UNIVERSIDAD DE MURCIA

ESCUELA INTERNACIONAL DE DOCTORADO

TESIS DOCTORAL

Regulation of glucose metabolism by telomerase in the health and disease

Regulación del metabolismo de la glucosa por telomerasa en la salud y enfermedad

D.ª Elena Naranjo Sánchez

2023

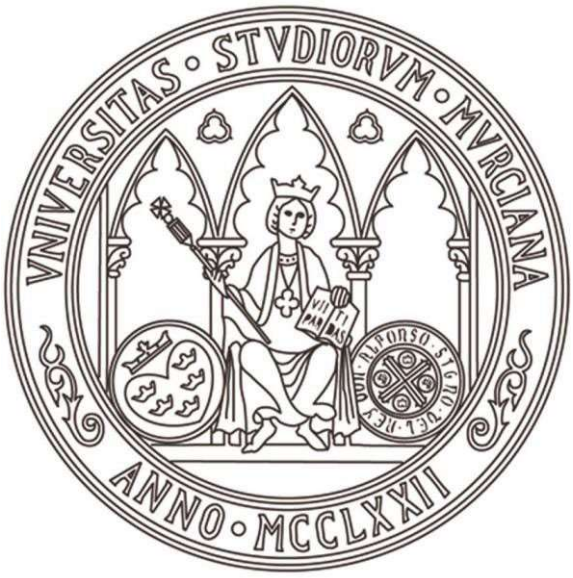

UNIVERSIDAD DE MURCIA

ESCUELA INTERNACIONAL DE DOCTORADO

TESIS DOCTORAL

Regulation of glucose metabolism by telomerase in the health and disease

Regulación del metabolismo de la glucosa por telomerasa en la salud y enfermedad

Autora: D.ª Elena Naranjo Sánchez

Directores: D.ª María Luisa Cayuela Fuentes,

D. Victoriano Mulero Méndez y

D. Jesús García Castillo

UNIVERSIDAD DE MURCIA

DECLARACIÓN DE AUTORÍA Y ORIGINALIDAD

DE LA TESIS PRESENTADA PARA OBTENER EL TÍTULO DE DOCTOR

D./Dña. Elena Naranjo Sánchez

doctorando del Programa de Doctorado en

Biología Molecular y Biotecnología

de la Escuela Internacional de Doctorado de la Universidad Murcia, como autor/a de la tesis presentada para la obtención del título de Doctor y titulada:

Regulation of glucose metabolism by telomerase in the health and disease / Regulación del metabolismo de la glucosa por telomerasa en la salud y enfermedad

y dirigida por,

D./Dña. María Luisa Cayuela Fuentes

D./Dña. Victoriano Mulero Méndez

D./Dña. Jesús García Castillo

DECLARO QUE:

La tesis es una obra original que no infringe los derechos de propiedad intelectual ni los derechos de propiedad industrial u otros, de acuerdo con el ordenamiento jurídico vigente, en particular, la Ley de Propiedad Intelectual (R.D. legislativo 1/1996, de 12 de abril, por el que se aprueba el texto refundido de la Ley de Propiedad Intelectual, modificado por la Ley 2/2019, de 1 de marzo, regularizando, aclarando y armonizando las disposiciones legales vigentes sobre la materia), en particular, las disposiciones referidas al derecho de cita, cuando se han utilizado sus resultados o publicaciones.

Si la tesis hubiera sido autorizada como tesis por compendio de publicaciones o incluyese 1 o 2 publicaciones (como prevé el artículo 29.8 del reglamento), declarar que cuenta con:

- *La aceptación por escrito de los coautores de las publicaciones de que el doctorando las presente como parte de la tesis.*
- *En su caso, la renuncia por escrito de los coautores no doctores de dichos trabajos a presentarlos como parte de otras tesis doctorales en la Universidad de Murcia o en cualquier otra universidad.*

Del mismo modo, asumo ante la Universidad cualquier responsabilidad que pudiera derivarse de la autoría o falta de originalidad del contenido de la tesis presentada, en caso de plagio, de conformidad con el ordenamiento jurídico vigente.

En Murcia, a 18 de mayo de 2023

Fdo.: Elena Naranjo Sánchez

Esta DECLARACIÓN DE AUTORÍA Y ORIGINALIDAD debe ser insertada en la primera página de la tesis presentada para la obtención del título de Doctor.

Información básica sobre protección de sus datos personales aportados	
Responsable:	Universidad de Murcia. Avenida teniente Flomesta, 5. Edificio de la Convalecencia. 30003; Murcia. Delegado de Protección de Datos: dpd@um.es
Legitimación:	La Universidad de Murcia se encuentra legitimada para el tratamiento de sus datos por ser necesario para el cumplimiento de una obligación legal aplicable al responsable del tratamiento. art. 6.1.c) del Reglamento General de Protección de Datos
Finalidad:	Gestionar su declaración de autoría y originalidad
Destinatarios:	No se prevén comunicaciones de datos
Derechos:	Los interesados pueden ejercer sus derechos de acceso, rectificación, cancelación, oposición, limitación del tratamiento, olvido y portabilidad a través del procedimiento establecido a tal efecto en el Registro Electrónico o mediante la presentación de la correspondiente solicitud en las Oficinas de Asistencia en Materia de Registro de la Universidad de Murcia

Table of contents

Abbreviations

µM	Micromolar
ADP	Adenosine diphosphate
AS	Antisense
ATP	Adenosine triphosphate
ChIRP	Chromatin Isolation by RNA-purification
CHT	Caudal hematopoietic tissue
CTNNB1	Catenin beta 1
CXCL14	Chemokine (C-X-C motif) ligand 14
DMSO	Dimethyl sulfoxide
DNA	Deoxyribonucleic acid
dpf	Days post-fertilization
drl	Zinc finger protein draculin
G-CSF	Granulocyte colony-stimulating factor
GFP	Green fluorescent protein
GLUD1/2	Glutamate dehydrogenase 1 and 2
GM-CSF	Granulocyte-macrophage colony-stimulating factor
H3	Histone 3
H4	Histone 4
hpf	Hours post-fertilization
hpi	Hours post infection
HPLC-MS	High-performance liquid chromatography-mass spectrometry
hpw	Hours post wound
IgG	Immunoglobulin G
IL17A	Interleukin 17A
IL1B	Interleukin 1 beta

LDH	Lactate dehydrogenase
LMNA/C	Lamin A/C
lncRNA	Long non-coding RNA
LPS	Lipopolysaccharide
lyz	Lysozyme
MDH2	Malate dehydrogenase 2
mM	Milimolar
Mo	Morpholino
mpeg1	Macrophage expressed 1
mpx	Myeloperoxidase
NAD^+	Nicotinamide adenine dinucleotide
NFKB	Nuclear factor κappa B
nM	NanoMolar
nm	Nanometers
NUP98	Nucleoporin 98
pγH2Ax	Phosphorylated histone variant H2AX
PBS	Phosphate buffer saline
PBST/PBT	Phosphate buffer saline with 0.1% tween-20
PBSTx	Phosphate buffer saline with 0.1% Triton-X
PDC	Pyruvate dehydrogenase complex
PDK	Pyruvate dehydrogenase kinase
PDP	Pyruvate dehydrogenase phosphatase
PFA	Paraformaldehyde
PFAS	Phosphoribosylformylglycinamidine synthase
PLA	Proximity Ligation Assay

RIP	RNA immunoprecipitation
RNA	Ribonucleic acid
ROS	Reactive oxygen species
rps11	Ribosomal protein subunit 11
RPS6KA1	Ribosomal protein subunit 6 kinase A1
S.D.	Standard deviation
S.E.M.	Standard error of the mean
SNP	Single nucleotide polymorphism
SOCS2	Suppressor of cytokine signaling 2
spint1a	Kunitz-type protease inhibitor 1
ST	*Salmonella Typhimurium*
TCA	Tricarboxylic acid
TERC	Telomerase RNA component
*terc*bs	*terc* binding site
TERT	Telomerase reverse transcriptase
T_H	Helper T lymphocyte $CD4^+$
TNFA	Tumor necrosis factor alpha

Summary

Telomerase is a complex composed by a catalytic subunit (TERT) and an RNA component (*TERC*) whose main function is telomere synthesis in eukaryotic cells. For that reason, telomerase has been related directly the aging and cancer. Nevertheless, both TERT and *TERC* are known to perform extracurricular or non-canonical functions, that is, independently of telomere lengthening.

The regulation of the cell energy metabolism plays an important role in the cell function, being the glucose metabolism one of the most studied in cancer and immune cells. In general terms, the regulation of both glycolysis and the Krebs cycle (TCA cycle) is fundamental for cell proliferation. However, also the generated metabolites in those pathways perform cell signaling functions, participate in the control of gene expression and have immunomodulatory roles.

In this doctoral thesis, we have described new extracurricular functions of TERT and *TERC* related to the regulation of glucose metabolism. In order to do that, we took advantage of zebrafish as an *in vivo* model, exploring these functions in two different disease models (chronic inflammation and cancer); and we have also used human cell lines for *in vitro* experimentation and in physiological condition approximations.

The objectives of this doctoral thesis are the following: 1) Validate and characterize the interaction between the pyruvate dehydrogenase complex and the telomerase components *TERC* and TERT. 2) Study the relationship between *terc* and the regulation of glucose metabolism in the context of chronic inflammation and the cancer immune response.

In the first chapter we performed a metabolic study and determined that *terc* expression was able to modify the glycolysis and TCA cycle metabolite composition. Likewise, we established that *terc* was playing a role as a long non-coding RNA, controlling the expression of the *ldhbb* gene, which encodes one isoform of the enzyme lactate dehydrogenase. Hence, we characterized this effect first in a chronic inflammation model by performing pharmacologic, transcriptomic, and functional studies; and second, in a cancer model, specifically studying the anti-tumor immune response *in vivo* by evaluating the tumor development and performing functional studies with several transgenic zebrafish lines.

In the second chapter, we based our studies in a proteomic analysis performed in zebrafish and found that the E1 subunit of the pyruvate dehydrogenase complex (PDC) was a possible *terc* interactor. In our studies, we validated this interaction in human cell lines using molecular biology and imaging techniques. Moreover, we checked by immunofluorescence and enzymatic activity assays that *TERC* expression could modify the PDC cell location, but not its enzymatic activity. Lastly, we confirmed that the interaction with PDC-E1 was also taking place with TERT, and that both telomerase components were interacting with the E2 subunit of the PDC, stablishing a new extracurricular function for both complexes.

Introduction

1. Telomeres and Telomerase: structure and functions

1.1. Telomeres

Telomeres are oligomeric DNA structures localized at the end of the eukaryotic chromosomes[1]. They are made by tandem repeat sequences which vary in copy number among organisms. In vertebrates, the telomeric sequences are composed by the TTAGGG hexanucleotide, that can be extended thousands of times[1; 2]. Another characteristic of the telomeric DNA is that it is a double stranded sequence for the most part, but it ends with a single stranded 3´overhang[3].

Telomeres are not coding sequences, that is, they don't contain genetic information. Nevertheless, they have a very relevant function in the cell since they protect the information contained in the genomic DNA. These protective sequences in the eukaryotic genome have been maintained throughout evolution, form yeast to mammals, revealing the importance of their presence in the cell[4].

However, due to the nature of the telomere structure, the telomeres also need protection form cellular exonucleases and other extracellular damages[5]. In order to maintain the telomere and chromosome stability, there is a series of proteins attached to the telomere repetitions called the shelterin complex[3; 6]. This six-protein complex is composed by the proteins POT1, TPP1, TIN2, TRF1, TRF2 and Rap1. The shelterin complex serves as a protection mechanism as well as it plays an important role in the nuclear localization of the telomeres and in the recruitment of specific proteins to the telomeres[6; 7].

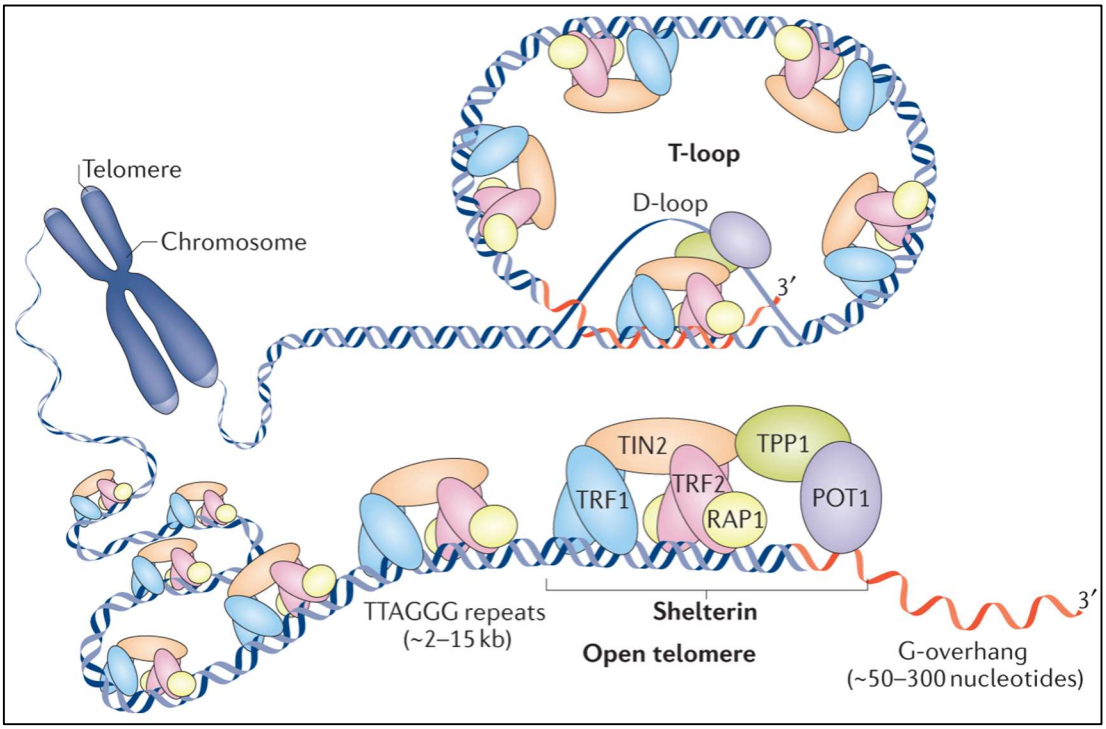

Figure 1. Localization and structure of telomeres. Adapted from (Lim and Cech, 2021)[8].

Even though the genomic DNA is protected by this nucleoprotein structure, it is known that each cellular division entails a small telomere shortening due to the impossibility of the replication machinery to complete the extension of the 3' ending of the DNA[9]. This implies that the cell cannot proliferate indefinitely due to the continuous loss of the chromosomal protection in each

division[10]. When this limit of divisions is reached (Hayflick limit), cells undergo a process called replicative senescence, in which they stop their cellular cycle and become unable to proliferate anymore[11]. However, some cells have mechanisms to maintain a continuous proliferation by avoiding this telomere attrition. One of most studied mechanisms that maintain the telomere length is the telomerase complex.

1.2. Telomerase complex

Telomerase is a ribonucleoprotein complex that has reverse-transcriptase activity[12; 13]. The main components of this complex are the protein called Telomerase Reverse-Transcriptase or TERT (the catalytic subunit; EC:2.7.7.49) and *TERC* (the RNA component), although also other accessory proteins such as Dyskerin are part of the complex[14; 15].

Telomerase is recruited by the sheltering complex proteins to the telomeric region during the S-phase of the cell cycle to perform the telomere elongation[16]. TERT uses *TERC* as a template to synthetize the telomeric sequence at the 3' overhang of the chromosomal DNA. After this elongation of the 3´ending, the DNA polymerase can now complete the other chain, thus achieving the maintenance of the telomere length in each DNA replication[2; 9; 11; 13].

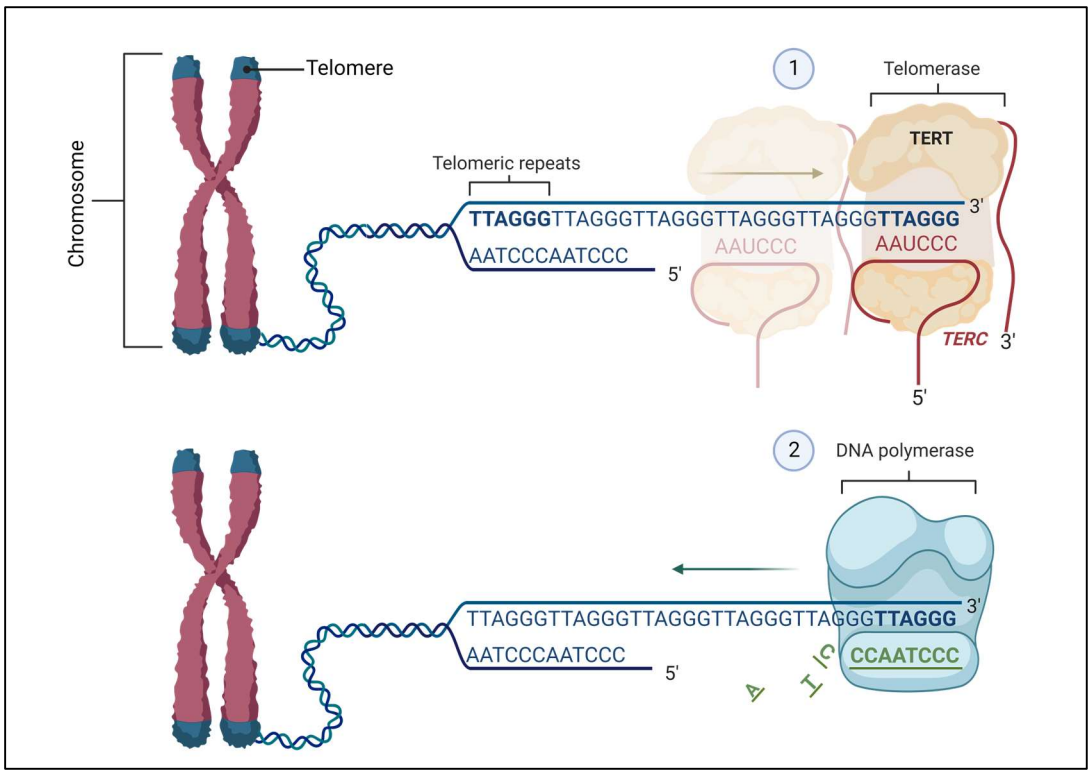

Figure 2. Synthesis of the telomeric sequence by telomerase. First telomerase extends the telomeric sequence thanks to its reverse-transcriptase activity using the *TERC* RNA as a template. After telomerase, the DNA polymerase now binds to the extended telomere and uses it to synthesize the lagging strand. Created with BioRender.com.

Since the telomerase function can overcome the limit of the cell divisions, the telomerase has been widely studied as a central player in aging, and cancer development and progression.

In multicellular organisms, telomerase is absent in most tissues and can only be found in embryonic and highly proliferative adult tissues[1; 7]. For that reason, most somatic cells undergo a telomere attrition throughout their cell divisions that ultimately leads to cell senescence. This senescent cells have been directly linked to the aging process, making the telomere length a common measure of the life expectancy[17].

As above mentioned, the expression of telomerase is restricted to specific tissues in the adult. However, its expression is commonly reactivated in cancer cells, since it enables a continuous proliferation[2]. Indeed, around 90% of tumors express TERT, becoming one of the most studied players in cancer and a target for cancer therapy[2; 18].

1.3. The extracurricular functions of telomerase

Besides telomere lengthening, TERT and *TERC* have other distinct roles in the cell that have been named as extracurricular or non-canonical functions[19-21]. A large part of the established extracurricular functions of TERT and *TERC* are due to their ability to bind to the DNA, acting as transcription factors.

1.3.1. Extracurricular roles of TERT

Overall, TERT expression has been directly associated to cancer progression by its role in maintaining chromosome stability through telomere elongation. Nonetheless, it's been demonstrated that TERT is involved in several processes that are key to cancer progression in a telomere-independent way, such as cell proliferation, stemness or cell migration[7; 22].

With the purpose of studying these extracurricular roles independent of its telomerase activity, mutant forms of TERT with no catalytic activity have been generated (DN-TERT). Several studies show that both the wild type and mutant TERT increase cell proliferation, cell adhesion and migration[23; 24]. Also, in Dr Cayuela's laboratory, TERT was found to regulate cancer cell invasiveness *in vivo*. In this case, both the mutant and wild type TERT increased the expression of a cluster of microRNAs called MIR500, and, specifically, the overexpression of *miR500* by TERT or the mutant form resulted in an increase in cancer cell invasiveness[25].

Moreover, the epithelial-to-mesenchymal transition (EMT), one of the hallmarks of cancer cell transformation has been found to be regulated by TERT in a telomere-independent fashion. TERT has been shown to activate one of the major pathways involved in EMT, which is the Wnt/β-catenin signaling pathway. TERT is able to directly interact with β-catenin, increase its nuclear translocation and bind to the promoter region of the Wnt/β-catenin target genes, ultimately activating their transcription[26; 27].

Another way in which TERT is linked to cancer progression independently of *TERC* and telomere lengthening, is by improving the binding of c-MYC to the promoter of its target genes. The ability of c-MYC to bind to the promoter of its target genes was impaired upon TERT deletion, and TERT overexpression resulted in an increase in the transcription of c-MYC target genes. Moreover, TERT was found to bind to and stabilize c-MYC at the promoter region of its target genes[28].

Other extracurricular roles of TERT point out to a relationship between TERT expression and the regulation of inflammation and oxidative stress.

The nuclear factor-kappa B (NF-κB) protein complex is a master transcription factor regulating inflammation and the immune response[29]. NF-κB can regulate TERT expression by binding to its promoter region[30]. However, also TERT can increase the transcription of NF-κB target genes, such as the pro-inflammatory cytokines interleukin 6 (IL-6) or the Tumor Necrosis Factor alpha (TNFα)[31; 32]. Nevertheless, this seems not to be a TERT exclusive role since *TERC* has also been shown to be involved in the regulation of the expression of NF-κB target genes. The activation of the NF-κB pathway is related to inflammation but also to cancer development[33], therefore, the communication between the telomerase complex and the NF-κB pathway stablishes a complex feed-forward loop between the inflammatory and the pro-oncogenic pathways in the cell.

All these extracurricular roles of TERT are related to their presence in the nucleus. However, it's been described that TERT has extracurricular roles in the mitochondria. Indeed, TERT has a canonical N-terminus mitochondria localization sequence (MLS), and it can be found inside the mitochondrial matrix[34; 35].

Since the mitochondrial DNA doesn't have telomeres, the presence of TERT in the mitochondria (mitochondrial TERT or mito-TERT) has been related to its extracurricular roles. One of them is the ability of TERT protect the mitochondrial DNA from the ultraviolet (UV) damage by binding to it[34]. Also, the mitochondrial TERT has been described to have an antioxidant role. Mitochondria are the main productors of reactive oxygen species (ROS) in the cell, which produce oxidative stress. Some studies show how the increase in the amount of mito-TERT not only improved the mitochondrial function by inhibiting the ROS production, but it also inhibited the ROS-mediated cell apoptosis[34; 36].

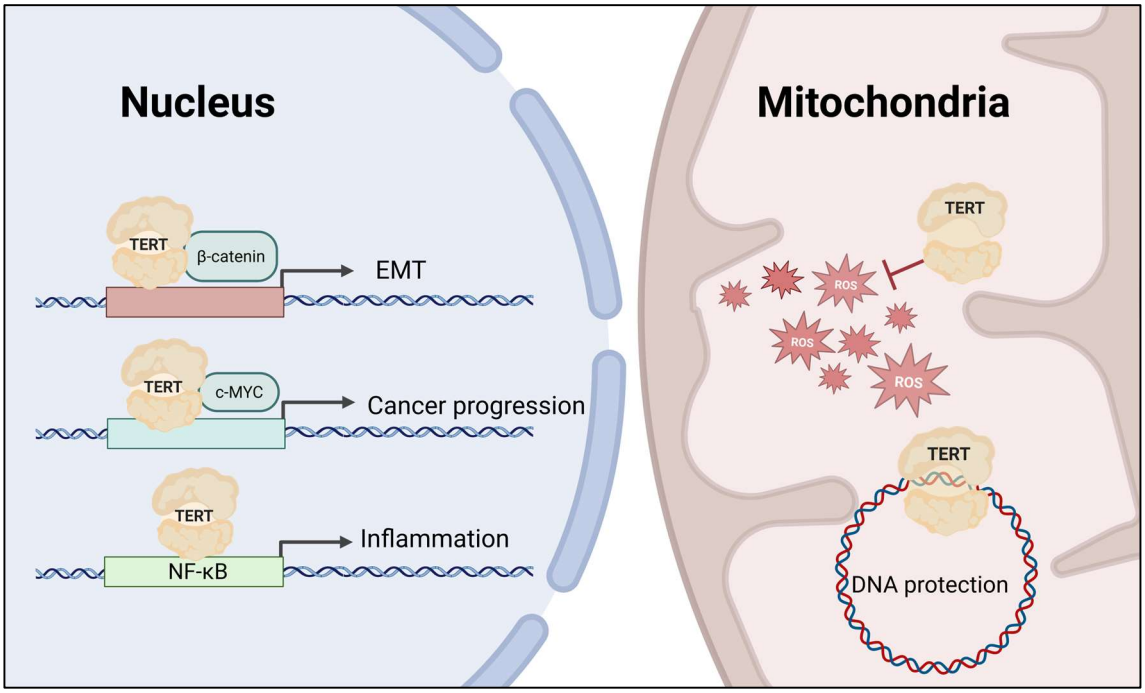

Figure 3. Representation of the extracurricular roles of TERT in the nucleus and mitochondria. Created with BioRender.com.

1.3.2. Extracurricular roles of *TERC*

As mentioned before, *TERC* has other functions besides telomere lengthening. Particularly, a Chromatin Isolation by RNA purification (ChIRP) study identified more than two thousand loci in the human genome which contained a *TERC* binding sequence[37], suggesting a role of *TERC* as a long non-coding RNA (lncRNA).

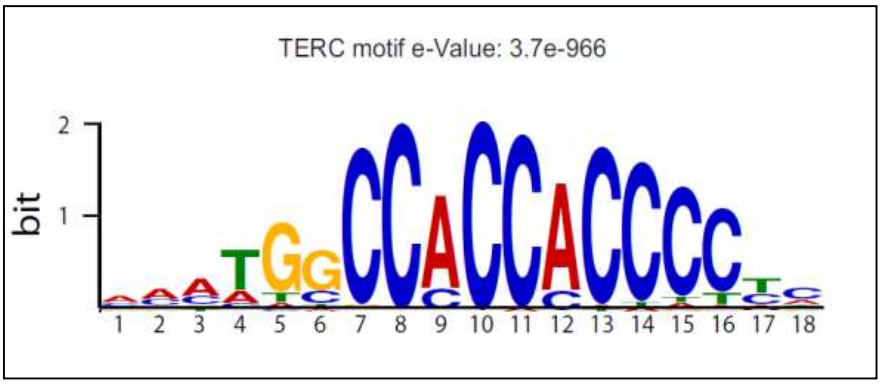

Figure 4. The cytosine-enriched motif corresponding to the *TERC*-binding sequence. Adapted from (Chu et al., 2011)[37].

Long non-coding RNAs (lncRNAs) are defined as transcripts longer than 200 nucleotides that lack the capacity to code for proteins[38; 39]. Most of the described functions of lncRNAs have to do with the control of gene expression. For instance, they are able to work as *cis* or *trans* elements, binding to specific motifs in the DNA that are nearby (*cis*) or far (*trans*) from the locus of their target gene[40]. They can also regulate gene transcription by acting as scaffolds for protein-protein interactions such as those between the elements of the transcription machinery. They can even change the chromatin spatial organization by controlling the localization of chromatin modificators[38].

In the case of *TERC*, studies have shown it to be an active player in multiple biological processes and pathways in the cell, independently of telomerase activity or telomere maintenance. These include establishing differential gene expression, directly controlling specific gene transcription, or even interacting with other RNAs.

As well as TERT, *TERC* can promote cell proliferation and cancer development through its non-canonical functions. Several studies reveal that the expression of *TERC* independently of TERT is needed to promote tumor development[41; 42]. Moreover, a recent study described how the expression of *TERC* increased the malignancy of gastric cancer cells by binding and sequestrating the microRNA *miR-423-5p*, which was found to have a positive effect inhibiting cell proliferation, migration and invasion[43].

Besides its non-canonical roles in cancer progression, *TERC* is accountable for several physiological processes related with the hematopoietic stem cell (HSC) differentiation and the immune function.

One example of that is the antiapoptotic role of *TERC* in $CD4^+$ T lymphocytes[44]. Specifically, an increase in *TERC* levels demonstrated to have a protective effect in $CD4^+$ T cells when treated with dexamethasone, independently of TERT expression. Furthermore, the knockdown of the endogenous *TERC* but not TERT in $CD4^+$ cells, activated the apoptosis signaling pathway by boosting the activity of caspase-3/7 and 9 without affecting the telomere length[44].

In another study, *TERC* was found to activate one of the major pathways controlling cell proliferation: the PI3K-AKT pathway. Specifically, *TERC* was shown to bind to the promoter region and activate the transcription of the PI3K-AKT target genes such as 3-Phosphoinositide Dependent Protein Kinase 1 (PDPK1). The role of *TERC* increasing the signaling of the PI3K-AKT pathway was found to be critical for the proliferation of activated $CD4^+$ T cells[45].

Other studies reveal a non-canonical function for *TERC* regulating the hematopoietic stem cell differentiation. In HSCs, a decrease in *TERC* expression resulted in impaired differentiation. Additionally, *TERC* reduction increased the expression of cellular senescence markers and the production of reactive oxygen species. This effect was demonstrated to be telomerase-independent since in induced pluripotent stem cells (IPSCs) with reduced *TERC* levels no telomere attrition was detected[46].

Also, studies performed in Dr. Cayuela's laboratory show how *TERC* absence leads to a defective production of neutrophils and macrophages (neutropenia and monocytopenia)[21]. In both human and zebrafish, *TERC* was demonstrated to function as a transcription factor needed for the expression of master myelopoietic genes such as the Colony Stimulating Factor 2 and 3 (*CSF2* and *CSF3*) and *SPI1*, and their zebrafish orthologous *csf3b*, *spi1a* and *spi1b*. This transcriptional regulation was found to be produced exclusively by *TERC* in a TERT-independent manner. The binding of *TERC* to its specific consensus sequence at the promoter regions of the genes, allowed the recruitment of the RNA polymerase II (RNApol II), therefore, enabling the expression of *CSF2/3* and *SPI1* and the correct formation of the myeloid population[47].

In addition to the role of *TERC* in the myelopoiesis and T lymphocytes, some evidence supports its role promoting the inflammatory response.

As commented before, *TERC* promotes the transcription of NF-kB target genes along with TERT. Nevertheless, *TERC* can promote the NF-kB signaling pathway also independently of TERT. The inhibition or overexpression of *TERC* in telomerase deficient or knock-down cells resulted in an increase and decrease, respectively, of the expression of pro-inflammatory cytokines such as IL-6 and IL-8. Moreover, *TERC* has been found to bind to the promoter region, and enhance the transcription, of the Tumor protein p63-regulated gene 1-like protein (TPRG1L), TYRO protein tyrosine kinase-binding protein (TYROBP) and Ubiquitin carboxyl-terminal hydrolase 16 (USP16) genes, which are up-regulated in patients with inflammation related disorders such as type II diabetes and multiple sclerosis[48].

Besides its presence in the nucleus and cytoplasm, *TERC* has also been found to be imported into the mitochondria[49]. In the mitochondria, *TERC* is processed into a shorter form (*TERC-53*), which is suggested to act as a reporter of the mitochondrial funciton[49]. The levels of *TERC-53* increase in the cytosol when there's a mitochondrial damage. Furthermore, the increase in *TERC-53*, seems to increase cell senescence markers both in *in vitro* and *in vivo* models, independently of telomerase activity or *TERC* levels[50].

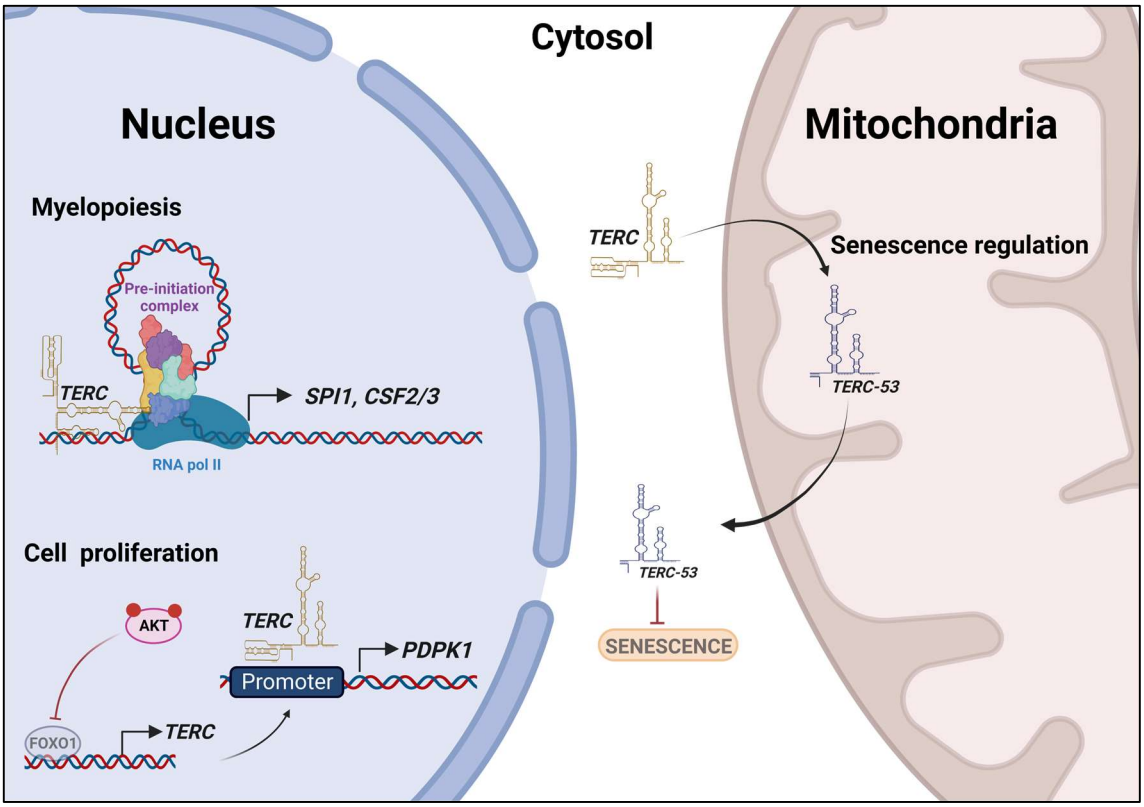

Figure 5. Representation of the extracurricular roles of *TERC*. In the nucleus, *TERC* regulates processes such as myelopoiesis and cell proliferation by binding to promoter regions and modiying gene expression. *TERC* is also imported into the mitochondria and processed into a shorter form (*TERC-53*) which is exported to the cytosol and regulates cell senescence. Created with BioRender.com.

2. Glucose metabolism

The cell metabolism is a very well-orchestrated succession of cellular processes by which cells obtain energy and precursors to maintain their synthetic and proliferative functions. The macromolecules and molecules involved in these processes are organized in pathways that are anabolic if they're aiming the synthesis of macromolecules or catabolic if the oxidation of molecules takes place to obtain energy[51]. One of the main catabolic pathways in the cell is the oxidation of glucose and it takes place in the cytosol (glycolysis) and in the mitochondria (tricarboxylic acid or TCA cycle and the electron transport chain or ETC). As a result, the molecules of glucose that enter the cell are catabolized to obtain energy in the form of adenosine triphosphate (ATP).

2.1. Glycolysis and TCA cycle

The uptake of glucose is done by two different kinds of transporters in the cell membrane: sodium–glucose linked transporters (SGLTs) and facilitated diffusion glucose transporters (GLUTs). The SGLTs are usually found in the small intestine and renal tubules, and they need a sodium concentration gradient to import glucose. On the other hand, GLUTs can introduce the glucose into the cell by a facilitated diffusion mechanism, and are present in all cell types[52].

Once glucose enters the cell, it must be activated to be catabolized, so the first step of glycolysis is the obtention of glucose-6-phosphate (G6P) by hexokinase (HK). The G6P is then converted into two molecules of glyceraldehyde 3-phosphate by four successive enzymatic reactions. These firsts steps of glycolysis are part of the preparatory phase, in which two molecules of ATP are consumed to introduce the phosphate groups in the enzymatic reactions. However, this ATP consumption will increase the ATP yield of the following steps[51].

In the payoff phase, each molecule of glyceraldehyde 3-phosphate is oxidized and phosphorylated by glyceraldehyde 3-phosphate dehydrogenase (GAPDH) to obtain 1,3-bisphosphoglycetate, which is converted into 3-phosphoglycerate and 2-phosphoglycerate by the successive reactions of phosphoglycerate kinase and phosphoglycerate mutase. Lastly, the enzyme enolase uses the 2-phophoglycetate molecules to produce phosphoenolpyruvate (PEP). The PEP molecules are used by the pyruvate kinase (PK) to produce pyruvate, which is the final product of glycolysis. In this payoff phase, four molecules of ATP are produced by each molecule of glucose. Considering that there was a consumption of two ATPs at the beginning of the pathway, the glycolysis only generates a total of 2 ATP molecules, being most of the energetic power still in the pyruvate molecules[51].

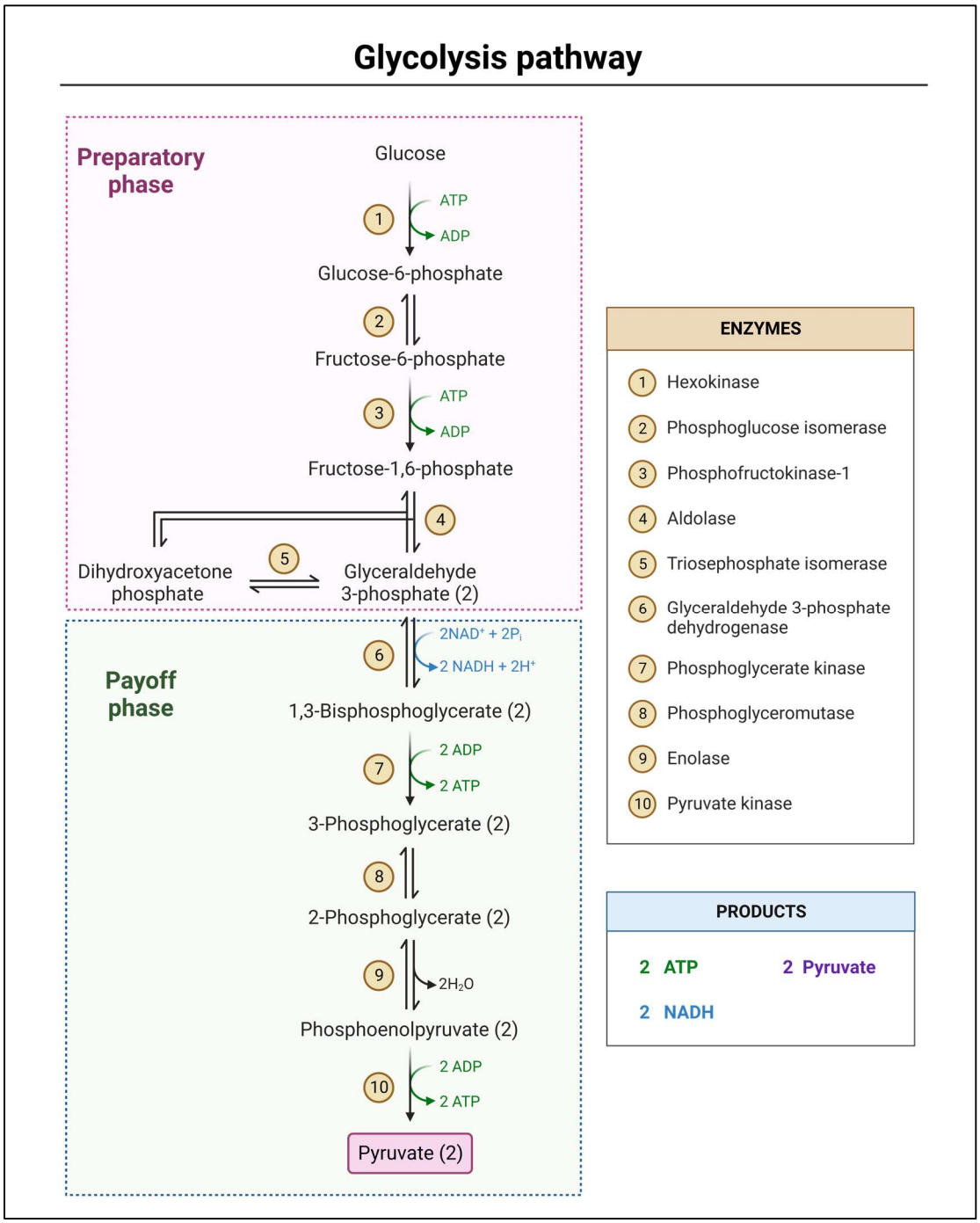

Figure 6. Schematic representation of the glycolysis pathway. In the preparatory phase, glucose is converted into two molecules of glyceraldehyde 3-phosphate by consuming two molecules of ATP. In the payoff phase, two molecules of pyruvate are generated along with four ATPs and two molecules of NADH. In brief, glycolysis yields a total of two molecules of ATP and two molecules of NADH. Created with BioRender.com.

Pyruvate can be further oxidized in the TCA cycle or it can be converted into lactic acid (lactate). The conversion of pyruvate into lactate is performed by the enzyme lactate dehydrogenase and it usually occurs under anaerobic conditions (hypoxia) or in specific cell types under normal oxygen conditions, such as in erythrocytes. Even though the production of lactate doesn't produce any extra ATP, the reaction catalyzed by lactate dehydrogenase consumes NADH, and

therefore produces NAD^+. This conversion is important to restore the NAD^+ molecules that were consumed in the payoff phase and makes it possible to continue with the flux of the glycolysis pathway[53].

However, in most tissues, pyruvate is oxidized by the pyruvate dehydrogenase complex (PDC) to obtain acetyl-CoA[51]. These two enzymes (lactate dehydrogenase and pyruvate dehydrogenase) are key in controlling the fate of the pyruvate molecule and, therefore, the amount of ATP produced by the cell and the way it is produced. The function and regulation of both enzymes will be covered in the next sections.

The TCA cycle (also called Krebs cycle) is a cyclic enzymatic pathway that takes place in the mitochondria. These cyclic reactions generate electrons which will be carried in the form of NADH and $FADH_2$, and later will be accepted by oxygen molecules in the electron transport chain to finally produce more ATP molecules. This process is called oxidative phosphorylation and yields a total of 36 ATP molecules per molecule of glucose[51; 53].

The first step in the cycle is the conversion of acetyl-CoA and oxaloacetate into citric acid (citrate). The acetyl-CoA can come from several sources, including the fatty acid and amino acid catabolism, but in the case of glucose catabolism, it comes from the oxidation of the pyruvate molecules by the pyruvate dehydrogenase complex. In the following reactions of the TCA cycle, citrate will be transformed into isocitrate, which will be decarboxylated by isocitrate dehydrogenase to produce α-ketoglutarate. A second decarboxylation of α-ketoglutarate will ultimately lead to the production of succinate.

These reactions comprise the first half of the TCA cycle and yield a total of two molecules of CO_2 (coming from the two decarboxylation steps) and two molecules of NADH for each acetyl-CoA entering the cycle. In the second half of the cycle, succinate gets reconverted into oxaloacetate in three enzymatic steps that will produce a molecule of $FADH_2$ and another molecule of NADH.

The TCA cycle is not only key in the oxidation of glucose. It generates metabolites that are intermediates or precursors in several biosynthetic pathways, such as fatty acids, amino acids and nucleotides. For that reason, the TCA cycle is considered an amphibolic pathway (both catabolic and anabolic)[51]. Moreover, the intermediates in the cycle can be replenished trough anaplerotic pathways, that is, pathways involved in other anabolic or catabolic processes, such as the amino acid metabolism[54].

Although the oxidation of glucose is aiming at energy production, both the glycolysis and the TCA cycle generate metabolites that are known to have signaling and regulatory functions besides being mere intermediate molecules. Furthermore, the enzymes participating in this process are known to have important roles in the cell in the regulation of gene expression and cell fate. In this regard, the study of the regulation of the glucose metabolism has been important in several fields such as immunology, cancer and aging[55-59].

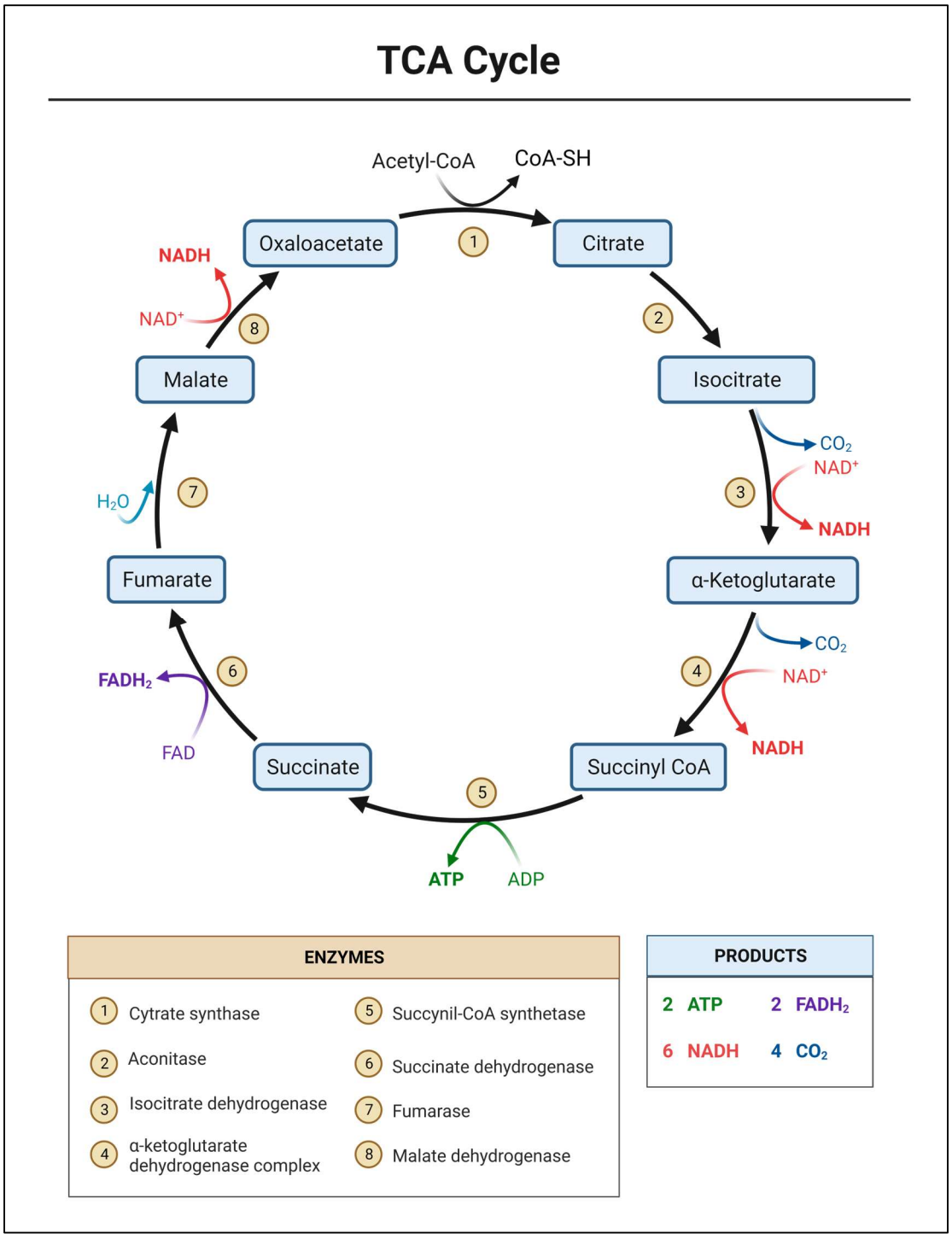

Figure 7. Schematic representation of the TCA cyle. In this cyclic pathway, the acetyl-CoA is transformed in succesive reactions that yield NADH, $FADH_2$ and ATP. The NADH and $FADH_2$ cofactors will transfer their electrons in the electron transport chain to produce more ATP molecules. The metabolites of the TCA cycle are also important for anabolic pathways, thus, the Krebs cycle defined an anphibolic pathway. Created with BioRender.com.

2.1.1. Lactate dehydrogenase

Lactate dehydrogenase or LDH (EC 1.1.1.27) is a cytosolic enzyme in charge of the conversion of pyruvate into lactic acid (lactate). It is tetramer composed by two different types of subunits that are encoded by two different genes. The subunit M, also called LDHA, is encoded by *LDHA* gene and the subunit H (LDHB) is encoded by *LDHB* gene[60]. In vertebrates, five different isoenzymes of LDH are found depending on the tetramer composition, ranging from LDH1 (all LDHB subunits) to LDH5 (all LDHA subunits)[61]. The abundance of each isoenzyme is different depending on the tissue energy requirements. For example, LDH1 is the predominant isoform in the heart whereas LDH5 is more abundant in tissues like the muscle or the skin[62; 63].

Besides *LDHA* and *LDHB*, there are another two genes encoding two special LDHs. One of them is *LDHC*, an exclusive form of male germ cells and spermatozoa[64]. The other one is *LDHD*, which encodes an LDH enzyme located inside the mitochondria that generates the isomer D-lactate instead of L-lactate, which is a hundred times less abundant[65].

In zebrafish, there are orthologs for every *LDH* gene except for *LDHC*, which probably appeared by an independent duplication of the *LDHB* gene in humans[64; 66]. Besides, due to the genome duplication in zebrafish[67], *LDHB* has two ortholog genes: *ldhba* and *ldhbb*. In the case of *LDHA* and *LDHD*, each one has its own ortholog: *ldha* and *ldhd*, respectively.

The reaction catalyzed by LDH is a reversible reaction and partially depends on the substrate availability[61; 68]. However, the subunit composition of the enzyme plays an important role in defining the enzyme affinity for pyruvate or lactate as a substrate, and that's why different tissues with different energy requirements have different LDH isoforms.

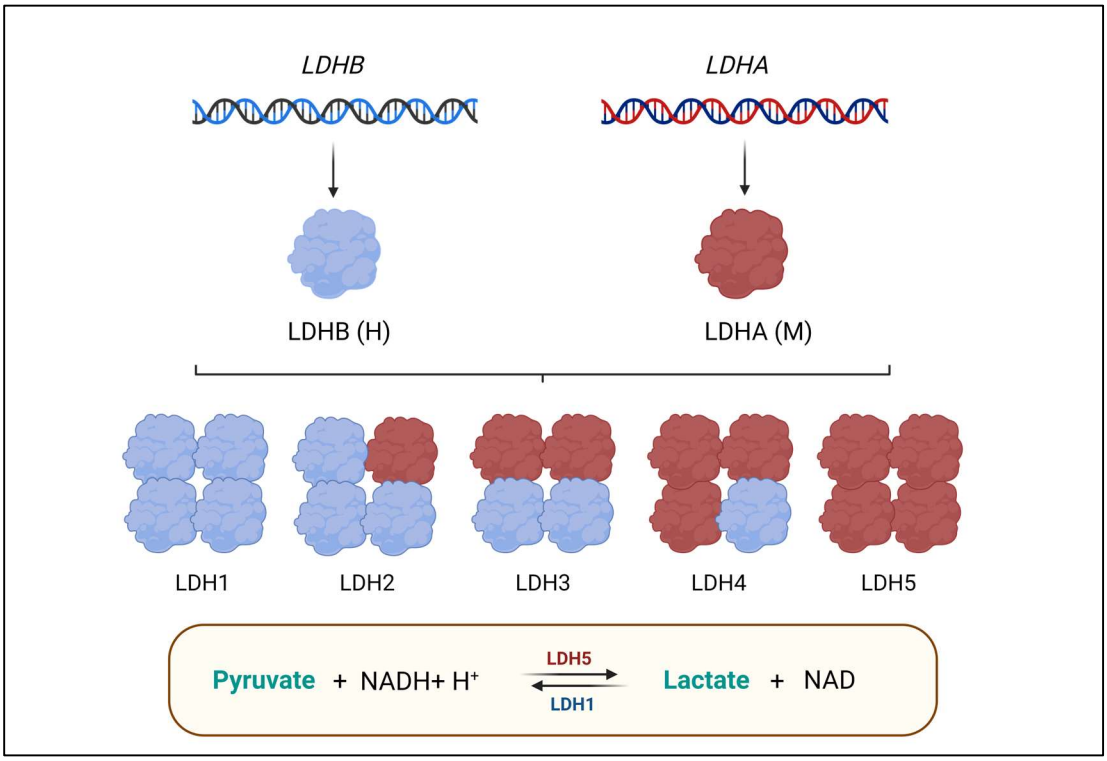

Figure 8. LDH isoenzymes and enzymatic reaction. Two genes code for two different subunits called H (LDHB) and M (LDHA). The two subunits compose the LDH tetramer in five different stequiometric arrangements: from all LDHB subunits (LDH1) to all LDHA subunits (LDH5). The reaction catalized by LDH depends on the subunit composition since LDHB usually transforms lactate into pyruvate whereas LDHA transforms pyruvate into lactate. Created with BioRender.com.

Even though LDHA and LDHB share almost 90% of similarity, only one key aminoacidic change in their catalytic center is enough to achieve a different affinity for the substrate[69]. As a result, LDH5 which is composed by all LDHA subunits, is more prompt to bind pyruvate and produce lactate, whereas LDH1 (all LDHB subunits) has a higher affinity binding lactate and producing pyruvate[69; 70]. Nevertheless, LDH1 is also able to produce lactate[71].

Although LDH activity varies according to the tetramer composition, there are two more levels of regulation for this enzyme. Through both transcriptional and post-translational modifications, the levels and activity of LDHA and LDHB are modified separately, thus increasing the level of complexity to study the regulation of this enzyme. These mechanisms have been widely studied in cancer cells since LDH has been stablished as a key protein that tumor cells need to fulfill their energy and proliferation requirements [72; 73].

The transcription of *LDHA* is positively regulated by transcription factors that are implicated in cell proliferation and oncogenic transformation, such as the Hypoxia-Induced Factor 1 alpha (HIF-1α) and c-MYC[74; 75]. The transcription regulation of *LDHB* is less well characterized, and whether its increase or decrease favors cancer development is still under debate. On the one hand, some transcription factors related to cancer progression have been identified to activate *LDHB* expression. That is the case of High-mobility group box 2 (HMGB2) and STAT3[76; 77]. On the other hand, it has been found that a common characteristic in several types of cancer cells is the hypermethylation of the promoter region of *LDHB*[78]. Specifically in prostate and pancreatic cancers, this epigenetic mark that leads to a decrease in *LDHB* expression and correlates with cancer development and invasiveness[79; 80].

As mentioned before, there are as well post-translational modifications (PTM) affecting LDHA and LDHB activities. Both phosphorylation and acetylation are common PTMs to LDHA and LDHB. In the case of LDHA, the phosphorylation at tyrosine 10 increases its enzymatic activity[81], whereas acetylation at lysine 5 inhibits the catalytic activity of LDHA. Moreover, this acetyl addition not only reduces its activity but also serves as a signal for the LDHA lysosomal degradation[82]. Interestingly, the phosphorylation of LDHB has a different effect on its activity. LDHB is phosphorylated at serine 162 by the kinase Aurora-A, changing its affinity for the substrate. Hence, the phosphorylated LDHB is more efficient producing lactate and nicotinamide adenine dinucleotide (NAD^+) instead of pyruvate and NADH (the reduced form of NAD^+)[83]. On the contrary, the acetylation of LDHB at lysine 392 has a similar effect as on LDHA, reducing its ability to convert lactate into pyruvate. Along with this finding, the deacetylation of LDHB by SIRT5 has been shown to produce and increase in its enzymatic activity[84].

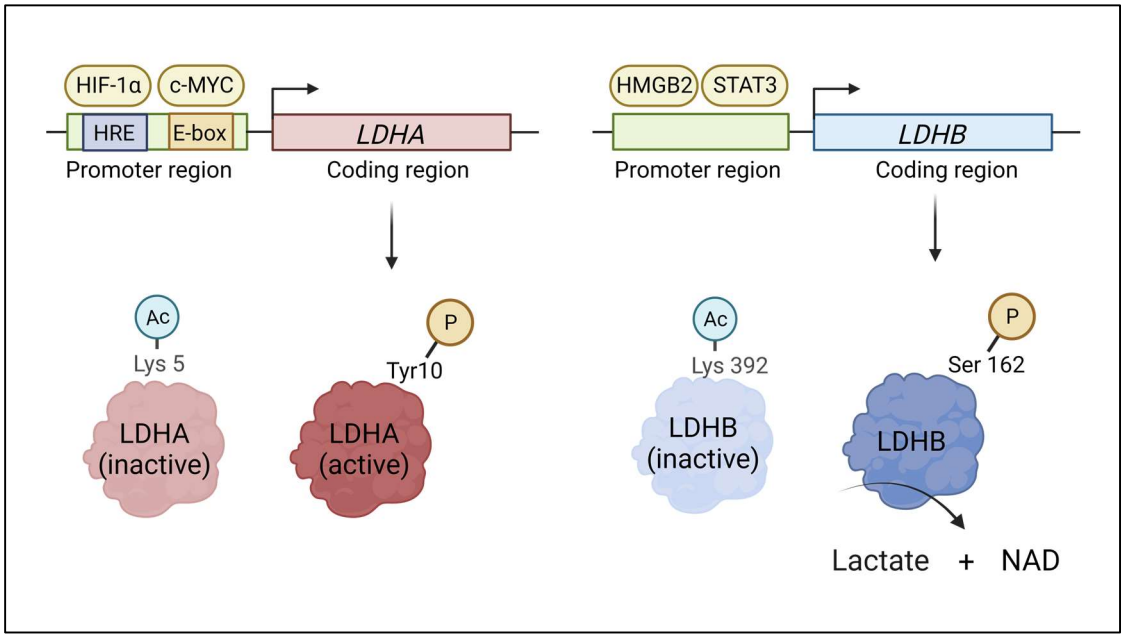

Figure 9. Transcriptional and protein regulation of LDH. The transcription of *LDHA* and *LDHB* is regulated independently and can be enhanced by several transcription factors by its binding at their promoter region. Also LDH activity can be modified at protein level by acetylation, which inhibits the function of both LDHA and LDHB, and by phosphorylation, which promotes lactate synthesis in both proteins. Created with BioRender.com.

2.1.2. LDH and lactate functions

The function of LDH has been described to be crucial to cancer cells, which have unlimited an uncontrolled proliferation[85]. In order to maintain that high level of proliferation, these cells undergo a metabolic adaptation which consists in the use of the glycolysis pathway as their main source of energy (ATP). This metabolic switch was first described by Otto Warburg, therefore, it was called the Warburg effect[86].

The Warburg effect has been described to be a common characteristic in most cancer cells. Since LDH is key to this metabolic adaptation, it has been established as one of the main targets in cancer therapy[72; 73; 87]. Nevertheless, the study of LDH as also unveiled the presence of extracurricular roles for this enzyme.

Although considered a cytoplasmic enzyme, LDH has been described to be present also in the nucleus (nLDH). nLDH is able to bind the DNA and regulate the transcription efficiency of several DNA polymerases[88; 89]. Furthermore, it is known that nLDH is involved in the regulation of gene transcription by regulating histone acetylation/deacetylation. However, it is unclear whether nLDH increases or decreases the activity of histone deacetylases (HDACs), since some studies show how the production of NAD^+ by LDH increases the function of acetylating proteins such as sirtuin 1 (SIRT1)[89], while others show a decrease in HDACs activity upon lactate accumulation[90]. Also, LDH has been described to promote EMT in cancer by increasing histone acetylation and the transcription of EMT genes such as *CTNNB1*, *RHOB*, and *TGFBR1*[91].

A special interest in the study of the LDH function and its regulation lies in the ability of this enzyme to control the production of lactate. Beyond being a product of an incomplete glycolysis, lactate has been established to be a metabolite with several and important signaling and regulatory functions under physiological conditions and in several diseases[92; 93]:

Specifically, the role of lactate has been studied in cancer, since it gets accumulated in the tumor microenvironment as a consequence of the tumor metabolism[94]. Lactate has been shown to affect the cells surrounding the tumor in multiple ways, but in all cases the final consequence is the promotion of tumor growth and metastasis. For instance, lactate affects the function of fibroblasts and other cells that form the tumor stroma, changing their metabolism to support the tumor metabolic requirements[95; 96]. Moreover, it can promote the formation of new vessels (angiogenesis) to increase the oxygen and nutrient supplies to the tumor cells[92]. Another way in which lactate is related to tumor progression is by its immunomodulatory functions, a topic that will be covered more extensively in following sections.

2.1.3. Pyruvate Dehydrogenase Complex

The Pyruvate Dehydrogenase Complex (PDH complex or PDC) is in an enzymatic complex located in the mitochondrial matrix of eukaryotic organisms and it is responsible for the conversion of pyruvate into acetyl-CoA[51]. The PDC is constituted by three different enzymes: pyruvate dehydrogenase (EC 1.2.4.1; PDH or E1), dihydrolipoyl transacetylase (EC 2.3.1.12; DLAT or E2) and dihydrolipoyl dehydrogenase (EC 1.8.1.4; DLD or E3)[97]. Although all of them constitute the whole Pyruvate Dehydrogenase Complex, the term 'complex' refers to the fact that all those subunits are usually found as a cluster with several copies of each one of them, resulting in a structure of several nanometers of diameter (30-50 nm)[51; 98; 99].

In order to obtain acetyl-CoA, the three enzymes perform consecutive reactions that require a total of five different cofactors: thiamine pyrophosphate (TTP), flavin adenin dinuclueotide (FAD), coenzyme A (CoA), NAD^+ and lipoate[51]. The E1 component is responsible for the first steps of the reaction. First, the pyruvate is decarboxylated, losing the acid group. The rest of the molecule is attached to TTP and is immediately oxidized, which generates the acetyl group and liberates the TTP. Next, the lipoyl component of the E2 enzyme joins to it and transfers the coenzyme A to this intermediate. That way, acetyl-CoA is produced. Lastly, the E3 enzyme uses FAD to regenerate the lipoate to its original oxidized form. The resulting $FADH_2$ transfers the remaining electrons to NAD^+ leading to the formation of NADH[97].

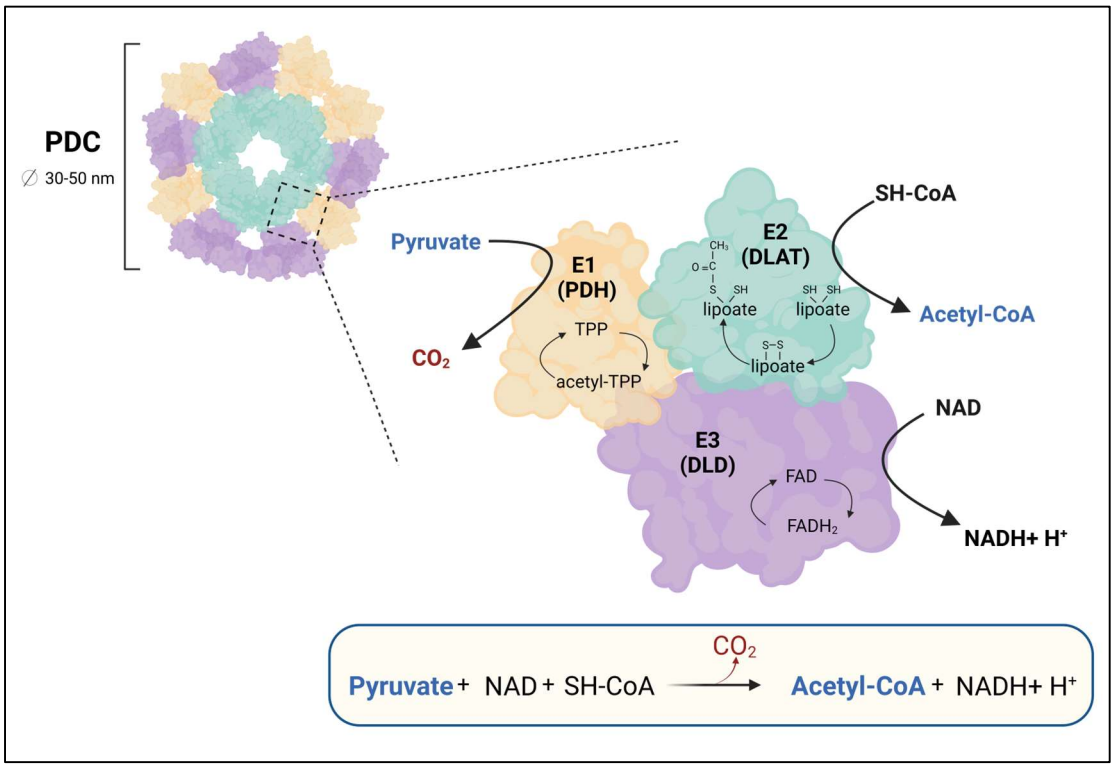

Figure 10. Pyruvate dehydrogenase complex (PDC) structure and enzymatic reaction. The PDC is composed by several copies of E1, E2 and E3 subunits in a variable amount. The E2 subunit is located in the core of the complex and the E1 and E3 are at the periphery. The three subunits use five different coenzymes in succesive reactions to produce acetyl-CoA from pyruvate. Created with BioRender.com.

The PDH (E1) enzyme is a heterotetramer composed by two alpha and two beta subunits (E1α and E1β). This enzyme is the one controlling the speed of the reaction of the PDC and is target of regulation by phosphorylation/dephosphorylation[100]. Three different phosphorylation sites at the PDC-E1α subunit have been identified: Ser^{232}, Ser^{293} and Ser^{300}. The modification of one or several of these serine residues has been shown to drastically reduce the activity of the PDC[101].

The pyruvate dehydrogenase kinases (PDKs) are the enzymes in charge of inhibiting PDC trough phosphorylation. There are four isoforms (PDK1, PDK2, PDK3 and PDK4), each one with a different specificity for the target serine residues in the E1α subunit and different patterns of expression among tissues[100].

The other key enzymes in control of PDC activity are the pyruvate dehydrogenase phosphatases (PDPs), which remove the phosphorylation mark, therefore activating the PDC. There are two isoforms of PDPs: PDP1 which is detected mainly in the heart and brain, and PDP2, which is present also in other tissues such as the liver and kidney. However, both isoforms can catalyze the de-phosphorylation of PDC[102].

The activity of the PDC can be allosterically inhibited by its own products: acetyl-CoA and NADH[51]. Besides, both PDKs and PDPs can be allosterically regulated by the products and substrates of the PDC. High levels of SH-CoA, NAD^+, or pyruvate (substrates) can inhibit PDKs, while high levels of acetyl-CoA or NADH (products) can activate PDKs and inhibit PDPs[51; 100]. Moreover, the activity of the PDC is also dependent on the energy requirements in the cell since ATP and ADP are allosteric regulators PDKs: high levels of ATP activate PDKs while high levels of ADP can inhibit their function[103].

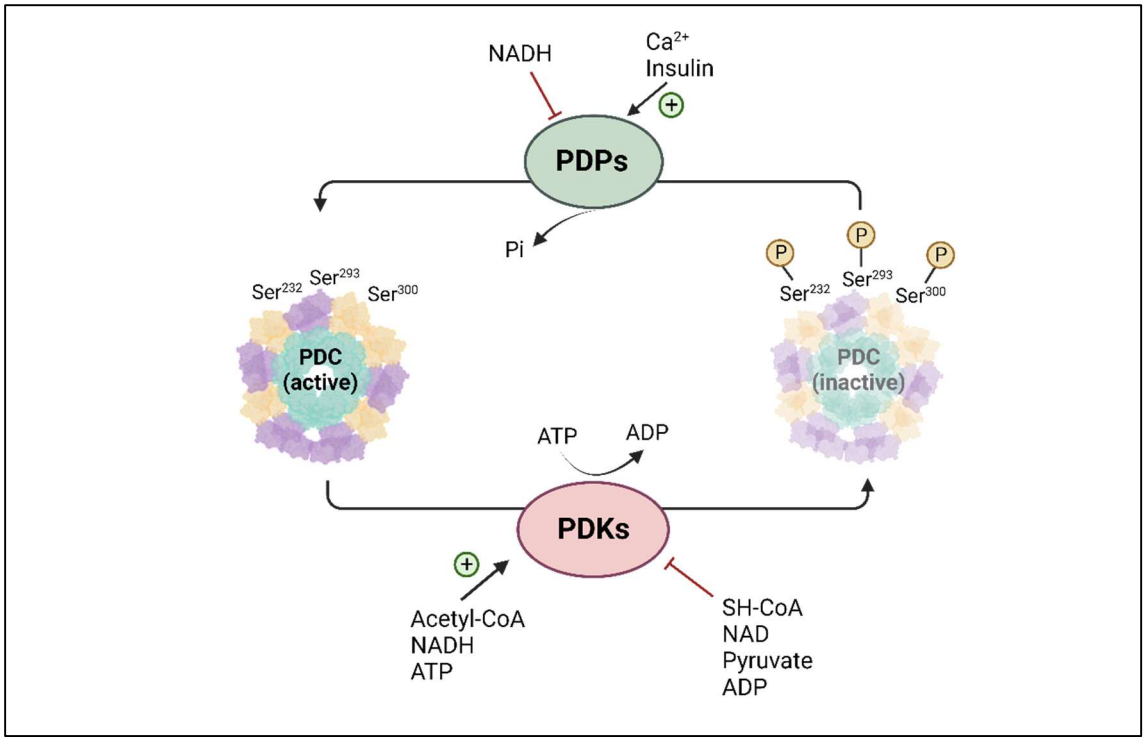

Figure 11. Regulation of PDC activity by phosphorylation. The phosphorylation of Ser^{232}, Ser^{293} and/or Ser^{300} at the E1α subunit of PDC by pyruvate dehydrogenase kinases (PDKs) inhibits PDC activity while dephosphorylation by pyruvate dehydrogenase phosphatases (PDPs) activates the PDC. Both PDKs and PDPs are allosterically regulated. Created with BioRender.com.

2.1.4. PDC and its non-canonical functions

Even though the PDC has been studied as a mitochondrial protein, this complex, as well as other glycolytic and TCA cycle enzymes, has other roles besides participating in the oxidation of glucose[104].

In addition to LDH, PDC can be translocated into the nucleus, where it takes part in the regulation of gene expression. Specifically, it has been reported that the production of acetyl-CoA in the nucleus by the PDC is directly related to the levels of histone acetylation and the transcription of genes related with cell cycle and proliferation[105]. Interestingly, the nuclear PDC corresponds only to active PDC, since only the non-phosphorylated form has been shown to be in the nucleus and none of the PDKs have been found in there.

The mechanism behind the translocation of the PDC remained unknown for several years after the discovery of its presence in the nucleus. The crossing of several mitochondrial membranes and the small pore size of the nuclear pores challenged the understanding on how this big-sized complex could be translocated into the nucleus. In a recent study, it's been shown that the whole PDC can translocate inside the nucleus through a non-canonical entry pathway, without involving the nuclear pores. Specifically, the tethering of mitochondria around the nucleus, creating points of contact with the nuclear envelope, facilitates the nuclear entry of the whole PDC. Specifically, the interaction between Lamin A (LMNA) and mitofusin 2 (MFN2) is crucial for mitochondria tethering and therefore, for PDC translocation[106]. However, this mechanism doesn't exclude the entry of the PDC subunits separately trough the nuclear pores.

The maximum amount of nuclear PDC (nPDC) is found during the S phase of the cellular division, when the DNA replication is taking place[105]. Proliferating stimulus such as serum, endothelial growth factor (EGF) and hypoxia promote mitochondria tethering around the nucleus, thus, PDC nuclear entry[105; 106]. Besides, other triggers and molecules have been described to affect nuclear PDC levels. Heat shock protein 70 (HSP70) is a chaperone that has been shown be bound to PDC subunits E1 and E2. Moreover, its nuclear levels correlated with nuclear PDC levels. And a decrease in HSP70 levels lead to a decrease in nPDC levels, indicating that HSP70 was important for the PDC entry into the nucleus (or the entry of the individual subunits)[105]. Other authors found that the presence of exogenous H_2S decreases nPDC levels. The S-suflhydration of PDC-E1 at Cys101 impaired PDC-E1 nuclear translocation, thus decreasing histone acetylation levels[107].

The levels of nPDC were first linked to an increase in H3K9 and H3K18 histone acetylation, thus promoting the cell-cycle progression[105]. Histone acetylation regulation has been shown to be directly related to aging in an evolutionary-conserved manner[55; 108]. Also, some works show how nPDC levels are key in regulating histone acetylation levels related to pluripotency and the embryonic development[109; 110]. Although PDC function and regulation has been widely studied as a potential target for cancer therapy due to its role controlling the pyruvate entry to the TCA cycle[111], the nuclear translocation of PDC expands the possible mechanisms by which PDC can be involved cancer progression, cell fate and aging.

3. The immune system and the inflammation response

3.1. Function and components of the immune system

The immune system is mainly composed of physical barriers and cellular responses whose function is the protection of the organism against tissue damage and pathogens. The first barrier that pathogens encounter is a physical barrier and is the cell epithelium, being the skin one of them[112].

The skin is composed by an external layer, the epidermis, and an internal layer, the dermis[113]. Although tight junctions between the skin cells impair the entrance of pathogens, also the synthesis of lipids, anti-microbial peptides and enzymes by the skin cells serve as a chemical barrier[114; 115].

Besides, the immune system also has a specific subset of cells in charge of defending the host from pathogens once they overcome the first line of defense above mentioned. These cells are generated in the hematopoietic tissue from progenitor cells in a process called hematopoiesis (the formation of blood cells) and are usually subdivided into innate immune cells and adaptative immune cells.

The innate immune cells represent the second line of defense. The cells that participate in the innate immune response are mainly monocyte/macrophages and neutrophils, that have the ability to phagocytize and eliminate pathogens. It is worth mentioned that, upon activation, macrophages can acquire pro or anti-inflammatory functions, classically defined as M1 or M2 macrophages, respectively. Other immune cells that are part of the innate immunity are natural killer cells (NKs), dendritic cells (DCs), eosinophils and basophils[116]. These cells can recognize conserved pathogen-associated molecular patterns (PAMPs) with specific membrane receptors called pattern recognizing receptors (PRRs)[112; 117].

The third line of defense is the adaptative immunity, which is constituted by T and B lymphocytes that recognize specific pathogen antigens. Some T lymphocytes are activated upon antigen presentation by other immune cells and initiate a clonal expansion to produce the lysis of targeted cells, whereas B lymphocytes produce immunoglobulins (antibodies) that bind to the extracellular pathogens to induce their elimination[118]. Additionally, some lymphocytes can acquire memory (T and B memory lymphocytes), improving the performance of the immune response in subsequent exposures to pathogens[119].

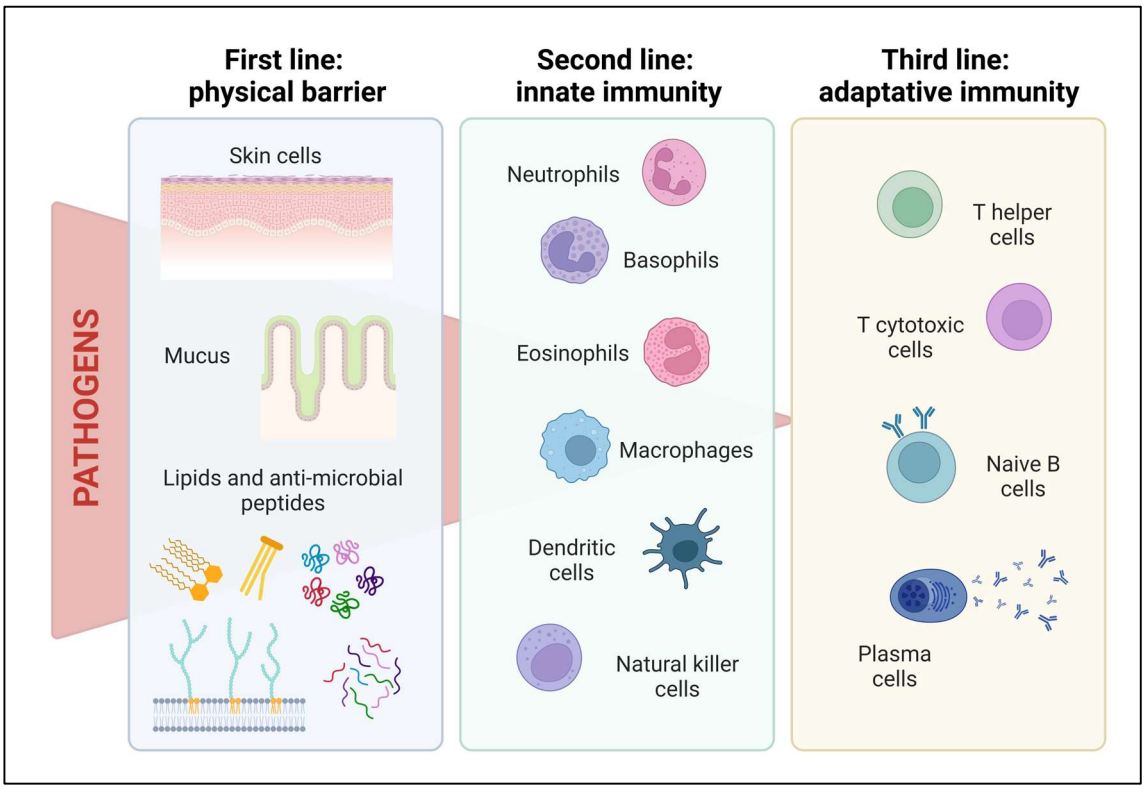

Figure 12. Lines of defense of the immune system. The immune system has several mechanisms to perform its function as a defense system. The first line of defense is a physical barrier while the second and third barriers are part of the cellular immunity. The second line is composed by cells of the innate inmunity and the third line of defense are cells from the adaptative immunity. Created with BioRender.com.

3.2. Regulation of metabolism in immune cell function

Nowadays there is clear evidence of the connection between the immune function and the cell metabolism[120-122]. The type and activity of immune cells not only determines their function in the organism but also their metabolic characteristics. The energy requirements for activated immune cells are not the same as for those cells that remain resting or those that are responsible of the trained immune response[121; 123]. The glycolysis, Tricarboxylic Citric Acid (TCA) cycle, phosphate pentose pathway (PPP) and fatty acid oxidation (FAO) are the main pathways involved in the metabolic changes that occur within the immune cells[120; 122].

One of the most studied metabolic adaptations is the switch between the use of the TCA and the glycolysis pathway as the main source of ATP for the cell (Warburg effect). Whereas the oxidative phosphorylation of glucose results in higher amounts of ATP per glucose molecule, aerobic glycolysis allows for a faster ATP production[121]. Besides, it serves as a source for the synthesis of intermediates that allow cell growth and proliferation and doesn't require an increase in the mitochondria biogenesis to support the production of energy. Another advantage in the use of glycolysis is that is not oxygen-depended. Therefore, cells can maintain their functionality in hypoxic conditions such as the tumor microenvironment[120].

Hence, aerobic glycolysis seems to be the pathway of preference in pro-inflammatory immune cells such as T_{H1} ($CD4^+$), T $CD8^+$ cytotoxic lymphocytes and M1 macrophages, while the TCA cycle

seems to be of greater importance in the metabolic requirements and immune function of Treg, Naïve T cells and M2 macrophages (anti-inflammatory)[122; 124; 125].

It may appear that for most immune cells the transitioning between the pro-inflammatory and the resting or anti-inflammatory state is clearly defined by this switch in the use of glucose. Nonetheless, new insights into the field of immunometabolism reveal the complexity of the regulation of the glucose metabolism in the immune response.

In the case of neutrophils, it is not possible to establish a key metabolic pathway controlling their immune functions. On the one hand, glycolysis has been shown to be relevant for its energy support and phagocytosis. On the other hand, their mitochondrial energy production has been proven to have an important role in their differentiation and also in their ability to follow chemoattractant signals[126; 127].

Besides, the connection between the glucose metabolism and the nuclear regulation of gene expression has already been extensively studied, establishing even more complex mechanisms of control of the immune cell function.

In M1 macrophages, the metabolic rewiring towards glycolysis not only results in changes in the cell energy production but also leads to changes in gene expression that regulate their activation state. One of these transcriptional changes takes place through a recently discovered histone modification: histone lactylation[128]. This epigenetic modification consists in the addition of lactate to some specific lysine residues in histones (Kla). Since M1 macrophages increase their glycolytic flux to support their proliferation, LDH activity increases, and so the production of lactate. Histone lactylation has been shown to be increased in M1 macrophages due to an increase in lactate production. Histone lactylation at specific promoters in M1 macrophages enhances the transcription of genes related with the M2 phenotype, acting as a modulator of the immune cell response at later time points of the polarization[128; 129].

Moreover, not only glycolysis, but also the Krebs cycle seems also to have a relevant role in the function of M1 macrophages. Since glycolysis serves as the main source of energy for these cells, the TCA cycle suffers a remodeling to increase the production intermediates such as of citrate, α-ketoglutarate or succinate instead of aiming at the production of ATP[130]. These metabolites now are no longer critical for the energy production of the cell but are key for the M1 phenotype as they also regulate the expression of cytokine genes through epigenetic modifications[130]. For instance, the production of α-ketoglutarate and succinate is increased in M1 macrophages since it increases the stability of the hypoxia-induced factor alpha (HIF-1α), which is crucial in regulating the cell function in hypoxic environments such as in cancer[130; 131]. Also, the TCA cycle has been shown to be important in M1 macrophages as they need it to produce antimicrobial metabolites such as itaconate[132]. Furthermore, plenty of TCA cycle metabolites are known to induce histone modifications that control gene expression, including the production of inflammatory cytokines and important signaling molecules such as reactive oxygen species (ROS) in activated macrophages[133].

3.3. Acute and chronic inflammation

Inflammation is a defensive response of the immune system to a given stimuli that causes disbalance in tissues or the organism homeostasis[134]. The classic inflammatory response is characterized by swelling, redness, pain, and warmness[112; 134]. All these phenomena are triggered by the immune system in order to increase the performance of the immune cells.

The inflammatory response can broadly be subdivided into acute and chronic inflammation, being the first normally more localized and transitory, while the second one is usually a systemic and maintained inflammation[135].

Although inflammation is a mechanism needed to reestablish tissue homeostasis, the timing and degree of the inflammatory response must be very well controlled to avoid damage in healthy tissues. That's why besides having activating mechanisms, immune cells also have deactivating strategies[136]. For instance, macrophages can acquire pro-inflammatory (M1 macrophages) or anti-inflammatory characteristics (M2 macrophages)[137]. Some molecules or cytokines such as the bacterial lipopolysaccharide (LPS) or interferon γ (INFγ) induce the M1 polarization. Other cytokines such as IL-4 induce the M2 polarization[138]. Also, T lymphocytes are subdivided into different subsets of cells depending on their function: $TCD8^+$ lymphocytes exert cytotoxic functions whereas $TCD4^+$ lymphocytes, also called T regulatory or helper cells, are able to suppress the function of other immune cells[112].

When the regulation mechanisms of inflammation are altered, it persists longer than necessary and turns itself into a process that causes additional damage instead of serving as a response to reduce it[136]. Systemic chronic inflammation is present in a wide range of diseases including cardiovascular disease, type 2 diabetes and obesity[135], and it has even been related to the aging process (inflammaging)[139]. However, there are also some chronic inflammatory diseases such as psoriasis, rheumatoid arthritis, or atopic dermatitis in which chronic inflammation affects a specific tissue or organ.

3.3.1. Psoriasis as a skin chronic inflammation disease

Psoriasis is a skin chronic inflammation disease with several clinical presentations[140; 141]. The most common form is psoriasis vulgaris which is characterized by the presence of well-defined red plaques with silvery scales in the skin[141; 142]. It can be triggered by genetic and environmental factors, and it involves an uncontrolled keratinocyte proliferation and the infiltration of immune cells in the skin due to an exacerbated immune response[141].

Whether the hyperproliferation of skin cells or the immune response initiates the skin chronic inflammation of psoriasis is still under debate[142]. Nevertheless, both keratinocytes and immune cells participate in the development of the disease.

Since keratinocytes are part of one of the main the physical barriers of the immune system (the skin), they are able to sense different kinds of PAMPs and other kinds of danger signals. Furthermore, they can react to them, synthetizing and releasing pro-inflammatory cytokines such as tumor necrosis factor alpha (TNFα), interleukin 1 beta (IL-1β) or interleukin 18 (IL-18). Some of these triggered-inflammatory pathways have been described to be upregulated in the psoriatic skin and amplified by keratinocytes[143; 144].

The other main players involved in the psoriatic chronic inflammation are a wide range of immune cells that produce pro-inflammatory cytokines and participate in the activation of other immune cells. Specifically, there is an increase in dendritic, T cells and neutrophils infiltrating the skin[145; 146].

In the psoriatic skin, dendritic cells produce interleukin 23 (IL-23) that induces the production of interleukin 17A (IL-17A) in several types of T cells. These wide range of T cells producing IL-17A are called T_{H17} lymphocytes[147]. In this inflammatory context, IL-17A stimulates keratinocytes to produce more IL-17A and other chemokines that attract neutrophils to the site of inflammation[146]. Moreover, neutrophils also become IL-17A producers, creating a complex feed-forward loop that amplifies the IL-17A pro-inflammatory signal[146; 148].

The IL-23/IL-17A axis seems to be one of the main signaling molecule pathways by which inflammation is initiated and maintained in chronic inflammation diseases[149]. Several monoclonal antibody therapies have been developed to target these cytokines and have successfully reduced the chronic inflammation in a range of diseases, including psoriasis[150; 151].

Other factors intervening in the pathology of inflammation in the psoriatic skin and that have been studied as targets for therapy are the levels of oxidative stress and the glucose metabolism.

Oxidative stress is defined by a disbalance between the levels of ROS produced by the cells and the molecules with antioxidant properties[152]. It is reported that the skin of psoriatic patients has higher levels of ROS. Moreover, those are known to be important for the pathogenesis of psoriasis[153; 154]. Some molecules that are classified as ROS are the superoxide anion ($O_2\bullet^-$), hydrogen peroxide (H_2O_2) and hydroxyl radical (HO^-)[155].

Neutrophils are known to produce large amounts of ROS as part of their antimicrobial function[146]. Due to the increase in neutrophil infiltration in the psoriatic skin, they may be one of the major sources of ROS in psoriasis, besides keratinocytes[155]. Moreover, the H_2O_2 gradient produced in the skin in both acute and chronic inflammation is known to induce neutrophil recruitment[156; 157], functioning as another feed-forward loop for inflammation and oxidative stress in the skin.

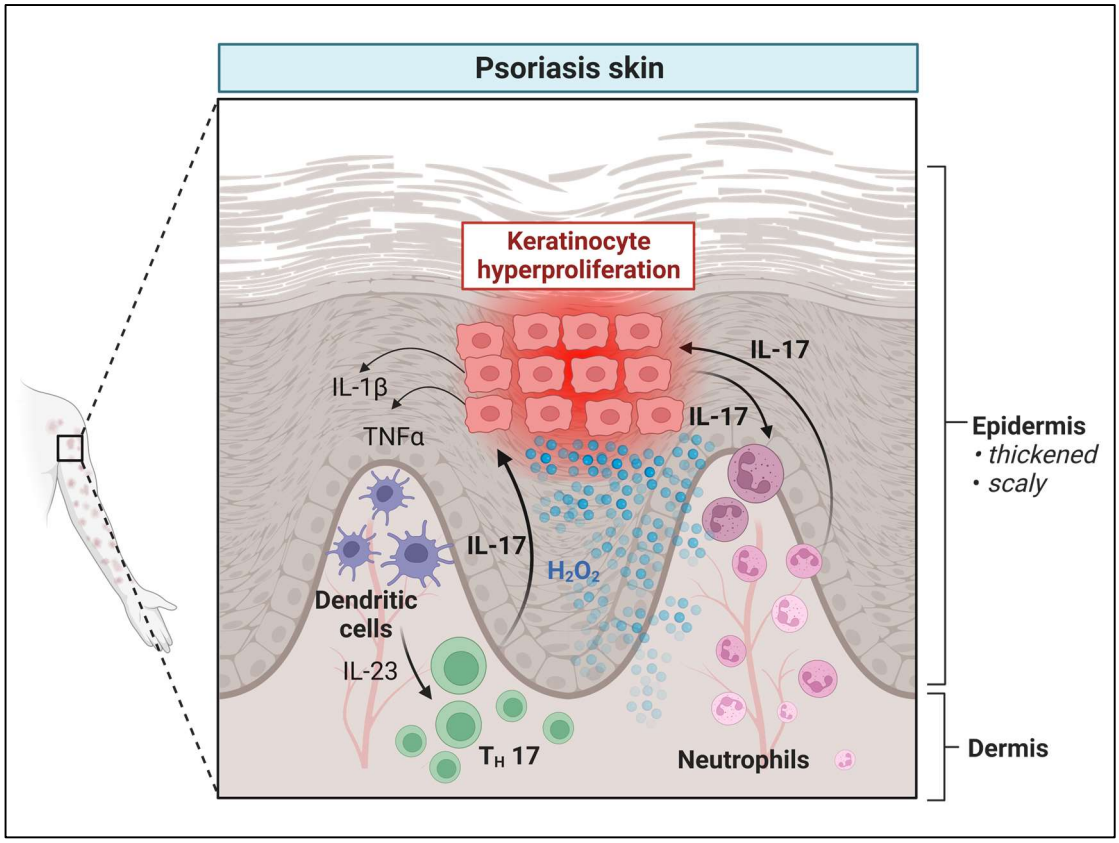

Figure 13. Schematic representation of the main molecular and cellular players of the psoriatic skin inflammation. Created with BioRender.com.

Recently, nicotinamide adenine dinucleotide (NAD^+) has been recognized as a key molecule in psoriasis controlling inflammation and oxidative stress in the skin. Specifically, the main enzyme controlling NAD^+ production, nicotinamide phosphoribosyltransferase (NAMPT) has been described to have a key role in psoriasis. An increase in NAD^+ levels results in increased H_2O_2 production, increased ROS production by NADPH oxidases, and an increase in general inflammation levels, while inhibition of NAMPT by FK-866 alleviates both oxidative stress and inflammation in both a psoriasis zebrafish model and in the human psoriatic skin[158]. Furthermore, NAD^+ levels and NAMPT expression are increased in the skin of psoriatic patients[158; 159] and are associated with keratinocyte proliferation[159].

As stated before, the chronic inflammation in psoriasis is explained by both an excessive inflammatory response and keratinocyte proliferation. As such, other studies have focused in describing mechanisms participating in the skin cell hyperproliferation of the psoriatic patients to find additional therapy strategies.

The glucose metabolism has been established to have a special role in the development of chronic inflammatory diseases, including psoriasis[160-162]. Usually, when cells need to support a high rate of cellular proliferation they increase their need for glucose, and they opt for a rapid, although not complete, oxidation of glucose trough the glycolysis pathway. Hence, both the uptake of glucose and the last product of the pathway, lactate, have been extensively studied in the context of cell hyperproliferation such as in the case of cancer cells and activated immune cells, as commented before[94; 163; 164].

The skin keratinocytes, which usually maintain a high rate of proliferation due to the physiological skin renovation, also rely extensively on glucose consumption to maintain their function[165]. In psoriasis, this dependence on glucose is more accentuated since the proliferation rate increases. In this sense, several studies have shown that the inhibition of GLUT1, one of the main the glucose transporter in keratinocytes, achieves an alleviation of inflammation in the psoriatic skin[165-167].

This metabolic adaptation in the hyperproliferating cells also leads to an accumulation of lactate in the inflamed tissue[168]. Lactate has been shown to participate in tumor progression, but it also has important roles in chronic inflammation controlling the immune response[169]. For instance, it has been reported that it is able to induce the production of IL-17A in T $CD4^+$ lymphocytes and retains them in the inflamed tissue, that way promoting the inflammation in rheumatoid arthritis[170; 171]. Also, LDHA, the enzyme in charge of lactate production, has been shown to promote inflammation by increasing ROS production in osteoarthritis mice models[172], linking the metabolite rewiring of the inflamed tissue with the increase in the levels of oxidative stress.

3.4. Immune response and inflammation in cancer

Another context in which the immune response plays a key role is in cancer. Due to the characteristics of the immune cell response that cancer cells trigger; inflammation has been considered as one of the hallmarks of cancer[173; 174].

The immune system is able to recognize the tumor cells due to the presence of antigens that make them different from normal cells, such as phosphatidylserine (normally in the inner cell membrane) or heat shock proteins (HSPs) that are usually overexpressed in cancer cells to adapt to the stress in the tumor microenvironment[175; 176].

Also, cancer cells usually have mutated or aberrant proteins due to the accumulation of mutations in their DNA[177]. Another way in which T cells sense the self and no-self is by identifying small peptides from inside the cell that are presented by the major histocompatibility complex (MHC). When cancer cells present a mutated peptide in their MHCs, they are recognized by T cells as malignant, and are eliminated. Hence, cancer cells often lose their antigenicity by avoiding the expression of MHCs, camouflaging themselves as part of their immune escape strategy.[178].

Interestingly, cancer cells produce chemokines to attract immune cells. By producing granulocyte and granulocyte-monocyte colony stimulating factors (G-CSF and GM-CSF), they induce a dysregulation in hematopoiesis and promote neutrophil and macrophage proliferation and mobilization to the tumor site[179]. However, these cytokines, rather than improving the immune response against the tumor, induce the arrival of immune cells with immunosuppressive characteristics (often immature neutrophils and macrophages). Besides, cancer cells produce another set of molecules to make sure that immune cells, once inside the tumor, reinforce the tumor progression[179; 180].

The M2 macrophage phenotype is associated with tissue remodeling, wound healing, and the inhibition of the inflammatory response since they also induce a T_{H2} lymphocyte phenotype[138]. M2 macrophages are producers of growth factors and angiogenic cytokines such as the epidermal growth factor (EGF) and the vascular endothelial growth factor (VEGF). These physiological roles that are needed after an injury, in the context of cancer, they are translated

into an inhibition of the anti-tumor response and the promotion of tumor growth and metastasis[181].

The production of IL-4 in the tumor microenvironment by cancer cells, induces M2 macrophage polarization and a T_{H2} regulatory response[182-184]. What is more, the lactate they produce due to their rapid proliferation, becomes another signaling molecule that induces the Treg and M2 polarizations. Several mechanisms have been described for lactate to produce this immune modulation. In the case of M2 polarization, it has been reported that lactate can activate signaling pathways important for the M2 phenotype such as the ERK-STAT3 signaling pathway, or the G-protein-coupled receptor 132 (GPR132)[169]. In lymphocytes, lactate inhibits the production of INFγ in $TCD8^+$ cells. However, lactate does not affect but increases the Treg function, which results in overall impaired anti-tumor T function[169; 185].

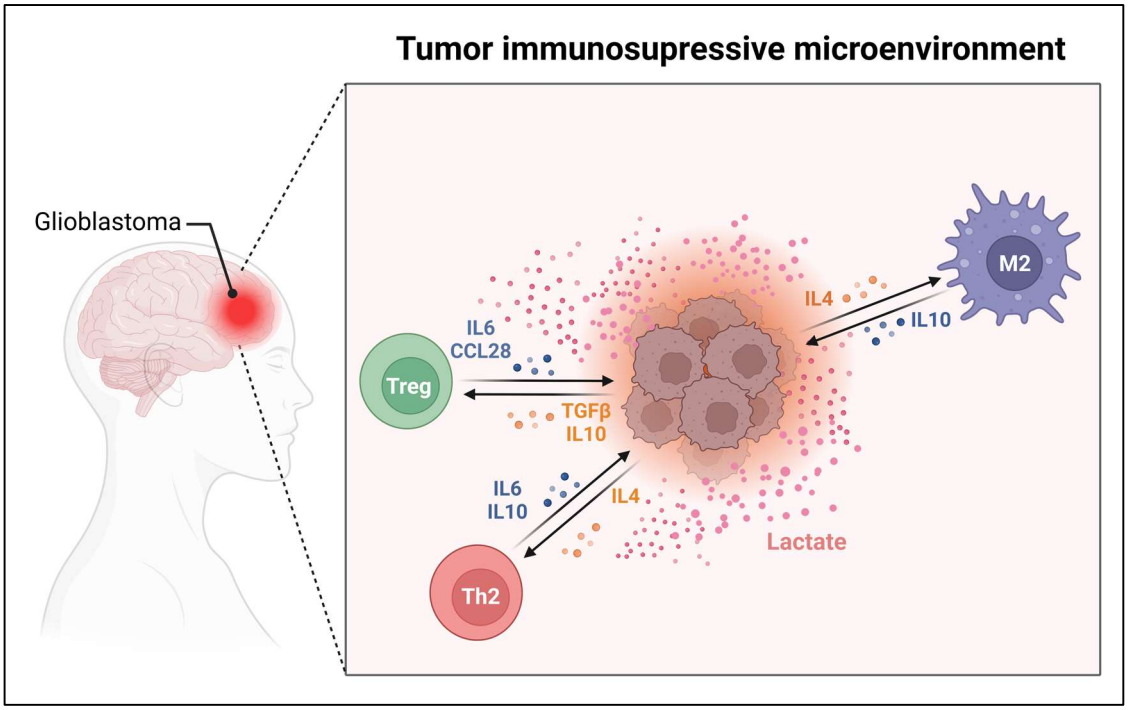

Figure 14. Schematic representation of the tumor immunosuppresive environment of glioblastoma. Tumor cells secrete cytokines to induce immune cell recruitment and polarization towards pro-tumor phenotypes such as Treg and Th2 lymphocytes, and M2 macrophages. Created with BioRender.com.

3.4.1. Cancer immunotherapy and glioblastoma

Due to the important role of immune cells in cancer progression, immunotherapy has emerged as a new approach to fight cancer, an several strategies have been developed to potentiate the anti-tumor immune response[177].

Glioblastoma multiforme (GBM) is the most common malignant brain tumor and one of the most aggressive brain cancers. Besides surgical resection and the application of chemotherapy and radiotherapy, the median survival of the patients is 15 months[186; 187]. The location of the tumor, the heterogeneity of mutations and deregulated signaling pathways in the tumor cells, and the immunosuppressive environment, make it hard to find successful conventional

therapies to fight this cancer[188; 189]. For that reason, a great effort has been made to develop effective immunotherapy treatments for glioblastoma tumors[190].

One of the major advances in immunotherapy is the development of Nivolumab, a monoclonal antibody that binds specifically to PD-1 receptor in T lymphocytes[191]. As commented before, cancer cells usually develop strategies to avoid the anti-tumor immune response. Hence, they often express PD-L1 and PD-L2, which are the ligands for PD-1[192]. The activation of PD-1 receptor by its ligands serves as checkpoint for T-cell deactivation, that way cancer cells can abrogate T cell function. The blockade of PD-1 with Nivolumab has been reported to be a very successful treatment for several types of solid tumors[193], although in glioblastoma tumors this strategy doesn't seem to be as efficient as in other types of cancer[194].

Another strategy to overcome the immunosuppressive environment of GBM has focused in reverting the M2 macrophage polarization induced by the tumor[181; 195]. Specifically in glioblastoma tumors, the M2 polarization not only affects the new recruited macrophages but also the ones already in the brain: the microglia.

Microglia are the tissue-resident macrophages in the central nervous system and, as well as other macrophages, they get activated when there is some kind of tissue damage and can be polarized to pro-inflammatory M1 or an anti-inflammatory M2 phenotype[195]. Microglia and macrophages are the most abundant cells infiltrating glioblastoma tumors[196]. Therefore, they are responsible for most of the immune response and inflammation in the tumor.

Some drugs and antibodies have been already developed to target key pathways involved in the M1 or M2 polarization. For instance, the inhibition of the colony stimulating factor 1 receptor (CSF1R), important for the M2 polarization, has been proven to have good effects in *in vitro* and in *in vivo* mice models. However, it seems that a positive effect in patients can only be achieved when used in combination with other therapies[195; 197]. Other proteins involved in the M1/M2-polarization signals are the Signal transducers and activators of transcription (STATs). One of the proteins in the family, STAT3, has been described to participate in the M2-polarization process, and the inhibition of the protein has been shown to activate macrophages and microglia, resulting in an inhibition of the glioblastoma growth in *in vitro* and *in vivo* models[181; 197].

In conclusion, although some immunotherapy strategies have reported promising results, in the present days there is no effective treatments for patients with glioblastoma tumors.

4. Zebrafish as a model for biomedical research

Animal models have been long and extensively used in research. In life sciences, the use of use of mammals such as mice is very frequent due to the genetic similarities with humans. Nevertheless, in the past years the use of zebrafish in biomedical research has been exponentially growing.

Zebrafish (Danio rerio) is a small tropical freshwater fish that belongs to the Cyprinidae family, Cypriniformes order[198]. Even though this fish can be viewed as distant relative of humans, zebrafish share 70% of genomic similarity with humans and, attending only to genes related to human diseases, 82% of them are conserved in the fish[199]. Additionally, as a vertebrate, the whole development of the organism is conserved, being established at first as a great model for developmental studies[198; 200].

Besides the genetic and developmental similarities, the increased use of zebrafish in research is explained by the several advantages that it has over other animals used such as mice.

One of the major advantages is their external fertilization and rapid embryo development (only 24 hours to complete organogenesis)[201]. This characteristic along with their high fecundity (≈100-200 eggs/female) an the small larvae size, make possible the use of a large number of individuals to perform the studies[202]. Also, zebrafish larvae can incorporate small molecules directly put into the water[203]. Taking into consideration all the above, zebrafish has become a great model for high throughput drug screening[204].

Moreover, the genome of zebrafish is fully sequenced[199]. This along with the external fecundation, makes very easy to genetically modify the zebrafish embryos. This can be done to model diseases or to perform functional studies. Moreover, there are several tools already developed to perform these genetic modifications. The knock-down of genes can be performed through microinjection of morpholinos[205], zinc-finger nucleases and transcription activator-like effector nucleases (TALENs). Also the use of CRISPR-Cas9 has been adapted for its use in zebrafish and has shown a very high efficacy to perform the genes knock-down[206]. On the other hand, gene overexpression can be accomplished by mRNA microinjection[202].

Besides transient gene regulations, stable transgenic and mutant lines can also be generated. The Gateway Tol2kit[207] and Gal4/UAS (upstream activating sequence)[208] transgenic tools are common systems used to generate transgenic lines in zebrafish.

The Gal4/UAS system is found in yeasts. The Gal4 protein a transcriptional activator that can bind to a small DNA sequence (UAS). The binding of Gal4 to those regions induces the recruitment of the transcription machinery, therefore initiating the transcription of the genes downstream the UAS sequence. The expression of Gal4 can be driven by different promoters, as well as different genes can be located downstream the UAS sequence. The use of the Tol2kit enables the introduction of the Gal4/UAS system in the zebrafish DNA by the Tol2 transposase, permitting endless combinations of specific tissue gene-modifications and facilitating the modelling of several diseases and the study of tissue-specific alterations[209].

Another great advantage of zebrafish is the larvae transparency. This characteristic enables *in vivo* labeling with fluorescent dyes, probes and/or proteins to perform developmental and carcinogenesis studies. This characteristic also allows to detect the presence of specific molecules in the context of a whole organism and in real time[210; 211].

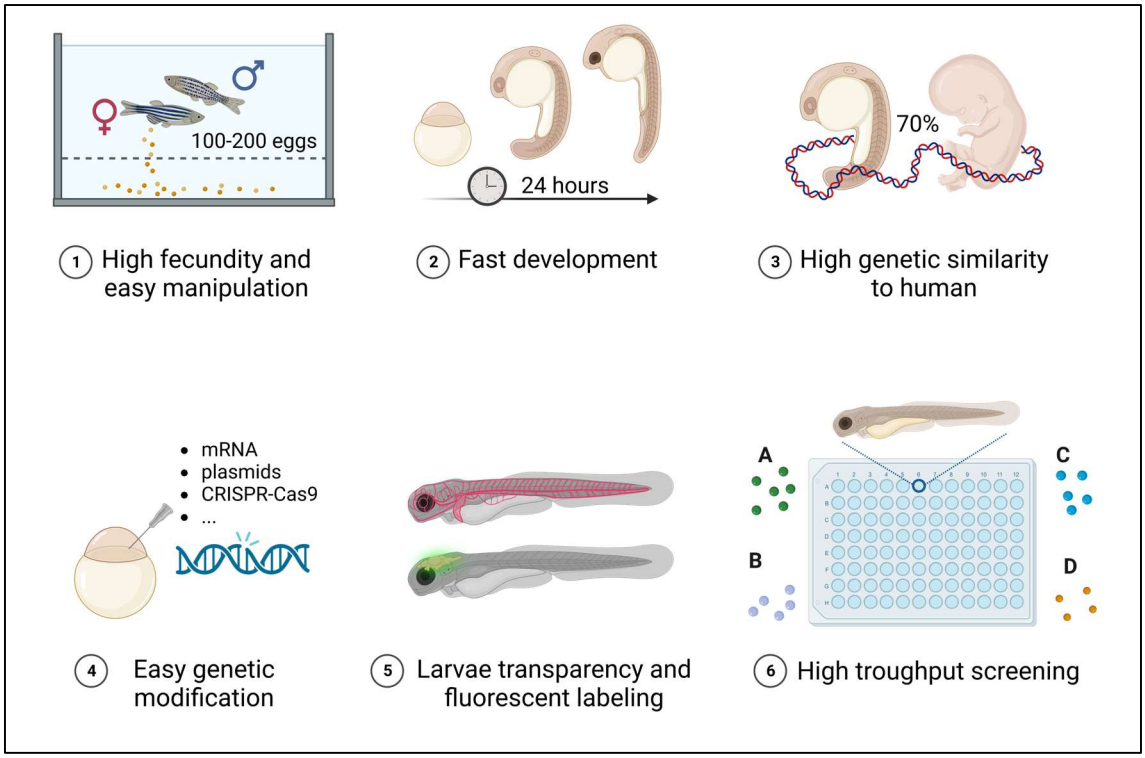

Figure 15. Zebrafish advantages over other vertebrate models in biomedical research. Created with BioRender.com.

4.1. Telomerase and zebrafish

Telomeres and telomerase are directly linked with the processes of aging, regeneration, and cancer. In the recent years, zebrafish has been used to study telomerase and the telomerase-related functions.

In regards to the telomerase complex components in zebrafish, the telomerase catalytic subunit (Tert) has conserved functional domains and residues with the human telomerase[212]. Also, the RNA component (*terc*) of telomerase zebrafish has a high conservation in structure and function with the human *TERC*[213; 214].

Contrary to humans, telomerase expression and activity has been detected in several tissues in zebrafish[215]. Nevertheless, their telomere length is similar to the one in humans (5-15 kb)[216]. This represents an advantage to the use of mice in the study aging and telomere disorders, since mice have telomere lengths ranging from 20-150 kb. Furthermore, the offspring of Tert-deficient mice need several generations of inbreeding to develop an aged phenotype[217].

Even though telomerase is expressed in several tissues in the fish, the telomere length in zebrafish has been described to be important for its lifespan. First, it's been demonstrated that telomeres get shorter with age in zebrafisfish[218]. And secondly, telomerase-deficient zebrafish show shorter telomeres and age faster[216; 219]. All these characteristics make zebrafish a great model to study aging and telomere disorders such as dyskeratosis congenita[21; 216].

In addition, zebrafish has also served as a great model to study non canonical roles of telomerase. A role of Tert independent of telomere length has been stablished to be important for the development of hematopoietic cells in zebrafish[220]. Furthermore, in Dr. Cayuela's lab,

deeper studies have shown a non-canonical function of telomerase RNA *terc* crucial for correct myelopoiesis[21]. And recently, new insights into this function have revealed the ability of *terc* to bind RNA polymerase II to regulate the transcription of master hematopoietic genes. These functions described in zebrafish have shown to be a conserved in humans, stablishing new targets for the treatments of neutropenias[47].

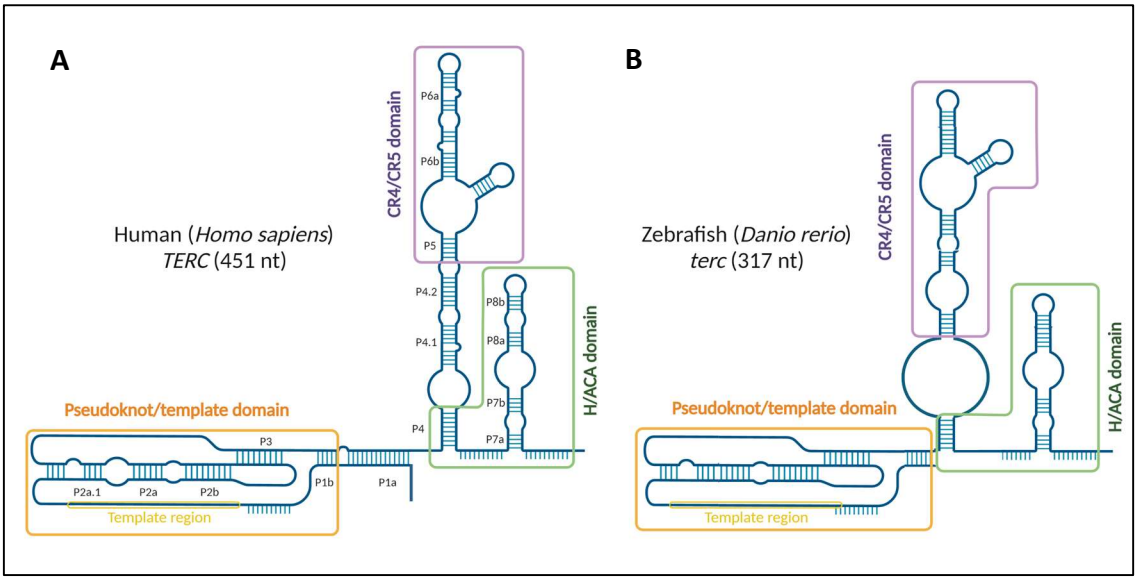

Figure 16. Structure similarities between human and zebrafish telomerase RNA. Both human (A) and zebrafish (B) telomerase RNAs have similar secondary structures. They both have a CR4/CR5 domain (purple), a psudoknot/template domain (orange) and a H/ACA domain (green). Created with BioRender.com.

4.2. Skin chronic inflammation zebrafish models

Zebrafish has shown to be a great model to study skin chronic inflammatory diseases such as psoriasis. Although some differences exist between the human and zebrafish skin, they also present some similarities. The overall structure of the skin in zebrafish follows the same distribution as in humans, with an external layer conforming the epidermis and an internal multilayered dermis[221]. Moreover, zebrafish has been established as a great model to study the immune response[222; 223] and, indeed, skin inflammation in zebrafish largely resembles the processes occurring in the human skin[221].

Several models of skin chronic inflammation have been already developed:

One of them is the *tnfatnfr2* morphant[157]. The knock-down of *tnfa* or its receptor *tnfr2* using morpholinos induced neutrophil mobilization to the skin, increased the production of pro-inflammatory cytokines such as *il1b*, and increased the production of H_2O_2 in keratinocytes. All in all, the *tnfatnfr2* morphant reproduces the skin inflammation phenotype seen in the psoriatic skin.

Another zebrafish model of skin chronic inflammation is a mutant in the serine peptidase inhibitor, Kunitz type 1a (Spint1a)[224]. The Spint1a protein is an inhibitor of matriptase 1a (St1a), which is expressed in the epidermis, among other epithelia. This mutation in *spint1a* produces the disruption of the skin integrity, a process that has also been reported to happen in the early

stages of psoriasis[225]. In the *spint1a* -/- model, keratinocytes loose contact with each other and acquire mesenchymal-like properties, resulting in the formation of aggregates due to their hyperproliferation. Moreover, it causes in an increase in keratinocyte cell death and consequent inflammation, as they have increased macrophage and neutrophil infiltration in the skin[224; 226].

Taking advantage of the zebrafish embryo transparency and *in vivo* cell visualization though the use of fluorescent transgenic lines, these psoriasis models have been combined with transgenic lines such as *lyz*:dsRED, in which neutrophils are labeled with red fluorescent. This enables the visualization and study of the skin chronic inflammation and the immune response live in a whole organism[157; 226].

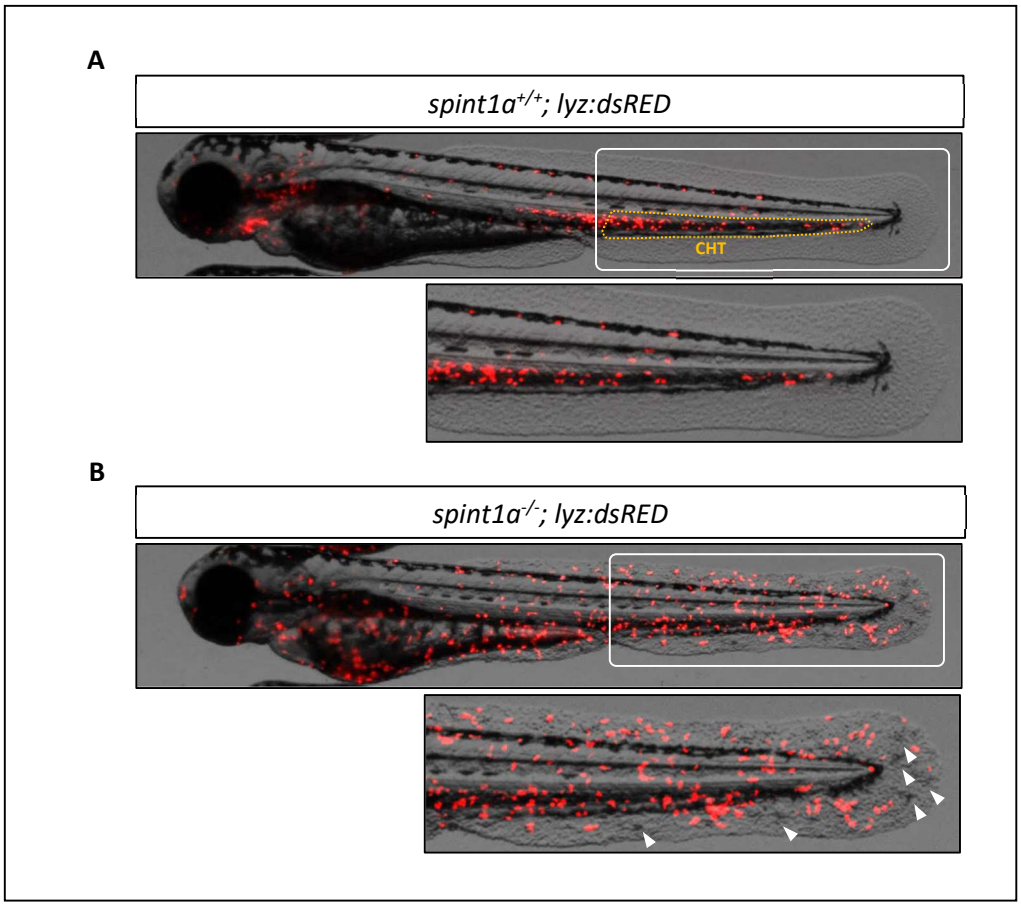

Figure 17. Images of wild type and mutant *spint1a* zebrafish larvae. Merged brightfield and red fluorescence channel images of wild type (A) and mutant (B) *spint1a* larvae. An image magnification of the tail is shown underneath each whole larva image (white rectangle area). Skin keratynocyte aggregates can be seen in the brighfield channel (white arroheads) whereas neutrophils are shown in red (*lyz:*dsRED). The mutant *spint1a* larvae have neutrophil inflitration in the skin due to inflammation, whereas neutrophils in the wild type larvae are mostly in the caudal hematopoietic tissue (CHT; yellow dotted line).

4.3. Cancer zebrafish models

Zebrafish serves also as a great animal model to study cancer. First of all, the cancer biology of zebrafish and humans is very alike. Zebrafish can develop cancer when exposed to mutagens, and their tumors are histologically similar to the ones in humans[227]. Moreover, zebrafish and humans share cell-cycle, tumor suppressor, and oncogenes that participate in cancer development in both organisms[228; 229].

Zebrafish can be used as a tool for cancer studies in many ways. One of the first approaches was large-scale forward genetic screens. In these kinds of studies, mutations were introduced in the DNA of adult zebrafish using chemicals, irradiation or by insertional mutagenesis (introducing viral or transposons vectors). After that, a correlation between the cancer phenotype and the introduced mutations was done to identify novel genes or pathways involved in tumor progression[228; 230].

Also, since human cancers share oncogene signaling pathways with zebrafish, the human tumors can be modelled in the fish. This has been used to identify driver mutations from passenger mutations in human cancers such as in melanoma[231]. Moreover, this also means that zebrafish is useful to identify potential drugs for the treatment of several cancers[229].

The transparency of zebrafish larvae has enabled the study of cell engraftment, invasiveness, and metastasis *in vivo*. Using xenograft cell transplantations, human cancer cells labeled with fluorescent markers can be introduced into the larvae without rejection[232]. Cells can be microinjected in the larvae yolk sac (heterotopic transplant) or orthotopically, in the same tissue the tumor develops normally. The fluorescent labeling allows the study of the tumor cells interactions with immune cells, cancer cell invasiveness, and proliferation[233]. Moreover, this can be done with tumor cells from patients. This approach in combination with the drug-screening potential of the zebrafish, makes possible the development of patient avatars in which to test hundreds of drugs to select a personalized treatment for each patient[234].

Without any doubt, the use of transgenic zebrafish lines has maximized the potential of zebrafish as a model to study cancer. The easy genetic manipulation of zebrafish has permitted the obtention of zebrafish with different fluorescent tissues such as vessels[235] or immune cells[236], but also with fluorescent tumors, meaning that cancer development and progression can be assessed *in vivo*[237]. In order to achieve that, the UAS/Gal4 system has been widely used.

The UAS/Gal4 system is used to drive the expression of oncogenes fused with fluorescent proteins in specific tissues, generating zebrafish models for different types of cancer. One of the most common cancer drivers is Ras protein, therefore, one of the main constructs used to generate cancer in zebrafish is an eGFP-HRAS^{G12V} fusion protein. In order to control the expression of the oncogene, an UAS sequence is placed upstream the fusion protein, and this construction can be inserted in the zebrafish to generate a stable transgenic line (*Tg*(UAS:eGFP-*HRAS*^{G12V}))[238]. This construction can also be microinjected in the fish along with the Tol2 transposase, generating a mosaic expression of the fluorescent oncogene[239]. However, it must be taking into consideration that a tissue-specific oncogene expression is only generated when the *Tg*(UAS:eGFP-*HRAS*^{G12V}) line is inbred with a tissue-specific Gal4-expressing transgenic line or when the UAS:eGFP-*HRAS*^{G12V} construction is microinjected in Gal4-expressing embryos. One example of this is the generation of the glioblastoma zebrafish model[240].

Specifically, the transgenic line *Et(zic4:*GAL4TA4,UAS:mCherry)$_{hmz5}$[241] was used to obtain the expression of *HRAS* in the zebrafish brain. In this zebrafish line, the *zic4* enhancer, which is

exclusive to the central nervous system (CNS), drives the expression of an optimized version of Gal4. In addition, the fluorescent protein mCherry labels the CNS, hence, the places of Gal4 expression. The glioblastoma model was then obtained through the somatic expression of GFP-*HRAS*^{G12V} by the inbreed of *zic4:*GAL4TA4,UAS:mCherry and UAS:GFP-*HRAS*^{G12V} zebrafish lines. Also, this glioblastoma can be generated in the germline by microinjecting a plasmid containing UAS:GFP-*HRAS*^{G12V} sequence.

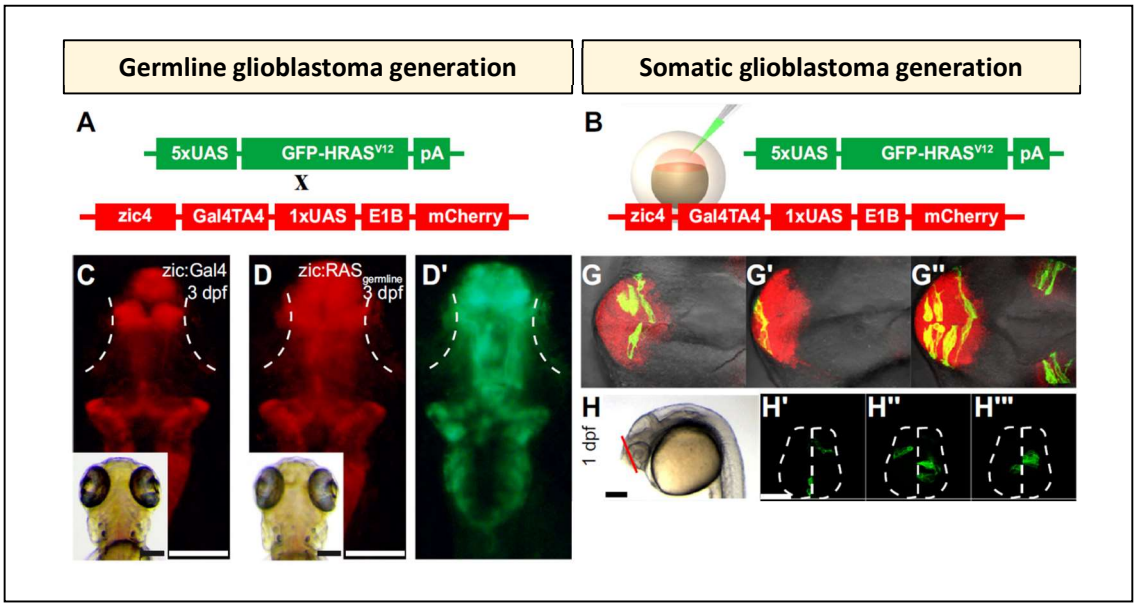

Figure 18. Germline (A) and somatic (B) generation of the glioblastoma zebrafish model. Adapted from (Mayrhofer et al., 2017)[239].

Objectives

The specific objectives of the present work are the following:

1. Study the relationship between *terc* and the regulation of glucose metabolism in the context of chronic inflammation and the cancer immune response.

2. Validate and characterize the interaction between the pyruvate dehydrogenase complex and the telomerase components *TERC* and TERT.

Chapter I

Regulation of glucose metabolism by *terc*:

PART 1. *terc* alleviates inflammation through the regulation of lactate metabolism

PART 2. *terc* inhibits glioblastoma growth by activating antitumor innate immunity

1. Introduction

Telomerase is a ribonucleoprotein complex whose main function is the synthesis of the telomeric DNA. The main components of this complex are TERT (the catalytic subunit) and *TERC* (the RNA component). Besides telomere lengthening, TERT and *TERC* perform extracurricular functions[19-21]. Particularly, in the case of the telomerase RNA, a Chromatin Isolation by RNA purification (ChIRP) study identified more than two thousand loci in the human genome which contained a *TERC* specific binding sequence (*TERC*-bs)[6], suggesting a role of *TERC* as a long non-coding RNA (lncRNA).

In that sense, *TERC* is accountable for several physiological processes related to the hematopoietic stem cell (HSC) differentiation and the immune function. For instance, *TERC* increases the anti-apoptotic signals in $CD4^+$ T lymphocytes, independently of TERT[44]. Another described extracurricular role for *TERC* is related to the production of myeloid cells and was depicted in our laboratory, where we described an evolutionary conserved mechanism by which *TERC* is needed for the production of neutrophils and macrophages[21]. *TERC* was demonstrated to function as a transcription factor, binding to its specific consensus sequence at the promoter regions of the master myelopoietic genes Colony Stimulating Factor 2 and 3 (*CSF2* and *CSF3*) and SPI1, and therefore allowing the recruitment of RNA polymerase II (RNApol II) and the correct formation of myeloid cells[47].

In hyperproliferating cells, such as in cancer and activated immune cells, a metabolic rewiring takes place to support the energy requirements of the increased cell proliferation. One of the most common metabolic adaptations is the use of the glycolysis pathway as the main source of ATP instead of performing a complete oxidative phosphorylation (Warburg effect)[94; 164]. Due to the importance of this metabolic adaptation, the regulation of the glucose metabolism of hyperproliferating cells can be targeted in order to control their function. Lactate dehydrogenase (LDH), which is responsible for lactate production, is one of the main players involved in this adaptation, thus, the roles of LDH and lactate have been studied in a wide range of diseases that involve cell proliferation[92].

Psoriasis is one of the most prevalent chronic inflammatory diseases[141], and it is characterized by a keratinocyte hyperproliferation and an increase in the immune cell infiltration in the skin, both resulting in a persistent chronic inflammation[150]. Although the IL-23/IL-17A axis is one of the main signaling molecule pathways involved in inflammation in psoriasis[149], also the levels of oxidative stress are known to have an important role in the pathogenesis of the disease[153; 154], and recently, nicotinamide adenine dinucleotide (NAD^+) has been identified as a key molecule controlling inflammation and oxidative stress in the psoriatic skin[158; 159].

The hyperproliferating keratinocytes of the psoriatic skin also have that constant rely on glycolysis to support their growth and proliferation. Moreover, the inhibition of GLUT1, one of the main the glucose transporter in keratinocytes, produces an alleviation of inflammation in the skin[165-167]. The increase in glucose consumption by keratocytes also leads to an accumulation of lactate in the inflamed tissue[168], which has been shown to have important roles in chronic inflammation controlling the immune response[169]. For instance, it has been reported to induce the production of IL-17A in T $CD4^+$ lymphocytes and to participate in the retention of the immune cells in the inflamed tissue, ultimately fostering inflammation in mice with rheumatoid arthritis[170; 171]. Also, LDH has been shown to promote inflammation by increasing ROS production in osteoarthritis mice models[172].

Even though the regulation of the glucose metabolism, and specially, the regulation of lactate production has shown to have an important immunomodulatory role in chronic inflammation diseases such as rheumatoid arthritis, its role in psoriasis has not been explored yet.

On the other hand, the regulation of the glucose metabolism in immune cells has been widely studied in the tumor immune response[161; 176]. In the tumor microenvironment, cancer cells secrete cytokines and other molecules that enable the tumor immune escape by inhibiting the immune cell function. Moreover, in this environment, immune cells become active players in the promotion of tumor growth[182].

Glioblastoma is very aggressive type of brain cancer, with an average survival time of 15 months for the patients[19]. Conventional therapy strategies have shown to not be enough to stop the cancer progression, being the highly immunosuppressive tumor microenvironment one of the characteristics that challenge the glioblastoma treatment[20]. For that reason, recent studies in glioblastoma therapy have focused on the development of new strategies to improve the immune response against the tumor (immunotherapy)[21]. With this purpose, the study of immunometabolism has raised interest in the context of glioblastoma tumors[22].

Many lncRNAs have been proven to be clearly implicated in the metabolic regulation of tumor cells, such as the *lncRNA-UCA1*, which increases the glucose metabolism by promoting the expression of the main enzyme in control of the glycolysis pathway: hexokinase 2 (HK2)[242]. However, only a few lncRNAs have been identified as to participate in this metabolic regulation in other types of cells with a similar metabolic adaptation, such as immune cells. One example is *Malat1*[243], which regulates the expression of mitochondrial pyruvate carriers (MPCs) in M2 macrophages, promoting the mitochondrial oxidation of glucose.

In this work, we study the relationship between the expression of the telomerase RNA (*terc*) and the glucose metabolism using zebrafish as an *in vivo* model. We show how *terc* expression is able to change the concentration of glycolysis and TCA cycle metabolites and we demonstrate that *terc* is able to change the expression of glycolysis-related genes such as *ldhbb*. Moreover, we explore the role of this metabolic *terc*-regulation in the context of skin chronic inflammation and the glioblastoma immune response.

2. Materials and Methods

2.1. Zebrafish lines and maintenance

All zebrafish (*Danio rerio* H., Cypriniformes, Cyprinidae) were raised and handled using standard procedures[244; 245]. All experiments comply with the Guidelines of the European Union Council (Directive 2010/63/EU) and the Spanish RD 53/2013. Experiments and procedures were performed as approved by the Bioethical Committee of the University Hospital Virgen de la Arrixaca (approval number A13211202).

The wild type zebrafish AB strain was obtained from the Zebrafish International Resource Center (ZIRC).

The transgenic zebrafish line *Tg(lyz:*dsRED) was kindly provided by Prof. Phil Crosier. In this transgenic fish, the promoter of the lysozyme C gene drives the expression of the red fluorescent protein dsRED2[246]. Thus, this transgenic line neutrophils are specifically labeled with red fluorescence.

The zebrafish line mutant for *spint1a* (*hi2217* mutant allele) was obtained in an insertional mutagenesis screen[247], and was kindly provided by Prof. Matthias Hammerschmidt.

The transgenic zebrafish line *Tg(zic4*:Gal4TA4, UAS:mCherry)$_{hzm5}$, (also called *zic:*Gal4; UAS:mCherry or *zic* in this work for simplicity) was kindly provided by Prof. Maria Caterina Mione from the Laboratory of Experimental Cancer Biology (CBIO, University of Trento). In this transgenic fish, the *zic4* promoter drives the expression of the red fluorescent protein mCherry in the central nervous system[240]. This tissue-specific regulation labels with red fluorescence the brain and the notochord in the transgenic fish.

The transgenic line *Tg(mpx*:eGFP) was kindly provided by Prof. Stephen A. Renshaw from the University of Sheffield. In this fish the neutrophil-specific myeloperoxidase promoter (*mpx*) controls the expression of the enhanced green fluorescent protein (eGFP), therefore the fish present neutrophils labeled in green[248].

The mutant zebrafish line for *tert* (allele hu3430), named *tert*$^{-/-}$ in this work, was obtained from the Sanger Institute and has been previously characterized[218].

The mutant line for *terc* (*terc*$^{-/-}$) was obtained in our laboratory, using the Transcription Activator-Like Effector Nuclease (TALEN) technology[47].

The transgenic lines *Tg(drl:terc)* and *Tg(drl:tert)* have a green heart reporter and were also generated in our laboratory using the *Gateway Tol2kit* system ([47], unpublished). In these fish, *terc* or Tert overexpression is driven by the *draculin* (*drl*) promoter, which is specific of cells of hematopoietic and angiogenic origin (hemangiogenic cells)[249].

Lastly, the transgenic line *Tg*(*mpeg1:*mCherryF*/tnfa:*eGFP-F), named *mpeg1*:mCherry;*tnfa*:eGFP in this work, was generously provided by Prof. Georges Lutfalla from the University of Montpellier[250]. In this case, the macrophage-specific *mpeg1* promoter drives the expression of mCherry while the Tumor Necrosis Factor *tnfa* promoter drives the expression of eGFP. The fish that have both genetic constructions have their macrophages labeled with red fluorescence and if macrophages polarize towards an M1 phenotype, they express Tnfα and, consequently, the eGFP protein.

2.2. Metabolite analysis

Targeted mass spectrometry and metabolite analysis were performed as previously described[251]. In short, samples were resuspended in 20µL HPLC grade water for mass spectrometry and 5µL were injected and analyzed using a hybrid 5500 QTRAP triple quadrupole mass spectrometer (AB/SCIEX) coupled to a Prominence UFLC HPLC system (Shimadzu) via selected reaction monitoring (SRM)[252]. Peak areas from the total ion current for each metabolite SRM transition were integrated using MultiQuant v2.0 software (AB/SCIEX).

2.3. Zebrafish morpholino and RNA microinjection

The specific morpholino targeting *terc* (Mo*terc*) and the control morpholino (Mostd) were obtained from Gene Tools and resuspended in nuclease-free water to 1 mM concentration (Table 1).

The RNAs of *terc* sense and antisense (S and AS) were obtained using pBlueScript zfTR KS+ plasmid generated in our laboratory. To produce the mRNAs, double stranded DNA sequence of the zebrafish *rps6ka1* and *socs2* genes was synthetized (IDT) and cloned into a pCS2P+ plasmid (Addgene) using NotI and EcoRI restriction enzymes (Invitrogen).

The plasmids were linearized with specific restriction enzymes and the mMESSAGE mMACHINE kit (Ambion) was used to produce the *in-vitro* transcribed RNAs following manufacturer's instructions. In the case of mRNAs, they were also polyadenylated using the Poly(A) Tailing kit (Invitrogen) following the manufacturer´s protocol.

MOs and RNAs were mixed in microinjection buffer (0.5x Tango buffer and 0.05% phenol red solution) and microinjected into the yolk sac or cell of one-cell-stage embryos using a Narishige IM3000 microinjector. The *terc* S and AS RNAs and the mRNAs of *rps6ka1* and *socs2* mRNAs were microinjected into the cell of one-cell stage zebrafish embryos at a concentration of 200 pg/egg. The working morpholino concentration is detailed in the table below (Table 1).

Name	Sequence (5´→3´)	Working dosis (ng/egg)
Mostd	CCTCTTACCTCAGTTACAATTTATA	1
Mo*terc*	TCAAGTTAATCTGCTCAGTGTTGTG	1

Table 1. Morpholino sequences and used concentration.

2.4. Zebrafish CRISPR-Cas9 microinjection

The genetic inhibition experiments were carried out using the CRISPR-Cas9 system and following the manufacturer´s indications. The predesigned guide RNAs (crRNAs) targeting the desired genes, the tracRNA (ref. 1072533) and the Cas9-V3 protein (ref. 1081058) were obtained from IDT. 1 µL of both crRNA (100 µM) and tracRNA (100 µM) were incubated at 95°C for 5 min and cooled at room temperature for 5-10 min to allow crRNA guide/tracRNA complex formation. 1.43 µL of IDT duplex buffer was added for a final complex concentration of 50 µM. The microinjection mixture was prepared with 1µL of crRNA guide/tracRNA complex, 0.2 µL of Cas9, 0.25 µL of phenol red and 2.55 µL of IDT duplex buffer. The mixture was kept in ice and injected into the yolk sac of one cell-stage zebrafish embryos using a NARISHIGE 300 IM microinjector (0.5-0.9 nl/egg). The name and sequence of the microinjected guide RNAs are listed below (Table 2).

crRNA Name	Species	Sequence (5´→3´)
Dr.Cas9.LDHA.1.AC	Zebrafish	GGTGGACGTGATGGAAGATA
Dr.Cas9.LDHBA.1.AC	Zebrafish	CTAACTCTCGTATTGTGGTG
Dr.Cas9.CXCL14.1.AC	Zebrafish	CATTTATTCGCTCAACACAG
Dr.Cas9.SOCS2.1.AC	Zebrafish	CTGCCATGAGAGACCTTAAA
Dr.Cas9.CTNNB1.1.AA	Zebrafish	CGTCCCTGAGTGGCAAAGGC
Dr.Cas9.PFAS.1.AD	Zebrafish	CAGCTGTGCAATCCTTCTTA
Dr.Cas9.RPS6KA1.1.AD	Zebrafish	ACACAGAGTACGCAGTGAAG

Table 2. List of crRNAs used in the zebrafish larvae.

The genomic DNA of the 3 dpf larvae microinjected with the control or the specific crRNAs was extracted with the Wizard® Genomic DNA Purification Kit (Promega) and the target region was amplified by PCR. The PCR product was sequenced, and the edition of the target locus was analyzed with the TIDE software (https://tide.nki.nl). The primers used for PCR and sequencing is listed in the table below (Table 3).

Name	Species	Sequence (5´→3´)	Application
F9-zf-rps6ka1-TIDE	Zebrafish	AGCAGCTTCACGGTAAGAACA	PCR/ Sequencing
R9-zf-rps6ka1-TIDE	Zebrafish	TTCAGTTGGATCCGTGCTTGT	PCR/ Sequencing
F-zf-pfas-TIDE	Zebrafish	CAGGATCATGCCTGTCGTGC	PCR/ Sequencing
R-zf-pfas-TIDE	Zebrafish	AAACATTTTAGGCTCCCCTGACA	PCR/ Sequencing
F9-zf-cxcl14-TIDE	Zebrafish	CGCCTGTCTATTCAGCCTCG	PCR/ Sequencing
R9-zf-cxcl14-TIDE	Zebrafish	ACAGTTGGACAAGCGTGAGG	PCR/ Sequencing
F7-zf-socs2-TIDE	Zebrafish	GTCACTCATCCGACTCCACG	PCR
R7-zf-socs2-TIDE	Zebrafish	TTGTGGGGGCGAACATTGTA	PCR
Rv6-zf-seq-TIDE-socs2	Zebrafish	CCAAATTGGTTCAAATGGCCCCT	Sequencing
zf_Ldha_I2/3_F	Zebrafish	GAGACCATTCCATTGGGGATCT	PCR
zf_Ldha_I3/4_R	Zebrafish	ACAGTGGAGCACATAGCTCAG	PCR
F-zf-gLDHA-nested	Zebrafish	GATCTGACCGATGAACTCGCC	PCR
R-zf-gLDHA-nested	Zebrafish	TCTTGTGCGTCTTGAGAAACAG	PCR/ Sequencing
Fw-zf-ldhbaE2/I3	Zebrafish	GCGTACTGCTTCGGGTAAGA	PCR
Rv-zf-ldhbaE6	Zebrafish	TTTGCACCACTCCATACGGG	PCR/ Sequencing

Table 3. List of primers used for PCR and/or sequencing of the target region for each crRNA.

2.5. Zebrafish glioblastoma generation

The glioblastoma was generated in the zebrafish as previously described[240]. Briefly, GFP-*HRAS_V12* oncogene was overexpressed in the zebrafish brain by the microinjection of the pT2MUASMCS-UAS:eGFP-*HRAS*_V12 plasmid (250 ng/µL) along with the mRNA of Tol2 transposase (250 ng/µl) into one-cell stage Tg(*zic4*:Gal4TA4, UAS:mCherry)$_{hzm5}$ embryos. Images of seven days post fertilization larvae (7 dpf) were acquired to measure the tumor size.

2.6. Gene expression analysis by RT-qPCR

Total RNA from zebrafish larvae or kidney marrow was extracted with TRizol (Thermo Fisher Scientific) using Direct-zol RNA Miniprep kit (Zymo Research). In the case of tail fins, the RNA extraction was performed using the RNAqueous-Micro Total RNA Isolation Kit. cDNA synthesis was performed using SuperScript IV VILO Master Mix (Invitrogen) following manufacturer's instructions. The quantitative PCR (qPCR) was performed in a StepOne Plus Real-time PCR System instrument (Applied Biosystems) using SYBR Premix Ex Taq (Perfect Real Time) (Takara). The following conditions were used for the amplification: 10 min at 95°C, followed by 40 cycles of 15s at 95°C, 1 min at 60°C, and finally a standard melting curve protocol 15s at 95°C, 1 min at 60°C and 15s at 95°C. The expression of each analyzed gene was normalized to the expression of the ribosomal protein S11 (*rps11*) gene in each sample using the comparative Ct method ($2^{-\Delta\Delta Ct}$). Each PCR was performed with triplicate samples and with at least two independent samples. The primers used are listed in the table below (Table 4).

Name	Species	Sequence (5´→3´)
zf terc-F1q	Zebrafish	GGTCTCACAGGTTTGGCTGT
zf terc-R2q	Zebrafish	TGCAGGATCAGTGTTTGAGG
zf tert-F2q	Zebrafish	CGGTATGACGGCCTATCACT
zf tert-R1q	Zebrafish	TAAACGGCCTCCACAGAGTT
FZF1_ldha	Zebrafish	CCCAAACATCATCAA GTACA
RZF1_ldha	Zebrafish	GATTTGAAACCACCAAAAGG
FZF1_ldhba	Zebrafish	CCTTGTGTCTGTGTTTAAGT
RZF1_ldhba	Zebrafish	TACAGCA GATTCAGAGGATG
FZF1_ldhbb	Zebrafish	GTGGTATCTTTACCTGGGAG
RZF1_ldhbb	Zebrafish	ACGCCATCTCTAATACTTGT
FZF1_ldhd	Zebrafish	ACTCCG ATTATACGGTGTTC
RZF1_ldhd	Zebrafish	GACGGATGGAAA AGAACAAA
FZF1_cxcl14	Zebrafish	GTGGTTCAAAATCTGGAAGG
RZF1_cxcl14	Zebrafish	ACATTTAGGCTTCAAACGTC
FZF2_ctnnb1	Zebrafish	CATTCTAGCCAGAGACATTC
RZF2_ctnnb1	Zebrafish	TAGGAGAATACAGCAACTGA
FZF1_socs2	Zebrafish	AAAACACTGGCTGGTATTG
RZF1_socs2	Zebrafish	AGATGGTGAAGAGGTAGTC
FZF1_idh1	Zebrafish	ATATGATGGGCGTTTCAAAG
RZF1_idh1	Zebrafish	ATACTTGGCCTTGTSCTCTT
FZF1_tbxas1	Zebrafish	TCTCAAGCTGACCTCATAAA
RZF1_tbxas1	Zebrafish	CCGGCCTATATAATAACCACA
FZF1_rps6ka1	Zebrafish	CACTATGATTGCTGGGTTTA
RZF1_rps6ka1	Zebrafish	GAGTGTCTTCTGGTCCATTA
FZF2_abl2	Zebrafish	ACATCCCAATCTAGTACAGT
RZF2_abl2	Zebrafish	TACTCGGTCACAATGTAGAA
FZF1_odc1	Zebrafish	TTGCTTGAGAGAAGTACACA
RZF1_odc1	Zebrafish	GCAAAAGAAACAGACGAATG
Fq-rps11	Zebrafish	ACAGAAATGCCCCTTCACTG
Rq-rps11	Zebrafish	GCCTCTTCTCAAAACGGTTC

Table 4. List of primers used for gene expression analysis by RT-qPCR.

2.7. *In vivo* luciferase assay

The luciferase plasmid containing the promoter region of *ldhbb* was obtained as follows: the genomic DNA of wild type larvae was extracted with the Wizard Genomic DNA Purification Kit (Promega) and used as template in a PCR amplification of the promoter region (1970pb upstream the transcription start site) of the *ldhbb* gene, using the Phusion High-Fidelity DNA polymerase from New England Biolabs (NEB) and the following primers F1-AAGGGGTACCGCACCAGGCGAAAGTATAAATGT and R1-AAGGGAGCTCGTGAGGGGATTACAATTAACCGA.

The PCR product was purified with the QIAquick PCR Purification kit (QIAGEN) and cloned into the luciferase reporter PGL3basic vector (Promega). Both the plasmid and insert were digested with Kpn I y Sac I restriction enzymes (Invitrogen) overnight at 37°C. The plasmid was also treated with Shrimp Alkaline Phosphatase (Promega) for one hour at 37°C. Both plasmid and insert were again purified with QIAquickPCR Purification kit (QUIAGEN) and the ligation step was done with T4 ligase (NEB) in a 1:3 proportion accordingly to the manufacturer's instructions.

The generated plasmid was transformed into One ShotTOP10 chemically competent *Escherichia coli* (ThermoFisher) by heat shock, accordingly with the manufacturer protocol. The plasmid was obtained from the bacteria by extraction with the GenElute™ HP Plasmid Midiprep kit (Sigma).

To perform *in vivo* luciferase assay, the Dual-Luciferase® Reporter Assay System kit (Promega) was employed. In brief, 250 ng of the luciferase construction (PGL3-p*ldhbb* plasmid) along with the Mo*terc* or *terc* RNA were microinjected into the yolk sac or the cell of one-cell stage wild type zebrafish embryos. The 2 dpf larvae were pooled into groups of 10 and lysed by mechanical homogenization in the provided lysis buffer at room temperature. The luciferase substrate was added prior to the luciferase measurement in each sample in an Optocom I luminometer (MGM Instruments).

2.8. Pharmacological treatments

The chorion of zebrafish embryos was manually removed at 24 hours post fertilization (hpf) and 20-25 embryos were sampled in wells of 6-well plates. The compounds were added at the indicated concentration into the egg water and 1% DMSO was used as a control. Larvae were treated for 48 hours more, and the egg water and treatments were changed after 24 hours. The larvae were maintained during the time of the treatment in a 28°C incubator and protected from light. The used compounds and concentrations are listed in the following table (Table 5).

Compound	Manufacturer	Concentrations
Sodium Oxamate	Sigma-Aldrich- O2751	100 µM
		1 mM
		10 mM
L-Sodium Lactate	PanReac AppliChem-A1004	25 mM
NAD	Cayman Chemical- 16077	1 mM
Talazoparib	Sigma-Aldrich- S7048	10 µM
FK-866 (Daporinad)	Selleckchem- S2799	10 µM

Table 5. Compounds and concentrations used to treat the zebrafish larvae.

2.9. NAD^+ and NADH luciferase determination

Three dpf larvae were anesthetized in cold PBS with tricaine and the tail fins of each larva was cut off (150-200 larvae per group). The tissue was collected and resuspended in 100-150 µL of a 1:1 mixture of PBS and NaOH 0.2 N with 1% dodecyltrimethylammonium bromide (DTAB). The sample was mechanically homogenized and kept in ice. Protein concentration was measured using Bradford reagent (Sigma).

The NAD^+ and NADH determination were performed with the NAD/NADH-Glo Assay kit from Promega (G9071) following manufacturer's instructions. For each sample, 10-15 µg of protein were used and NAD^+ and NADH levels were determined. A NAD^+ (Cayman Chemical 16077) and NADH (Biosynth NN12622) standard curve (0-400 nM) was used to obtain the exact concentration in each sample.

2.10. Microarray gene expression analysis

The RNA of the tail fin was extracted using RNAqueous-Micro Total RNA Isolation Kit (Invitrogen) following manufacturer's instructions. RNA quantification and quality was evaluated using a NanoDrop One Spectrophotometer (Thermo Fisher Scientific) and an Affimetrix Zebrafish Array Strip 1.1 ST (901802) from Thermo Fisher Scientific was used to perform the transcriptomic microarray analysis.

2.11. Transcriptomic data of psoriasis patients

The Gene Expression Omnibus (GEO) database (https://www.ncbi.nlm.nih.gov/geo/) was used to obtain transcriptomic data from punch biopsies of healthy individuals and psoriatic patients (GDS4602).

2.12. Zebrafish whole larvae immunofluorescence

The zebrafish larvae were fixed with paraformaldehyde 4% in PBS overnight at 4°C. They were washed four times for 5 minutes in PBS and two times in PBS with 0.2% Triton (PBStx). Then larvae were treated with 2 mg/mL Collagenase A (Sigma) in PBS for 30 minutes and washed three times in PBStx. Later, they were incubated in glycine (50 mM in PBStx) for 10 minutes, washed 5 minutes in PBStx, and blocked in blocking buffer (1% DMSO, 1% normal goat serum or fetal bovine serum, 1% BSA and 0.7% Triton-X in PBS) for 2 hours at room temperature. The incubation with the primary antibody for microglia (1:50 anti-4C4, mouse monoclonal Becker Laboratory, University of Edinburgh) or for Histone H2A.X phosphor Ser139 (1:250 Genetex GTX127342) was performed overnight at 4°C, diluted in blocking buffer. The next day, the larvae were washed three times for 15 minutes in PBStx and incubated with the secondary antibody (1:200 dilution of goat anti-mouse Alexa Fluor-647 or goat anti-rabbit Alexa Fluor 488) overnight. Lastly, they were washed twice in PBStx for 15 min and three times in PBS for 15 min.

2.13. H_2O_2 determination

The measurement of H_2O_2 levels was performed as previously described[157; 158] using a live cell fluorescein dye. Briefly, 3 dpf larvae were incubated with 50 µM acetyl-pentafluorobenzene

sulphonyl fluorescein (H_2O_2 probe) (Cayman Chemical) in egg water for one hour in the dark. After probe incubation, imaging was carried out immediately.

2.14. Sudan black neutrophil staining

The 7 dpf larvae were fixed in methanol-free paraformaldehyde 4% in PBS overnight at 4°C. The next day, the larvae were washed two times for 5 minutes in PBS and were incubated in Sudan black (Sigma - 380B-1KT) for 12 minutes. Larvae were washed two to three times for 30 minutes with 70% ethanol (until the liquid was clear) and were progressively rehydrated with 50% and 25% ethanol solutions in PBT (0,1% Tween-20 PBS). Finally, they were placed in PBT and images were acquired immediately after the staining with a Leica M165 C stereomicroscope equipped with a Leica DMC 5400 camera.

2.15. Neutrophil wound migration assay

The complete transection of the tail was performed with a disposable sterile scalpel in the 3 dpf larvae previously anesthetized in buffered tricaine (164 mg/mL). Then, they were mounted in 1% (w/v) low-melting-point agarose dissolved in egg water, and images were acquired at the selected times at 28.5°C in a LEICA M205 FA stereomicroscope. Neutrophils recruited to the wound area (between the arterio-venous loop and the end of the tail) were manually counted.

2.16. Salmonella infection

The otic vesicle and systemic infection experiments were carried out using *Salmonella Typhimurium* (ST 12023). The bacteria were cultured in Luria-Bertani (LB) broth plates and the day before the infection, one single colony was grown overnight in liquid LB medium. The day of the infection, the ST culture was diluted 1/5 in LB with 0.3 M NaCl and incubated at 37 °C with agitation until 1.4-1.6 optical density at 600 nm was reached (about 1-1.5 hours). Lastly, 600 µl of bacterial culture were diluted adding 400 µl of sterile PBS and the microinjection mixture was prepared with 20 µL of the diluted bacteria (or 20 µL of PBS as control) plus 2 µL of phenol red. Larvae of 2 dpf were anaesthetized in embryo medium with tricaine and placed in an agar plate. Around 100 bacteria per larvae were microinjected into the otic vesicle for local infection or Cuvier duct for systemic infection. At 4 and 6 hours post infection (hpi), the larvae with the infection in the otic vesicle were anesthetized in egg water with buffered tricaine and placed in an agar plate to acquire the images of the recruited macrophages to the site of infection. The larvae with the systemic infection were also anesthetized at 6 hpi (peak of recruitment) and processed for FACS analysis. Larvae were crushed to homogenization with a sterile scalpel and treated with liberase (Roche) at 1:65 (vol/vol) in PBS for 30 minutes at 28°C, pipetting up and down every 10 minutes. To stop the reaction, fetal bovine serum (FBS) was added to a final concentration of 5% and samples were kept in ice from this point onwards. The cell suspension was filtered through a 70-micron cell strainer, washed with 5%FBS in PBS, filtered again through a 40-micron cell strainer and washed again. The suspension was centrifuged at 650g for 5 minutes and resuspended in PBS. Lastly, cells were fixed with 0.5% PFA in PBS for 20 min at RT, washed twice with PBS and kept at 4°C overnight.

The next day, the cell suspension was analyzed with a DB LRSFortessa X-20 cytometer. The percentage of $mCherry^+$, GFP^+, doble positive cells and fluorescent intensity of the cells was calculated using the BD FACSDiva™ Sorftware v8.0.

2.17. Zebrafish larvae imaging

The zebrafish larvae were anesthetized in a petri dish with a solution of 164 mg/L of tricaine in egg water and images were acquired using a Leica M205 FA fluorescent stereomicroscope equipped with a Leica DFC365 FX camera. The LASX software was used to perform the area and fluorescence quantification analysis. The neutrophil dispersion and aggregate number were manually quantified in the acquired images.

2.18. Microglia imaging and quantification

The immunostained larvae were mounted in 1.5% low melting point agarose (Life Technologies) in E3 (5mM NaCl, 0.17 mM KCl, 0.33 mM $CaCl_2$, 0.33 mM $MgSO_4$) for the microglia image acquisition. Z-stacks images were taken with a step size of 80 µm in an inverted Leica TSP8 confocal microscope. For the quantification of $4C4^+$ cells, only cells within the brain (telencephalon, tectum, and cerebellum) were counted for each sample using the 'To count microglia' plugging for ImageJ developed by the members of the of the CBIO Advanced Imaging Core Facility (AICF) at the University of Trento.

2.19. Statistical analysis and data representation

All statistical analysis and data representations were performed using GraphPad Prism version 8.0.0. The statistical test used in each particular experiment is stated in the corresponding figure legend.

3. Results

3.1. The expression of telomerase RNA (*terc*) alters glycolysis and TCA cycle metabolite composition

A metabolomic analysis was carried out in 3 days post fertilization (dpf) zebrafish larvae in which *terc* expression was modified. The expression of *terc* was decreased through a morpholino microinjection (Mo*terc*), while *terc* levels were increased by microinjecting the *terc* RNA (*terc* S) in the embryos. A standard morpholino (Mo std) and the antisense RNA of *terc* (*terc* AS) were used as controls.

After analyzing the metabolomic composition of the samples, we focused on studying the metabolites whose concentration had the opposite behavior when modifying *terc* levels. We found out that the levels of several metabolites related to glycolysis and tricarboxylic acid (TCA) cycle changed in accordance with *terc* expression. Specifically, the levels of 3-phosphoglycerate, phosphoenolpyruvate and succinyl-CoA where reduced, and the levels of lactate, succinate and oxaloacetate significantly increased when reducing *terc* expression (Fig. 19). As mentioned, the opposite effect in the metabolite concentration was observed when increasing *terc* levels in the larvae, and statistically significant changes were detected in the levels of fructose 1,6-bisphosphatase, 3-phosphoglycerate, phosphoenolpyruvate and acetyl-CoA (Fig. 19).

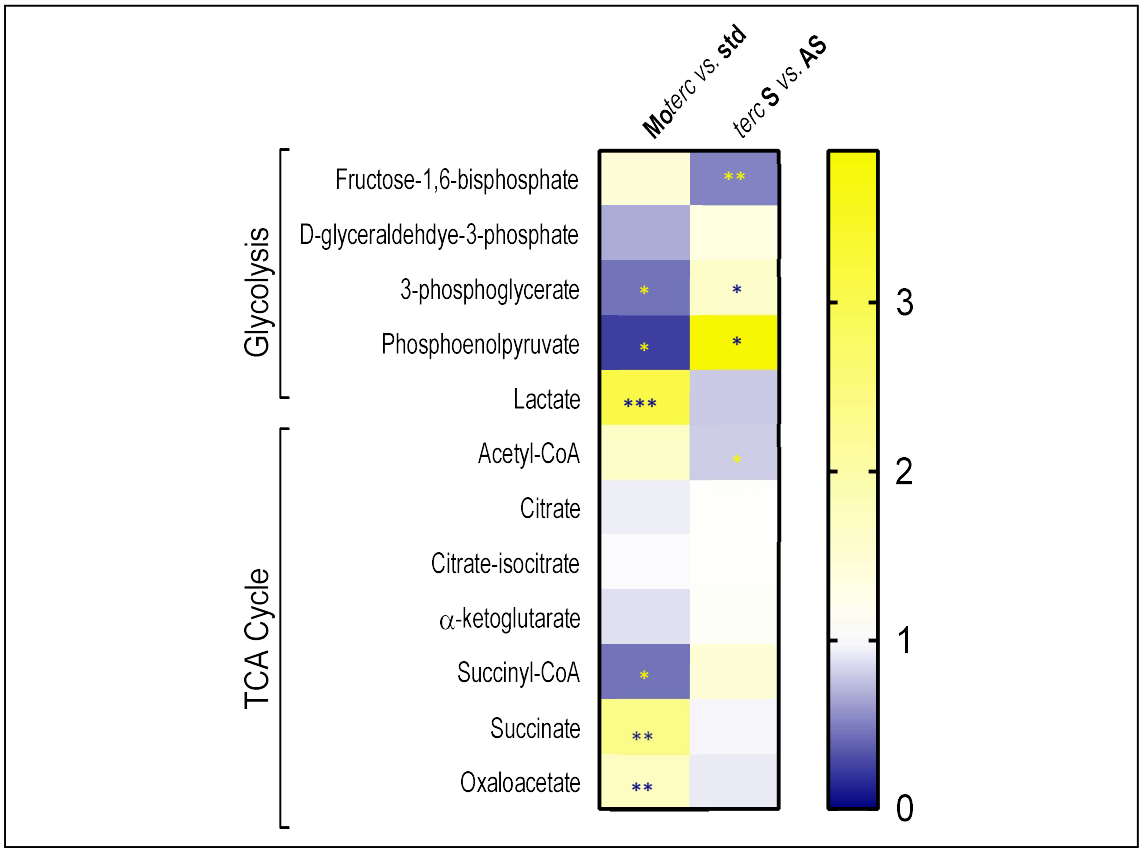

Figue 19.*terc* expression modifies the levels of glycolytic and TCA cycle metabolites. Heatmap showing the glycolytic and TCA cycle metabolite composition in 3 days post fertilization (dpf) zebrafish larvae after decreasing (Mo*terc* vs. std) or increasing (*terc* S vs. AS) *terc* expression. Only those metabolites that showed the opposite behaviour when changing *terc* expression are shown. Metabolites that present statistically significant changes are labelled as * pvalue≤0.05, ** pvalue≤0.01, ***pvalue≤0.001.

In this context, we came out with two possible situations that could be occurring to induce those variations in the metabolite concentration. One of them would be that the levels of *terc* could be changing the activity of the enzymes in charge of synthetizing or consuming those metabolites. Another possibility would be that the total levels of those enzymes were increasing or decreasing due to changes in *terc* expression. Since *terc* is able to bind the DNA and regulate gene expression[21; 37], we hypothesized that *terc* levels could be regulating the glycolytic metabolite concentration trough changes in the expression of genes encoding the enzymes participating in these pathways.

3.2. The expression of the *ldhbb* gene is regulated by *terc* expression

One of the metabolites with the highest changes in concentration was lactate. The levels of lactate increased when *terc* expression decreased, whereas lactate concentration declined when *terc* was overexpressed (Fig. 19). Given that the enzyme that generates lactate is lactate dehydrogenase (Ldh), we looked for the consensus *terc*-binding sequence (*terc*bs) at the promoter region of the genes coding for that enzyme in the zebrafish.

In the zebrafish, four genes code for LDH isoforms: *ldha*, *ldhba*, *ldhbb* and *ldhd*. Using the ensembl database (https://www.ensembl.org/index.html) a possible *TERC*-binding sequence (*terc*bs) was found at the promoter region of the *ldhbb* gene[253]: CCACCACCACC (Fig. 20A). In order to know if *terc* expression was important for *ldhbb* expression, we microinjected the morpholino against *terc* in zebrafish embryos and checked *ldhbb* expression through RT-qPCR in 3 dpf larvae. Strikingly, *ldhbb* expression decreased when using the *terc* morpholino (Fig. 20C).

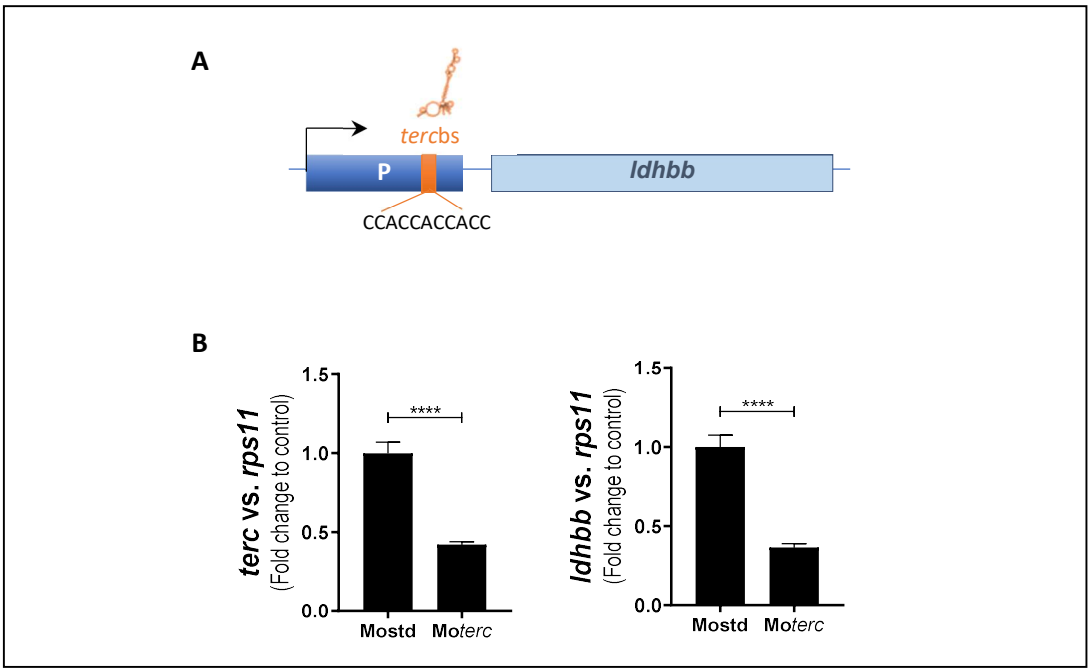

Figure 20. The expression of *ldhbb* decreases in the *terc*-deficient larvae. (A) Schematic representation of the *terc*-binding sequence (*terc*bs) found at the promoter region of *ldhbb* gene using the ensembl website. (B) RT-qPCR of 3 dpf larvae microinjected with a standard morpholino (Mostd) or the morpholino against *terc* (Mo*terc*) to decrease *terc* expression. The expression of *terc* and *ldhbb* was measured and normalized to Mostd samples. The mean ± standard error of the mean (S. E. M) for each group is shown. P value was calculated using Man-Whitney test, ****p≤0.0001.

3.3. *terc* regulates *ldhbb* expression through the promoter region of *ldhbb*

To further confirm if *terc* was able to regulate *ldhbb* expression through the *terc*bs at the promoter region of the gene, an *in vivo* luciferase assay was performed. The sequence 2 kb upstream the *ldhbb* gene that had the *terc*-binding sequence was cloned into a reporter plasmid containing the luciferase gene (Fig. 21A). This construction was microinjected in the zebrafish embryos along with the *terc* morpholino or the standard morpholino as a control. The 3 dpf larvae were used for the luciferase assay, in which we could confirmed that the luciferase activity of *terc* morpholino larvae significantly decreased (Fig. 21C).

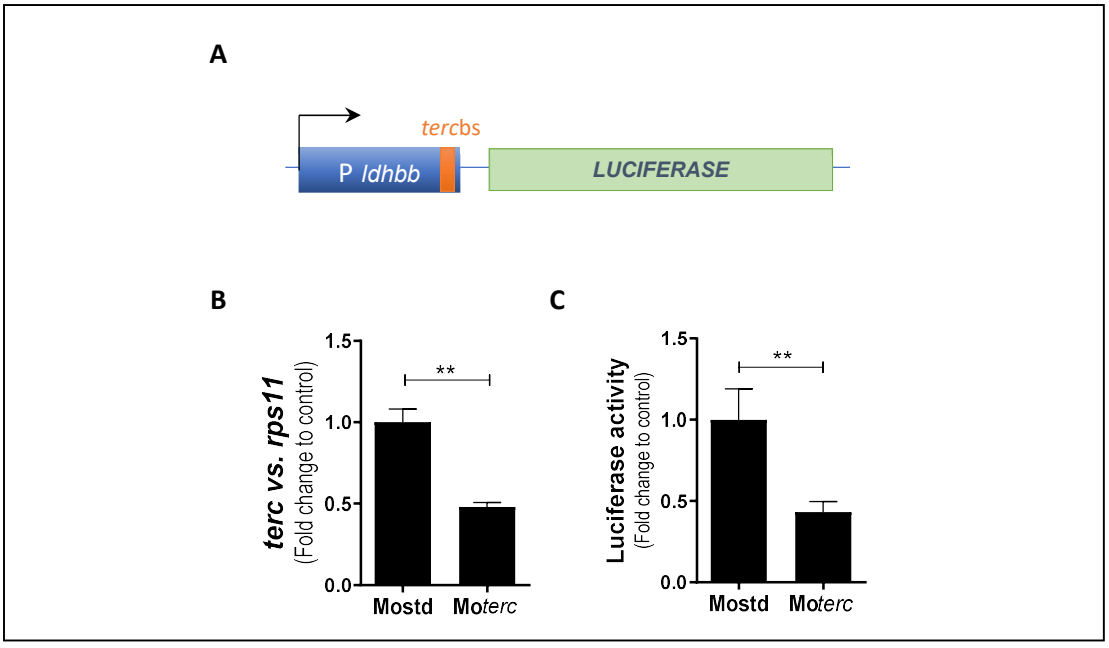

Figure 21. *terc* controls *ldhbb* expression through its promoter region. (A) Schematic representation of the luciferase construction microinjected in the zebrafish embryos. The promoter region of *ldhbb* containing the *terc*bs was cloned upstream the luciferase gene. (B) RT-qPCR of *terc* in 3 dpf larvae microinjected with the luciferase construction and Mostd or Mo*terc*. (C) Quantification of the luciferase signal of the microinjected larvae normalized to Mostd larvae. The mean ± S.E.M. for each group is shown. P value was calculated using Man-Whitney test, **p≤0.01

The *ldhb* (a and b) genes are both orthologous of the *LDHB* human gene, although in the zebrafish, the gene is duplicated. The *ldha* zebrafish gene corresponds to the human LDHA. The LDHB enzyme is known to preferably convert lactate into pyruvate, while LDHA is prompt to transform the pyruvate into lactate. Thus, the increase in lactate when *terc* expression is reduced may be caused by a decrease in *ldhbb* expression.

3.4. The expression of *ldhbb* is regulated in the zebrafish hematopoietic tissue by *terc* levels

It is known that the immune cells regulate their energy metabolism depending on their function and their resting/activation state. Since changes in *terc* expression induce changes in the expression of *ldhbb* and the glycolytic metabolite composition in the larvae, we wondered if those changes could also be seen specifically in the hematopoietic lineage in adult zebrafish.

For that reason, first we decided to study if the regulation of *ldhbb* was taking place in the zebrafish hematopoietic tissue (kidney marrow). The expression of the four genes coding for Ldh in zebrafish was studied in the kidney marrow of 6-month-old fish by RT-qPCR. Specifically, four different genetic backgrounds were used to elucidate the *terc* involvement in *ldh* gene expression. Wild type fish (WT) were used as controls, *terc* knock out fish (*terc*$^{-/-}$) were used to identify changes in the absence of *terc* and, lastly, *drl:terc* fish were used to determine changes due to *terc* overexpression. In addition, *tert* knock out zebrafish (*tert*$^{-/-}$) were chosen to identify changes related to the canonical function of telomerase. The *drl:terc* transgenic zebrafish line overexpress *terc* under the draculin (*drl*) promoter. This promoter is specific for cells in the cardiac tissue but also for hematopoietic cells. Therefore, *terc* overexpression is specific to the hematopoietic tissue in those fish.

The results show that *terc*$^{-/-}$ fish have almost an indetectable amount of *terc* while *drl:terc* fish have a 12-fold increase in *terc* expression in the kidney marrow compared to the wild type ones (Fig. 22A). *drl:terc* fish had a 2-fold increase compared to wild type fish (Fig. 22A). In the case of *tert*$^{-/-}$ fish, they have a truncated TERT protein with no enzymatic activity, but the expression of messenger RNA can be detected (Fig. 22D). Similarly, to zebrafish larvae, the expression of *ldhbb* was regulated by *terc* levels: *terc*$^{-/-}$ hematopoietic tissue had a decreased expression of *ldhbb* (Fig. 22B). Besides, the *ldhba* expression also increased in the *terc*-overexpressing hematopoietic tissue (Fig. 22C).

In the case of *ldha* and *ldhd*, some changes in expression were detected in all genetic backgrounds (Fig. 22E and 22F). However, the more distinct changes were found in *terc*$^{-/-}$ fish, in which both genes were increased 5 to 6 times (Fig. 22E and 22F). Since *terc*$^{-/-}$ fish have a reduced *ldhbb* expression, this increase may be explained by a genetic compensation mechanism in those fish.

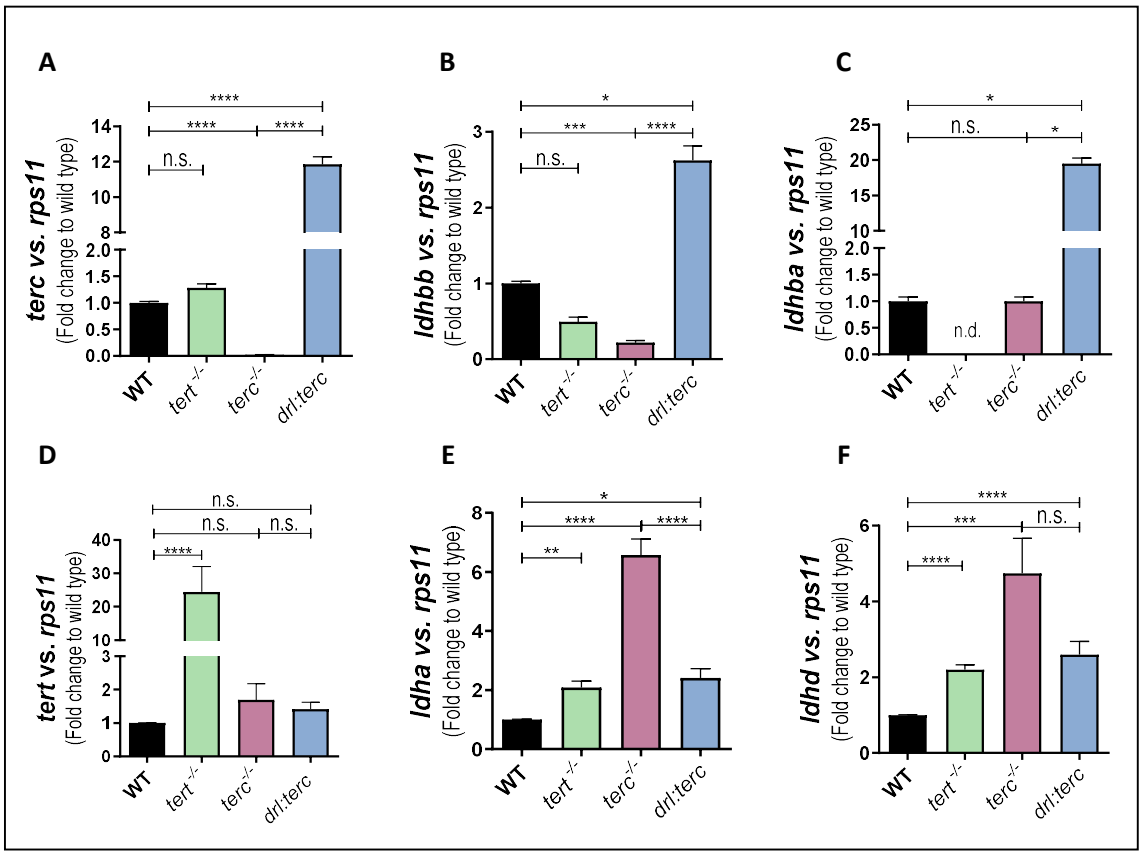

Figure 22. Expression of the *ldh* genes in the kidney marrow of wild type, *tert*$^{-/-}$, *terc*$^{-/-}$ and *drl:terc* fish. Four kidney marrows were pooled in two groups of two to perform the RT-qPCR in each genotype. (A and D) *terc* and *tert* expression were measured as control. (D) *tert*$^{-/-}$ fish have an increase in a short form of *tert* mRNA. (B and C) The expression of *ldhbb* and *ldhba* change in accordance to *terc* expression. (E and F) The expression of *ldha* and *ldhd* is increased in *terc*$^{-/-}$ larvae. The mean ± S.E.M. for each group is shown. P values were calculated using Kruskal-Wallis and Dunn's multiple comparisons test, n.s.: not significant,*p≤0.05, **p≤0.01, ***p≤0.001, ****p≤0.0001.

On the basis of *terc* regulation of lactate levels in the zebrafish larvae, we aimed at evaluating the effects of *terc* expression in two different disease models, both involving an immune response due to an inflammation process: chronic inflammation and the cancer immune response. Due to the established role of lactate in other chronic inflammatory diseases, in the first part of this chapter (Part 1) we decided to test the effects of lactate regulation in chronic inflammation to later study *terc* involvement. Lastly, in Part 2, we evaluated the effects of *terc* expression in the immune cells in the context of the cancer immune response.

PART 1

terc alleviates inflammation through the regulation of lactate metabolism

3.5. The pharmacological inhibition of Ldh and exogenous lactate reduce the inflammation levels in a zebrafish model of psoriasis

To assess the role of Ldh in a zebrafish model of skin chronic inflammation, *spint1a*$^{-/-}$ larvae were treated with sodium oxamate, a pyruvate analog that inhibits the LDH activity. Hence, 24 hour-post-fertilization (hpf) larvae were exposed to oxamate for 48 hours by adding the compound into the embryo water. After the treatment, images were acquired, and the number of skin aggregates and neutrophil dispersion were quantified.

As expected, the *spint1a* mutant larvae had increased keratinocyte aggregates and neutrophil infiltration in the skin compared to wild type *spint1a*$^{+/+}$ larvae (Fig. 23A and 23B). The treatment with oxamate reduced keratinocyte aggregates and neutrophil infiltration in the skin in a dose dependent manner (Fig. 23A and 23B). The concentration of 10 mM of oxamate was chosen to perform the following experiments, since it showed the most potent anti-inflammatory effect.

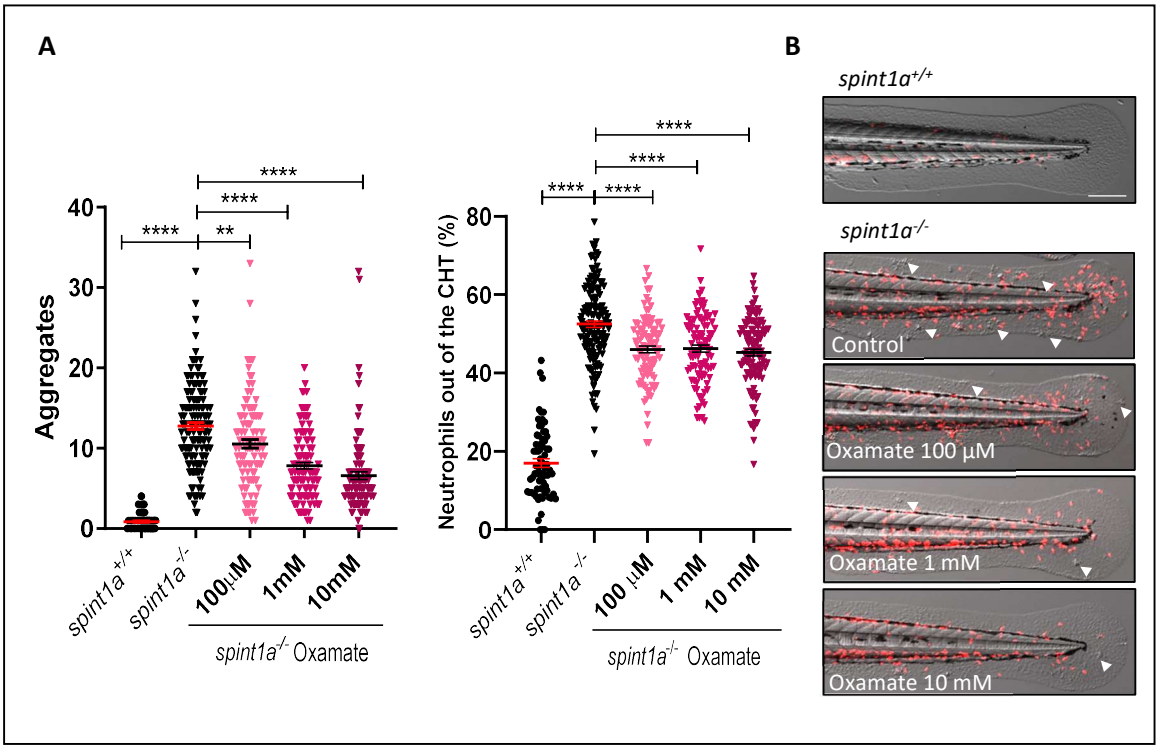

Figure 23. The treatment with oxamate reduces keratinocytes aggregates and neutrophil skin infiltration.(A) Quantification of skin aggregates and neutrophil dispersion out of the CHT in the tail of 72hpf larvae after treatment with different doses of oxamate. Mean ± standard error of the mean (S.E.M) is shown for each group and each dot represents a larvae. (B) Representative images of the tail of the wild type (*spint1a*$^{+/+}$) and chronic inflammation (*spint1a*$^{-/-}$) zebrafish larvae treated with oxamate. Merged brightfield and red fluoresecent channel are shown. Skin aggregates can be seen in the brighfield channel (white arroheads), whereas neutrophils are shown in red (*lyz:*dsRED). Scale bar= 200 µm . P values were calculated using Brown-Forsythe and Welch's ANOVA tests followed by Dunnett's T3 multiple comparisons test **p≤0.01, ****p≤0.0001.

In order to investigate a possible direct relationship between the inhibition of LDH by oxamate and the reduction of the inflammation, *spint1a* $^{-/-}$ larvae were treated with lactate, the product of LDH, and a combination of both oxamate and lactate. Surprisingly, larvae treated with 25 mM of lactate had a reduction in both the neutrophil dispersion and the skin aggregate formation, whereas the combination of both oxamate and lactate led to a decrease in neutrophil dispersion.

Nevertheless, the number of aggregates in the latter remained at the same level as untreated *spint1a* deficient larvae (Fig. 24A and 24B).

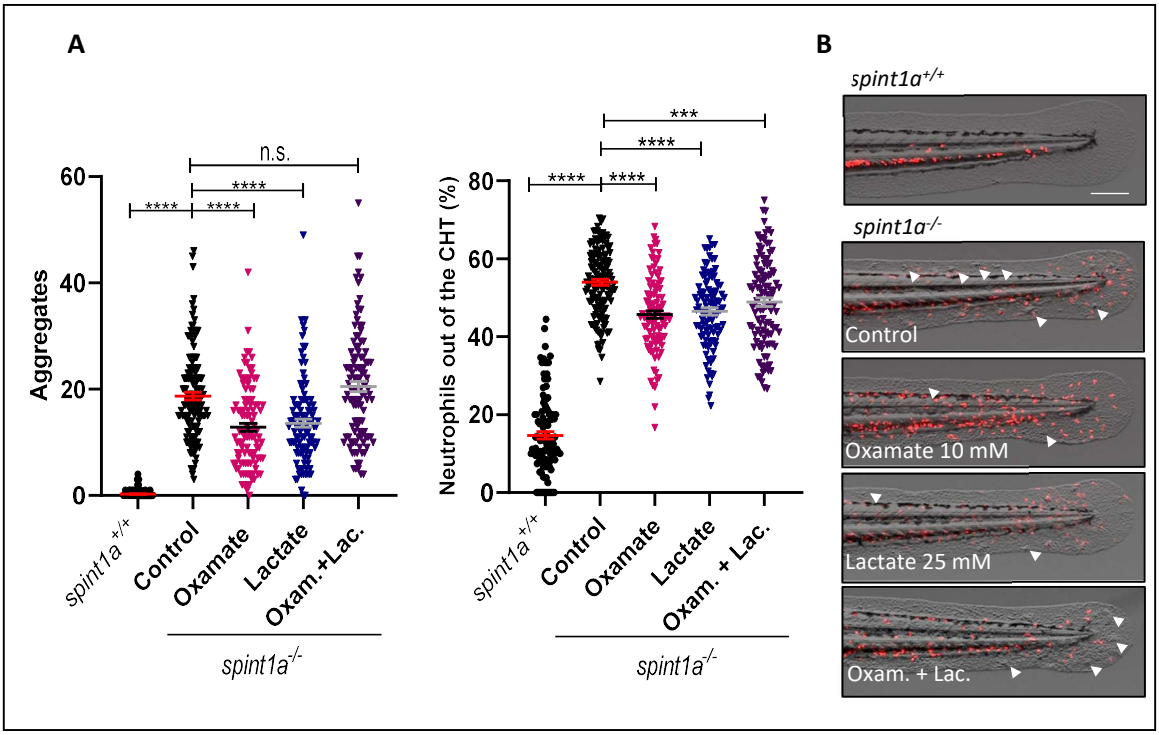

Figure 24. The addition of exogenous lactate alleviates inflammation. (A) Quantification of skin aggregates and neutrophil dispersion out of the CHT in the tail of 72hpf larvae after treatment with oxamate, lactate and the combination of both. Mean ± S.E.M. is shown for each group and each dot represents a larvae. (B) Representative images of the tail of the wild type (*spint1a*$^{+/+}$) and chronic inflammation (*spint1a*$^{-/-}$) zebrafish larvae with the oxamate, lactate or the treatment combination (Oxam.+Lac.). Merged bright field and red fluoresecent channel are shown. Skin aggregates can be seen in the brighfield channel (white arroheads) whereas neutrophils are shown in red (*lyz:*dsRED). Scale bar= 200 µm. P values were calculated using Brown-Forsythe and Welch's ANOVA tests followed by Dunnett's T3 multiple comparisons test n.s.: not significant, ***p≤0.001, ****p≤0.0001.

Since the reaction catalyzed by the LDH enzyme is reversible and dependent on the abundance of the substrate and the product, we hypothesized that the addition of lactate may be decreasing the inflammation in the skin by modifying the enzymatic reaction equilibrium towards the production of pyruvate and NADH instead of lactate and NAD^+ (Fig. 25). That is, the addition of an excess of lactate would be mimicking the effect of the LDH inhibition.

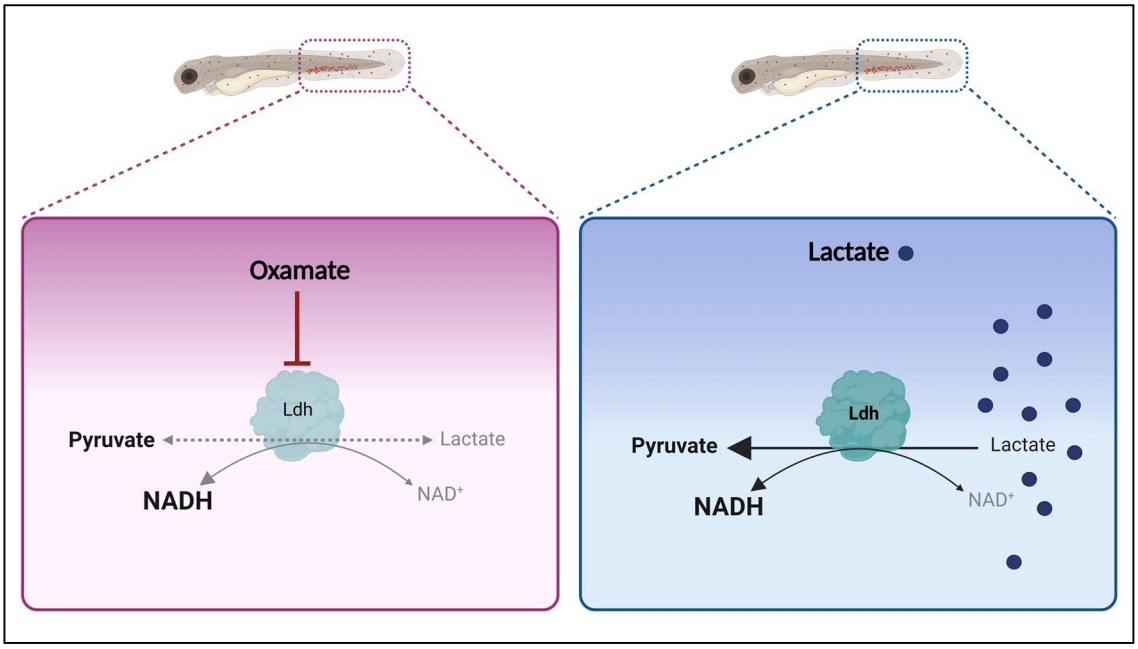

Figure 25. Representation of the possible mechanism by wich both lactate and oxamate alleviate inflammation. The inhibition of Ldh by oxamate in the left panel causes a decrease in the production of lactate and NAD^+. The addition of exogenous lactate in the right panel would shift the direction of the enzymatic reaction. The presence of excess substrate (lactate) would be unbalacing the reaction towards the production of pyruvate and NADH, decreasing NAD^+ levels as well. Created with BioRender.com.

To further confirm that the inhibition of Ldh was directly contributing to mitigate skin inflammation, we used the CRISPR-Cas9 technology to perform the genetic inhibition of the two most expressed genes in zebrafish coding for Ldh isoforms. *spint1a*$^{-/-}$ embryos were microinjected with crRNA guides targeting *ldha* and *ldhba*, that are the homologs of the human *LDHA* and *LDHB*. The *ldha* gene is mostly expressed in the muscle tissue, although it is also present in the zebrafish skin. On the contrary, the *ldhba* gene is the predominant isoform in the zebrafish skin[254].

Neither the microinjection of the *ldha* or *ldhba* guides alone, nor the combination of both produced any recovery of the skin inflammation in the *spint1a*-deficient larvae (Fig. 26A and 26B). Even though the guides successfully edited the selected genes (Fig. 26C and 26D), this unexpected result may be explained due to the presence of other *ldh* isoforms in the skin of the larvae such as *ldhbb* or *ldhd*, and the impossibility to target all of them with this genetic inhibition, in contrast to the pharmacological inhibition with oxamate. In fact, in the samples microinjected with the *ldha* guide, the expression of the *ldha* gene is reduced but not completely abrogated (Fig. 26E). In addition, other *ldh* isoforms are expressed at the same level as in control samples (Fig. 26E).

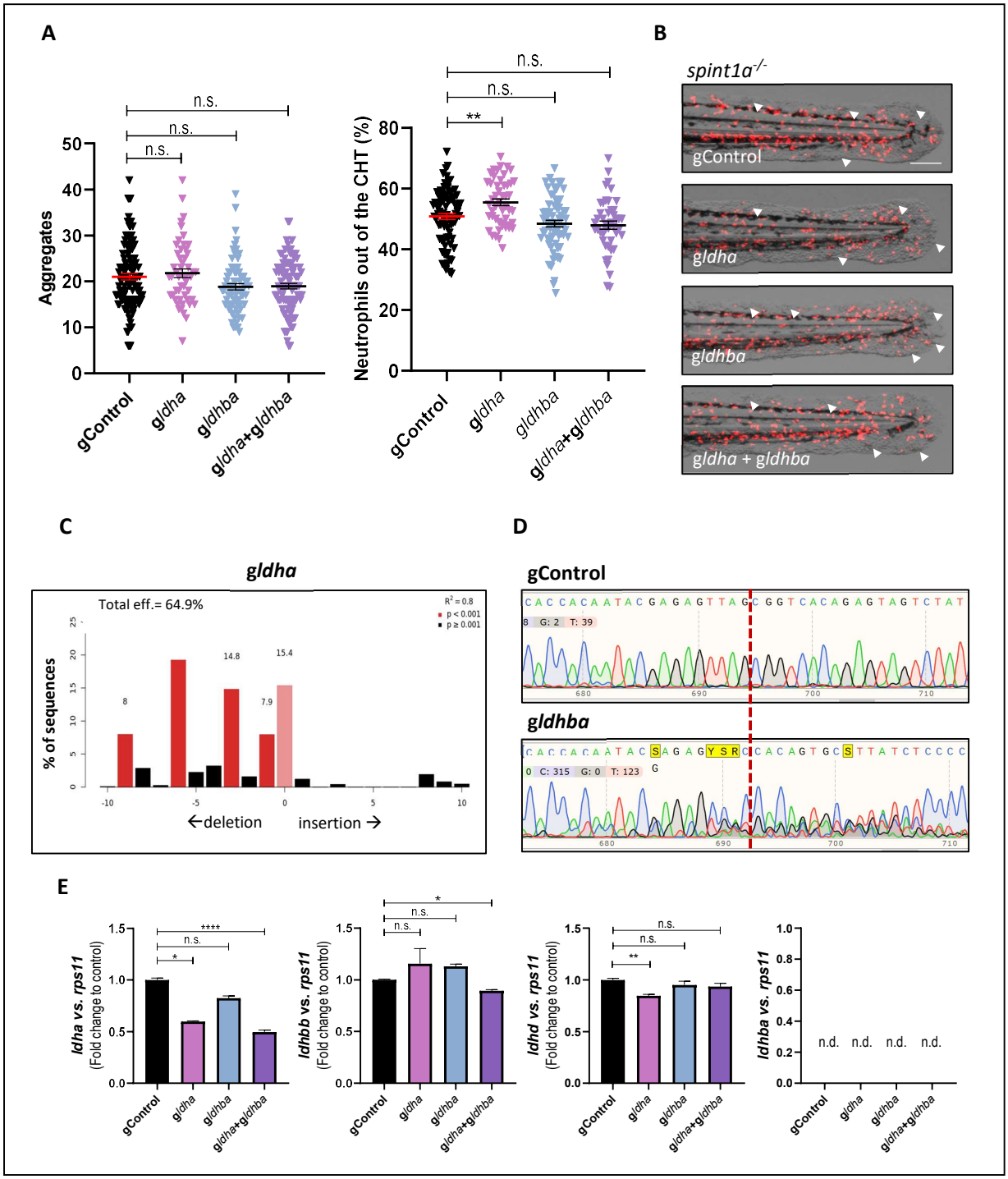

Figure 26. The genetic inhibition of *ldha*, *ldhba* or its combination does not alleviate skin inflammation. (A) Quantification of skin aggregates and neutrophil dispersion in the tail of 72hpf larvae after the microinjection of crRNAs control (gControl) or targeting *ldha* (g*ldha*), *ldhba* (g*ldhba*) or both (g*ldha* + g*ldhba*). Mean ± S.E.M. is shown for each group and each dot represents a larvae. (B) Representative images of the tail of *spint1a*$^{-/-}$ zebrafish larvae microinyjected with the mentioned crRNAs. Scale bar= 200 µm. (C) Graph showing the efficacy of edition of the g*ldha* (total eff.= 64.9%) and percetange and position of insertions and deletions found in the target sequence. The analysis was performed using the TIDE software (https://tide.nki.nl/) after uploading the sanger sequencing data from samples microinjected with gControl or g*ldha*. (D) Sanger sequencing results of samples microinjected with control or *ldhba* crRNAs. Note the peak mixture around the dotted red line, indicating the genome editing at the target sequence by the g*ldhba*-Cas9 complex. (E) Gene expression of the different *ldh* genes in the microinjected zebrafish larvae, n.d.: not detected. P values were calculated using Brown-Forsythe and Welch's ANOVA tests followed by Dunnett's T3 multiple comparisons test (A) and Kruskal-Wallis test followed by Dunn's multiple comparisons test (E), n.s.: not significant, *p≤ 0.05, **p≤0.01, ****p≤0.0001

3.6. The treatment with either oxamate or lactate restores the NAD^+/NADH balance in *spint1a* $^{-/-}$ larvae

An appropriate NAD/NADH balance has been shown to play a key role in the skin homeostasis of the *spint1a*$^{-/-}$ skin inflammation model as well as in patients with psoriasis[158]. Since the LDH catalyzes a reversible reaction that uses NADH or NAD^+, changes in the reaction equilibrium due to the lactate addition or directly the enzyme inhibition by oxamate, could cause changes in the NAD^+/NADH balance and, eventually, changes in the skin inflammation state (Fig. 25). To test this hypothesis, the *spint1a* mutant larvae were treated with a combination of NAD^+ and lactate or NAD^+ and oxamate.

It has been shown that treating *spint1a*$^{-/-}$ larvae with NAD^+ worsens the skin inflammation ([158] and Fig. 27A). The lactate in combination with NAD^+ reduced the skin inflammation to the same level as the control *spint1a* deficient larvae (Fig. 27A and 27B). The oxamate was able to slightly reduce the level of inflammation caused by the addition of NAD^+, since the aggregate number and the neutrophil dispersion was reduced in comparison with the group treated with NAD^+ alone (Fig. 27C and 27D). However, the aggregate number was still higher than in the control *spint1a*$^{-/-}$ larvae (Fig. 27C). These results suggest that the exogenous lactate and the inhibition of LDH by oxamate may be increasing the NADH levels and restoring the NAD^+/NADH balance.

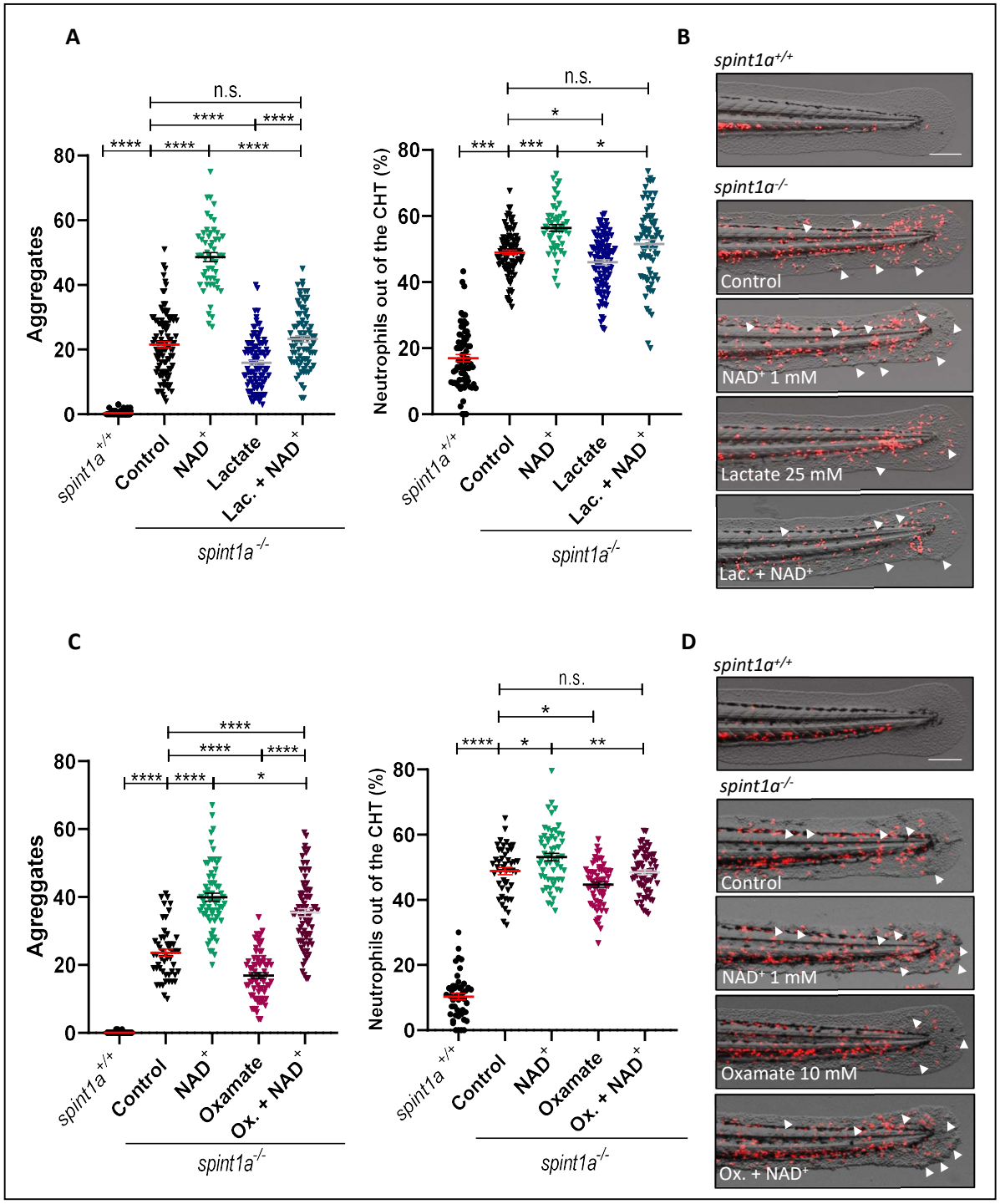

Figure 27. Either lactate or oxamate treatment rescue NAD⁺-driven inflammation. (A and C) Quantification of skin aggregates and neutrophil dispersion out of the CHT in the tail of 72hpf larvae after treatments. Mean ± S.E.M. is shown for each group and each dot represents a larvae. (B and D) Representative images of the tail of the wild type (*spint1a*$^{+/+}$) and chronic inflammation (*spint1a*$^{-/-}$) zebrafish larvae with the treatments. Merged bright field and red fluoresecent channel are shown. Skin aggregates can be seen in the brighfield channel (white arrowheads) whereas neutrophils are labeled in red (*lyz:*dsRED). Scale bar= 200 µm. P values were calculated using Brown-Forsythe and Welch's ANOVA tests followed by Tamhane's T2 multiple comparisons test n.s.: not significant, *p≤ 0.05, **p≤0.01,***p≤0.001, ****p≤0.0001.

Next, we aimed to evaluate whether the treatments were indeed modifying the NAD^+/NADH balance in the larvae. For that we measured NAD^+ and NADH levels in the tail fin using a cycling enzyme luciferase method. We chose this part of the larvae because it is a skin-enriched tissue. The levels of NAD^+ and NADH were measured for each sample and then the NAD^+/NADH ratio was calculated (Fig. 28B). As expected, the NAD^+/NADH ratio for the skin of *spint1a* $^{-/-}$ larvae was higher than the one for *spint1a*$^{+/+}$, (Fig. 28C). Confirming our hypothesis, the treatment with either lactate or oxamate returned the NAD^+/NADH ratio to the levels of the *spint1a*$^{+/+}$ (Fig. 28C), indicating that the alleviation of the skin phenotype caused by the treatments may be due to changes in the concentration of NAD^+ and NADH.

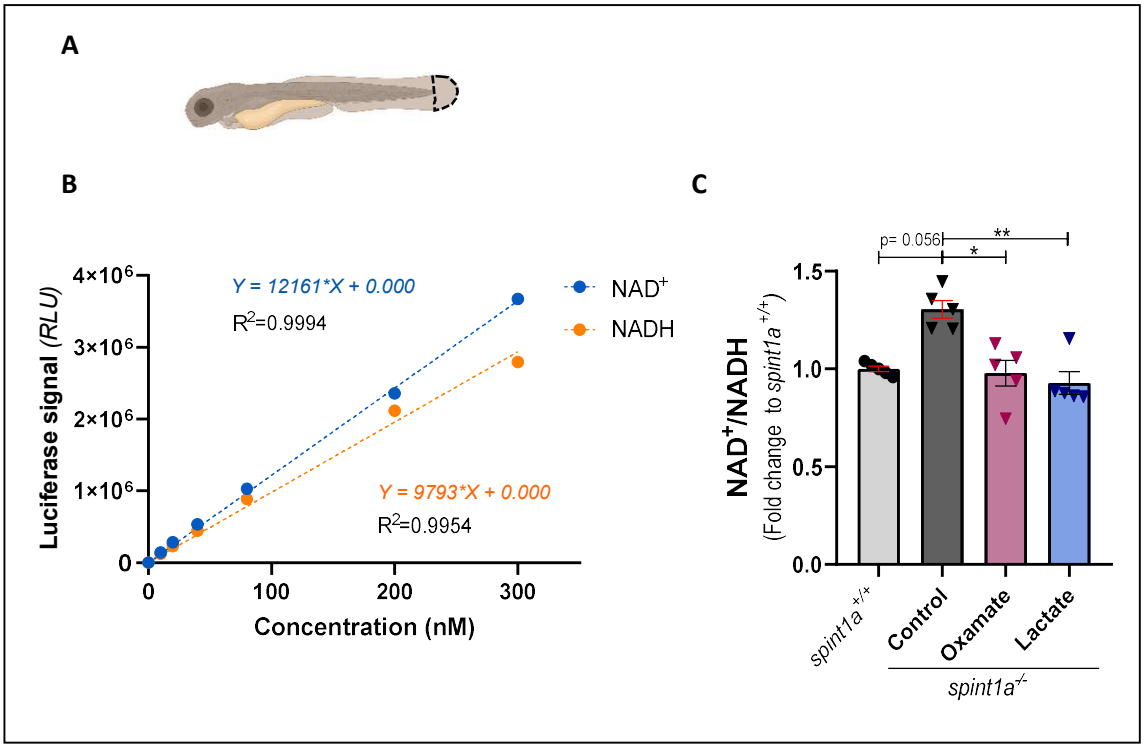

Figure 28. The treatment with either oxamate or lactate reduces the NAD^+/NADH ratio of *spint1a*$^{-/-}$ larvae. (A) Schematic representation of a 72 hpf zebrafish larvae. The area inside the doted black line indicates the tissue collected to perform the NADH and NAD^+ measurement. (B) Standard curves for NAD^+ and NADH. Solutions of 0, 20, 40, 80, 200 and 300 mM of pure NAD^+ and NADH were used to obtain the curves. (C) Quantification of the NAD^+/NADH ratio measured in the control and treated larvae. The values for NAD^+ and NADH were obtained for each sample and the NAD^+/NADH ratio was calculated. Then the obtained value was normalized to *spint1a* wild type larvae (*spint1a*$^{+/+}$). Mean ± S.E.M. is shown for each group and each dot represents a pool of around 150 tail fins. P values were calculated using Kruskal-Wallis test followed by Dunn's multiple comparisons test, *p≤ 0.05, **p≤0.01.

3.7. The treatment with oxamate reduces DNA damage and oxidative stress in *spint1a* deficient larvae

The *spint1a* mutant embryos have higher levels of DNA damage than the wild type larvae. This DNA damage is known to be partially dependent on the levels of NAD^+ since the inhibition of one of the main enzymes in charge of synthesizing NAD^+, Nicotinamide phosphoribosyltransferase (NAMPT), reduces the amount of DNA damage in the larvae[158]. Given that oxamate and lactate treatments are able to reduce the NAD/NADH ratio in *spint1a*$^{-/-}$ larvae, we decided to test whether these treatments were also affecting the amount of DNA damage. Therefore, we performed an immunostaining of the DNA damage marker pγH2Ax in both control and treated larvae (Fig. 29C). The larvae were also treated with FK-866 and talazoparib as controls. Talazoparib is an inhibitor of poli-ADP ribose 1 (PARP1), an enzyme involved in DNA repair. Thus, talazoparib was used a positive control due to its ability to increase the amount of DNA damage.

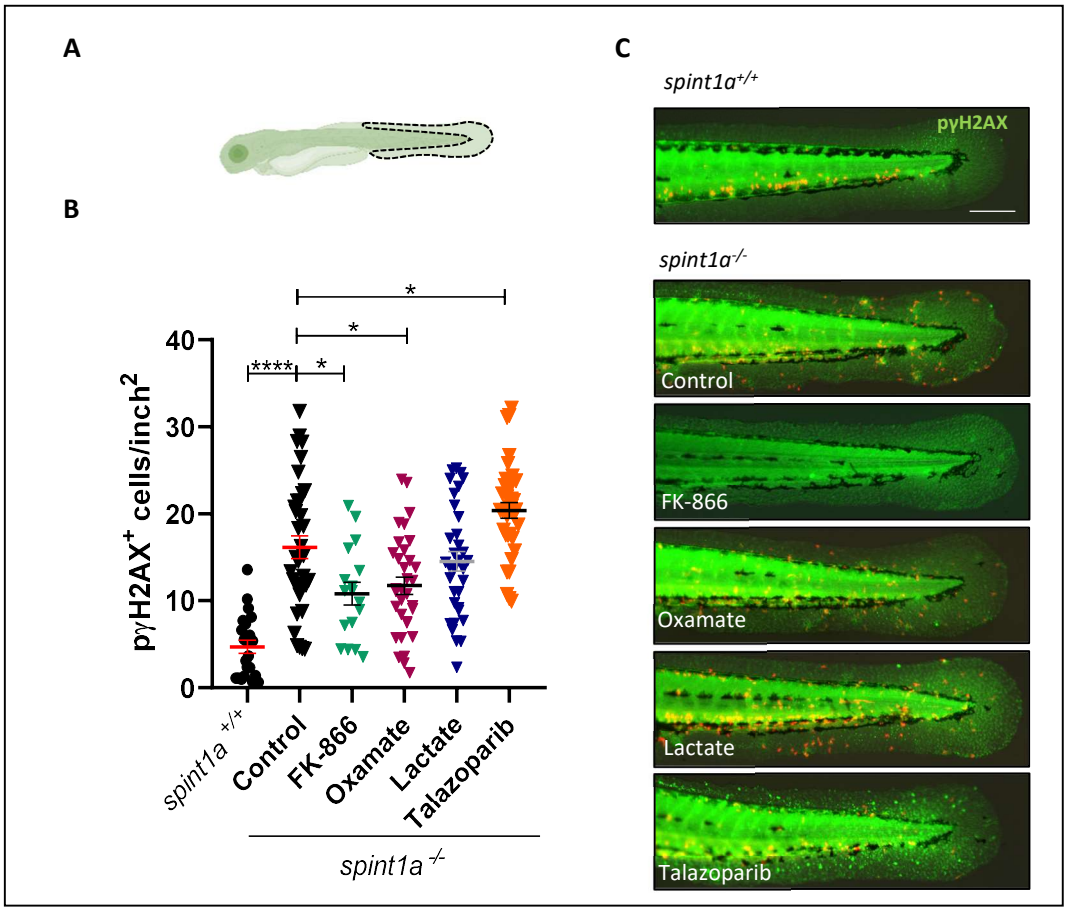

Figure 29. The treatment with oxamate reduces DNA damage in the *spint1a* mutant larvae. (A) Schematic representation of a 3 dpf zebrafish larvae. The area inside the doted black line indicates the area used to perform the image quantification. (B) Quantification of the number of pγH2AX positive cells per square inch using imageJ software. Mean ± S.E.M. is shown for each group and each dot represents a larvae. (C) Representative images of the pγH2AX immunostaining (merged red and green fluorescent channels). The green fluorescent signal in the skin of the larvae corresponds to pγH2AX positive cells, which accumulate in the skin aggregates. Neutrophils are labeled in red and maintain their fluorescence after the staining (*lyz:dsRED*). Scale bar= 200 µm. P values were calculated using Brown-Forsythe and Welch's ANOVA tests followed by Dunnett's T3 comparisons test, *p≤ 0.05, ****p≤0.0001.

Even though the treatment with lactate slightly reduced the number of pγH2Ax positive cells, only the treatment with oxamate showed a significant reduction of the pγH2Ax staining, almost to the same level as the treatment with FK-866 (Fig. 29B).

Another characteristic of the *spint1a* mutant embryos is their high levels of oxidative stress[158]. Because of that, they have increased levels of oxygen reactive species (ROS) such as hydrogen peroxide (H_2O_2). Besides, the treatment with NAD^+ increases the amount of H_2O_2 in *spint1a*$^{-/-}$ larvae. The two tested compounds were able to revert the inflammation and restore the NAD^+/NADH balance, so it was of interest to know if the treatments with oxamate and lactate were also causing a decrease in the oxidate stress levels of the larvae.

The oxidative stress of the larvae was then measured by the detection of H_2O_2. A fluorescent probe detecting H_2O_2 levels was added in the water and, after one hour of incubation in the dark, images were acquired, and the fluorescence intensity of the skin was analyzed (Fig. 30A). The image quantification revealed that only the treatment with oxamate but not the treatment with lactate, was again able to decrease the levels of H_2O_2 in the larvae (Fig. 30B and 30C).

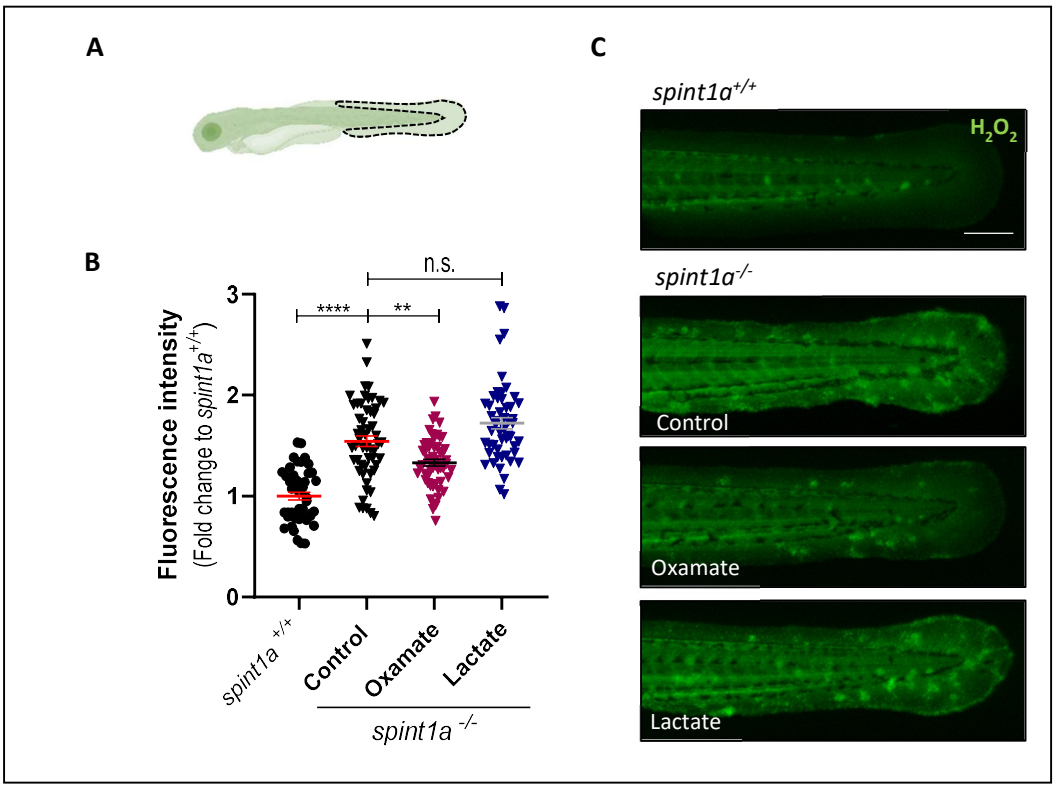

Figure 30. The treatment with oxamate reduces H_2O_2 levels in *spint1a*$^{-/-}$ larvae. (A) Schematic representation of a 3dpf zebrafish larvae. The area inside the doted black line indicates the area used to perform the image quantification. (B) Quantification of the fluorescent signal of the H_2O_2 probe per square centimeter. The values were calculated and normalized to *spint1a*$^{+/+}$ control larvae. Mean ± S.E.M. is shown for each group and each dot represents a larvae. (C) Representative images showing the fluorescent green signal from the H_2O_2 probe in the zebrafish control and treated larvae. Scale bar= 200 µm. P values were calculated using Brown-Forsythe and Welch's ANOVA tests followed by Dunnett's T3 comparisons test, n.s.: not significant, **p≤0.01, ****p≤0.0001.

3.8. A microarray analysis reveals putative genes involved in the alleviation of the inflammatory phenotype after oxamate and lactate treatment.

With the purpose of identifying key genes that could be mediating the alleviation of the skin inflammation observed with oxamate and lactate treatments, a transcriptomic analysis was carried out. Tail fins of *spint1a*$^{+/+}$ and *spint1a*$^{-/-}$ larvae along with the tail fins of *spint1a*$^{-/-}$ larvae treated with lactate or oxamate were collected to perform the gene expression analysis.

We found 56 genes that were upregulated in both treatments at the same time, and 36 genes that were downregulated (fold change threshold ±1.2, p value≤0.05) (Fig. 31A and 31C). These genes were used to perform a KEGG enrichment analysis to reveal specific molecular pathways that could be regulated by the treatments. The analysis showed that the metabolic and signaling pathways (MAPK signaling pathway, neuroactive ligand-receptor interaction, calcium signaling pathway) were among the most enriched ones (Fig. 31B and 31D). Also, a few of the identified pathways were only represented in one of the treatments, including cellular senescence, cellular cycle, or cytokine-cytokine receptor interaction (Fig. 31B and 31D).

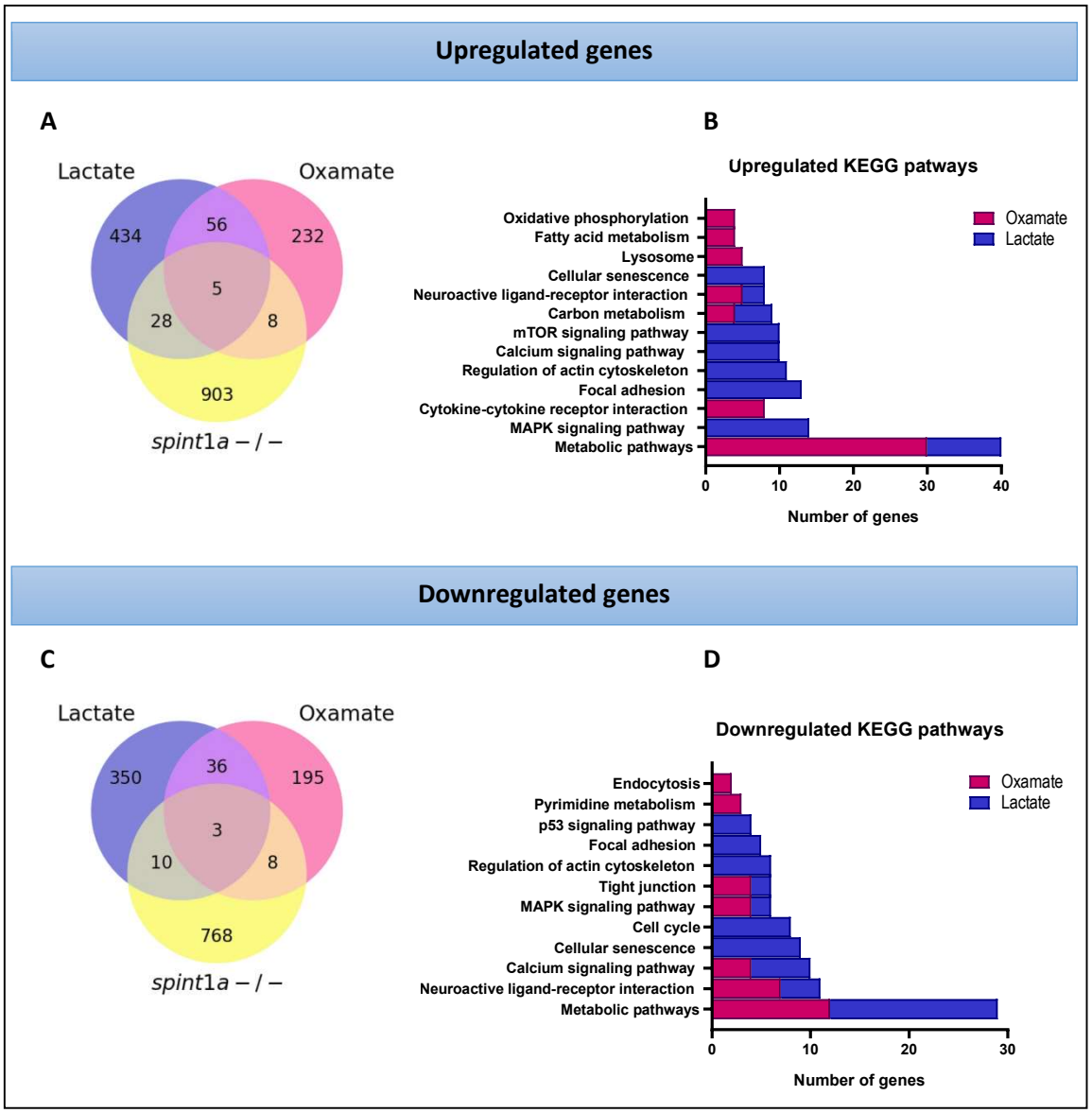

Figure 31. The microarray analysis shows that the genes regulated by oxamate and lactate treatments are mainly involved in metabolic pathways. (A and C) Venn diagrams showing the genes up or downregulated in the treatments with lactate (blue) and oxamate (magenta) versus *spint1a*$^{-/-}$ control larvae (yellow). The overlapping regions correspond to genes commonly up or downregulated by two or more groups and the number inside each region represents the number of genes. There are 56 commonly upregulated genes in the treatments with lactate and oxamate and 36 commonly downregulated genes. (B and D). Representation of the KEGG pathway-enrichment analysis. The number of genes in each treatment is represented by a colored bar. The dark or light blue bars correspond to the number of genes (up or downregulated respectively) with the lactate treatment. The dark or light magenta bars correspond to the number of genes (up or downregulated respectively) with the oxamate treatment. The KEGG analysis shows that most up and downregulated genes in both treatments are related to metabolic pathways, followed by signaling pathways (MAPK signaling pathway and neuroactive ligand-receptor interactions).

The common genes to both treatments that were annotated in databases were grouped attending to their KEGG pathway classification and some of the genes related with cell proliferation, metabolism and/or chemokines (Fig. 32) were chosen to validate the microarray data by RT-qPCR (Fig. 33).

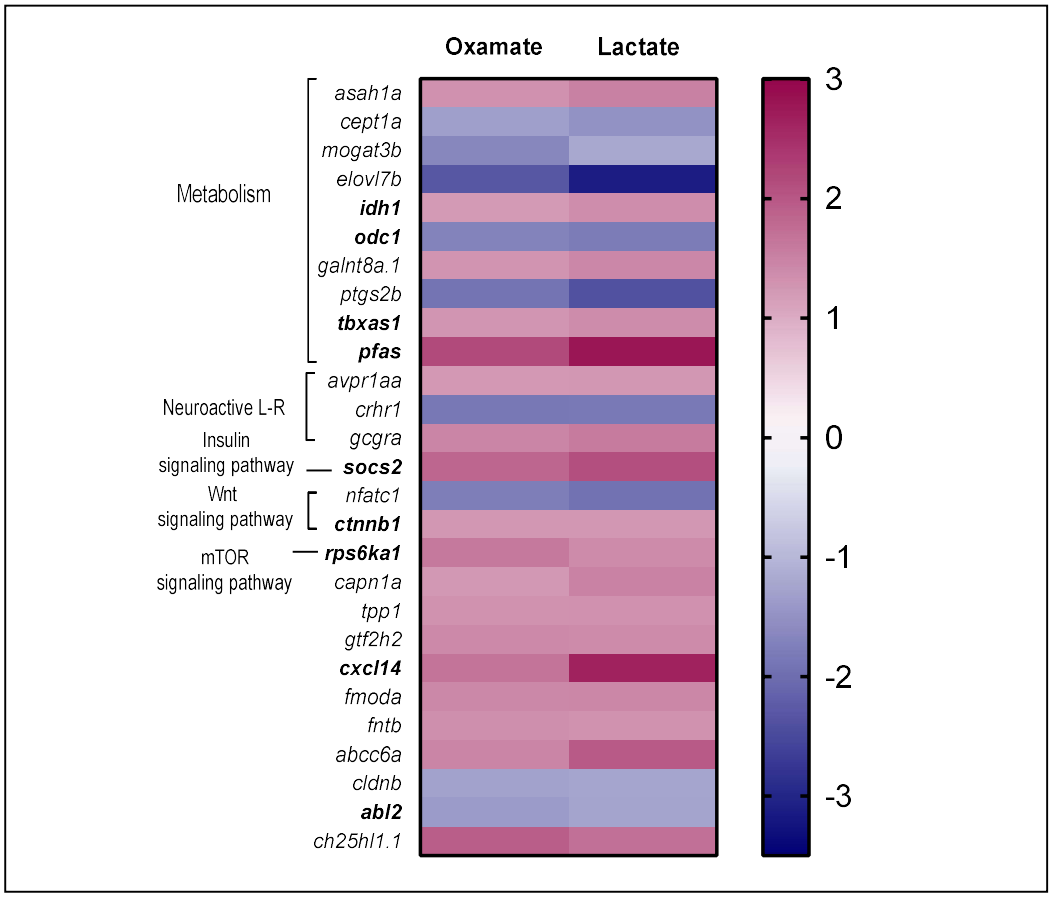

Figure 32. Heatmap showing the commonly up and downregulated genes by oxamate and lactate. The value of the fold change for each gene in each treatment is represented in each square. The color indicates if it is downregulated (blue) or upregulated (magenta) and the intensity of the color corresponds to the fold change value, as indicated in the legend at the right. The genes were classified attending to their KEGG pathway, which is indicated for some of them in the left. The genes in bold were the ones chosen to validate the array results by RT-qPCR.

Overall, the transcript levels of the selected genes correlated with the microarray results with some exceptions. The expression of C-X-C motif chemokine ligand 14 (*cxcl14*) (Fig. 33A), suppressor of cytokine signaling 2 (*socs2*) (Fig. 33B), isocitrate dehydrogenase 1 (*idh1*) (Fig. 33C), thromboxane A synthase 1 (*tbxas1*) (Fig. 33D), catenin beta 1 (*cnntb1*) (Fig. 33F) and ribosomal protein S6 kinase a polypeptide 1 (*rps6ka1*) (Fig. 33G) was similar to the expression data obtained in the microarray analysis, whereas the expression of Ornithine Decarboxylase 1 (*odc1*) and ABL proto-oncogene 2 (*abl2*) did not follow the same expression pattern (Fig. 33E and 33H).

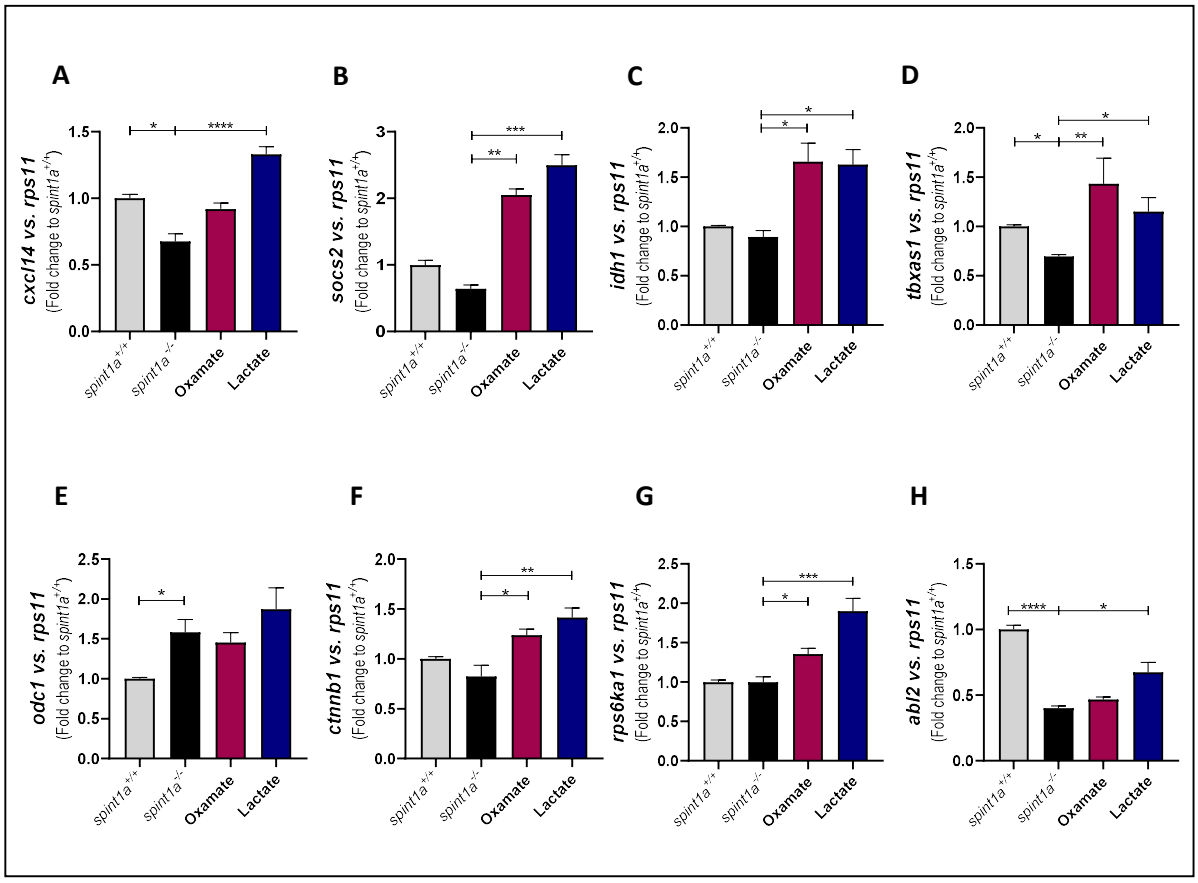

Figure 33. Validation of the microarray results by RT-qPCR. Tail fins of control *spint1a*$^{+/+}$ and *spint1a*$^{-/-}$larvae, and *spint1a*$^{-/-}$ treated with oxamate and lactate were collected. The results are an average of three independent experiments. Most of the analyzed genes showed the same regulation indicated by the array results, with the exception of *odc1* and *abl2*. Mean ± S.E.M. is shown for each group. P values were calculated using Kruskal-Wallis test followed by Dunn's multiple comparisons test, *p≤ 0.05, **p≤0.01, ***p≤0.001, ****p≤0.0001.

3.9. The expression of *LDHA* increases in psoriatic human skin and positively correlates with *IL1B* expression

We have previously shown that the regulation of Ldh enzymatic activity is important for the skin homeostasis in a zebrafish model of skin inflammation. Therefore, we next decided to investigate if Ldh could also have a role in the regulation of the inflammation in the skin of psoriatic patients. Using the Gene Expression *Omnibus* (GEO) database (https://www.ncbi.nlm.nih.gov/geo/), we obtained transcriptomic data from skin punch biopsies of healthy individuals and psoriatic patients (GDS4602). The biopsies for each patient were obtained from their skin lesions and a healthy area, so we could analyze the levels of the genes of interest in these two kinds of samples.

In this dataset, we looked for the transcript levels of *LDHA* and *LDHB*. On the one hand, we found that the mRNA levels of *LDHA* were reduced in the healthy skin of the psoriatic patients compared to control healthy skin. However, they increased in the skin lesions. On the other hand, the levels of *LDHB* did not change in the healthy skin of the psoriatic patients, but they also increased in the psoriasis lesions (Fig. 34A).

Once we observed that the mRNA levels of *LDHA* and *LDHB* increased in the lesioned skin of the psoriatic patients, we aimed at exploring if there was a correlation with the expression of inflammatory genes. We focused on the expression of cytokines related to the Th17 response characteristic of psoriasis, such as interleukin 17 (*IL17A*) and interleukin 23 (*IL23A*). Also, we checked the expression of a well-known gene involved the inflammatory response: interleukin 1β (*IL1B*).

Although the mRNA levels of neither *LDHA* nor *LDHB* correlated with *IL17A* or *IL23A* levels (Fig. 34C and 34D), we found that *LDHA* levels positively correlated with those of *IL-1B* (Fig. 34B), indicating that *LDHA* could be important to regulate the levels of the inflammation in the skin of the patients.

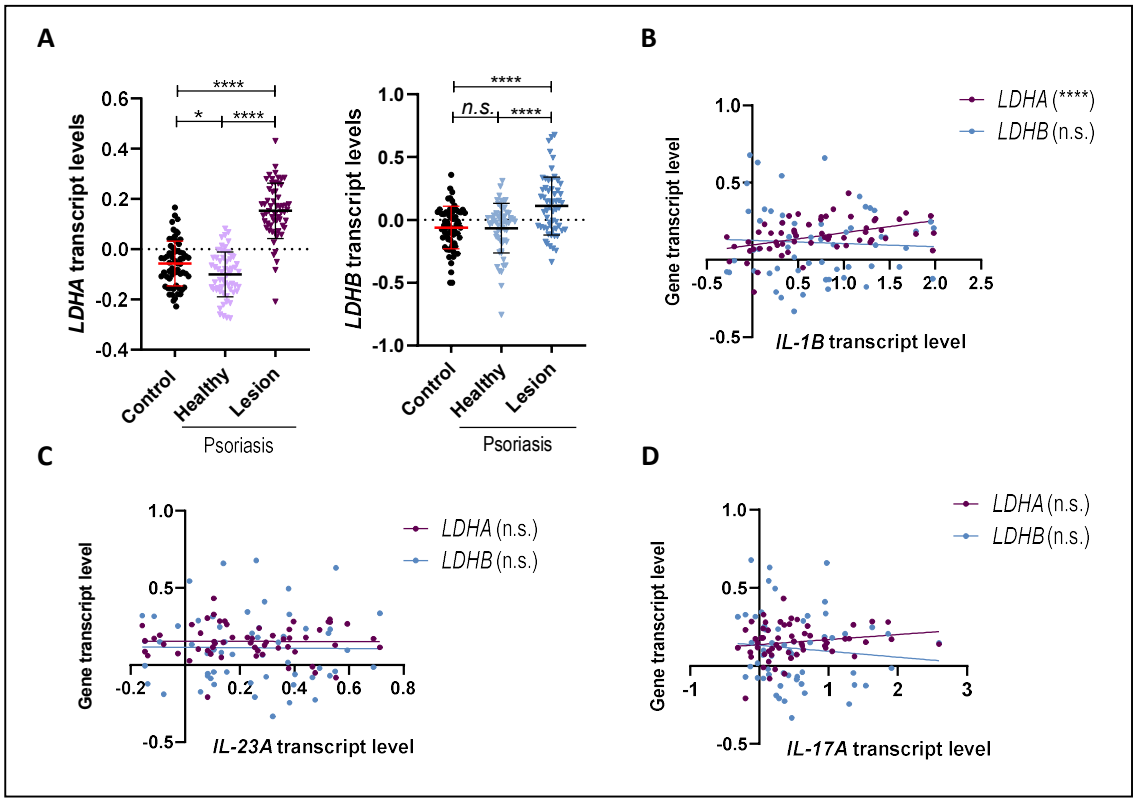

Figure 34. The transcript levels of *LDHA* and *LDHB* increase in the psoriatic lesions and positively correlate with *IL-1B* expression. Transcriptomic data obtained from GEO database (GDS4602) of skin biopsies of healthy individuals (control) and healthy and skin lesions of psoriatic patients. (A) Transcript levels of *LDHA* and *LDHB* in the skin samples. P values were calculated using Brown-Forsythe and Welch's ANOVA tests followed by Games-Howell's multiple comparisons test, n.s.: not significant, *p≤0.05, ****p≤0.0001. (B, C and D) Correlation between *LDHA* and *LDHB* mRNA levels and the ones of pro-inflammatory cytokines *IL1B*, *IL23* and *IL17A*. Linear regression for each gene is shown. P values were calculated using Pearson's correlation coefficient, n.s.: not significant, ****p≤0.0001.

3.10. The expression of *CXCL14*, *SOCS2* and *CTNBB1* decrease in the skin lesions of the psoriatic patients

Since we conducted a microarray study in zebrafish in which we determined some candidate genes that could be taking part in the alleviation of the skin inflammation, we wondered if the expression of those genes was affected in the skin of the psoriatic patients. Besides, the expression of some of the studied genes was not only changed by the oxamate and lactate treatments but it was also affected in the skin of the *spint1a* mutant larvae (Fig. 33A, 33B and 33D-F).

Interestingly, the transcript levels of some of the studied genes in the microarray were the opposite of what we had described in the zebrafish skin. The mRNA levels of *TBXAS1* and *RPS6KA1* increased in the lesioned skin of the psoriatic patients (Fig. 35A and 35E), whereas *tbxas1* decreased and *rps6ka1* levels did not change in *spint1a*$^{-/-}$ larvae. Besides, the mRNA levels of both genes increased by oxamate and lactate treatments (Fig. 33D and 33G).

Other genes such as *PFAS* and *ODC1* did not change their transcript levels in the psoriatic human skin or did it very weakly (Fig. 35F and 35G). However, *CXCL14*, *CTNNB1* and *SOCS2* mRNA levels decreased both in the skin of the psoriasis patients (Fig 35B-D) and in the studied zebrafish

model of psoriasis. Moreover, all of them increased by oxamate and lactate treatments (Fig. 33A, 33B and 33F).

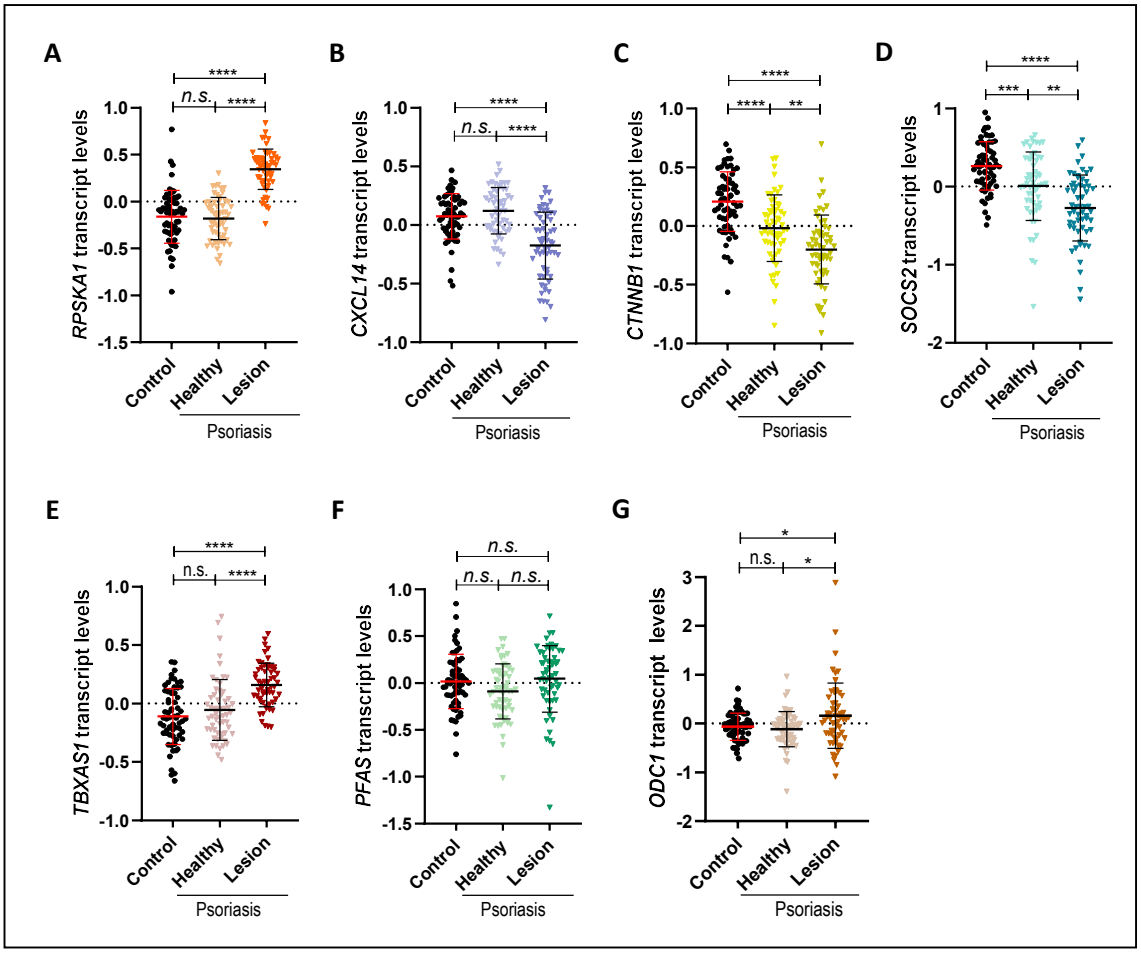

Figure 35. Differential expression in healthy and psoriatic human skin of altered genes in the zebrafish *spint1a*$^{-/-}$ larvae. Transcriptomic data obtained from GEO database (GDS4602) of skin biopsies of healthy individuals (control) and healthy and skin lesions of psoriatic patients. (A) mRNA levels of *RPS6KA1*, (B) *CXCL14*, (C) *CTNNB1*, (D) *SOCS2*, (E) *TBXAS1*, (F) *PFA*) and (G) *ODC1* in the skin samples. P values were calculated using Brown-Forsythe and Welch's ANOVA tests followed by Games-Howell's multiple comparisons test, n.s.: not significant, *p≤0.05, **p≤0.01, ***p≤0.001, ****p≤0.0001.

3.11. mRNA levels of *RPS6KA1* positively correlate, while *CXCL14* negatively correlate with the mRNA levels of *LDHA* and pro-inflammatory cytokines

We also checked in psoriatic skin lesions if there was a correlation between the transcript levels of all these genes found in the zebrafish microarray and the inflammatory cytokines mentioned before. Out of the seven genes, we only found some correlations in the case of *RPSKA1*, *CXCL14* and *CTNNB1* (Fig. 36A-C).

We unexpectedly found that the transcript levels of *RPS6KA1*, that increased in the lesions of the psoriatic patients, positively correlated with those of *IL1B* and *IL17A* (Fig. 36A and 36B). Conversely, the levels of *CTNNB1* negatively correlated with those of *IL23* (Fig. 36C). In the case of the mRNA levels of *CXCL14*, decreased both in human and zebrafish psoriatic skin, negatively correlated with those of *IL1B* and *IL17A* (Fig. 36A and 36B).

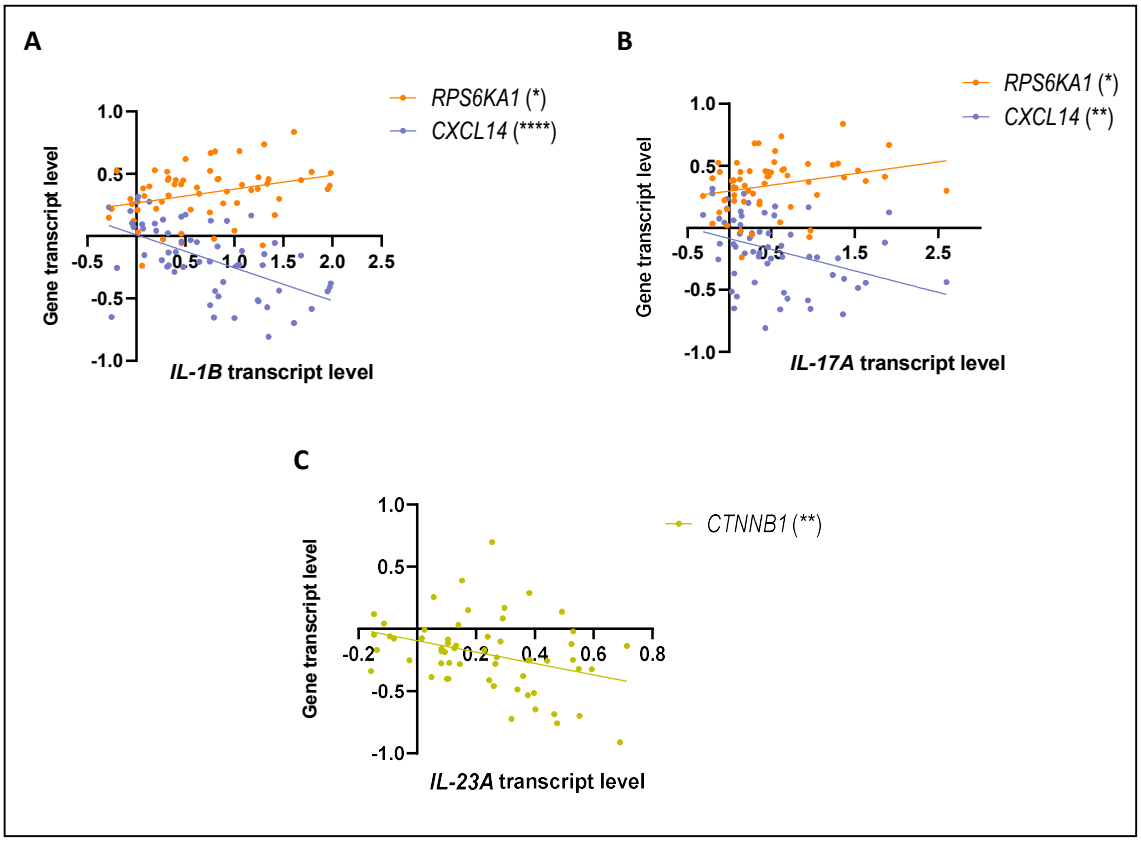

Figure 36. The transcript levels of *RPS6KA1*, *CXCL14* and *CTNNB1* correlate with the ones of inflammatory cytokines. Transcriptomic data obtained from GEO database (GDS4602) of skin lesions of psoriatic patients. The correlation between the transcript levels of *RPS6KA1*, *CXCL14* and *CTNNB1* and the pro- inflammatory cytokines (A) *IL1B*, (B) *IL17A* and (C) *IL23A* was studied in the samples. Linear regression for each gene is shown. The negative slope of *CXCL14* and *CTNNB1* indicates a negative correlation. P values were calculated using Pearson's correlation coefficient, n.s.: not significant, *p≤0.05, **p≤0.01, ****p≤0.0001.

Lastly, we analyzed the correlation between the transcript levels of these three genes, namely *RPS6KA1*, *CXCL14*, *CTNNB1*, and *LDHA* and *LDHB*, to determine if indeed this differential gene expression could be caused by the increase in *LDHA* or *LDHB* seen in the psoriatic lesions (Fig. 34A). The mRNA levels of *CTNNB1* did not correlate with neither those of *LDHA* nor *LDHB*. Nevertheless, *RPS6KA1* levels positively correlated with those of *LDHA* and negatively with those of *LDHB*. In the case of *CXCL14*, its levels negatively correlated only with those *LDHA* (Fig. 37A and 37B).

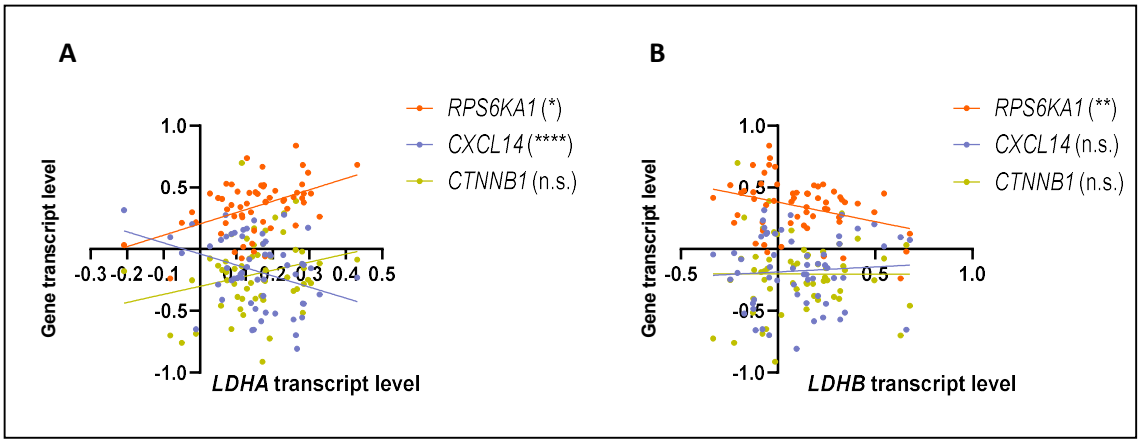

Figure 37. The mRNA levels of *RPS6KA1*, *CXCL14* and *CTNNB1* do not completely correlate with the expression of *LDHA* and *LDHB*. Transcriptomic data obtained from GEO database (GDS4602) skin lesions of psoriatic patients. The correlation between the transcript levels of *RPS6KA1*, *CXCL14* and *CTNNB1* and (A) *LDHA* and (B) *LDHB* genes was studied in the samples. Linear regression is shown for each group. A negative slope indicates a negative correlation. P values were calculated using Pearson's correlation coefficient, n.s.: not significant, *p≤0.05, **p≤0.01, ****p≤0.0001.

3.12. The overexpression of *socs2* and *rps6ka1* did not alter the inflammation levels in the *spint1a*-deficient larvae

Once explored the transcriptional changes taking place in the zebrafish *spint1a*$^{-/-}$ larvae treated with oxamate and lactate, and the transcriptional changes in the psoriatic human patients, we decided to perform functional studies in the zebrafish in order to test if the regulation of some of the identified genes had an impact in the development of the skin inflammation.

The genes that showed the best correlation with the zebrafish array results were selected to examine their role in the inflammation phenotype. The mRNAs *socs2* and *rps6ka1*, two of the overexpressed genes, were in *vitro* synthetized and microinjected in the zebrafish *spint1a* mutant embryos. The results indicated that neither the overexpression of *rps6ka1* or *socs2* mRNAs nor its combination (Fig. 38A) reduced the skin aggregate formation or neutrophil dispersion (Fig. 38B and 38C).

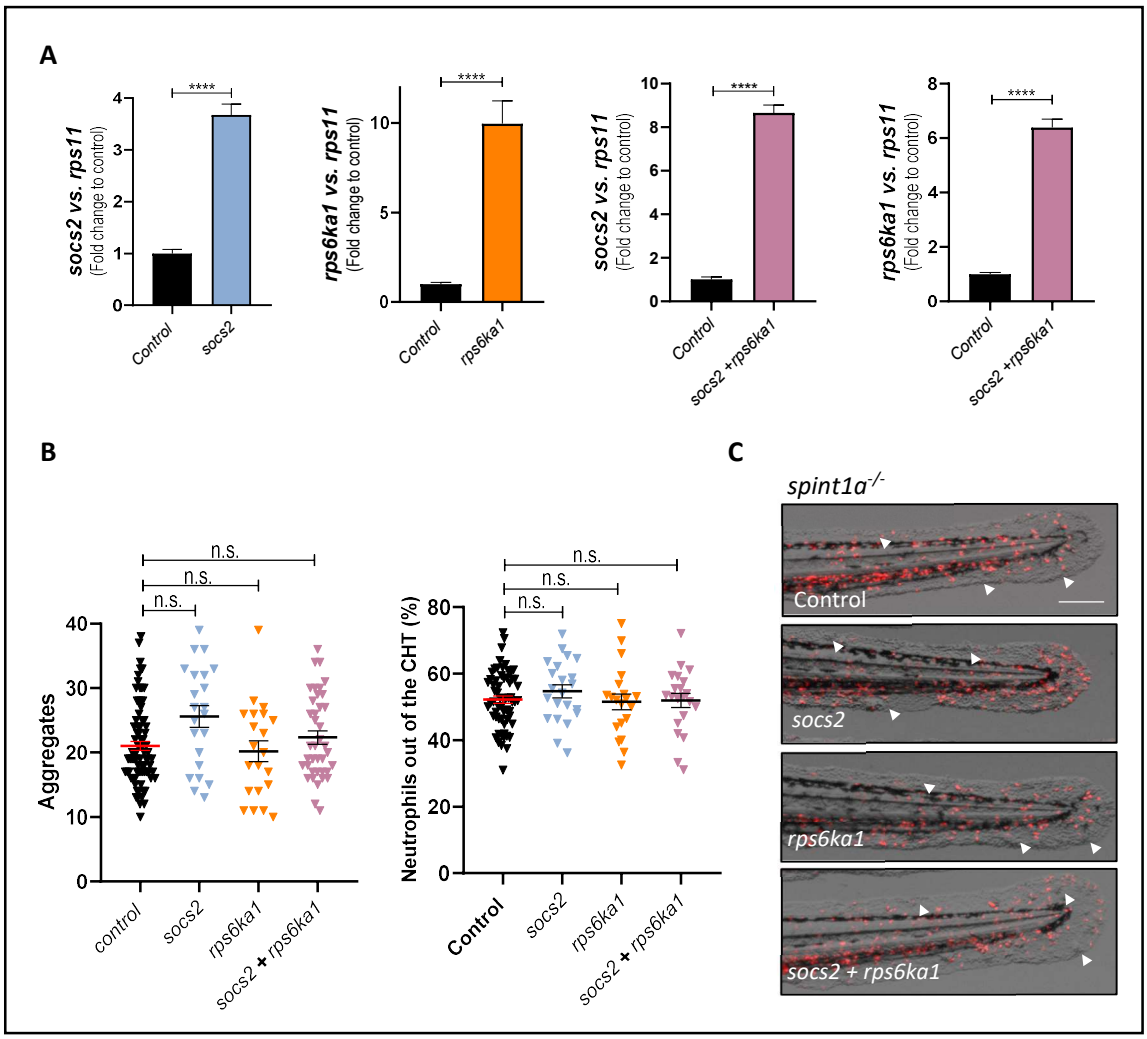

Figure 38. The overexpression of *socs2*, *rps6ka1* or its combination fail to alleviate inflammation of *spint1a* mutant larvae. (A) RT-qPCR of the microinjected 72 hpf larvae showing the mRNAs overexpression. Mean ± S.D. is shown. P values were calculated using Man-Whitney test, ****p≤0.0001. (B) Quantification of skin aggregates and neutrophil dispersion out of the CHT in the tail of 72hpf larvae after treatments. Mean ± S.E.M. is shown for each group and each dot represents a larvae. P values were calculated using Brown-Forsythe and Welch's ANOVA tests followed by Dunnett's T3 multiple comparisons test, n.s.: not significant. (C) Representative images of the tail of *spint1a*$^{-/-}$ zebrafish larvae microinjected with a control RNA or the mRNAs of *socs2* and *rps6ka1*. Merged bright field and red fluoresecent channel are shown. Skin aggregates can be seen in the brighfield channel (white arrowheads) whereas neutrophils are labeled in red (*lyz:*dsRED). Scale bar= 200µm.

3.13. The genetic inhibition of *socs2* and *rps6ka1* did not compromise the anti-inflammatory effect of oxamate

To elucidate whether the lack of these genes impaired the reduction of the skin inflammation observed when treating with oxamate, the *spint1a* mutant embryos were microinjected with CRISPR-Cas9 RNA guides targeting the selected genes and then treated with oxamate. Besides *socs2* and *rps6ka1*, some other upregulated genes were selected, such as *pfas*, *cxcl14* and *cnntb1* (Fig. 32). Four out of the five tested guides successfully edited the locus of the target genes. However, the guide targeting *cxcl14* was not able to perform the expected edition due to the presence of two SNPs in the target sequence (Fig. 39A).

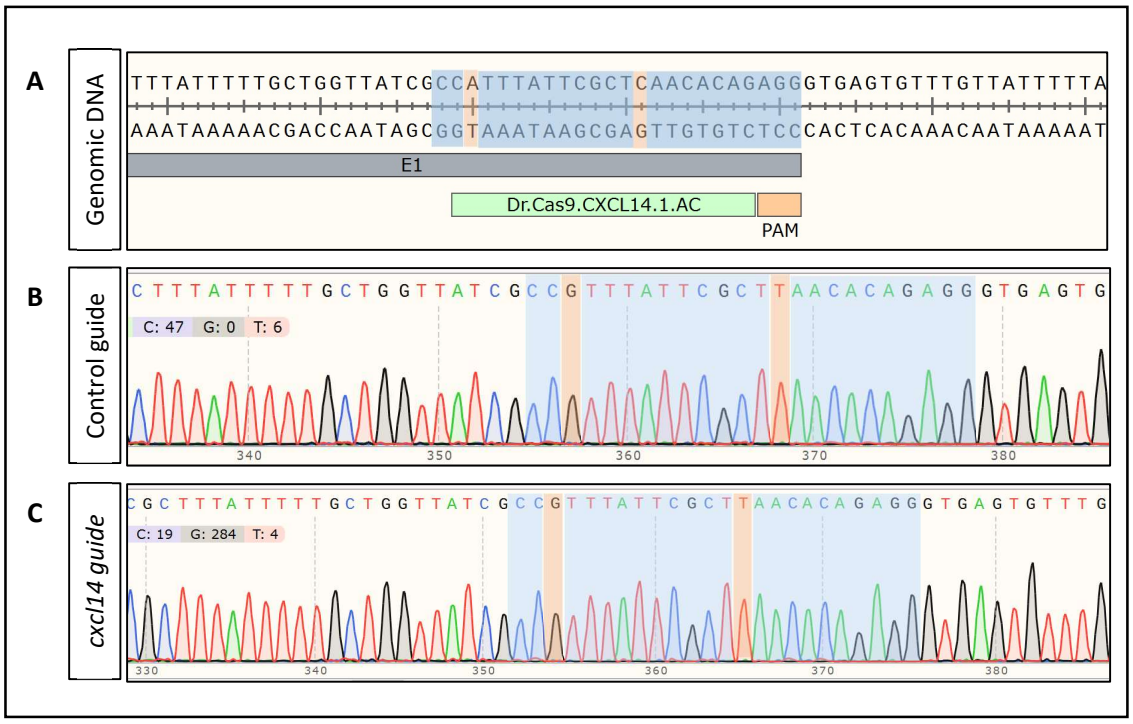

Figure 39. SNPs found in the target sequence of the *cxcl14* crRNA. (A) Genomic DNA sequence for the *cxcl14* zebrafish gene (https://www.ensembl.org/index.html). The green rectangle comprises the target sequence recognized by the predesigned crRNA for *cxcl14*. (B) Sanger sequencing of the genomic DNA of zebrafish larvae microinjected with a control crRNA. (C) Sanger sequencing of the genomic DNA of zebrafish larvae microinjected with *cxcl14* crRNA. The lack of mixture of sequences indicates that there was no edition in that region after the crRNA/Cas9 microinjection. The nucleotides highlighted in blue indicate the sequence that is bound by the RNA guide and the nucleotides highlighted in orange correspond to the SNPs that were found.

The knock-down of *ctnnb1* caused morphological abnormalities in *spint1a*$^{+/+}$ and *spint1a*$^{-/-}$ larvae, even when reducing the amount of guide microinjected (Fig. 40A and 40B).

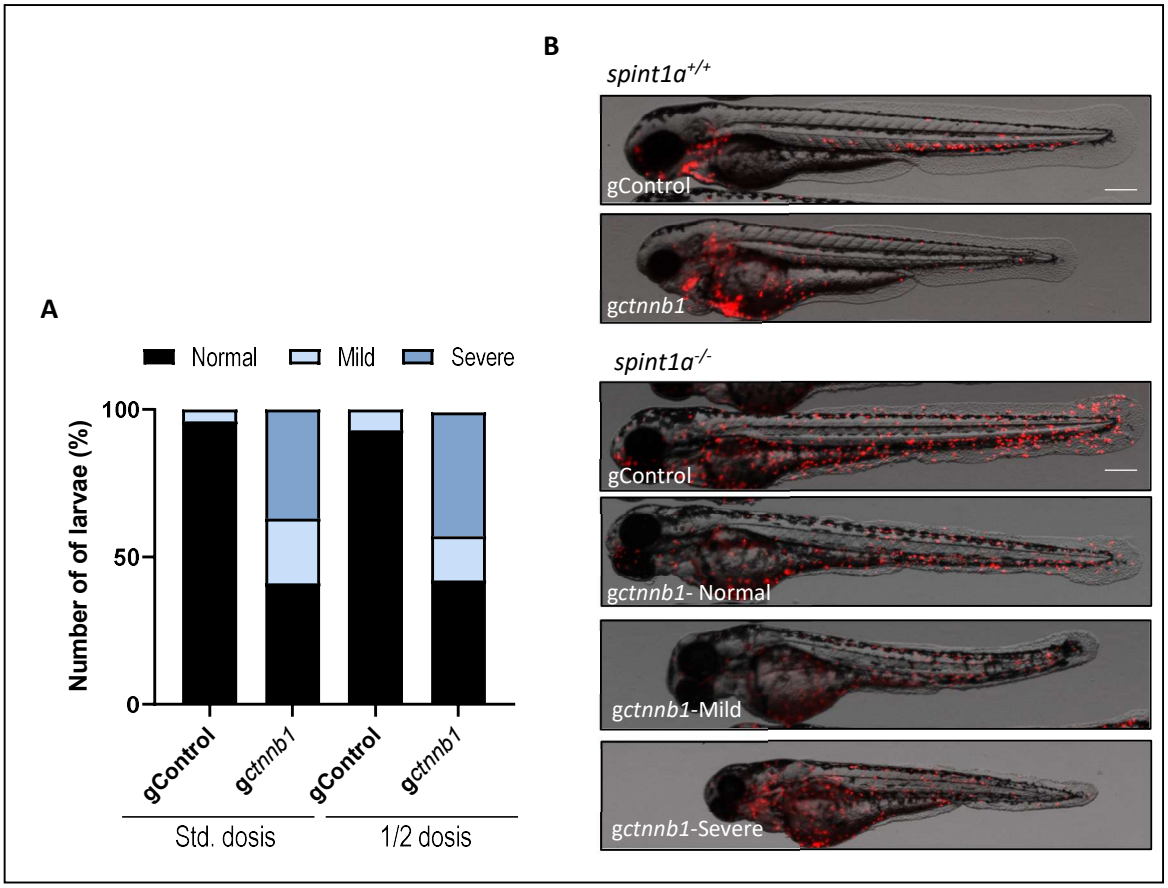

Figure 40. The genetic inhibition of *ctnnb1* gene causes develomental abnormalities in the zebrafish larvae. (A) Quantification of *spint1a*$^{-/-}$ larvae that presented malformations after *ctnnb1* crRNA microinjection. The colors indicate the phenotype of the larvae: normal development (black), mild malformations (light blue) and severe malformations (blue). The guide was microinjected at the standard and half dosis (std. and 1/2, respectively), without obtainig a decrease in the percentage of larvae with malformations. (B) Representative images of wild type (*spint1a*$^{+/+}$) and chronic inflammation larvae (*spint1a*$^{-/-}$) with at 72hpf after microinjection of control or *ctnnb1* crRNAs (gControl and *gctnnb1*). Merged bright field and red fluoresecent channel are shown, where neutrophils are shown in red. Scale bar= 200 µm.

The crRNAs targeting *socs2*, *rps6ka1* and *cnntb1* successfully edited the target loci (Fig. 41A-C). In the case of the guide targeting *pfas*, although it was editing the locus with a high efficacy (84,5%), the main modification was a deletion of three nucleotides, which does not change the reading frame of the gene and most likely fails to alter the protein function (Fig. 41A). Nevertheless, the *socs2* and *rps6ka1* crRNAs showed a high efficacy of edition and properly insertion/ deletion positions (Fig. 41B and 41C).

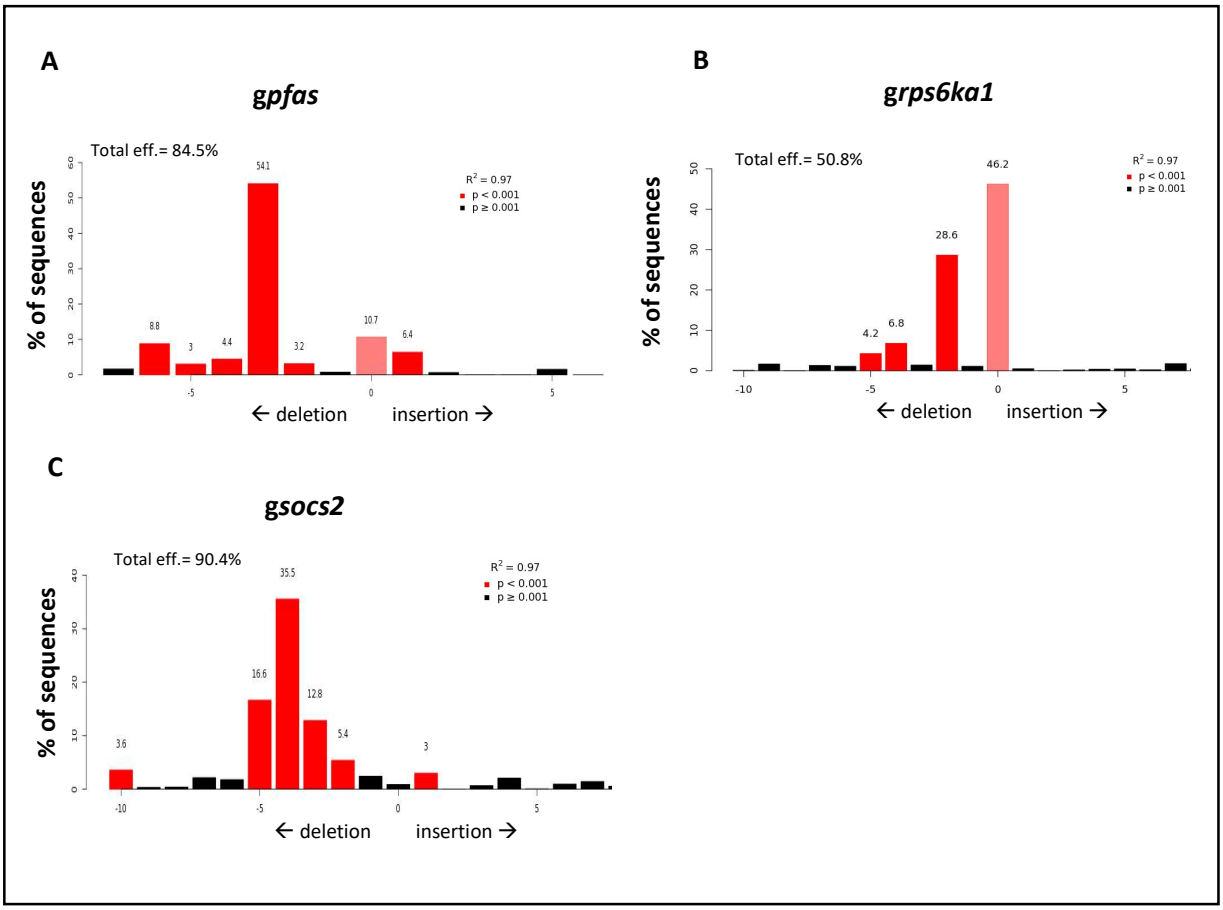

Figure 41. Efficiency of CRISPR-Cas9 targeting *pfas*, *rps6ka1* and *socs2*. Graphs showing the efficacy of edition for each crRNA (total eff.) and percetange and position of insertions and deletions found in the target sequence. The analysis was performed using the TIDE software (https://tide.nki.nl/) after uploading the sanger sequencing data from samples microinjected with gControl or the targeted crRNAs (g*pfas*, g*rps6ka1* or g*socs2*).

Lastly, the microinjection of *pfas*, *socs2* or *rps6ka1* crRNAs alone did not impair the reduction in the inflammation caused by oxamate. The number of aggregates in both control and the edited larvae treated with oxamate was similarly reduced compared to the untreated ones (Fig. 42A and 42B).

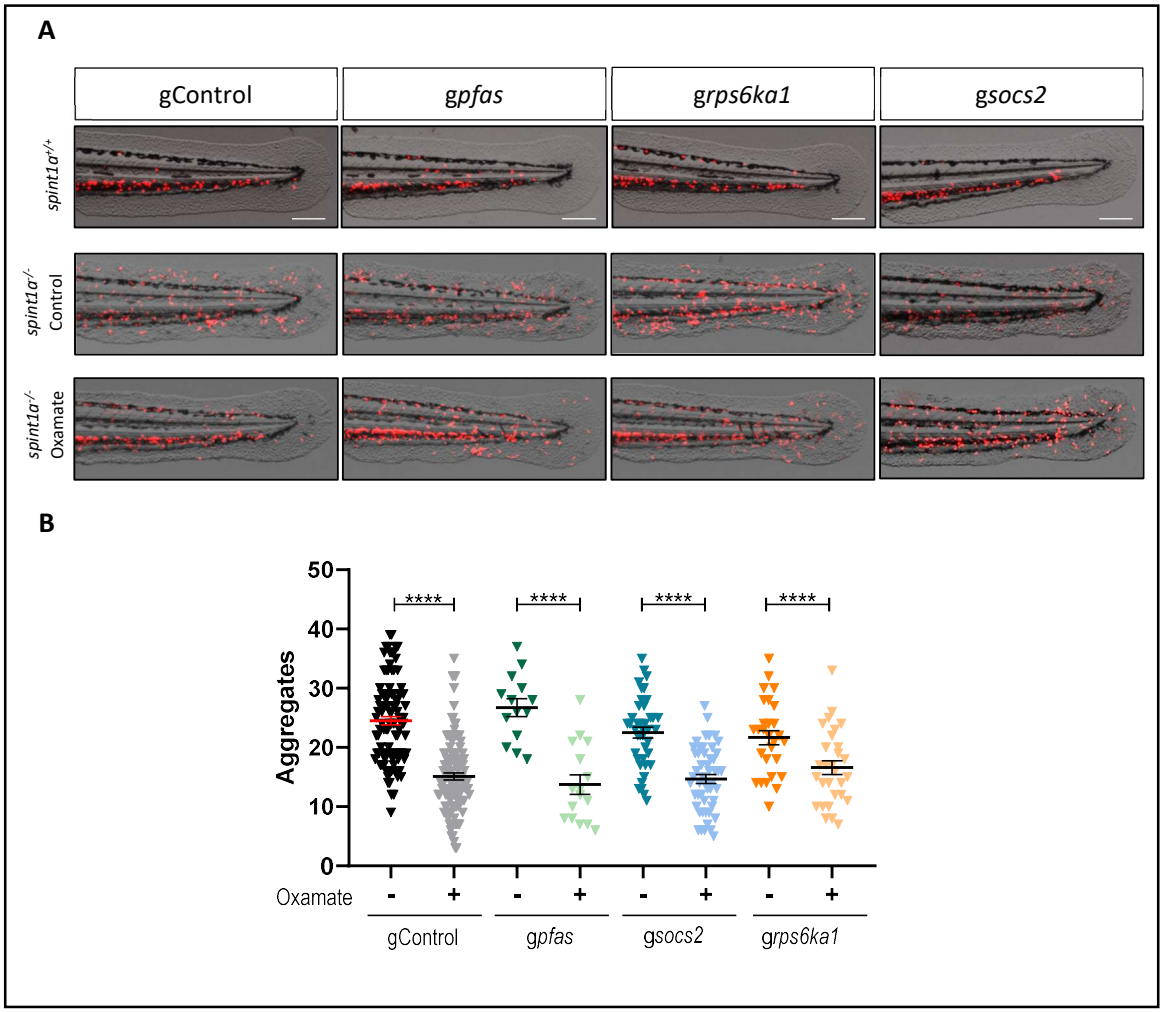

Figure 42. (A) Representative images of the tail of zebrafish larvae microinjected with a control crRNA (gControl) or a crRNA targeting *pfas*, *socs2* or *rps6ka1* (g*pfas*, g*socs2* and g*rps6ka1*) with and without oxamate treatment. Merged bright field and red fluoresecent channel (neutrophils) are shown. Scale bar= 200 µm. (B) Quantification of skin aggregates in the tail of 72hpf *spint1a*$^{-/-}$ larvae after guide microinjection and treatment with oxamate. Mean ± S.E.M. is shown for each group and each dot represents a larvae. P values were calculated using Brown-Forsythe and Welch's ANOVA tests followed by Unpaired t with Welch's correction test ****p≤0.0001.

3.14. *terc*$^{-/-}$ larvae show decreased skin aggregate formation and neutrophil infiltration

So far, we have characterized the effect of lactate modulation in a model of skin chronic inflammation, stablishing that the decrease in lactate production is able to ameliorate the inflammation. Since *terc* levels change the transcription of one of the genes coding for *ldh* in the zebrafish (Fig. 20), we decided to explore if *terc* expression could also affect the levels of inflammation in the *spint1a*$^{-/-}$ model.

In order to accomplish that, we used CRISPR-Cas9 edition technology against the *spint1a* gene to induce the skin chronic inflammation condition in wild type and *terc*$^{-/-}$ larvae. The *terc*$^{-/-}$ larvae were obtained by the breeding of *terc*$^{-/-}$ fish and they show barely any *terc* expression (Fig. 43A) and decreased neutrophil number, as expected[21] (Fig. 43B and 43C). The number of neutrophils was quantified with a Sudan black staining. Sudan black stains neutrophils specifically and they can be seen as black cells in the larvae (Fig. 43C).

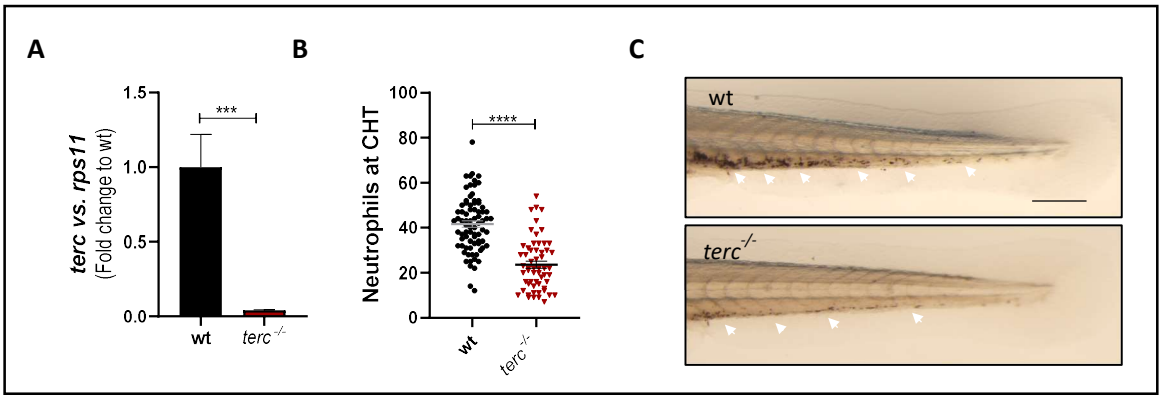

Figure 43. *terc*$^{-/-}$ larvae have reduced neutrophil number. (A) RT-qPCR of wild type and *terc*$^{-/-}$ 72 hpf larvae showing the *terc* expression. Mean ± S.E.M. is shown. (B) Neutrophil cuantificaction in the caudal hematopoietic tissue (CHT) of wild type and *terc*$^{-/-}$ 72 hpf larvae. Each dot represents a larvae. Mean ± S.E.M. is shown. (C) Representative birghtfield images of the Sudan black neutrophil staining. Neutrophils can be seen as black dots in the CHT (white arrowheads). The staining was performed in wild type larvae and *terc*$^{-/-}$ larvae. Scale bar= 200 µm. P values were calculated using Man-Whitney test, ***p≤0.001, ****p≤0.0001.

Interestingly, *terc*/*spint1a*-deficient larvae showed reduced keratinocyte aggregate numbers and neutrophil dispersion than *terc* wild type larvae (Fig. 44A-D). Moreover, the same experiment was repeated with *tert*$^{-/-}$ larvae, and they showed no differences in the aggregate formation (Fig. 44E and 44F), indicating that the reduction in the aggregate number in the *terc*$^{-/-}$ larvae seemed to be independent of telomerase function and telomere length.

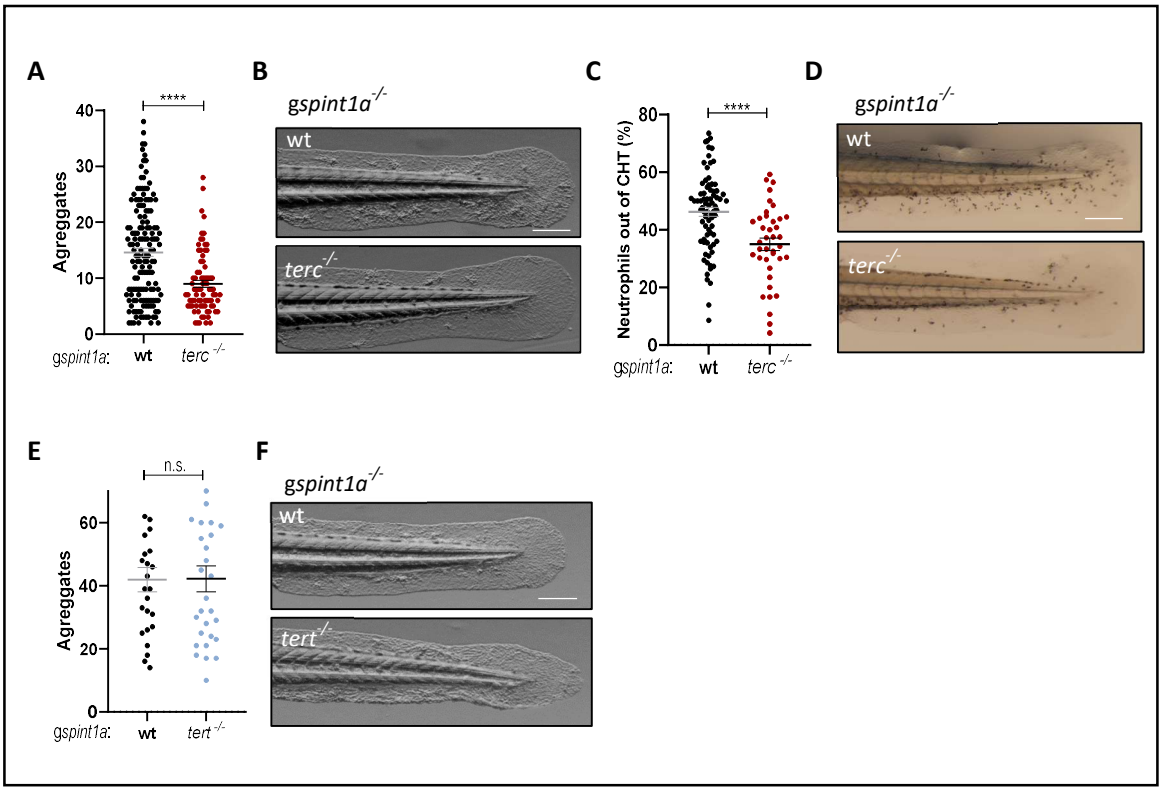

Figure 44. *terc/spint1a*-deficient larvae have reduced aggregate number and neutrophil dispersion independently of Tert. (A and E) Quantification of skin aggregates in the tail of 72hpf wild type and *terc*$^{-/-}$ or *tert*$^{-/-}$ larvae after *spint1a* crRNA microinjection (g*spint1a*). Mean ± S.E.M. is shown for each group and each dot represents a larvae. (B and F) Representative brightfield images showing aggregates in the tail of wild type and *terc*$^{-/-}$ or *tert*$^{-/-}$. Scale bar= 200 µm. (C) Quantification of neutrophil dispersion out of the CHT in the tail of 72hpf larvae. Mean ± S.E.M. is shown for each group and each dot represents a larvae. (D) Representative birghtfield images of the Sudan black neutrophil staining. Neutrophils can be seen as black dots in the larvae. Scale bar= 200 µm. P values were calculated using Man-Whitney test, n.s.: not significant,****p≤0.0001.

PART 2

terc inhibits glioblastoma growth by activating antitumor innate immunity

3.15. *terc* overexpression in the hematopoietic lineage reduces glioblastoma tumor size independently of *tert* expression

Considering that both the metabolomic and gene expression results pointed out to a regulation of the glycolytic metabolism by *terc* (Fig. 19, 20A and 21C), we hypothesized that those metabolic changes could be affecting the function of the immune cells in the zebrafish. We then decided to test the effects of *terc* overexpression in the blood cells in a zebrafish cancer model. That way, we could track *in vivo* tumor development and the immune response.

We used a model of glioblastoma since the development and size of the tumor can be easily detected and measured, and the immune response in this type of cancer is especially relevant for the cancer progression. To generate the glioblastoma, we used the transgenic line *zic:Gal4*; *UAS:mCherry* (*zic*:Gal4 for simplicity) and the *UAS:GFP-HRAS_G12V* plasmid. The *zic*:Gal4 fish have the brain and notochord labelled with the red fluorescent protein mCherry. The microinjection of the UAS:GFP-*HRAS_G12V* construction in those fish leads to the expression of oncogenic *HRAS_G12V* in the brain and nervous tissue . Since the green fluorescent protein GFP is fused to the HRAS_G12V, the tumor can be directly observed because of its green fluorescence.

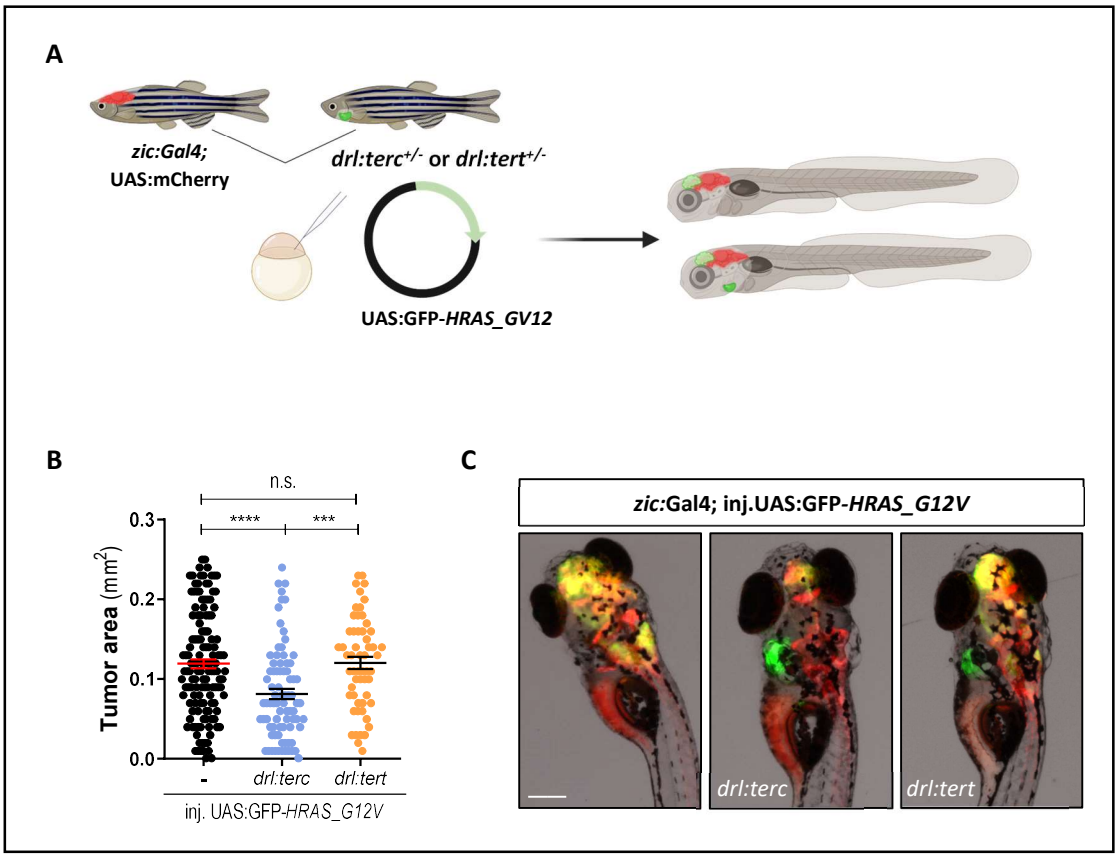

Figure 45. The overexpression of *terc* in the hematopoietic lineage decreases glioblastoma tumor size. (A) Schematic representation of the glioblastoma generation in wild type, *drl:terc* and *drl:tert* larvae. Created with BioRender.com. (B) Tumor size quantification in 7 dpf larvae. Mean ± S.E.M is shown for each group and ach dot represents a larvae. (C) Representative images of the tumor size in the larvae. Merged brightfield, red and green fluorescent channels are shown. The brain is seen in red while the heart of the *drl:terc* and *drl:tert* larvae is seen in green. The glioblastoma is shown in yellow due to the colocalization of red fluorescence signal from the brain and the green signal from the tumor (GFP-HRAS_G12V-expressing tissue). Scale bar= 200 µm. P values were calculated using Brown-Forsythe and Welch's ANOVA tests followed by Games-Howell's multiple comparisons test, n.s.: not significant,***p≤0.001, ****p≤0.0001

The offspring of the *drl:terc*$^{+/-}$ and the *zic:Gal4* fish was microinjected with the *UAS:GFP-HRAS_G12V* plasmid to obtain both the larvae with glioblastoma (control) and larvae with glioblastoma and *terc* overexpression in the hematopoietic lineage (Fig. 45A). The *drl:terc* fish can be differentiated from the wild type fish since they have a fluorescent reporter gene that results in the GFP expression in the heart (green heart). After the oncogene microinjection, the tumor area was measured in 7 dpf larvae. Surprisingly, the tumor area of the *drl:terc* fish was significantly reduced compared to control larvae (Fig. 45B and 45C). Furthermore, the same experiment was repeated this time with *drl:tert*$^{+/-}$ fish (overexpression of the catalytic subunit of telomerase in the hematopoietic linage), and no tumor growth changes were observed (Fig. 45B and 45C). These results indicated that the decrease in tumor size seemed to be specific to *terc* overexpression in the hematopoietic cells.

3.16. *terc* overexpression in the hematopoietic lineage increased the number of glioblastoma-recruited neutrophils

Since increased *terc* levels leads to increased neutrophils and macrophages[21], we first studied if there were changes in the number of those cells around the tumor. The reduction in the tumor size could be explained in that case as a result of an increase in the number of immune cells instead of a better response of the immune cells.

To study the neutrophil number around the tumor area, a Sudan black staining was performed. The number of neutrophils in the head of *drl:terc* fish was similar to wild type fish (Fig. 46A and 46B). Although *drl:terc* fish have increased number of neutrophils, those are predominantly localized in the caudal hematopoietic tissue (CHT) of the larvae, so the number of circulating neutrophils number may not be altered. Interestingly, there was a significant increase in the number of neutrophils in the head of the *drl:terc* larvae with glioblastoma (Fig. 46A and 46B). However, due to the limitations of this technique, we could not confirm if those neutrophils were just around the tumor or if they were indeed infiltrating the tumor.

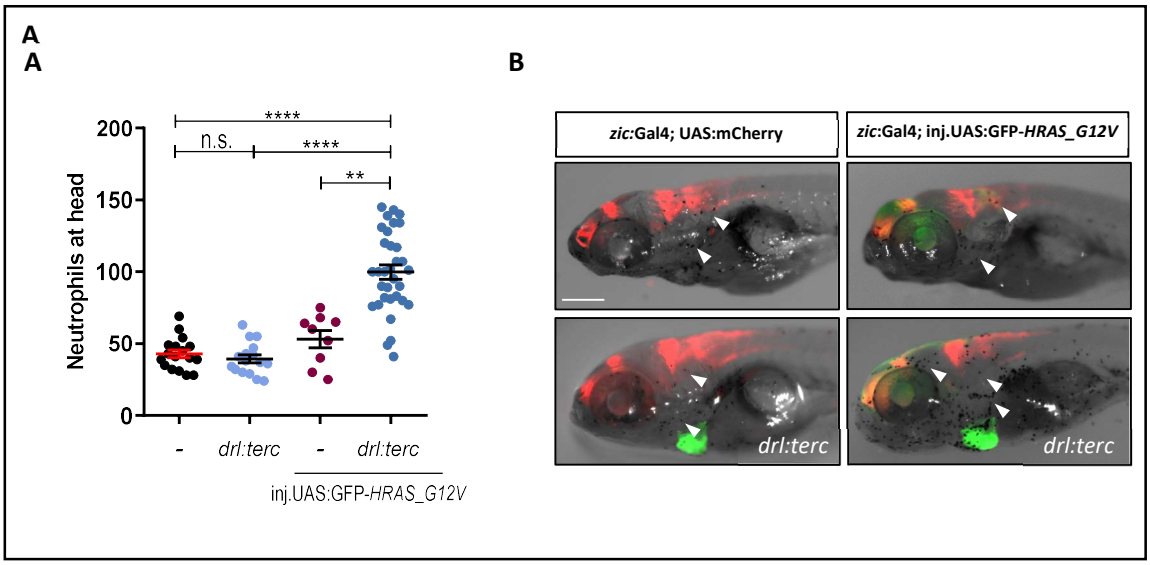

Figure 46. *drl:terc* larvae with glioblastoma have increased number of neutrophils in the head. (A) Quantification of the neutrophils in the head of the 7 dpf larvae. Mean ± S.E.M is shown and each dot represents a larvae. (B) Representative images of the sudan black neutrophil staining. Merged brightfield, red and green fluorescent channels are shown. Neutrohpils can be seen as black dots in the larvae (white arrowheads). The staining was performed in control larvae (*zic:*Gal4 and *drl:terc*) and larvae with glioblastoma (inj. UAS:GFP-*HRAS_G12V*). Scale bar= 200 µm. P values were calculated using Kruskal-Wallis test followed by Dunn's multiple comparisons test, n.s.: not significant,**p≤ 0.01, ****p≤0.0001.

3.17. Neutrophil migration to wound is not altered in larvae overexpressing *terc* in the hematopoietic lineage

Since the number of neutrophils in the head only increased in *drl:terc* larvae upon tumor development, we investigated if neutrophil recruitment improved in those fish compared to the wild type ones. To study neutrophil migration, we used the transgenic zebrafish line *mpx:eGFP*, in which neutrophils can be tracked *in vivo* due to its green fluorescence. The *drl:terc* and *mpx:eGFP* fish were bred to obtain larvae with *terc*-overexpressing and green fluorescent neutrophils. The recruitment assay was performed in 3 dpf larvae, using *mpx*:*eGFP* larvae as the wild type control. The complete transection of the tail was performed to follow up neutrophil migration to the wound from 1 to 8 hours post wounding (hpw) (Fig. 47A). In both groups the peak of migration was observed at 4 hpw and no differences in the number nor the migration pattern of the *drl:terc* neutrophils was detected (Fig. 47B and 47C).

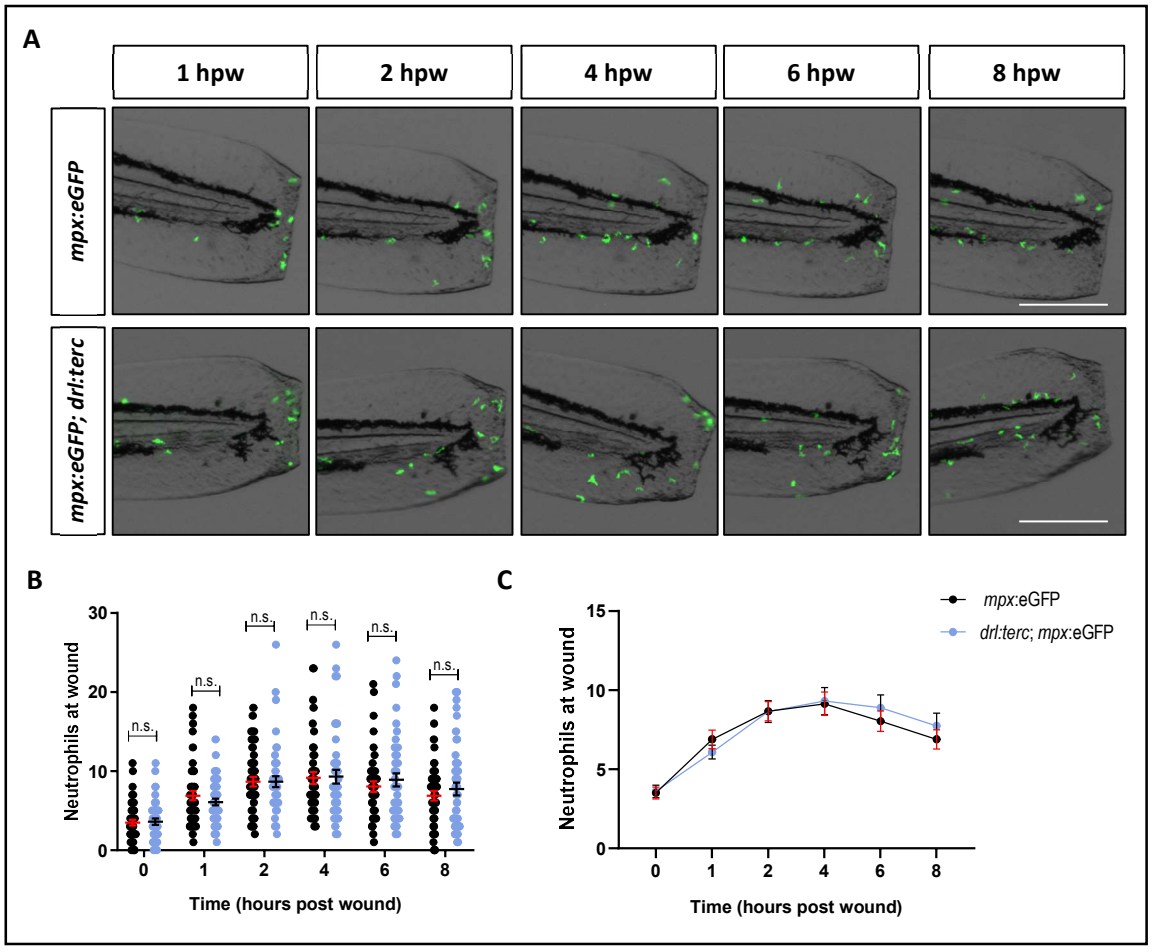

Figure 47. Neutrophil migration is not altered in *drl:terc* larvae. (A) Representative images of the neutrophil migration assay in 3dpf control (*mpx*:eGFP) and *drl:terc* larvae (*mpx*:eGFP*; drl:terc*). Merged brightfield and green fluorescent channel are shown. Neutrophils in both groups are shown green. Scale bar= 200µm. (B) Quantification of the number of neutrophils at the wound area. Mean ± S.E.M is shown for each group and each dot represents a larvae. (C) Migration kinetics of control and *drl:terc* larvae. Mean ± S.E.M is shown for each group. P values were calculated using two-way ANOVA with Geisser-Greenhouse correction followed by Sidak's multiple comparisons test, n.s.: not significant.

3.18. The microglia number is not affected in larvae overexpressing *terc* in the hematopoietic lineage

We then focused on studying the tissue-specific brain macrophages (microglia). The microglia cells come from primitive macrophages that colonize the brain and are the first immune cells in contact with the glioblastoma.

We performed a whole larva immunostaining to count the number of microglia cells in the brain of *drl:terc* and wild type larvae. Also, *drl:tert* larvae were used as control. The microglia cells were quantified in z-stacks images of the brain of the larvae using a specific ImageJ software plugin. We found that there were no changes in the number of cells in the *drl:terc* larvae compared to the wild type ones (Fig. 48A and 48B). Moreover, the number of microglia cells in the larvae with glioblastoma was no different in the wild type and *drl:*terc or *drl:tert* larvae (Fig. 48A and 48C).

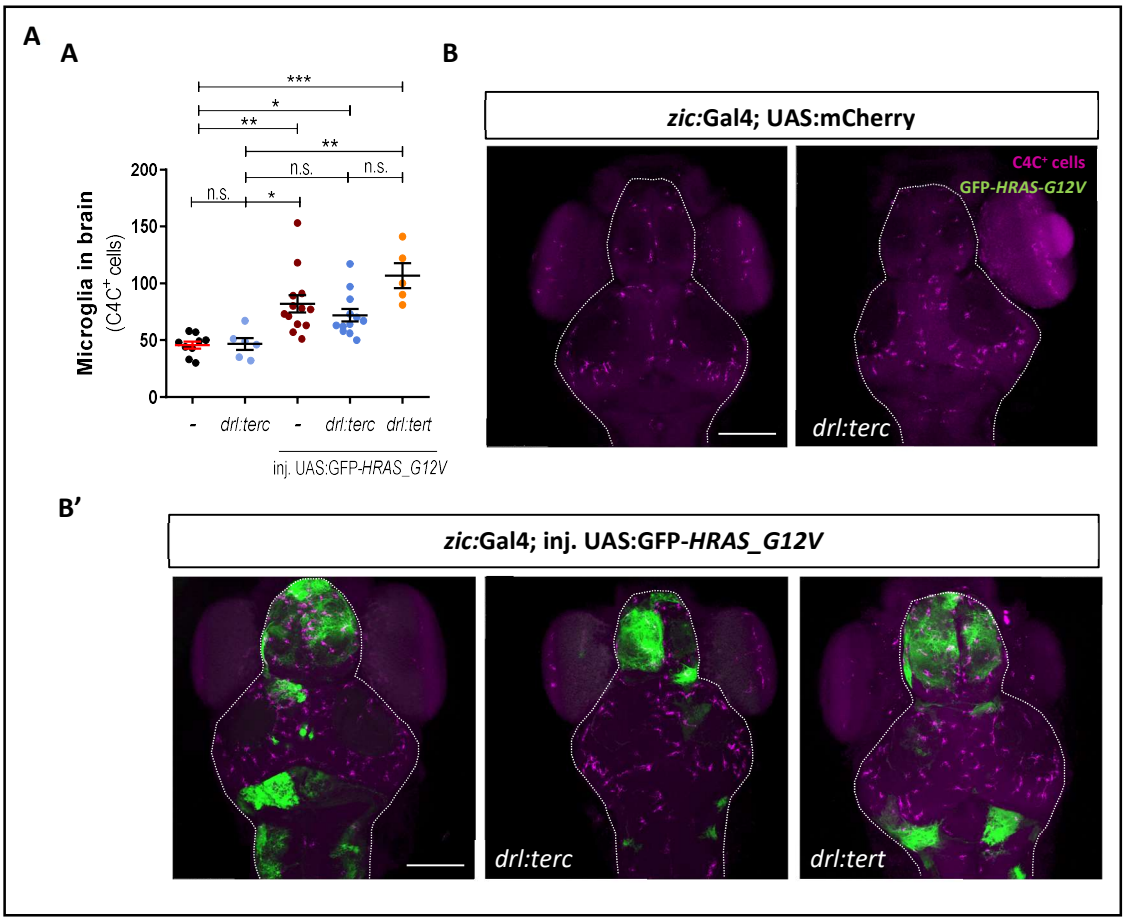

Figure 48. The number of microglial cells is not affected in *drl:terc* larvae. (A) Quantification of the number of microglial cells in the brain of 7 dpf larvae. Mean ± S.E.M is shown for each group and each dot represents a larvae. (B and B') Representative confocal images of the microglia immunostaining in whole larvae. The microglia cells are shown in magenta ($C4C^+$ cells) and the tumor tissue is shown in green (GFP-*HRAS_G12V*). The brain (quantification area) is inside the white dotted line. All images represent maximum intensity projections of confocal stacks. Scale bar= 198 µm. P values were calculated using Kruskal-Wallis test followed by Dunn's multiple comparisons test, n.s.: not significant, * p≤0.05, **p≤ 0.01, ***p≤0.001.

3.19. *terc* expression does not affect macrophage polarization in response to bacterial infection

Macrophages can be classified in different stages depending on their activity. The M0 state corresponds to resting macrophages while activated macrophages are categorized into two groups: M1 if they are performing pro-inflammatory functions or M2 if they have anti-inflammatory roles. It is also known that those changes in the state of activated macrophages (from M1 to M2 or vice versa) are linked to modifications in their energy metabolism. M1 macrophages rely more on an incomplete glycolysis to obtain energy, whereas M2 macrophages tend to obtain ATP through the complete oxidative phosphorylation of glucose. We hypothesized that if the *terc*-overexpressing cells from the macrophage lineage were experimenting changes in their metabolism, there should be also changes in their polarization status.

To identify changes in polarization *in vivo*, we used the *mpeg1:*mCherry; *tnfa*:*eGFP* zebrafish line. We can detect macrophages in these larvae due to their red fluorescence. Besides, since M1 macrophages start expressing Tnfa, due to the *tnfa*:*eGFP* reporter, they become doble fluorescent (red and green positive cells). Hence, we can detect M2 macrophages based on their red fluorescence and M1 macrophages based on the number of doble positive cells for red and green.

In order to induce the M1 polarization and also to follow the macrophage recruitment, 2 dpf larvae were locally infected in the otic vesicle with *Salmonella* Thyphimurium (ST). The *terc*-overexpressing larvae were obtained by microinjecting the *terc* RNA into the *mpeg1:*mCherry; *tnfa*:*eGFP* embryos. Also, a control RNA was microinjected. Images of the site of infection were taken 4 and 6 hours post infection (hpi), when the peak of recruitment is reached. Unfortunately, although the recruited macrophages were polarized, individual cells could not be counted in the infection area (Fig. 49A). Thus, the number of polarized cells was quantified based on the ratio between the green and the red fluorescent signal in the otic vesicle. In the analyzed time points after the infection, no changes in polarization were observed in the *terc*-microinjected larvae versus the control larvae (Fig. 49B and 49C).

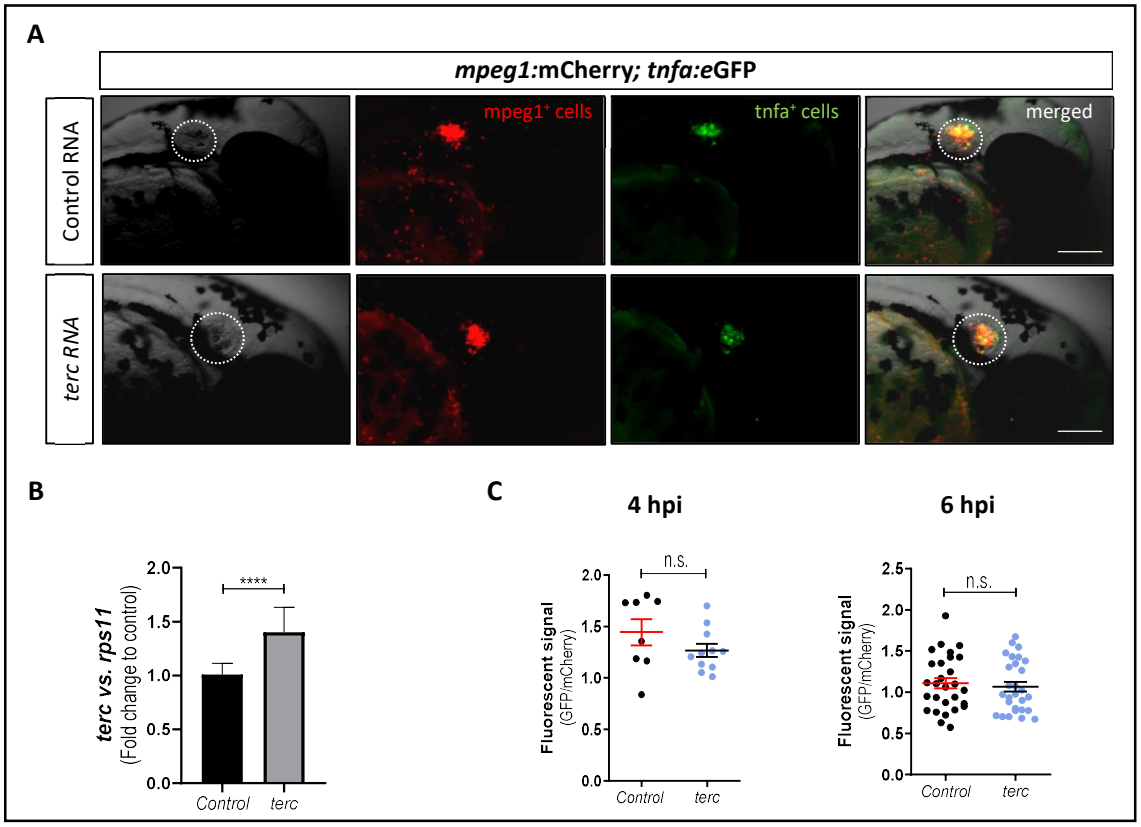

Figure49. *terc* overexpression does not modify macrophage polarization. (A) Representative images of 2 dpf larvae infected with ST in the otic vesicle (white dotted line) at 6 hours post infection (hpi). Macrofages are shown in red (mpeg1$^+$ cells) while polarized M1 macrophages are shown in geen (tnfa$^+$ cells). Scale bar= 198 µm. (B) RT-qPCR of *terc* showing *terc* overexpression in the *terc*-microinjected larvae. Mean ± S.E.M is shown. (C) Polarized M1 macrophage quantification. The ratio between the green and the red fluorescent intensity was calculated in the otic vesicle area at 4 and 6 hpi. Mean ± S.E.M is shown for each group and each dot represents a larvae. P values were calculated using Man-Whitney test, n.s.: not significant,****p≤0.0001.

Lastly, with the aim of counting individual polarized macrophages, we decided to do a systemic infection in the *mpeg1:*mCherry; *tnfa*:*eGFP* larvae and analyze the macrophage populations through flow cytometry. First, we manipualted *terc* levels by microinjecting the larvae with the *terc* RNA or the *terc* morpholino. Two dpf larvae were infected with ST in the duct of Cuvier and six hours post infection, the larvae were processed to obtain a cell suspension (Fig. 50A). Cells were fixed in 0.5% PFA and kept in PBS at 4ºC until the next day, when they were analyzed through FACS. In the flow cytometry analysis, the population of mCherry positive cells was detected and the number of doble positive cells for mCherry and GFP was quantified (Fig. 50B, 50D and 50G). Also, the GFP signal intensity was measured as a way of detecting differences in *tnfa* expression in the M1 macrophages (Fig. 50C, 50E and 50H). Neither the increase nor the decrease in *terc* expression resulted in significant changes in the percentage of polarized M1 macrophages (Fig. 50G) nor in the *tnfa* levels measured through the GFP signal intensity (Fig. 50H).

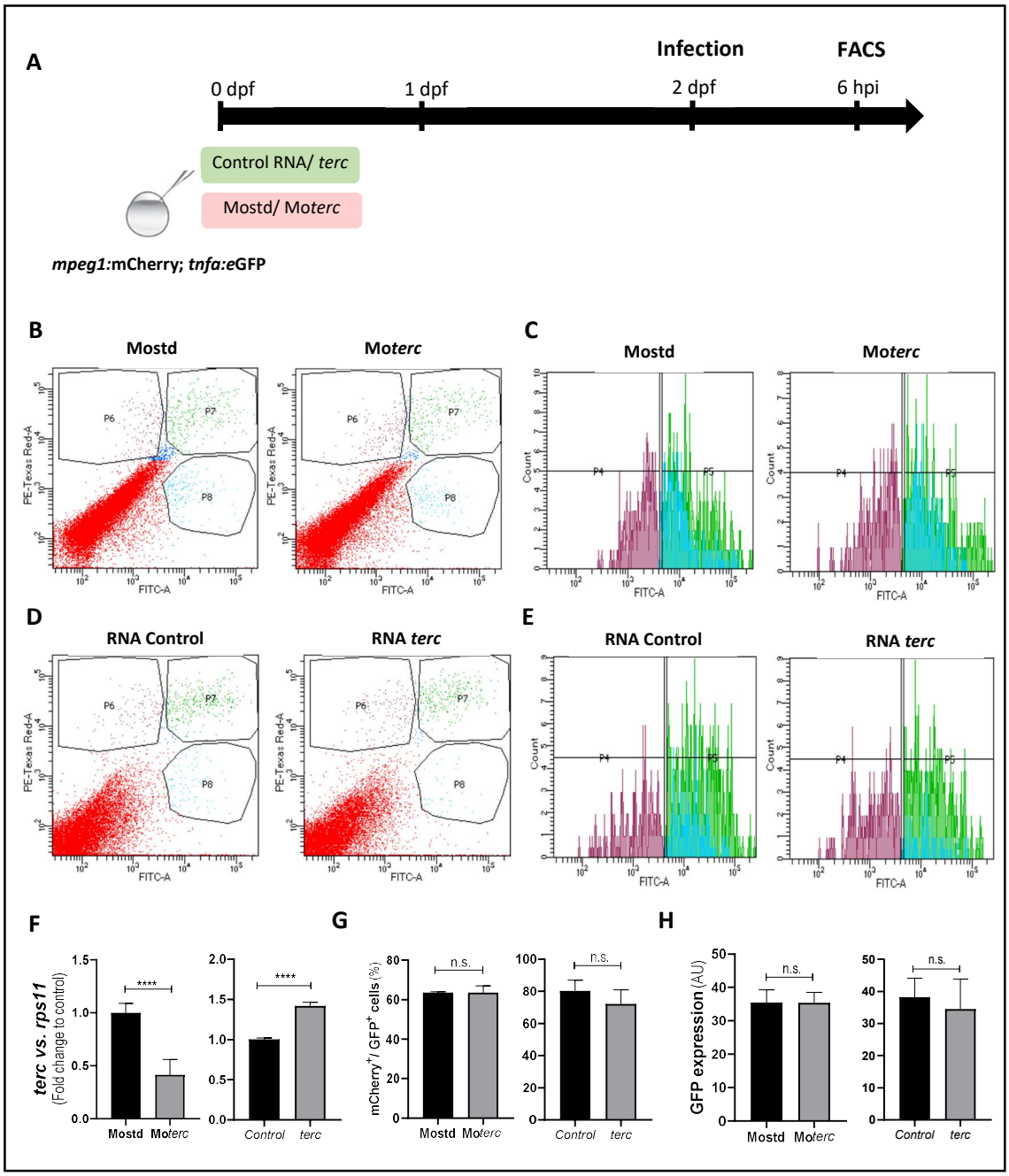

Figure 50. *terc* expression does not affect macrophage polarization. (A) Schematic representation of the infection protocol in larvae with *terc* downregulation or overexpression. (B and D) Dot plots of the fluorescent cell populations in the infected larvae obtained through flow cytometry analysis. The red versus the green fluorescent signal is represented and each dot represents a cell. The red population outside the limited areas corresponds to the background autofluorescent signal. The P6 population in magenta are mpeg$^+$ cells only (M2 macrophages) while the P7 population in green are *mpeg1*$^+$/*tnfa*$^+$ cells (M1 macrophages). The P8 population in light blue are tnfa$^+$ cells only. (C and E) Histograms of the GFP intensity signal in the cells of P6, P7 and P8 populations. The peaks at the right of the graph indicate GFP expression (P7 and P8) while the ones in the left indicate no GFP expression (P6). (F) RT-qPCR of *terc* showing *terc* downregulation or overexpression in the microinjected larvae. (G) Quantification of the percentage of M1 macrophages (*mpeg1*$^+$/*tnfa*$^+$ cells) over the total number of macrophages (mpeg$^+$ cells). (H) Quantification of the mean GFP intensity signal in the P7 population. (F, G and H) Mean ± S.E.M is shown in each graph. P values were calculated using Man-Whitney test, n.s.: not significant,****p≤0.0001.

The same experiment was repeated this time breeding the *mpeg1:*mCherry; *tnfa*:*eGFP* fish with *drl:terc* fish to obtain *terc* overexpression specifically in the hematopoietic cells (including macrophages). The infection experiment was performed as described above, but selecting after the infection the doble positive larvae for *mpeg1:*mCherry; *tnfa*:*eGFP* and triple positive larvae for *mpeg1:*mCherry; *tnfa*:*eGFP* and green heart (*drl:terc*) (Fig. 51A). Yet again, no differences were found in the percentage of polarized M1 macrophages (Fig. 51B and 51E) nor in TNFα expression (Fig. 51C and 51F).

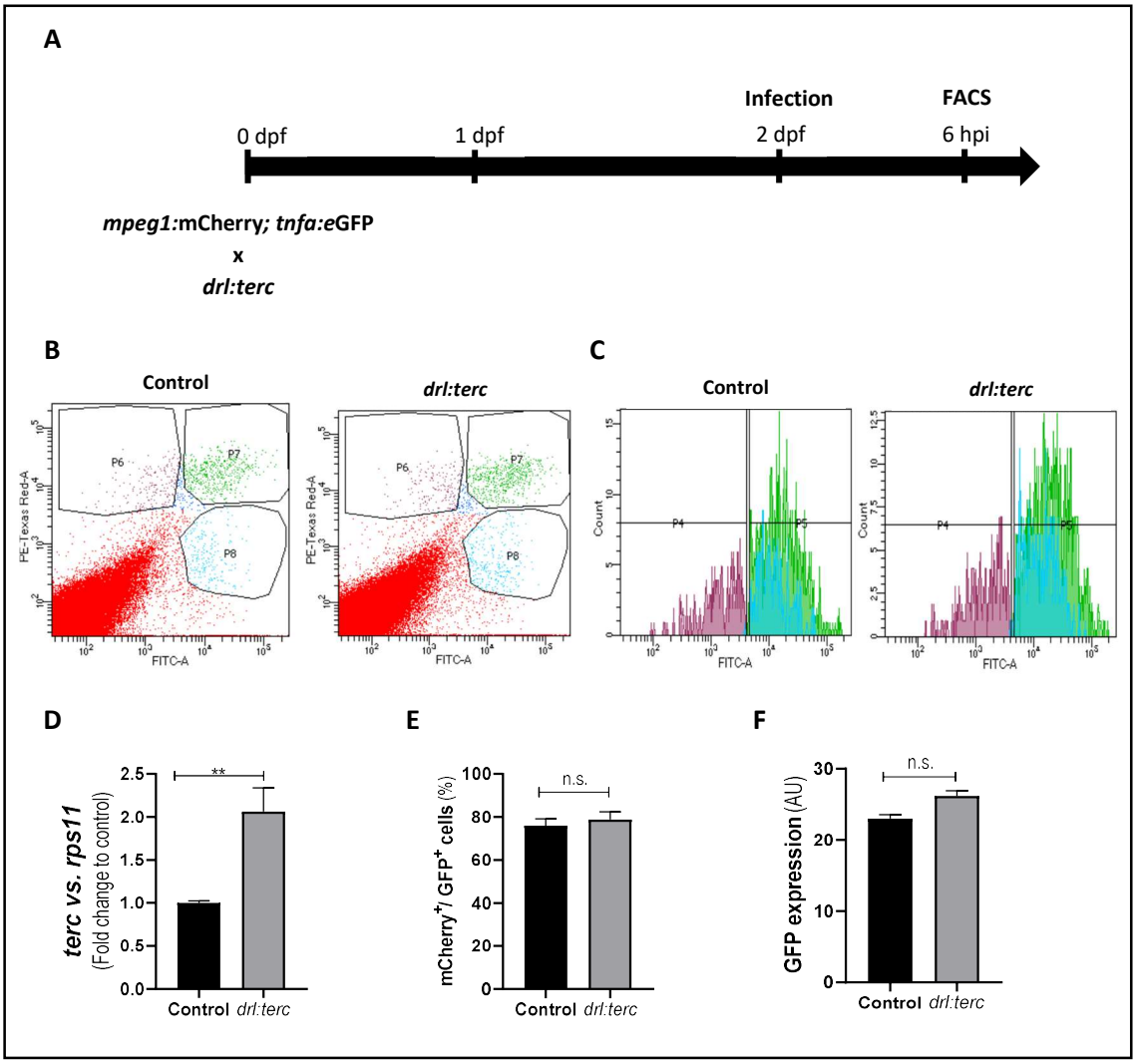

Figure 51. *terc* overexpression in hematopoietic cells does not alter macrophage polarization. (A) Schematic representation of the infection protocol in wild type and *drl:terc* larvae. (B) Dot plots of the fluorescent cell populations in the infected larvae obtained through flow cytometry analysis. The red versus the green fluorescent signal is represented and each dot represents a cell. The red population outside the limited areas corresponds to the background autofluorescent signal. The P6 population in magenta are *mpeg1*$^{+}$ cells only (M2 macrophages) while the P7 population in green are *mpeg1*$^{+/}$*tnfa*$^{+}$ cells (M1 macrophages). The P8 population in light blue are tnfa^{+} cells only. (C) Histograms of the GFP intensity signal in the cells of P6, P7 and P8 populations. The peaks at the right of the graph indicate GFP expression (P7 and P8) while the ones in the left indicate no GFP expression (P6). (D) RT-qPCR of *terc* showing *terc* overexpression in *drl:terc* larvae. (E) Quantification of the percentage of M1 macrophages (*mpeg1*$^{+}$/*tnfa*$^{+}$ cells) over the total number of macrophages (*mpeg1*$^{+}$ cells). (F) Quantification of the mean GFP intensity signal in the P7 population. (D, E and F). Mean ± S.E.M is shown in each graph. P values were calculated using Man-Whitney test, n.s.: not significant,**p≤0.01.

4. Discussion

The telomerase RNA is known to have extracurricular functions independently of telomere lengthening activity. In our laboratory we have described an extracurricular function for *terc* regulating myelopoiesis by binding though a specific consensus sequence at the promoter region of the main myelopoiesis regulatory genes, *SPI1* and *CSF3*, and recruiting RNA polymerase II to initiate their transcription[21; 47].

It has been reported that the *terc*-binding motif is present in more than 2000 loci in the whole human genome, indicating that it could be regulating the transcription of many other genes[37]. In addition, there are also many identified lncRNAs involved in the regulation of the glucose metabolism, such as lncRNA-UCA1[242; 255], which increases the expression of hexokinase 2 (HK2) or lncRNA-AC020978, which is expressed under hypoxic conditions and increases the expression of several glycolytic enzymes[256].

Considering all the above, we decided to test if *terc* expression could be affecting the glucose metabolite composition by performing a metabolomic analysis in zebrafish larvae upon manipulation of *terc* expression. Our results provide the first evidence of telomerase RNA regulating the glucose metabolism. We found that the concentration of several metabolites related to glycolysis and the TCA cycle changed according to *terc* expression. One of the most salient metabolite changes was found to be in lactate, which increased when reducing *terc* expression and decreased upon *terc* overexpression. We found the consensus *terc*-binding sequence (*terc*bs) at the promoter region of *ldhbb* gene and demonstrated that *terc* expression was able to regulate the expression of *ldhbb* though its promoter region. We also show that the regulation of *ldhbb* by *terc* not only occurred in the zebrafish larvae, but also in the adult hematopoietic tissue, the kidney marrow. To further characterize this regulation, an additional *in vivo* luciferase experiment should be performed by mutating the consensus *terc*-binding sequence at the *ldhbb* promoter. Moreover, a Chromatin Isolation by RNA Purification (ChIRP) assay would be key to detect *terc* RNA bound at this promoter region.

Once established this regulation, we aimed at studying the impact of *terc* expression in two different disease models in which lactate has an important immunomodulatory function, first focusing on a model of skin chronic inflammation. Due to the relationship between the glucose metabolism and cell proliferation, the regulation of glucose uptake and use by the cell have been widely studied in the progression of chronic inflammatory diseases that are linked to cell hyperproliferation such as psoriasis[160]. For instance, inhibition of the main glucose transporter GLUT1 has been shown to have a positive effect reducing keratinocyte hyperproliferation and inflammation in zebrafish, mouse, and human psoriatic skin[165-167].

Besides cell proliferation, the way glucose is metabolized by the cell creates a specific metabolite composition that directly and indirectly regulates gene expression and cell function. Some key glucose-derived metabolites have been identified to have this signaling and regulatory functions[57; 257]. Specifically, lactate has been described as one of those metabolites, and it has been reported to have immunomodulatory functions[128; 169; 170].

For that reason, before stablishing the impact of *terc* regulation in chronic inflammation, we decided to characterize the effect of lactate regulation in a model of skin chronic inflammation such as the *spint1a*-deficient zebrafish. This model has a characteristic phenotype of keratinocyte aggregates and neutrophil skin infiltration that makes it a unique model great for drug screening, besides all the other advantages of the work with zebrafish, such as their easy

genetic modification, fast development, and larvae transparency, which enabled us to determine inflammation status in a whole vertebrate *in vivo*.

We found that the inhibition of Ldh by oxamate alleviated the inflammatory phenotype of this model, reducing both the neutrophil infiltration in the skin and the number of skin aggregates, a surrogate of keratinocyte proliferation. Unfortunately, we could not confirm this result through genetic inhibition of *ldha*, *ldhba* or both. As stated before, the presence of other *ldh* isoforms in the zebrafish skin or the impossibility to abrogate completely *ldha* and *ldhba* expression may explain this result. Thus, it would be interesting to generate a skin-specific *ldha* and *ldhba* knock out zebrafish line to confirm whether skin inflammation is impaired or reduced in those fish.

The treatment of the *spint1a*$^{-/-}$ larvae with lactate also alleviated the skin inflammation. This unexpected result led us to hypothesized that not only the production of lactate, but also changes in the NAD^+/NADH balance caused by Ldh regulation could be mediating the recovery of skin homeostasis in the larvae. We demonstrated that the inhibition of Ldh by oxamate and the excess exogenous lactate were in fact decreasing the NAD^+/NADH ratio, as shown in the functional rescue experiments performed and the measurement of NAD^+ and NADH levels in the skin of treated and untreated *spint1a* mutant larvae. The NAD/NADH balance has been previously reported to be essential for the skin inflammation in zebrafish models and patients with psoriasis[158]. Furthermore, our results confirm other studies which have stablished that excess lactate directly contributes to NAD^+/NADH levels in the cell[258; 259].

Although both oxamate and lactate reduced the NAD^+/NADH ratio in the *spint1a*-deficient larvae, when measuring DNA damage and oxidative stress in the treated larvae, we could only see a reduction in H_2O_2 production and pγH2Ax$^+$cells by oxamate. This may be implying that those effects may not only be caused due to changes in the NAD^+/NADH balance but also to a decrease in lactate production by oxamate. Further studies will be required to clarify this issue.

Additionally, we studied the transcriptomic changes caused by oxamate and lactate treatments in the skin of *spint1a*-deficient larvae. Although we focused on studying common regulated genes by the treatments, some of the identified genes were only exclusive of one treatment. On the one hand, these specific genes regulated by oxamate may be interesting to identify key players involved in the oxidative stress and DNA damage responses that may explain the reduction in H_2O_2 production and pγH2Ax$^+$cells seen exclusively with this treatment. On the other hand, the genes regulated by both treatments could be mediating the inflammation alleviation due to their involvement in metabolic, cytokine signaling and proliferation pathways. Some of them (*rps6ka1*, *socs2*, *ctnnb1*, *pfas* or *cxcl14*) were chosen to study *in vivo* their implication in the development of the skin inflammation. Although we could not perform the studies regarding *cxcl14*, *ctnnb1* and *pfas* by different reasons, we could stablish that neither gain- nor loss-of-function of *socs2* and *rps6ka1* were enough to cause changes in the inflammation status of the larvae, pointing out to the complex effects played by lactate metabolism in inflammation.

Besides our studies performed with the *spint1a*$^{-/-}$ zebrafish model, we conducted an exploratory analysis using transcriptomic data from the skin of psoriatic patients available in the GEO database (GDS4602). We found that the transcript levels of *LDHA* and *LDHB* increased in the skin lesions of psoriatic patients. Moreover, the positive correlation found between *LDHA* and *IL1B* expression in the samples could be indicating a role for *LDHA* promoting skin inflammation in the patients.

We also evaluated the expression in the human samples of some of the differentially expressed genes in the skin of the mutant *spint1a* larvae. Overall, not all genes behaved as previously seen in the zebrafish model, such as *RPS6KA1*, *TBXAS1* and *PFAS*. Surprisingly, the mRNA levels of *RPS6KA1*, which was upregulated by both treatments in the zebrafish skin, positively correlated with the mRNA levels of *LDHA* and negatively with *LDHB*. Besides, *RPS6KA1* mRNA levels positively correlated with the expression of the genes encoding the proinflammatory cytokines IL1B and IL17A. *LDHA* is prompt to convert pyruvate into lactate, whereas *LDHB* has the opposite affinity. These transcriptomic results seem to be linking lactate production to *RPS6KA1* expression and an increase in inflammation in the human skin, differing from the results obtained in the zebrafish.

CXCL14, *CTNBB1* and *SOCS2* were found to be downregulated both in the zebrafish and human skin samples. Besides, their expression in zebrafish increased upon treatment with both oxamate and lactate. In addition, *CXCL14* levels correlated negatively with *LDHA, IL1B* and *IL17A*. CXCL14 is relatively new discovered cytokine, and its roles are not well-defined yet[260]. It is known to be produced by a variety of immune cells and skin cells (among others), and it has been found to have antimicrobial and chemoattractant roles[260; 261]. One study has shown a reduction of CXCL14 protein expression in psoriasis lesions[261], and links the lack of this protein to the susceptibility of the patients to bacterial infections. Moreover, other studies also find CXCL14 to have an anti-inflammatory role since its overexpression leads to a decrease in pro-inflammatory cytokines[262]. Therefore, it will be worthy to investigate the relevance of the crosstalk between lactate metabolism and CXCL14 in skin inflammation.

One of the most interesting results of this study is the alleviation of skin inflammation by *terc* deficiency, independently of Tert. *terc* deficiency results in decreased *ldhbb* expression. This gene is mostly expressed in the liver, where it converts lactate to pyruvate. Since *ldhba* is the most expressed Ldh isoform in the zebrafish skin, *terc* deficiency will lead to increased lactate concentrations in the liver due to *ldhbb* reduced expression; however, in the skin, the excess lactate from the liver, can be transformed into pyruvate, decreasing the NAD^+/NADH ratio, which, in turn, will alleviate the oxidative stress and inflammation (Fig. 52).

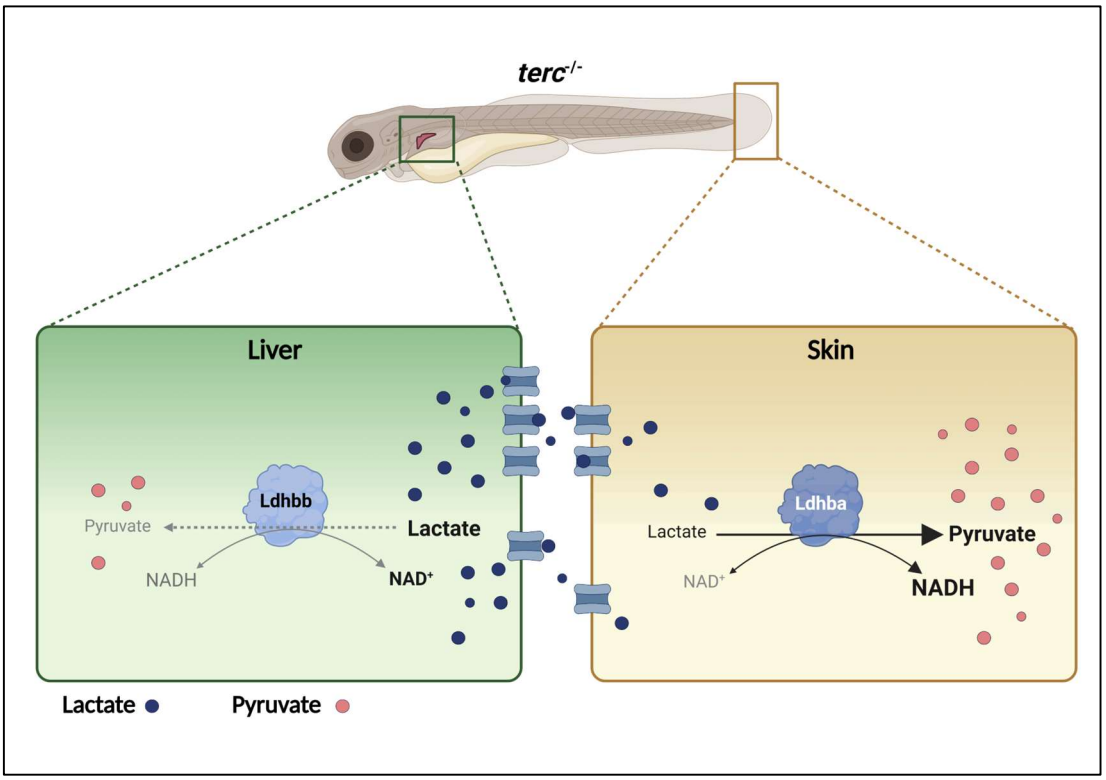

Figure 52. Possible mechanism for skin inflammation alleviation in *terc/spint1a*-deficient larvae. The reduced expression of *ldhbb* in the liver results in lactate accumulation. The excess lactate reaches the skin, where it is converted into pyruvate by *ldhba*. The enzymatic reaction of *ldhba* yields NADH molecules, which reestablish the NAD^+/NADH balance in the inflamed skin.

Besides reporting a novel *terc* non-canonical function modifying lactate production trough regulation of *ldhbb* expression and performing an exploratory analysis on *terc* impact in the development of chronic inflammation in the *spint1a*$^{-/-}$ larvae, we conducted a second study in order to characterize the implications of *terc* overexpression in the immune cells in the context of the tumor immune response. First, we found that overexpression of *terc* in the hematopoietic linage, which results in myelopoiesis activation[47], results in decreased size of the glioblastoma tumor, and this effect was also independent of Tert. When encountering this remarkable result, we looked for the players involved, starting with neutrophils. We have described that *drl:terc* fish have an enhanced myelopoiesis, and thus, an increased number of neutrophils[47]. However, we do not know if the changes found in *ldhbb* expression in *drl:terc* hematopoietic tissue could change their function. Even though we could detect increased neutrophil number around the tumor area (head) in the *drl:terc* fish with glioblastoma, we found that there were no differences in the migration to wound of *terc*-overexpressing versus wild type neutrophils. It is known that glioblastoma tumor cells induce neutrophilia and promote neutrophil recruitment by secreting granulocyte and granulocyte-macrophage colony-stimulating factors (G-CSF and GM-CSF), two of the major cytokines that induce neutrophil production and mobilization[263]. In addition, other neutrophil-chemoattractant cytokines, such as CXCL1 and CXCL2, are produced under neuroinflammatory conditions[264; 265]. Nevertheless, neutrophil recruitment only seems to increase in *terc*-overexpressing neutrophils in the context of the glioblastoma-induced inflammation but not in the acute inflammation caused in the wound assay. In the latter, the first signal for neutrophil recruitment in is an H_2O_2 gradient produced by epithelial cells[156], whereas this signaling pathway has not been reported to occur in in glioblastoma. It would be

interesting to study the differences in the chemoattractant cytokine gradients of glioblastoma and the one happening in the wound and see if *terc* overexpression could be changing the expression of cytokine receptors in the neutrophils, promoting the migration to the glioblastoma but not to the wound.

Although the role of neutrophils in tumor progression is not well elucidated, a higher number of neutrophils specifically in glioblastoma tumors has been largely described to promote tumor progression and correlates with poor prognosis[263; 266; 267]. However, our results show a higher number of neutrophils in the larvae with a reduced tumor. Moreover, we cannot confirm that *terc*-overexpressing neutrophils are indeed infiltrating the tumor and whether they contribute to restrain tumor growth. Therefore, we decided to study the role of microglia, since they are the main immune cells in close contact with the tumor[195]. The embryonic microglial cells come from primitive macrophages in the zebrafish that colonize the brain at about 60 hours post fecundation (hpf)[268]. Since *terc* overexpression increases the macrophage number, it could also be increasing the microglia in the brain. Unexpectedly, the number of microglia cells in *drl:terc* larvae was no different from the wild type larvae, and that was also the case in the larvae with glioblastoma. This result indicated that the tumor size reduction was not due to an increase in the amount of microglia in the tumor.

Given that *terc* overexpression was not changing the amount of microglia cells and our results indicated that *terc* was causing changes in the glucose metabolism, we further investigated if *terc* was affecting macrophage polarization. Macrophages (including microglia) can be classified into M1 and M2 depending on their pro-inflammatory or anti-inflammatory characteristics, and it has been widely reported that changes in the way they oxidize glucose are key in determining their polarization status[56; 269; 270]. We induced the activation of macrophages in the zebrafish by performing a bacterial infection[250] (locally in the otic vesicle and systemically by introducing the bacteria in the Cuvier Duct), and we found that changes in *terc* expression did not affect macrophage polarization. Although changes in *terc* levels affect glucose metabolism, it may not be enough to rewire completely the mechanisms participating in macrophage of polarization. Besides the metabolic changes, specific cytokines, several transcription factors, signaling pathways and chromatin remodeling enzymes participate to produce a specific polarization M1 or M2 phenotype[271]. Unfortunately, we could not evaluate macrophage polarization in the tumor microenvironment, which is known to affect the overall immune function[174] and, specifically the microglia polarization[195; 272]. In that sense, it would be interesting to address polarization markers in the microglia around the tumor (wild type and *drl:terc*) to completely discard that *terc* expression is not affecting microglia polarization.

In order to have an idea of which other cells may be playing a role in the decrease of glioblastoma size, we looked at the protein interactome of the Draculin protein using the STRING database (https://string-db.org/).

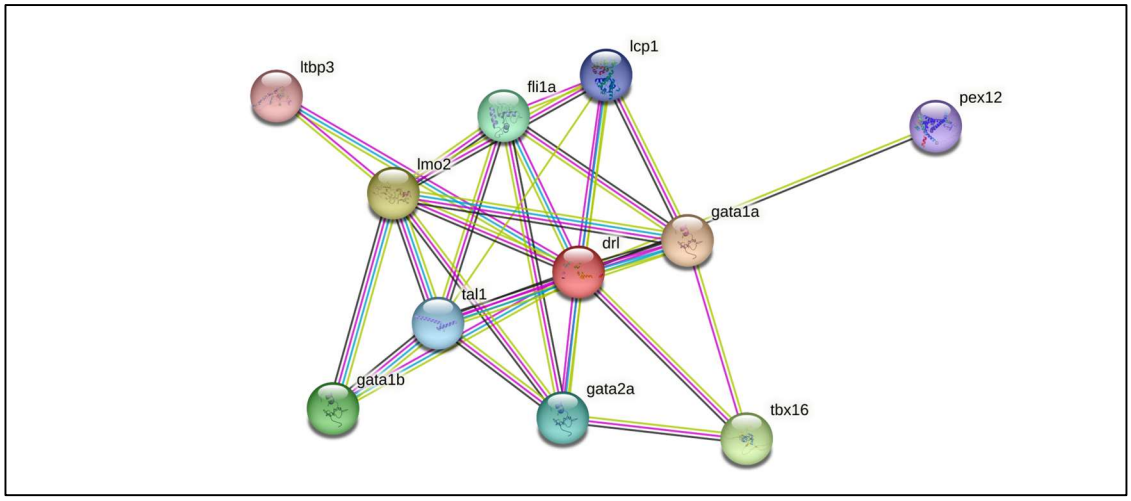

Figure 53. Draculin protein interactions found in STRING database. Each conecting line indicates a type of interaction described in the literature between two proteins (colored spheres). The color of each line indicates the kind of interation: pink and blue lines indicate known interactions. The black lines indicate co-expression and the other colored lines indicate predicted interactions. The studied protein (drl) is indicated with a red-color sphere.

The Draculin protein, whose expression is driven by the draculin (*drl*) promoter, interacts with master transcription factors and specific proteins of hematopoietic stem cells (HSCs) and progenitors, such as *lcp1*, *gata1a* and *gata1b*, indicating that it is present in those cells, as previously described[273] (Fig. 53).

In the zebrafish embryos, the HSCs arise from the hemogenic endothelial cells (HECs), which also generate the common endothelial cells (ECs). Indeed, HECs and ECs have a common progenitor[274]. In this protein interactome, besides finding HSCs markers, we also found proteins present in endothelial cells or that participate in the EC generation, such as the Friend leukemia integration 1 transcription factor (*fli1a*)[274; 275], LIM Domain Only 2 (*lmo2*)[276] and T-cell acute lymphocytic leukemia protein 1 (*tal1*)[277] (Fig. 53). Hence, we can infer that in our *drl*:*terc* transgenic line, *terc* is being overexpressed not only in hematopoietic cells but also in endothelial cells. Solid tumors such as glioblastoma induce the formation of new blood vessels (angiogenesis) to ensure nutrients reaching the tumor cells[278; 279]. It would be interesting to study if the tumor-promoted angiogenesis is different in the *drl:terc* fish, resulting in the reduction of the tumor size reported in this work.

In conclusion, here we describe a new non-canonical function for the telomerase RNA (*terc*) participating in the regulation of glucose metabolism. *terc* expression is able to induce changes in the concentration of glucose-derived metabolites and regulates the transcription of *ldhbb* gene though its promoter region. Moreover, we report that only *terc* but not *tert* overexpression in the hematopoietic cell population leads to a reduction in glioblastoma size, revealing a telomerase-independent function. Further studies are needed to determine the exact molecular players involved in this anti-tumor function of *terc* and whether there is any relationship to its effect on metabolism.

Chapter II

Characterization of pyruvate dehydrogenase and telomerase interaction

1. Introduction

Telomerase is a ribonucleoprotein complex in charge of telomere synthesis, consisting of a catalytic subunit (TERT) and an RNA component (*TERC*)[280]. More specifically, TERT, which has a reverse-transcriptase activity, uses *TERC* as a template to synthetize the telomeric sequence[12; 13]. Nevertheless, it is known that TERT and *TERC* have other extracurricular roles that are independent of telomerase activity and telomere lengthening[19-21].

TERT has been shown to regulate cell signaling pathways related to cell proliferation and migration by binding at promoter regions and interacting with transcription factors such as β-catenin and c-MYC, increasing the transcription of their target genes[22; 26; 28]. In the case of *TERC*, it's been described that it can bind to a specific sequence in the DNA (*TERC*-binding sequence), which is presented in more than 2000 loci in the genome, indicating its role as a long-noncoding RNA (lncRNA)[37]. As such, *TERC* has been shown to promote cell proliferation by activating the transcription of genes in the PI3K-AKT pathway[45]. Furthermore, in our laboratory, we have described that *TERC* plays an important role in the transcription of master myelopoietic genes, controlling the production of neutrophils and macrophages in a TERT-independent manner[21; 47]. In addition, both telomerase components (TERT and *TERC*) are known to be imported into the mitochondria, where they also perform independent non-canonical functions[34; 50].

With the aim of further explore the mechanism by which *TERC* regulated myelopoiesis, we discovered its ability to bind RNA polymerase II (RNApol II), thus increasing the transcription of master myelopoietic genes[47]. In light of this observation, we hypothesized that *TERC* could be playing other non-canonical roles by interacting with other proteins. We therefore performed a proteomic analysis to identify the *terc*-interacting proteins using zebrafish as an *in vivo* model. Surprisingly, we found that most *terc* protein interactors were involved in metabolic pathways (Elena Martínez-Balsalobre PhD thesis, unpublished results).

Metabolic enzymes stablish an axis of communication between the nucleus, mitochondria, and the cytoplasm, and they are important to perform regulatory and sensing functions for the cell to adapt to nutrient availability and stress conditions. These functions besides their catabolic activities have been named as moonlighting functions[281; 282].

In this regard, a long list of enzymes participating in the glycolytic pathway and the Tricarboxylic Acid Cycle (TCA) have been identified to be present in the nucleus, such as pyruvate kinase muscle isoenzyme 2 (PKM2)[283], lactate dehydrogenase (LDH)[88], the pyruvate dehydrogenase complex (PDC)[105] or malate dehydrogenase 2 (MDH2)[284]. These enzymes are able to control gene expression by modifying histone acetylation and methylation levels, but also, they can bind to transcription factors to potentiate or inhibit the transcription of their target genes[104].

The Pyruvate Dehydrogenase Complex (PDC) is a mitochondrial enzymatic complex that is able to produce acetyl-CoA from pyruvate[51]. The PDC is constituted by three different enzymes: pyruvate dehydrogenase (PDH or E1), dihydrolipoyl transacetylase (DLAT or E2) and dihydrolipoyl dehydrogenase (DLD or E3)[97]. The PDC-E1 is an heterotetramer composed by two alfa and two beta subunits (E1α and E1β), and phosphorylation or dephosphorylation of the E1α subunit at Ser^{232}, Ser^{293} or Ser^{300} controls the PDC activity[100]. The phosphorylation of one or several of these serine residues by the pyruvate dehydrogenase kinases (PDKs) inhibits the activity of the PDC whereas the dephosphorylation of these residues by the pyruvate dehydrogenase phosphatases (PDPs) restores its activity[101].

The PDC has been described to be translocated into the nucleus during the S phase of the cellular cycle. Once inside, the nuclear PDC (nPDC) is able to produce acetyl-CoA and increase the levels of acetylation of H3K9 and H3K18, thus, promoting cell-cycle progression[105]. In addition, other studies show how nPDC levels are key in regulating histone acetylation related to pluripotency and the embryonic development[109; 110]. Interestingly, the nPDC is only active PDC, since only the non-phosphorylated form has been shown to be in the nucleus and none of the PDKs have been found in there[105].

Besides nuclear translocation, another moonlighting function of several metabolic enzymes is their ability to bind RNAs[285; 286]. Although the function behind this RNA-binding activity has not been elucidated for all the identified enzymes with this ability, some of them have shown to perform regulatory functions. That is the case of enzymes such as the cytosolic aconitase (aconitase 1), whose catabolic activity is impaired under low iron conditions; however, in this context, it is starts to bind and stabilize mRNAs related to iron homeostasis[287]. Another well-studied example of metabolic enzyme binding RNA is Glyceraldehyde 3-phosphate dehydrogenase (GAPDH), which has been shown to bind mRNAs, controlling their transcription, as well as tRNAs, viral RNAs and even the telomerase RNA[288].

In this study we report the interaction between the telomerase RNA (*TERC*) and the PDC-E1 in both zebrafish and two different human cell lines. To our knowledge, this is the first study showing the ability of the PDC to bind RNAs. We determined that this interaction is taking place inside and outside the cell nucleus, and that the nuclear translocation of PDC-E1 is affected by *TERC* levels. Moreover, we show that this interaction is not exclusive to the telomerase RNA since also TERT was found as an interactor of PDC-E1. Finally, we also described that both telomerase components are in close proximity with the PDC-E2 subunit, indicating that the telomerase complex could be interacting with the whole PDC and performing a new non-canonical function.

2. Materials and Methods

2.1. Cell culture and transfection

HL60 and MOLM-13 cell lines were cultured in RPMI (Lonza) supplemented with 10% fetal bovine serum (FBS), 1% glutamine and 1% penicillin/ streptomycin at 37°C in a 5% CO_2-humidified atmosphere. HeLa cells were cultured in DMEM (Lonza) supplemented with 10% fetal bovine serum (FBS), 1% glutamine and 1% penicillin/ streptomycin in the same conditions.

HL60 shC and sh*TERC* cell clones were obtained by lentiviral transduction. HL60 cells were incubated overnight with a mixture of shRNA-containing lentiviral particles (1-2.5 lentiviral particles/20 cells, Santa Cruz Biotechnology) and 8 µg/ml of polybrene (Sigma). On the next day, the transduction medium was replaced with fresh medium, and cells were incubated for another 24 h. To select stable clones expressing shRNAs against *TERC*, cells were split 1:3 and selected for 2 weeks (4 passages) in medium containing 2 µg/mL of puromycin (Sigma).

HeLa cells were seeded to 70%-80% confluency and transfection was performed with Lipofectamine RNAiMAX (Invitrogen) for siRNAs, and Lipofectamine™ 2000 (Invitrogen) for plasmid transfection following the manufacturer's instructions. Briefly, lipofectamine-siRNA and lipofectamine-plasmid complexes were prepared in OptiMEM Reduced Serum Medium (Gibco) and added to the cells. After 4 hours, transfection medium was replaced with fresh medium and cells were left for 24 to 48 hours before collecting them.

The used siRNAs were purchased from Santa Cruz Biotechnology: control siRNA-A (sc-37007), TERC siRNA (sc-106994) and TERT siRNA (sc-36641).

The plasmids used were the following: pCS2 mt-GFP (BamHI minus) was a gift from Michael Klymkowsky (Addgene plasmid #15681, unpublished). pBABE-puro-hTERT (pBABE-TERT for simplicity) was a gift from Bob Weinberg[289] (Addgene plasmid # 1771). pBABEpuro U3-hTR-500 (pBABE-*TERC* in this work for simplicity) was a gift from Kathleen Collins[290] (Addgene plasmid # 27666).

2.2. Nuclei Isolation in HL60

The nuclei isolation was performed as previously described[291]. Briefly, the cells were washed 2 times with phosphate-buffered saline (PBS) for 5 minutes at room temperature (RT) and resuspended in 2 mL of nuclear solubilization buffer (10 mM Tris-HCl, pH 7.4, 10 mM NaCl, 3 mM Mg_2Cl, 0.3% Igepal) containing a protease inhibitor cocktail (Sigma). Cells were incubated for 30 min in ice and centrifuged for 5 minutes at 500g at 4°C to collect nuclei. The supernatant (cytoplasmic fraction) was centrifuged at 21.000xg for 30 min at 4 °C to remove cell debris and cellular organelles. The nuclei were washed with nuclear solubilization buffer without Igepal and centrifuged for 5 min at 500g and 4°C four times.

2.3. Nuclei isolation in HeLa

The nuclei of HeLa cells were isolated following 3 different protocols.

First, nuclei were obtained following the protocol used for HL60 cells, but incubating cells in lysis buffer for 1 hour instead of 30 min.

Second, nuclei isolation was performed with NE-PER™ Nuclear and Cytoplasmic Extraction Reagents (Thermo Fisher Scientific) following manufacturer's instructions, with some modifications. Briefly, cells were collected by centrifugation and washed with PBS once. Cell lysis was performed with ice-cold CER I buffer for one hour in ice, vortexing every 10 minutes. After lysis, CER II buffer was added, and the sample was incubated in ice for an additional minute. Sample was centrifuged at 16 000xg for five minutes and the supernatant (cytoplasm) was collected. The nuclear pellet was washed once with CER I buffer before nuclei lysis with ice-cold NER buffer.

Lastly, nuclei purification was performed using the Nuclei PURE prep kit from Sigma (NUC201) following manufacturer's instructions. HeLa cells were washed with ice cold PBS and lysed in lysis buffer supplemented with DTT and 0.1-0.5% Triton X-100 (Sigma Aldrich). Cells were then incubated in ice for 0.5-2 hours, vortexing 10 seconds every 30 minutes. Cell lysate was carefully placed in a 1.8-2M glucose cushion prepared in a Beckman ultracentrifuge tube (Ultra-Clear Centrifuge Tubes, Beckman Catalog #344058) and centrifuged at 30,000xg for 45 min at 4°C in a swinging bucket ultracentrifuge. The supernatant containing the cytoplasmic fraction was recovered, and proteins were precipitated with trichloroacetic acid (TCA). The pellet containing nuclei was washed once with Nuclei PURE Storage Buffer and resuspended in the same buffer. A sample of the isolated nuclei were stained with DAPI 1:1000 in PBS and adhered to confocal dishes with Corning Cell-Tak adhesive and analyzed for cytoplasmic membrane contamination using a confocal microscope.

2.4. RNA immunoprecipitation (RIP)

RNA immunoprecipitation experiments were performed as previously described[292]. HL60 whole cells or nuclei were washed twice with PBS and crosslinked in 1%formaldehyde in PBS for 10 min at RT with rotation, followed by the addition of 1/10 volume of fresh glycine 1.25M in PBS. Cells were then washed twice with cold PBS and lysed in RIPA buffer (50 mM Tris pH 7.4, 150 mM NaCl, 1mM EDTA, 0.5 mM DTT, 0.1% SDS, 1% NP-40, 0.5% sodium deoxycholate) containing a protease inhibitor cocktail (Sigma) and RNase inhibitors (Thermo Fisher Scientific). Lysates were centrifuged at 21,000xg for 10 min at 4°C and pre-cleared with washed Protein G Sepharose beads (GE Healthcare Life sciences) for 1 hour at 4°C with rotation. The extract was quantified using Bradford reagent (Sigma) and 2-5% of the sample was kept at 4°C as Input. The immunoprecipitation was performed by adding 1 µg of antibody (Table 7) per 1 mg of precleared protein extract and overnight incubation at 4°C with rotation. The sample was incubated with the Protein G Sepharose beads 1 hour at 4°C with rotation, washed 3 times for 5 minutes with RIPA buffer and one time with RIPA high salt buffer (RIPA buffer with 1 M NaCl). Beads and Input sample were resuspended in 50 µl of RIPA buffer and incubated with 5 µL of Proteinase K (20 mg/ml, Roche) for 1 hour at 65°C. The Input and precipitated RNAs were purified using the RNeasy Mini Kit (QIAGEN) following the RNA Cleanup protocol provided by the manufacturer. Finally, they were reverse transcribed and subjected to qPCR for detection of *TERC* or control RNAs (*ACTIN* or *U6*).

2.5. RT-qPCR

The total RNA of whole cells was obtained with Direct-zol RNA Miniprep kit (Zymo Research) accordingly to the manufacturer's instructions and cDNA synthesis was performed using SuperScript IV VILO Master Mix (Invitrogen).

Quantitative gene expression was performed by qPCR in a StepOne Plus Real-time PCR System instrument (Applied Biosystems) using SYBR Premix Ex Taq (Perfect Real Time; Takara). The PCR conditions were 30 seconds (s) at 95°C followed by 40 cycles of 5s at 95°C, 20s at 60°C and finally, a melting curve protocol: 15s 95°C, 1 min 60°C and 15s 95°C. The levels of expression of each gene were normalized with the expression levels of *ACTIN* using the comparative Ct method ($2^{-\Delta\Delta Ct}$). In all cases, each PCR was performed with triplicate samples. The used primers are shown in Table 6.

Name	Species	Sequence (5´→3´)
hTERC-F3q	Human	CCCTAACTGAGAAGGGCGTA
hTERC-R3q	Human	GCTCTAGAATGAACGGTGGAA
FH1-TERT	Human	AGAACGCAGGGATGTC
RH1-TERT	Human	CAGCTTGAGCAGGAATG
ACTIN-Fw	Human	CCACCCCACTTCTCTCTAAGGA
ACTIN-Rv	Human	ACCTCCCCTGTGTGGACTTG
RN-U6 F2	Human	CTCGCTTCGGCAGCACA
RN-U6 R2	Human	ACGAATTTGCGTGTCATCCT

Table 6. List of primers used for RT-qPCR.

2.6. RNA-pull down

RNA immunoprecipitation experiments were performed as described[292]. The *in vitro*-transcribed and biotin-labeled *TERC* and control (*GFP*) RNAs were generated with the mMESSAGE mMACHINE kit (Ambion), adding biotin RNA labeling mix (Roche) instead of 2x dNTP/CAP mix provided by the kit.

To perform the RNA-pull down, HL60 cells were collected and washed twice with PBS. Later, the cell pellet was resuspended and homogenized in RIP buffer (25 mM Tris pH 7.4, 150 mM KCl, 0.5 mM DTT, 0.5% NP-40). The sample was centrifuged at 21,000xg for 10 min at 4°C to remove cell debris and pre-cleared by incubating the sample with washed Dynabeads MyOne Streptavidine C1 magnetic beads for 1h at 4°C with rotation. After bead incubation, protein concentration was quantified using a standard curve and Bradford reagent (Sigma). 2-5% of the sample was kept as Input. An equal volume of 2x RNA structure buffer (20 mM Tris pH 7.0, 0.2 M KCl, 20 mM $MgCl_2$) was added to 3 µg of each biotinylated RNA, incubated at 70°C for 5 min and cooled down to room temperature (RT) for 20 min to allow RNA folding. Finally, 1x RNA structure buffer was added up to 100 µL. The folded RNA was bound to 20 µL of washed streptavidin beads for 1 hour at RT with rotation and at least 1 mg of the pre-cleared protein extract was incubated with the RNA-loaded beads overnight at 4°C with rotation. The beads were washed 5 times for 5 min with 1 mL of RIP buffer and the RNA-protein complexes and INPUT sample were eluted in 30 µL of NuPAGE LDS sample buffer (Termo Fisher Scientific) boiling at 90°C for 10 min. Finally, samples were subjected to polyacrylamide gel electrophoresis (PAGE) followed by western blotting with the selected antibodies (Table 7 and 8).

2.7. Western blot

For mitochondria and nuclear isolation analysis, SDS-PAGE experiments were performed as described previously[293]. Briefly, cells were pelleted, washed twice with PBS and lysed on ice cold RIPA buffer (Sigma, R0278) containing PMSF, protease inhibitor cocktail, sodium orthovanadate, and sodium fluoride, for 30 min, vortexing every 10 min. Samples were centrifuged at 10 000 rpm at 4°C for 20 min and the protein concentration in the lysates was measured using a BCA kit (Thermo Fisher Scientific, 23227) following manufacturer's instructions. Samples were prepared in 2x Laemmli sample buffer (Sigma Aldrich S3410) and boiled for 5 minutes at 100˚C. Protein electrophoresis was done in 12% polyacrylamide gels and transferred onto nitrocellulose membranes (BioRad) using a Trans-blot turbo transfer (Bio Rad). Ponceau S staining (Thermo Fisher Scientific) was performed to assess efficient loading and transferring. The membranes were blocked with 5% bovine serum albumin (BSA) (w/v) in tris-buffered saline with tween-20 (TBST) for 1 hour at RT and further incubated with the primary antibodies (Table 7) in TBST 5% BSA overnight at 4°C. The following day, membranes were washed 5 times for 5 minutes with TBST and incubated with the appropriate secondary antibodies coupled to horseradish peroxidase (Cell Signaling Technology, Table 8) for one hour at RT. After several washes with TBST, proteins were detected with enhanced chemiluminescence reagent (ECL) (Thermo Fisher Scientific) and imaged on a ChemiDoc MP Imaging System.

To analyze total lysates cells were harvested, washed twice in PBS and lysed in RIPA buffer (50 mM Tris-HCl, pH 7.4, 150 mM NaCl, 1 mM EDTA, 0.5 mM DTT, 0.1% SDS, 1% NP-40, 0.5% sodium deoxycholate) containing a protease and phosphatase inhibitor cocktail (Sigma) and the histone deacetylase inhibitor Trichostatin A (Sigma). Samples were then incubated on ice for 10 min with frequent vortexing and centrifuged at 21,000xg for 10 min at 4°C. The supernatant was collected, and protein concentration was measured using Bradford reagent (Sigma). Proteins were subjected to polyacrylamide gel electrophoresis (4–15% Mini-PROTEAN® TGX™ Precast Protein Gels, #4561084) and humid-transferred onto nitrocellulose membranes (Bio-Rad) or methanol-activated PVDF membranes (Bio-Rad), in the case of detecting acetylated proteins. The membranes were blocked with 5% (w/v) skim milk (BD Life Sciences) in TBST for 1 hour at RT and later they were incubated with primary antibodies (Table 7) diluted in TBST 5% skim milk overnight at 4°C. The next day, membranes were washed 5 times for 5 minutes with TBST and secondary antibody incubation (Cythiva, Table 8) was performed in TBST 5% skim milk for one hour at RT. After several washes with TBST, proteins were detected with enhanced chemiluminescence reagent Cytiva Lifescience™ Amersham™ ECL™ Prime and imaged on a ChemiDoc XRS Imaging System.

2.8. Proximity Ligation Assay (PLA)

PLA for specific RNA–protein interaction was performed as described[47; 294]. Briefly, HL60 or HeLa cells were seeded in poly-L-Lys coverslips, washed once with PBS, and fixed in 4% formaldehyde for 30 min on ice. Cells were permeabilized with 1% saponin in PBS for 1 hour and blocked with blocking buffer (10 mM Tris-acetate pH 7.5, 10 mM magnesium acetate, 50 mM potassium acetate, 250 mM NaCl, 0.25 mg/ml BSA, 0.05% Tween 20) and 20 µg/ml sheared salmon sperm DNA (sssDNA) for 1 hour at 4°C. Then, cells were incubated with 100 nM *TERC* sense or antisense oligonucleotide probes (*TERC*-sense probe 5´ TCCGGAGGCACCCACTGCCACCGCGAAGAGTTGGGCTCTGTCAGCCAAAAAAAAAAAAAAAAAAAATA TGACAGAACTAGACACTCTT 3´ and *TERC*-antisense probe 5´ AGCAGCTGACATTTTTTGTTTGCTCTAGAATGAACGGTGGAAAAAAAAAAAAAAAAAAAAATATGAC

AGAACTAGACACTCTT 3´) pre-heated at 70°C for 3 min in blocking buffer. Cells were washed three times with PBS and blocked in PBST (PBS 0.1% Tween 20) containing 1% BSA and 20 µg/mL salmon sperm sheared (sss) DNA at RT for 1 h.

Samples were washed once with PBS, once with 300 mM NaCl, 30 mM sodium citrate buffer pH 7 (2xSSC) with 0.1% Tween 20, washed again with PBS, and then incubated with the selected primary antibodies (Table 7), or no antibody as control, in PBST at RT for 1 h. The appropriate species-specific minus PLA probe (Duolink PLA Fluorescence kit, Sigma) was diluted 1:5 into PBST containing 20 µg/mL sssDNA and incubated for 20 min at RT. After three washes with PBS, the coverslips were incubated with the probe solution for 1 h at 37 °C.

PLA for specific protein–protein interaction was performed as described[295]. Briefly, HL60 or HeLa cells were seeded in poly-L-Lys coverslips and fixed and permeabilized as described above. Then cells were blocked with Duolink block solution (Sigma) for 1h at RT followed by primary antibody incubation (Table 7) or no antibody as negative control, overnight at 4°C. Primary antibodies were prepared at the dilution indicated in Table 7 using Duolink antibody dilution buffer (Sigma). The next day, samples were washed with 5% BSA in PBS twice for 10 min. Then, the corresponding species-specific minus PLA probe (Duolink PLA Fluorescence kit, Sigma) was diluted 1:5 into Duolink antibody dilution buffer and incubated for 20 min at RT. Finally, PLA probe was added to the samples and incubated for 1h at 37°C.

Ligation, amplification and labeling steps in both RNA-protein and protein-protein PLA, were performed using the Duolink PLA Fluorescence kit (Sigma), following manufacturer's instructions. Samples were washed twice with buffer A and incubated with fresh ligation mix for 30 min at 37 °C. They were washed twice again with buffer A and further treated with fresh amplification mix for 100 min at 37 °C. Finally, cells were washed twice with buffer B and mounted onto glass slides in Duolink PLA Fluorescence mounting medium with DAPI (Sigma).

To couple mitochondria staining to PLA, cells were previously labeled using MitoTracker Red CMXRos (Thermo Fisher Scientific). In HL60 cells, the staining was done with 250 nM of MitoTracker for 30 min at 37°C and in HeLa cells with 500 nM for 45 min at 37°C. Next, cells were washed once with medium and twice with PBS, protecting from light. HL60 cells were then attached to poli-L-lysine confocal dishes or coverslips for 30 min to continue with the PLA protocol.

2.9. Cell cycle analysis

shC and sh*TERC* HL60 cells were collected and washed twice with PBS and centrifuged in cytometer tubes at 1000 rpm for 2 minutes. The cell pellet was immediately fixed adding 1 mL of ice cold 70% ethanol while vortexing. Cells were centrifuged again at 1000 rpm for 2 minutes and kept in 70% ethanol at 4°C for at least 30 minutes until propidium iodide staining. Cells were then washed two times with cold PBS in order to remove ethanol, treated with 100 µg/mL of Ribonuclease A (Sigma) for 10-15 min and with propidium iodide (Sigma) at a concentration of 50 µg/mL in PBS for another 10 min. The cell cycle analysis was performed using a BD FACSCanto II flow cytometer and ModFit LT V5.0.9 software.

2.10. Immunostaining

HL60 or HeLa cells were seeded in poly-L-Lys coverslips, washed once with PBS, and fixed in 4% formaldehyde in PBS at RT for 20 min. Cells were permeabilized with 0.3% Triton-X in PBS for 10 min at RT on a shaker. Later, cells were blocked in PBS with 1% BSA and 0.1% saponin. Samples were incubated with primary antibody (Table 7) diluted in blocking solution for 1 hour at RT in a humid chamber. Cells were washed twice with 0.1% Triton in PBS (PBST) and incubated with secondary antibody (Alexa Fluor Goat anti-rabbit 594, Invitrogen) diluted at 1:200 in PBS with 1% BSA for 30 min at RT and protected from light. In addition, Hoechst reagent was added at 1:1000 concentration together with the secondary antibody for nuclei staining. Finally, coverslips were mounted in Dako fluorescent mounting medium.

2.11. Confocal imaging and co-localization analysis

RNA-protein PLA and immunofluorescence images were acquired on a Leica TCS SP8 confocal microscope by tandem scanner of 405 nm and 561 nm lasers and sequential scanner when using the 488 nm laser. All images were acquired with a 63x/1.4 oil objective with a resolution of 1024x1024 pixels. In these images, co-localization analysis was performed using ImageJ software with Intensity Correlation Analysis plugging in selected z-stacks slices after image de-convolution with Huygens Essential (Scientific Volume Imaging B.V) software.

Protein-protein PLA and nuclei isolation images were acquired on a ZEISS LSM 710 confocal microscope with a 40x/1.4 oil objective (1024x1024 pixel resolution). Each channel was independently and sequentially scanned with only one excitation wavelength active during each scan to avoid overlap between the different dye emissions. After acquisition, images were processed with ZEN software (Carl ZEISS AG).

2.12. Pyruvate dehydrogenase (PDC) activity colorimetric assay

The activity of the PDC (PDH) was evaluated with the Pyruvate Dehydrogenase Kit from Abcam (ab287837) following manufacturer's instructions. Briefly, cells were lysed in ice cold PDH Assay Buffer and centrifuged to remove cell debris. 46 µl of HL60 or HeLa cell protein extracts corresponding to 25 000 and 1000 000 cells respectively, were mixed with 2 µl of PDH developer reagent and with 2 µl of PDH substrate in wells of 96-well clear plate with flat bottom. 1µl of PDH Positive Control (NADH) was used as positive control. Protein extracts were incubated without PDH substrate to correct the cell background absorbance. Sample absorbance was measured at 450 nm in kinetic mode every 10 min for 60 min at 37°C in a CLARIOstar® Plus plate reader. The reading from sample background controls was subtracted from its paired sample and two time points (T1 & T2) in the linear range were chosen to calculate the pyruvate dehydrogenase activity of the samples.

2.13. Mitochondria isolation in HeLa

Mitochondria were isolated with the Mitochondria Isolation Kit for Cultured Cells from Abcam (ab110170) following manufacturer's instructions. In brief, confluent HeLa cells were scrapped and resuspended in Reagent A at a concentration of 5 mg/mL. Cells were disrupted using a 2 mL Dounce homogenizer and centrifuged at 1000xg for 10 min at 4°C. The supernatant was

collected, and this step was repeated with the pellet, resuspending this time in Reagent B. The supernatants from both steps were combined and centrifuged at 12 000xg for 15 min at 4°C. The pellet (mitochondria) was used for the subsequent protein quantification and PDC activity determination.

2.14. Pyruvate dehydrogenase activity dipstick assay and band quantification

Determination of PDC activity in isolated mitochondria was performed using the Pyruvate dehydrogenase (PDH) Enzyme Activity Dipstick Assay Kit (ab109882) following the manufacturer's instructions. 25 µg of total protein extracts from isolated mitochondria of HeLa cells was incubated with the dipstick containing the PDC antibody that captures the PDC in the sample is in its native form in the dipstick membrane. After washing the dipstick with sample buffer, it was incubated with the activity buffer, containing diaphorase and nitroblue tetrazolium (NBT). PDC activity is visualized by coupling PDC-dependent production of NADH to the reduction of NBT in the presence of excess diaphorase, forming an insoluble intensely colored precipitate at the capture line (Fig. 54). PDC activity was measured by quantification of the band intensity using a flat top scanner and ImageJ software.

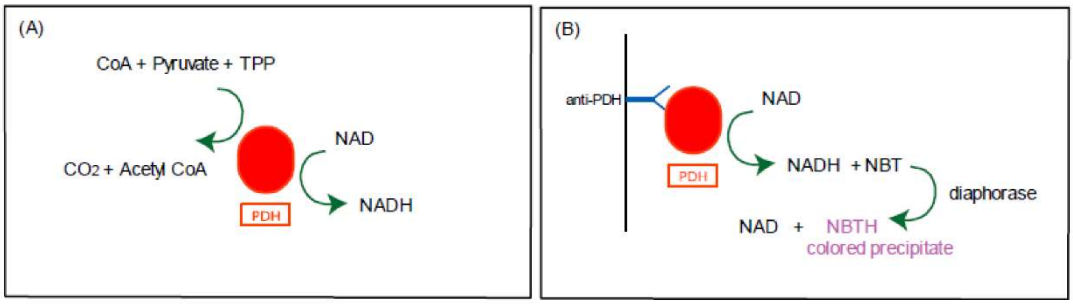

Figure 54. Schematic representatiton of PDH activity reaction. (A) The PDH activity reaction generates NADH. (B) The NADH produced is coupled to the reduction and precipitation of a colored dye. Figure obtained from Abcam.

2.15. Statistical analysis and data representation

All statistical analysis and data representations were performed using GraphPad Prism version 8.0.0. The statistical test used in each experiment is stated in the corresponding figure legend.

Target protein	Species	Dilution and application	Manufacturer	Reference
MDH2 (1G12)	Mouse	1:500 WB	Santa Cruz Biotechnology	sc-293477
GLUD1/2 (C-10)	Mouse	1:1000 WB	Santa Cruz Biotechnology	sc-515542
H3 total	Rabbit	1:1000 WB	Abcam	ab1791
Acetyl-histone H3	Rabbit	1:1000 WB	EMD Millipore	06-042
Acetyl-histone H4	Rabbit	1:1000 WB	EMD Millipore	06-866
TERT	Rabbit	1:100 IF/PLA	Rockland	600-401-252
PDC-E1α (PDHA1)	Rabbit	1:500 WB	Abcam	ab168379
PDC-E1β (PDHB)	Rabbit	1:200 IF/PLA 1µg/mg IP 1:1000 WB	Abcam	ab155996
PDC-E1 (PDHA1)	Mouse	1:200 PLA	Abcam	ab110334
PDC- E1α p-S293	Rabbit	1:1000 WB	Abcam	ab92696
PDC-E2 (DLAT)	Rabbit	1:100 PLA	Abcam	ab126224
PDC-E2 (DLAT)	Mouse	1:100 PLA	Abcam	ab69304
PDC-E2 (C-1)	Mouse	1:100 PLA	Santa Cruz Biotechnology	sc-166899
Lamin A/C	Mouse	1:1000 WB	Cell signaling Technology	#4777S
Tom20	Rabbit	1:500 WB	Santa Cruz Biotechnology	sc-11415
NUP98	Rabbit	1:1000 WB	Cell signaling Technology	#2598S
αTubulin	Mouse	1:1000 WB	Sigma	T6199
Total RNApol II	Mouse	1:1000 WB	Abcam	ab817
Anti-mitochondria (MTC02)	Mouse	1:1000 WB	Abcam	ab3298
β-actin-HRP (C4)	Mouse	1:1000 WB	Santa Cruz Biotechnology	sc-47778
Rabbit IgG Isotype control	Rabbit	1µg/mg IP	Thermo Fisher Scientific	10500C

Table 7. List of primary antibodies used, application and concentration.

Target protein	Species	Dilution and application	Manufacturer	Reference
Mouse IgG, HRP-linked antibody	Horse	1:2500 WB	Cell Signaling Technology	#7076
Rabbit IgG, HRP-linked antibody	Goat	1:2500 WB	Cell Signaling Technology	#7074
Mouse IgG HRP-Linked Whole Ab	Sheep	1:1000 WB	Cytiva	NA931
Rabbit IgG, HRP-linked $F(ab')_2$ fragment	Donkey	1:1000 WB	Cytiva	NA9340

Table 8. List of primary antibodies used, application and concentration.

3. Results

3.1. Telomerase RNA interacts with the E1 component of the pyruvate dehydrogenase complex in zebrafish and human

Previous results obtained in our laboratory showed that *TERC* plays a non-canonical role in myelopoiesis by interacting with and recruiting RNA polymerase II to the promoter of myeloid genes and activating its transcription[47]. Therefore, we speculated that *TERC* could be playing additional non-canonical roles by interacting with other proteins. To address this hypothesis, a proteomic analysis to identify the protein interactome of *TERC* in zebrafish was performed in our lab. *TERC*-interacting proteins were isolated by RNA pull-down experiments followed by mass spectrometry. Proteins identified in at least two out of three independent experiments were considered positive interactions and then classified according to their implication in different pathways using the KEGG database. Interestingly, *TERC*-interacting-proteins involved in metabolic pathways were the most enriched. Specifically, the carbon metabolism and the oxidative phosphorylation were some of the most represented pathways (Elena Martínez-Balsalobre PhD thesis, unpublished results). The identified *TERC*-interactors that belonged to those pathways are listed in the table below (Table 9).

Gene symbol	Protein name	EC number
***pdhb* (Z), *PDHB* (H)**	Pyruvate dehydrogenase E1 component subunit beta	EC:1.2.4.1
***mdh2* (Z), *MDH2* (H)**	Malate dehydrogenase 2	EC 1.1.1.37
***glud1a* (Z), *GLUD1* (H)**	Glutamate dehydrogenase 1a	EC 1.4.1.3
***atp2a1l* (Z), *ATP2A1* (H)**	ATPase sarcoplasmic/endoplasmic reticulum Ca2+ transporting 1, like	EC 7.2.2.10
***atp5f1c* (Z), *ATP5F1C* (H)**	ATP synthase F1 subunit gamma	EC 7.1.2.2
***atp5pb* (Z), *ATP5PB* (H)**	ATP synthase peripheral stalk-membrane subunit b	-
***atp5pd* (Z), *ATP5PD* (H)**	ATP synthase peripheral stalk subunit d	-
***atp5po* (Z), *ATP5PO* (H)**	ATP synthase peripheral stalk subunit OSCP	-

Table 9. *terc* potential interactors involved in carbon metabolism and oxidative phosphorylation. Table showing the gene symbol of the identified zebrafish interactors (Z) and their human ortholog (H). The protein name and EC entry number are also presented.

Next, we sought to validate in human cell lines some of these proteins interacting with *terc* in the zebrafish. The possible interaction of *TERC* with MDH2, GLUD1A and PDHB (PDC-E1) was analyzed in human leukemia cells (HL60 or MOLM-13) using RNA pull-down or RNA immunoprecipitation (RIP) experiments. We were able to validate only the interaction of *TERC* with PDC-E1 (Fig. 55A and 55C). Although in the RNA-pull down experiments the interaction was validated with a whole cell extract, in the RIP experiments, a significant interaction could only be observed when using nuclear extracts (Fig. 55B and 55C).

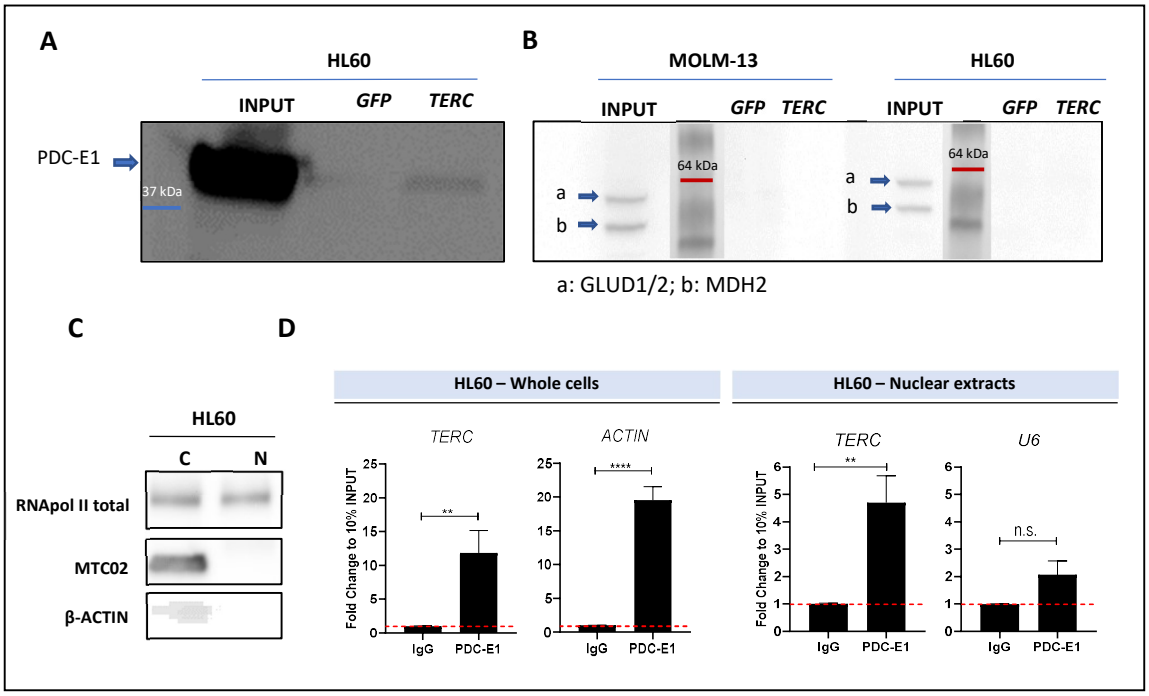

Figure 55. Validation of *TERC* interaction with PDC-E1 in HL60 cells. (A) Western blot of RNA-pull down eluates performed in HL60 and MOLM-13 cells using anti-PDC-E1, anti-GLUD1/2 and anti-MDH2 antibodies. The RNA of GFP was used as control. A specific interaction is only detected when using *TERC* RNA. (B) Western blots of RNA-pull down eluates performed in HL60 and MOLM-13 cells using anti-GLUD1/2 and anti-MDH2 antibodies. (C) Western blots of cytoplasmic and nuclear fractions of HL60 cells. The abscense of cytoplasmic and mitcochondrial markers (β-actin and MTC02) and the presence of the nuclear protein RNApol II indicates the purity of the nuclear extract. (D) RT-qPCR performed with the RIP eluates of HL60 cells and their isolated nuclei. The samples were immunoprecipitated with anti-PDC-E1 or IgG as a control and the enrichment in *TERC*, *ACTIN* and *U6* RNAs was detected. *ACTIN* was used as control in the whole cell samples whereas the lnc-RNA *U6* was used as control in the nuclear extracts. The mean ± S.E.M. for each sample is shown. P values were calculated using Man-Whitney test, n.s.: not significant, **p≤0.01, ***p≤0.001,****p≤0.0001.

3.2. The *TERC*-PDC-E1 interaction takes place in multiple sites in the cell

It has been shown that the pyruvate dehydrogenase complex (PDC) can be translocated into the nucleus[105].Other studies describe the presence of *TERC* inside the mitochondria[49]. Therefore, it was interesting for us to explore the specific location of the interaction between *TERC* and PDC-E1 withing the cell. For that, an RNA-protein proximity ligation assay (PLA) was performed in HL60 cells. This kind of assay is performed maintaining the cell structure, so the interactions occurring *in vivo* in the cell can be detected. This technique is similar to an immunofluorescent staining since it uses specific primary antibodies and also secondary antibodies to amplify the signal. If the molecules of interest interact with each other at a distance below 40 nm, it will be visualized due to a specific fluorescent signal[295]. (Fig. 56).

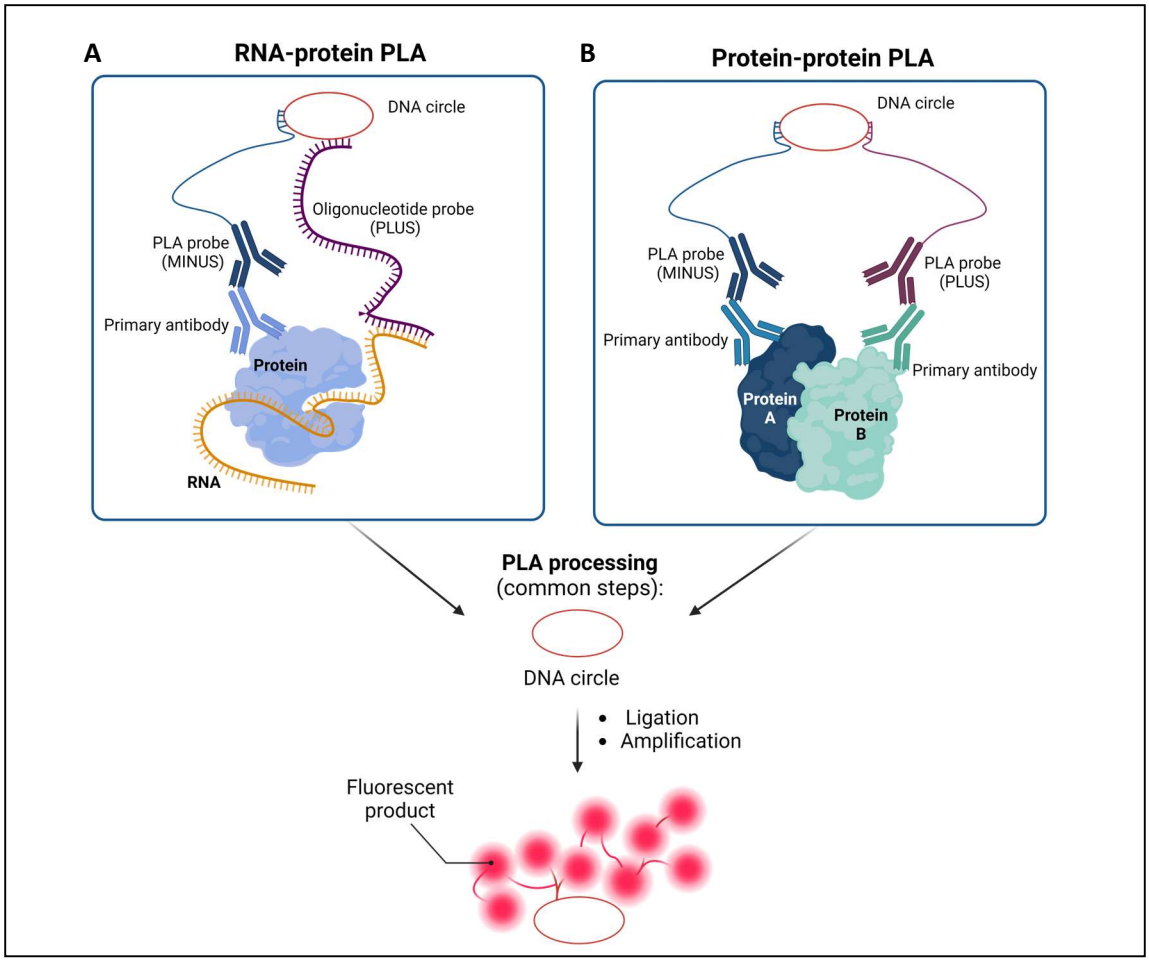

Figure 56. Schematic representation of the RNA-protein and protein-protein proximity ligation assay (PLA). (A) RNA-protein PLA. A primary antibody is used to recognize the protein of interest while an antisense oligonucleotide probe is used to detect the RNA molecule. (B) Potein-protein PLA. Two primary antibodies of different species (such as mouse and rabbit) are employed to detect the two proteins of interest. After incubation with primary antibodies and/ or probes, specific secondary antibodies that contain a ligation/hydridization arm are used (PLA PLUS and MINUS probes). In the PLA processing steps (common to both techniques), a specific ligase creates a DNA circle between the two probe arms. Later, a polymerase is added, resulting in the generation of a fluorescent product that indicates the place of interaction between the studied molecules. Created with BioRender.com.

The PLA was originally developed to detect protein-protein interactions. In this case, a variation of that protocol was used to detect an RNA-protein interaction[294]. A specific primary antibody was used to detect PDC-E1, and a probe with an antisense sequence was designed to bind to *TERC*. In addition, two different conditions were tested as negative controls: a sample without primary antibody and the antisense probe, and another control with the primary antibody and a sense probe (same sequence as *TERC*) (Fig. 57A and 57B). As a positive control, a primary antibody against RNA polymerase II (RNApol II) and the *TERC* antisense probe were used[47] (Fig. 57C). Surprisingly, a positive PLA signal for *TERC*-PDH interaction was found both inside and outside of the nucleus of the cells (Fig. 57D).

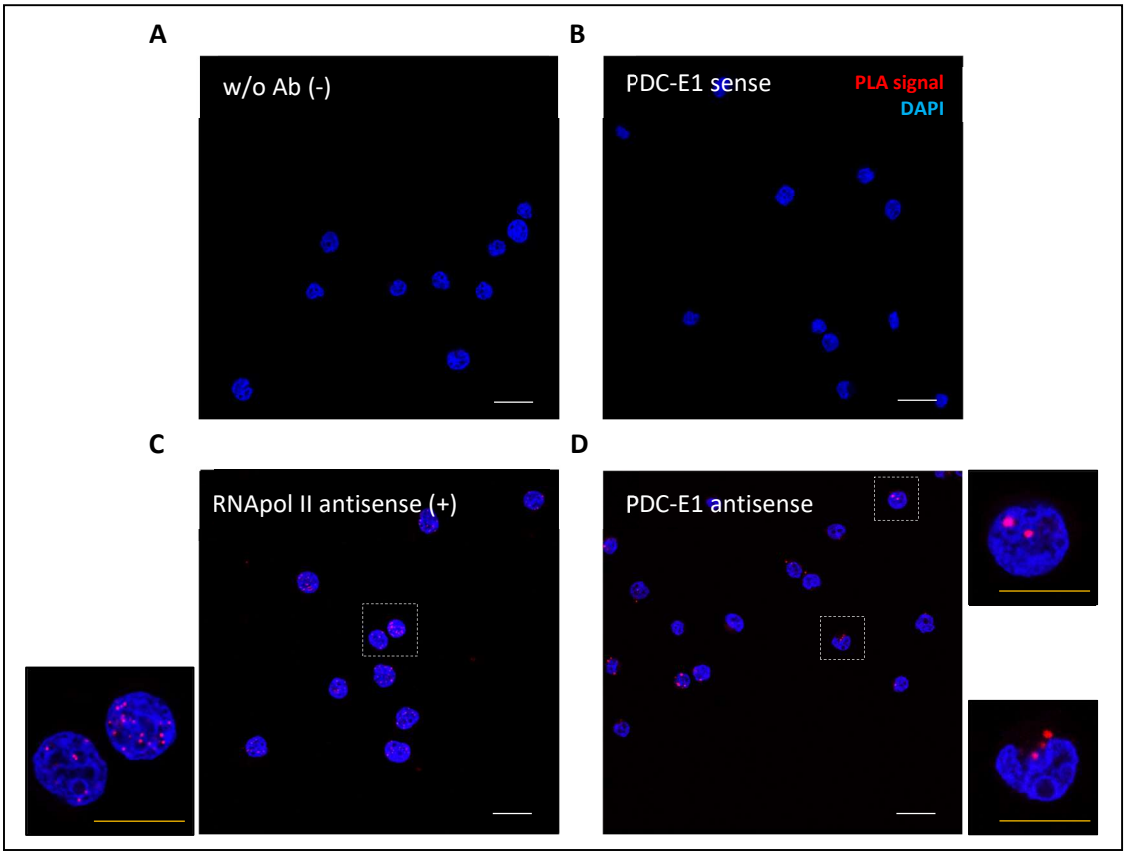

Figure 57. *TERC* and PDC-E1 interaction occurs inside and outside of the nucleus. Representative images of the RNA-protein PLA experiment in HL60 cells. The foci of red fluorescence (PLA signal) indicate the sites of interaction between *TERC* and the studied protein. The cell nucleus is stained with DAPI (blue). (A-B) Negative controls without the anti-PDC-E1 antibody or with the sense *TERC* probe. (C) Positive control with anti-RNA pol II and *TERC* antisense probe. (D) Interactions between *TERC* and PDC-E1 inside and outside the nucleus of the cells. Scale bar= 10 µm (yellow), 20 µm (white).

To find out if the PDH-*TERC* interaction outside of the nucleus was taking place in the mitochondria, we performed PLA experiments coupled to mitochondria staining with Mitotracker. After the image acquisition, a colocalization analysis was performed in imageJ to determine the degree of overlap between the green channel (PLA signals for *TERC* and PDC-E1 interaction) and the red channel (mitochondria).

There are several methods to analyze colocalization. One of them is to use the Manders' coefficients (M1 and M2)[296]. These coefficients range from 0 to 1 depending on the percentage of overlapping area between the signal of the two channels of interest. A value of 1 indicates total colocalization (100%) and a value of 0 indicates no colocalization (0%). We used the M2 value to study the amount of green area (PLA signal) overlapping with the red area (mitochondria). In the analyzed cells, values for M2 coefficient ranged from 0 to 0.4, indicating a very low level of colocalization (data not shown). Nevertheless, each M2 value is calculated for every cell, and some of them had multiple PLA signals (including those inside the nucleus). Therefore, we couldn't rule out the possibility that some, but not all of the PLA signals could be co-localizing with the mitochondria, resulting in an overall low M2 value.

Since the Manders' coefficients method was not useful to determine these possible situations of partial colocalization, the shape of the ICA (Intensity Correlation Analysis) plot and scatter

plots for each cell were used to determine the place of the interaction between *TERC* and PDC-E1. In both kinds of graphs, the intensity and overlap of two fluorescent signals is shown, although different formulas are applied to obtain a specific representation[297]. The visual representation that these graphs provide for total, partial co-localization or no co-localization is shown in Figure 58.

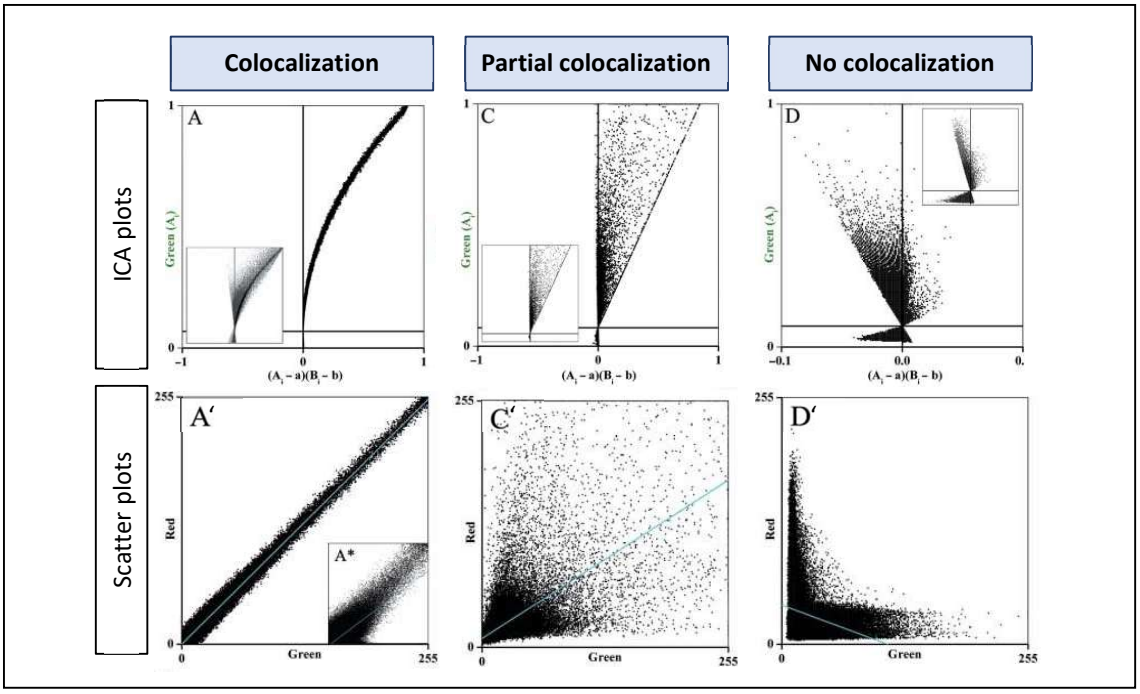

Figure 58. ICA and scatter plot examples of total, partial or no colocalization. In the upper pannel the Intensity Correlation Analysis (ICA) plot for the green channel is represented. The ICA plot is specific for each channel and the distribution of the cloud indicates the level of colocalization. The right side of the x axis indicates total colocalization if forming a C shape (A) or partial colocalization if the cloud is spread (C). The presence of pixels along the left side of the x axes indicates no colocalization (D). The scatter plots examples are shown on the lower pannel. The scatter plot is a representation of the correlation between the pixel intensity of the green and the red channel using Pearson's coefficient. A straight line representation indicates total colocalization (A') whereas the partial colocalization is shown as a cloud all over the graph (C'). The situations of no colocalization are shown as an L-shaped graph (D'). Figure adapted from (Bolte S. and Cordelières F.P., 2006)[12].

Considering the shape of both the ICA plot for the green channel and the scatter plot, the image analysis revealed that most PLA signals outside the nucleus were not colocalizing with the mitochondrial signal (Fig. 59D-F). Only some cells had one or two PLA signals that colocalized with the mitochondria (Fig. 59A and 59B), that were represented as situations of partial colocalization. The ICA plot representation for the red channel was not considered in the analysis because the area of the mitochondria signal is way larger than the one colocalizing, so always a no colocalization plot was showing. These results suggest that the interactions between *TERC* and PDC-E1 observed in the cytosol were taking place mainly outside the mitochondria.

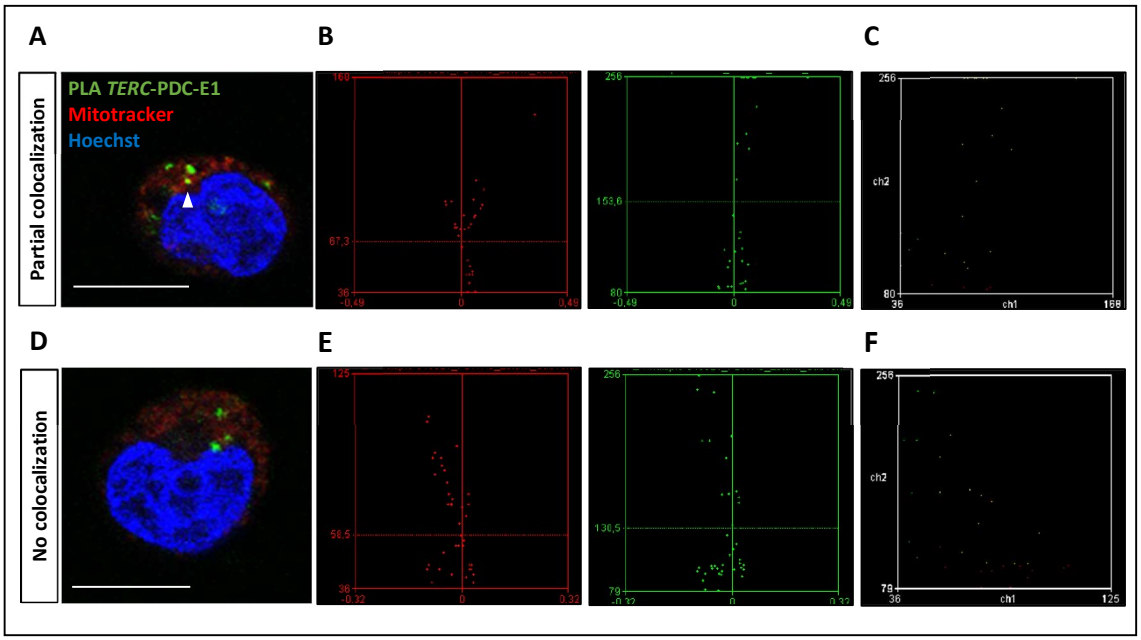

Figure 59. The interaction between *TERC* and PDC-E1 is produced mainly outside the mitochondria. (A and D) Confocal images of the *TERC*-PDH PLA (green) in HL60 cells stained with mitotracker (red). The white arrowhead indicates the place of colocalization between the green and the red signal. Scale bar= 10 µm. (B and E) ICA plots of the red and the green channel in each cell. (C and F) Scatter plots for each cell. The upper green ICA plot along with the upper scatter plot show the partial colocalization between the PLA signal and the mitchondria. The green ICA plot and scatter plot in the bottom show a situation of no colocalization.

3.3. *TERC* modulates the levels of nuclear PDC-E1

Next, we aimed at studying the biological significance of the interaction between *TERC* and PDC-E1. Since the interaction was occurring both inside and outside the nucleus, we first decided to test whether *TERC* was involved in the PDC translocation.

The translocation of PDC into the nucleus is produced mainly during the S phase of the cell cycle[105]. To stablish if *TERC* levels could be important for the nuclear translocation of PDC, control HL60 cells and HL60 cells with reduced *TERC* levels by RNA interference (shC and sh*TERC*, respectively[47]) were synchronized by serum starvation overnight, and samples were collected after 4 hours of serum addition, when the maximum number of S-phase cells was reached (data not shown). To determine nuclear PDC (nPDC) levels, an immunostaining for PDC-E1 was performed followed by a co-localization analysis. The colocalization was determined using the Manders' coefficients, focusing on the M2 value: amount of red signal (PDC) inside the blue signal (nucleus). Given that the majority of PDC is outside the nucleus, the M2 value was expected to be very low. However, this time we could compare between samples (shC and sh*TERC*), so we could stablish if that level changed upon decreasing *TERC* levels.

Although the *TERC* expression in the sh*TERC* clone only decreased in by 30% (Fig. 60B), the colocalization analysis revealed that there was a slightly increase in nPDC-E1 levels in those cells compared to the shC HL60 cells (Fig. 60C).

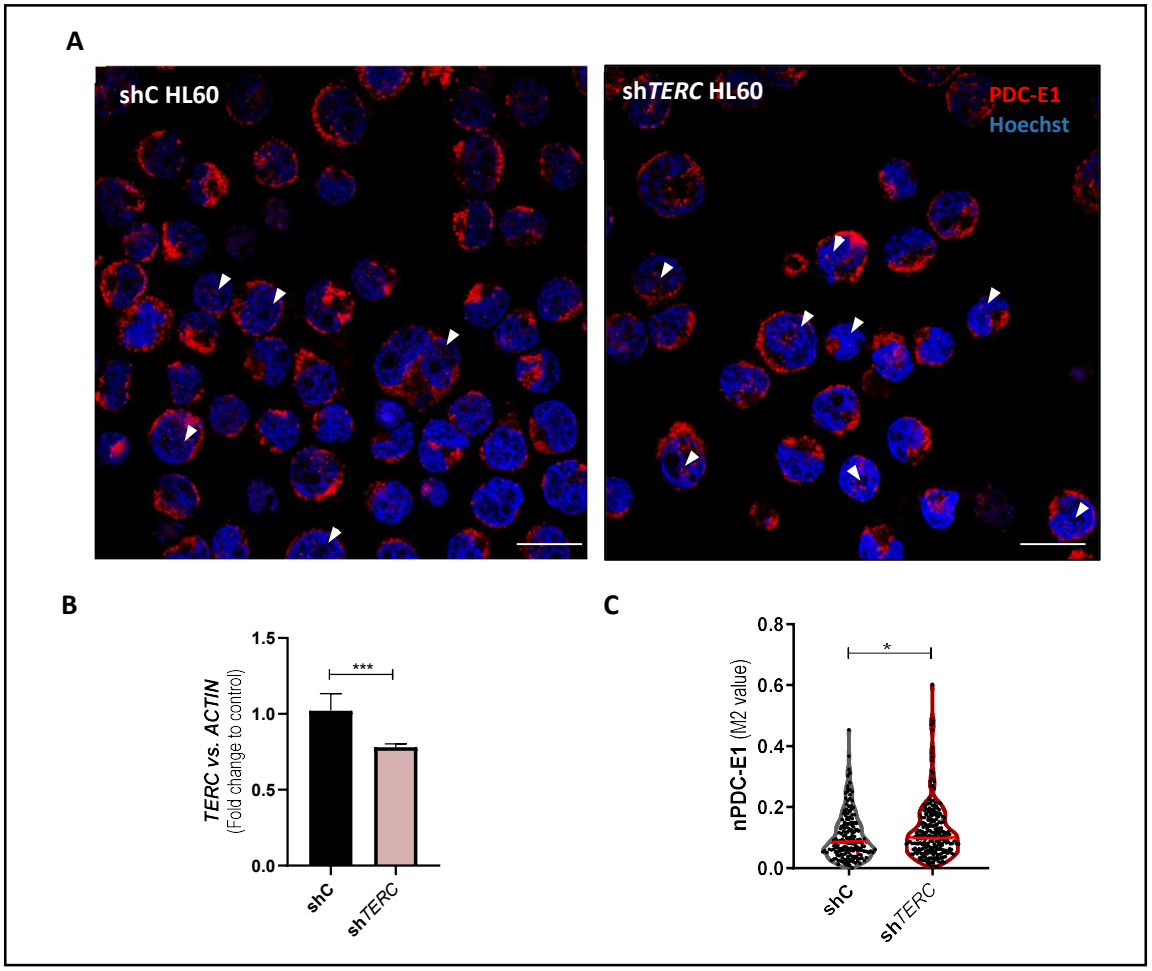

Figure 60. The decrease in*TERC* levels increases the amount of nuclear PDC-E1. (A) Representative confocal images of PDC-E1 immunostaining (red) in shC and sh*TERC* HL60 cells. The white arrowheads indicate cells with nPDC-E1. Scale bar= 20 µm. (B) RT-qPCR of shC and sh*TERC* HL60 cells showing the decrease in *TERC* levels in the sh*TERC* clone. The mean ± S.D. for each group is shown. P value was calculated using Man-Whitney test, ***p≤0.001. (C) Quantification of the levels of nuclear PDC-E1 (nPDC-E1). The imageJ software was used to determine the M2 Manders' coefficient, which indicates the amount of PDC-E1 inside the nucleus. Each dot represents a cell nucleus. The median for each sample is shown. P value was calculated using Welch's t test, *p≤0.05.

3.4. The decrease in *TERC* expression does not affect the total levels of histone acetylation.

The nuclear localization of PDC has been directly related with an increase in histone acetylation. The increase in PDC in the nucleus leads to an augmented production of acetyl-CoA that is used by the acetylases to modify the histones. Specifically, the acetylation levels of histone 3 (H3) and histone 4 (H4) increase upon PDC nuclear translocation[105]. Since *TERC* inhibition resulted into an increment of the levels of nPDC-E1, total levels of acetylated H3 and H4 (Ac-H3 and Ac-H4) were quantified by western blot in both shC and sh*TERC* HL60 cells (Fig. 61A). Nevertheless, no changes in total acetylation levels were found either in H3 or in H4 (Fig. 61B).

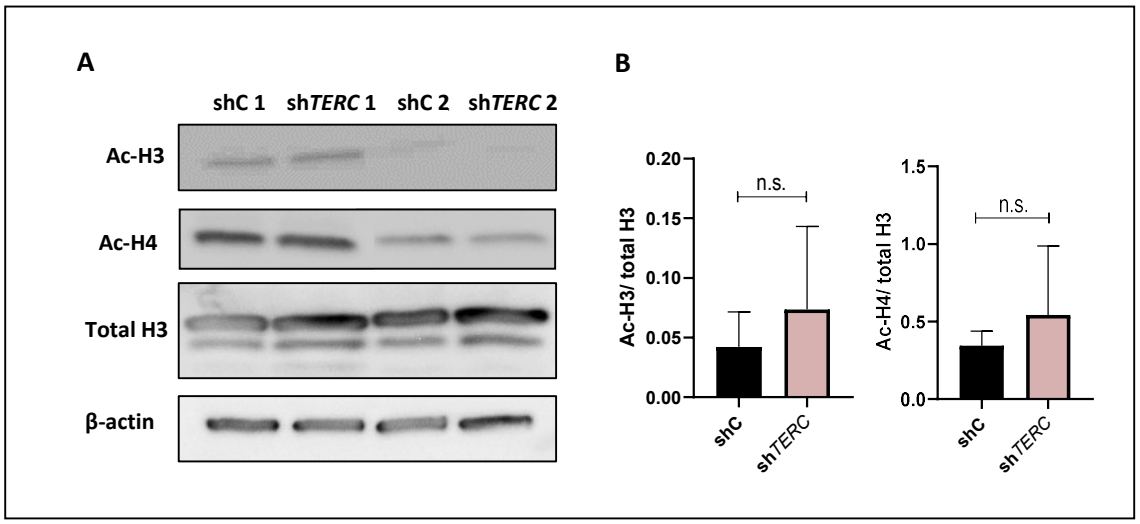

Figure 61. The decrease in *TERC* levels does not affect total levels of aceytaled histone 3 and 4. (A) Western blot membranes of acetylated H3 (Ac-H3) and H4 (Ac-H4) in two different shC and sh*TERC* HL60 clones. The levels of total H3 and β-actin were also dermined. (B) Western blot quantification. The total levels of H3 were normalized to β-actin and then used to normalized the levels of Ac-H3 and Ac-H4 in the samples. The mean ± S.E.M. for each group is shown. P value was calculated using Man-Whitney test, n.s.: not significant.

3.5. The decrease in *TERC* levels does not change PDC-E1 activity

With the purpose of evaluating if the interaction with *TERC* was modifying the activity of the enzyme, we quantified PDC activity through a colorimetric method using a commercial kit. We obtained shC and sh*TERC* HL60 protein extracts and samples were incubated with pyruvate (the substrate of PDC). The rest of the protein extract was used as background. The absorbance of each sample was measured every ten minutes for one hour and two time points were selected in the linear range to calculate the PDC activity (increase in absorbance). The results showed that PDC activity did not change upon decreasing *TERC* levels (Fig. 62B and 62C).

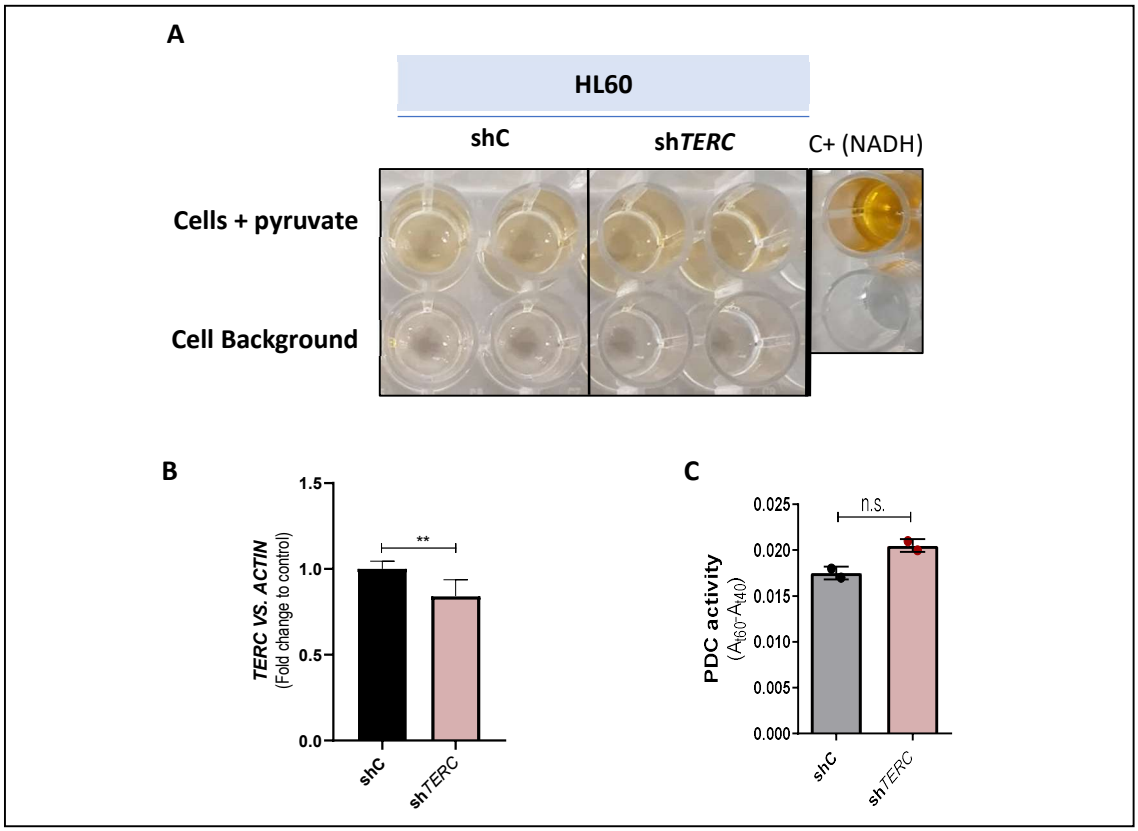

Figure 62.The decrease in *TERC* expression does not affect PDC-E1 activity. (A) Image showing the plate sample distribution and color at the final time of the PDC activity determination. In the right, a well with the possitive control provided by the kit is shown (NADH). The well below corresponds to the blank withouth cells. (B) RT-qPCR of shC and sh*TERC* HL60 cells showing the decrease in *TERC* levels in the sh*TERC* clone. (C) PDC activity quantification. The absorbance at 450 nm in the 40 and 60 minutes time points was chosen to determine the increase in PDC activity in the samples. (B and C) The mean ± S.D. for each group is shown. P value was calculated using Man-Whitney test, n.s.: not significant,**p≤0.01.

3.6. The interaction between *TERC* and PDC-E1 is also occurring in HeLa cells

We use HeLa cells to further confirm the TERC- PDC E1 interaction in another cell line. The HeLa cells are epithelial cells that can be easily transfected with siRNAs or plasmids to decrease or increase the expression of a protein or RNA of interest.

The interaction between *TERC* and PDC-E1 was confirmed using RNA-protein PLA. In this case a positive PLA signal was found both inside and outside of the cell nucleus, corroborating what we previously described in HL60 cells (Fig. 63D).

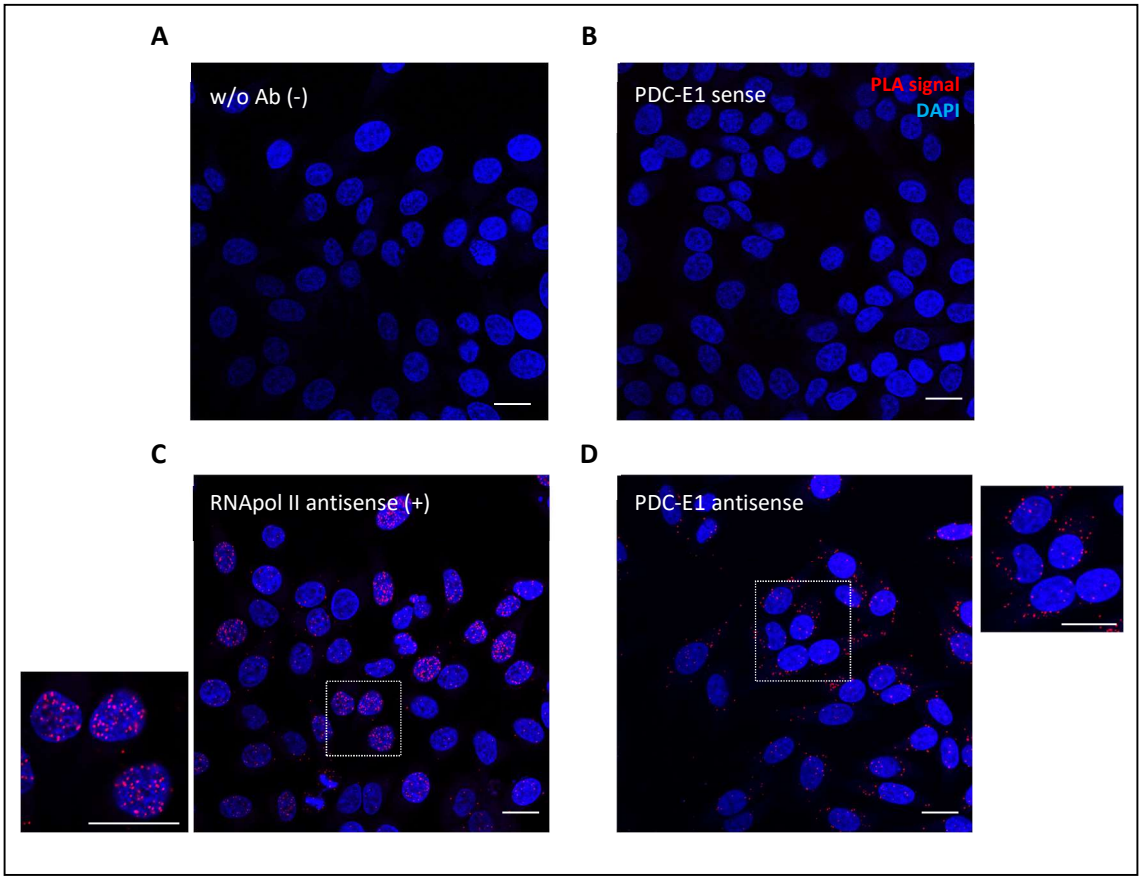

Figure 63. *TERC* and PDC-E1 interaction is confirmed in HeLa cells. Representative images of the RNA-protein PLA experiment in HeLa cells. The foci of red fluorescence (PLA signal) indicate the places of interaction between *TERC* and the studied protein. The cell nucleus is stained with DAPI (blue). (A-B) Negative controls without the anti-PDC-E1 antibody or with the sense *TERC* probe. (C) Positive control with anti-RNA pol II and *TERC* antisense probe. (D) Interactions between *TERC* and PDC-E1 inside and outside the nucleus of the cells. Scale bar= 20 µm.

3.7. *TERC* modulates the levels of nuclear PDC-E1

Next, we studied the PDC-E1 localization in HeLa cells upon modulating *TERC* levels. Cells were transfected with si*TERC* to decrease *TERC* levels, or with a plasmid (pBABE-*TERC*) to overexpress *TERC*. A scramble siRNA (siC) or a plasmid expressing GFP (pCS2-mtGFP) were used as controls. Then, cells were cell-cycle synchronized and an immunostaining and nuclear co-localization analysis were done. As shown in HL60 cells, we observed that a decrease in *TERC* levels lead to an increase in the levels of nPDC-E1 (Fig. 64A-C). Moreover, the overexpression of *TERC* resulted in a reduction of the amount of nPDC-E1, suggesting that *TERC* is important to control PDC-E1 localization in HeLa cells (Fig. 64A', 64B' and 64C).

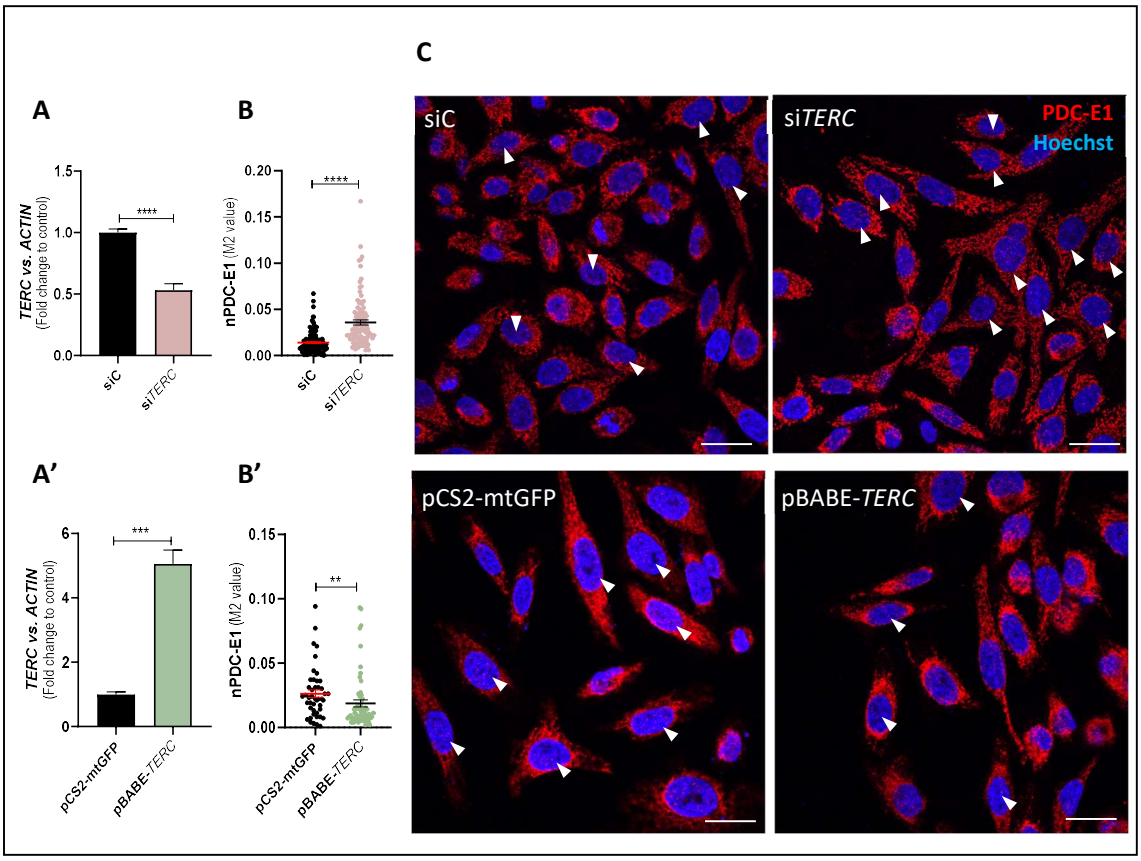

Figure 64. *TERC* levels can modify the amount of nuclear PDC-E1. (A and A') *TERC* levels quantified by RT-qPCR in HeLa cells transfected for 24 hours with si*TERC* to decrease *TERC* expresion or the pBABE-*TERC* plasmid to increase *TERC* expresion. The siC RNA and pCS2-mtGFP plasmid were used as controls. The mean ± S.D. for each group is shown. (B and B') Quantification of the levels of nuclear PDC-E1 (nPDC-E1). The imageJ software was used to determine the M2 Manders' coefficient, which indicates the amount of PDC-E1 inside the nucleus. Each dot represents a cell nucleus. The mean ± S.E.M. for each sample is shown. (C) Representative confocal images of PDC-E1 immunostaining (red) in the transfected HeLa cells. The cell nucleus is shown in blue (Hoechst). The white arrowheads indicate cells with nPDC-E1. Scale bar= 20 µm. P values were calculated using Mann-Whitney test, **p≤0.01, ***p≤0.001, ****p≤0.0001.

3.8. The change in *TERC* levels does not alter PDC-E1 activity

The PDC-E1 activity was also quantified in protein extracts of HeLa cells transfected with si*TERC* or pBABE-*TERC* using the same colorimetric method as described previously. In this case, neither the decrease nor the increase in *TERC* levels changed PDC-E1 activity in the whole cell lysate (Fig. 65B and 65C).

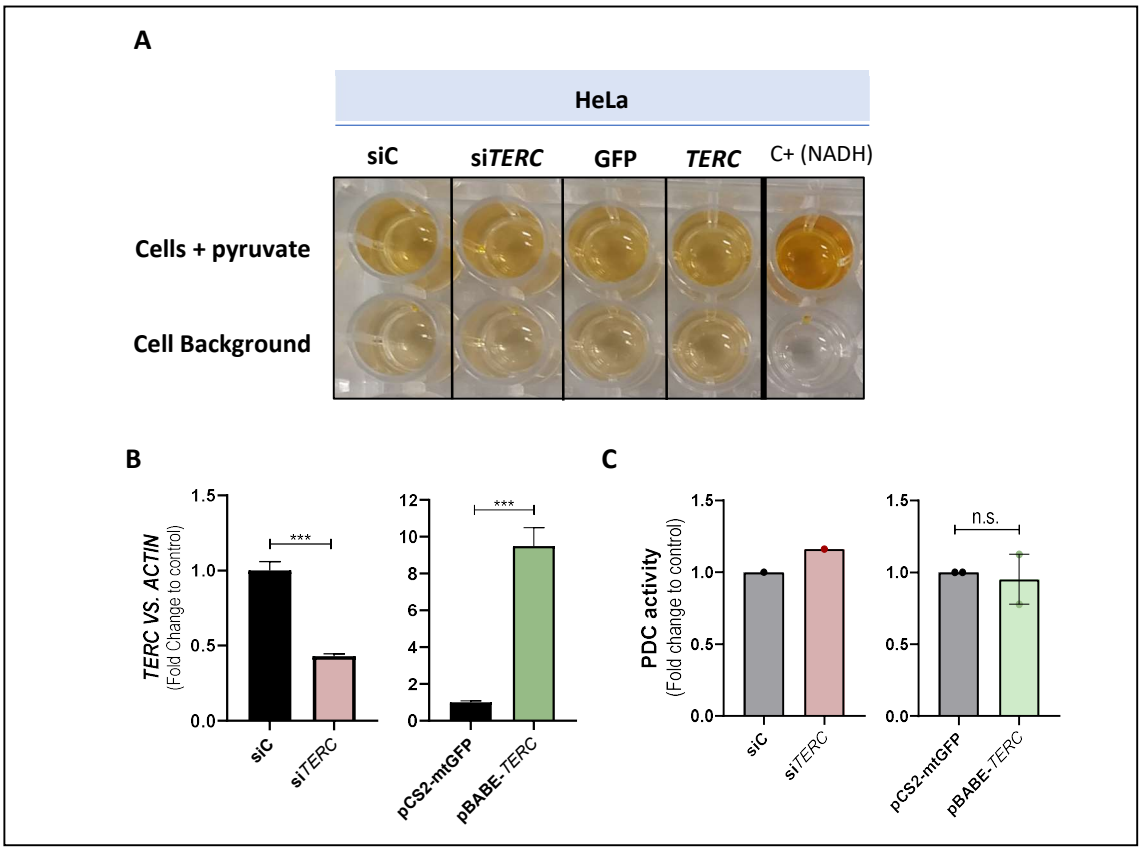

Figure 65. *TERC* expression does not affect PDC activity. (A) Image showing the plate sample distribution and color at the final time of the PDC activity determination. In the right, a well with the possitive control provided by the kit is shown (NADH). The well below corresponds to the blank withouth cells. (B) RT-qPCR of transfected HeLa cells showing the decrease in *TERC* levels upon siRNA transfection (si*TERC*) and the increase in expression with the plasmid transfection (pBABE-*TERC*). (C) PDC activity quantification. The absorbance at 450 nm in the 40 and 60 minutes time points was chosen to determine the increase in PDC activity in the samples. The measurements were then normalize to control samples. (B and C) The mean ± S.D. for each group is shown. P value was calculated using Man-Whitney test, n.s.: not significant,***p≤0.001

3.9. The telomerase catalytic subunit (TERT) interacts with PDC-E1

It is known that *TERC* and TERT play non-canonical functions independent of telomere lengthening. However, those functions can be performed by each component separately or forming a complex[32]. Hence, to establish whether TERT was also involved in the interaction with PDC-E1, we performed protein-protein PLA assays. In this protein-protein PLA we used two primary antibodies to detect TERT and PDC-E1. As a positive control of interaction, the antibodies against the E1 and E2 components of the PDC were used (Fig. 66A and D).

In the PLA experiments, we detected a positive interaction signal inside and outside of the cell nucleus in both HL60 and HeLa cells, the same distribution observed for *TERC* and PDC-E1 interaction (Fig. 66C and 66F). Besides, an increase in the number of interactions occurred when we overexpressed TERT (pBABE-hTERT) (Fig. 66H).

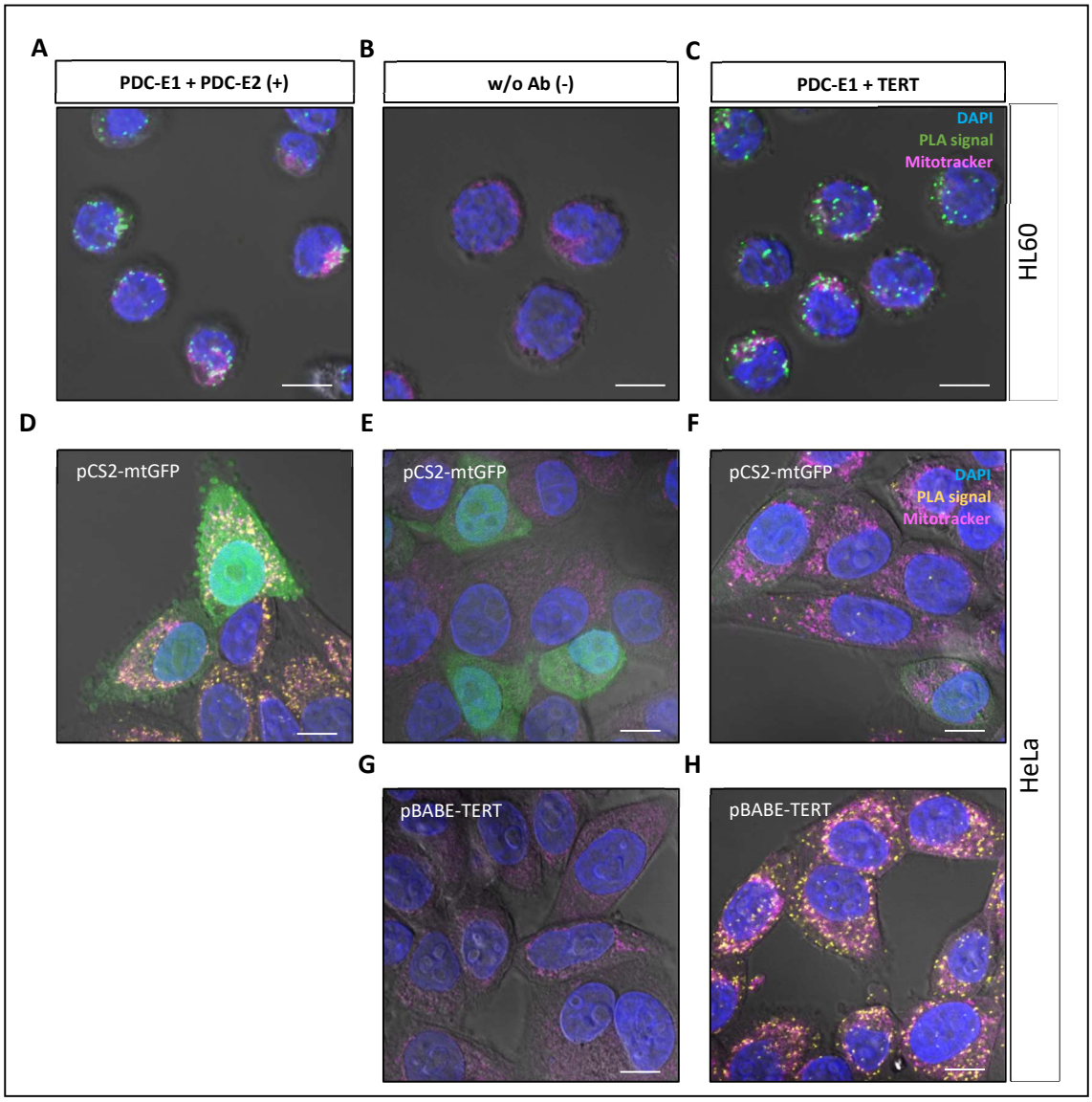

Figure 66. The interaction between TERT and PDC-E1 is confirmed by PLA. Representative confocal images of the TERT-PDC-E1 PLA in HL60 and HeLa cells. The PLA foci of interactinon can be seen in green in the upper panel (A-C) and in yellow in the other images (D-H). Mitochondria are stained with mitotracker (magenta) and the green cells correspond to HeLa cells transfected with the pCS2-mtGFP plasmid. (A and D) Positive control with anti-PDC-E1 and PDC-E2. (B, E and G) Negative controls without the primary antibodies. (C, F and H) Foci of interaction between TERT and PDC-E1 in the nucleus and cytoplasm of HL60 cells and HeLa cells. The number of foci increases upon transfection with the pBABE-TERT plasmid. Scale bar= 10 µm.

3.10. The isolation of pure nuclei in HeLa cells could not be achieved

The activity of PDC is regulated by phosphorylation of the E1 component. Three different serine residues can be phosphorylated: Ser^{232}, Ser^{293} and Ser^{300}. The modification of one or several of these serines has been shown to drastically reduce the activity of the PDC[101]. The pyruvate dehydrogenase kinases (PDKs) are the enzymes in charge of phosphorylating the PDC-E1. Since PDKs are not present in the cell nucleus[105], all nuclear PDC is active. According to our results, *TERC* levels do not affect PDC-E1 activity in whole cell lysates. However, *TERC* levels seemed to be important for nuclear PDC-E1 localization. For that reason, we aimed at studying PDC activity only in the nucleus of the transfected HeLa cells. Unfortunately, even though several protocols were tested to obtain pure nuclei of HeLa cells (refer to materials and methods), those could not be isolated with a significant level of purity. When analyzing the cellular fractions by western blot, an increase in the amount of nuclear proteins could be detected, indicating the nuclei were being enriched in the fractionation (Fig 67A and 67B). Nevertheless, the cytoplasmic and mitochondria proteins were present, indicating that membranes and cytoplasmic components were still attached to the cell nuclei (Fig. 67A-C).

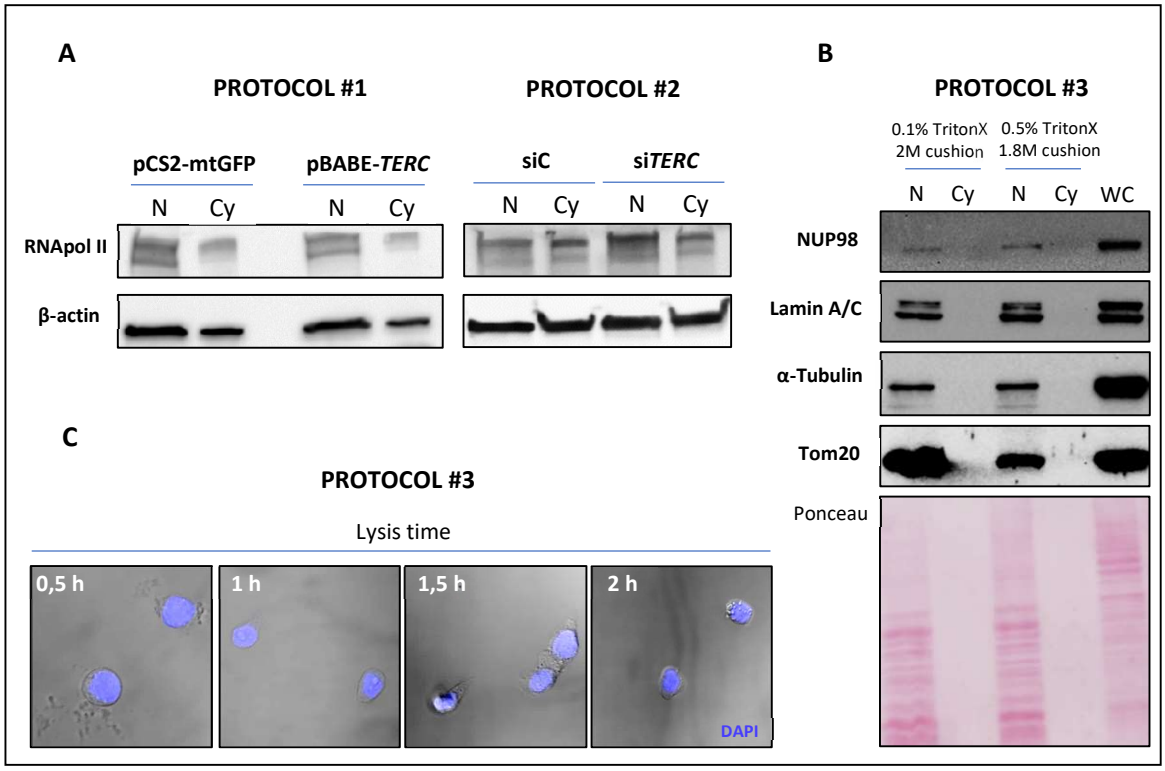

Figure 67. Three different protocols were tested to obtain pure nuclei out of HeLa cells. (A) Western blot membranes of nuclear (N) and cytoplasmic fractions (Cy) of HeLa cells incubated with anti RNA pol II and anti β-actin. The fractions were obtained using two different protocols utilizing homemade (protocol 1) and commercial buffers (protocol 2). Both consisted in a first step of lysis followed by differential centrifugation. The enrichment in RNA pol II shows the nuclei enrichment in the N fraction. The presence of β-actin in the nuclear fraction indicates the presence of cytoplasmic components along with the nuclei. (B) Western blot membranes of nuclear (N), cytoplasmic (Cy) fractions and whole HeLa (WC) cells incubated with anti NUP98, Lamin A/C, α-Tubulin and Tom20. The fractions were obtained using two variations of a protocol with a first step of lysis with TritonX followed by density gradient centrifugation with a glucose cushion (protocol 3). The Ponceau staining shows the no-recovery of the cytoplasmic fraction after the nuclear isolation protocol. The presence of α-Tubulin and Tom20 in the N fraction indicates the presence of cytoplasmic and mitochondrial components along with the nuclei. (C) Representative confocal images of isolated nuclei after performing the standard protocol 3 with four different lysis times. Nuclei are stained with DAPI (blue). The presence of cytoplasmic membranes around the nuclei shows their incomple isolation.

3.11. PDC activity is reduced in the mitochondria of TERT-overexpressing cells

Due to the impossibility to isolate pure nuclei, we decided to measure the PDC activity in isolated mitochondria. Also, because of the interaction found between TERT and PDC-E1, these experiments were done in HeLa cells transfected with siRNAs or plasmids to knock down or overexpress both telomerase components independently.

In this case, the PDC activity quantification was done using an immunocapture-dipstick assay, a more accurate method to determine PDC activity[105]. In this method, the cell or tissue lysate is absorbed into a nitrocellulose membrane (dipstick) that captures specifically the PDC. Later on, the dipstick with the bound PDC is incubated with a substrate that generates a color precipitate. The intensity of the color band that appears correlates to the PDC activity (Fig. 68A).

The mitochondria of the transfected HeLa cells were isolated, and their purity was evaluated by western blot (Fig. 68C). The determination of PDC activity in the HeLa knocked down for *TERC* and TERT could only be performed once. In this samples, no significant changes in PDC activity were found (Fig. 68B and 68D). The overexpression experiment was performed four times. The quantification of the band intensity indicated that the increase in *TERC* levels didn't cause any changes in PDC activity, which confirms our previous results (Fig. 68B and 68D). Unexpectedly, TERT overexpression caused a reduction in the mitochondrial PDC activity (Fig. 68B and 68D).

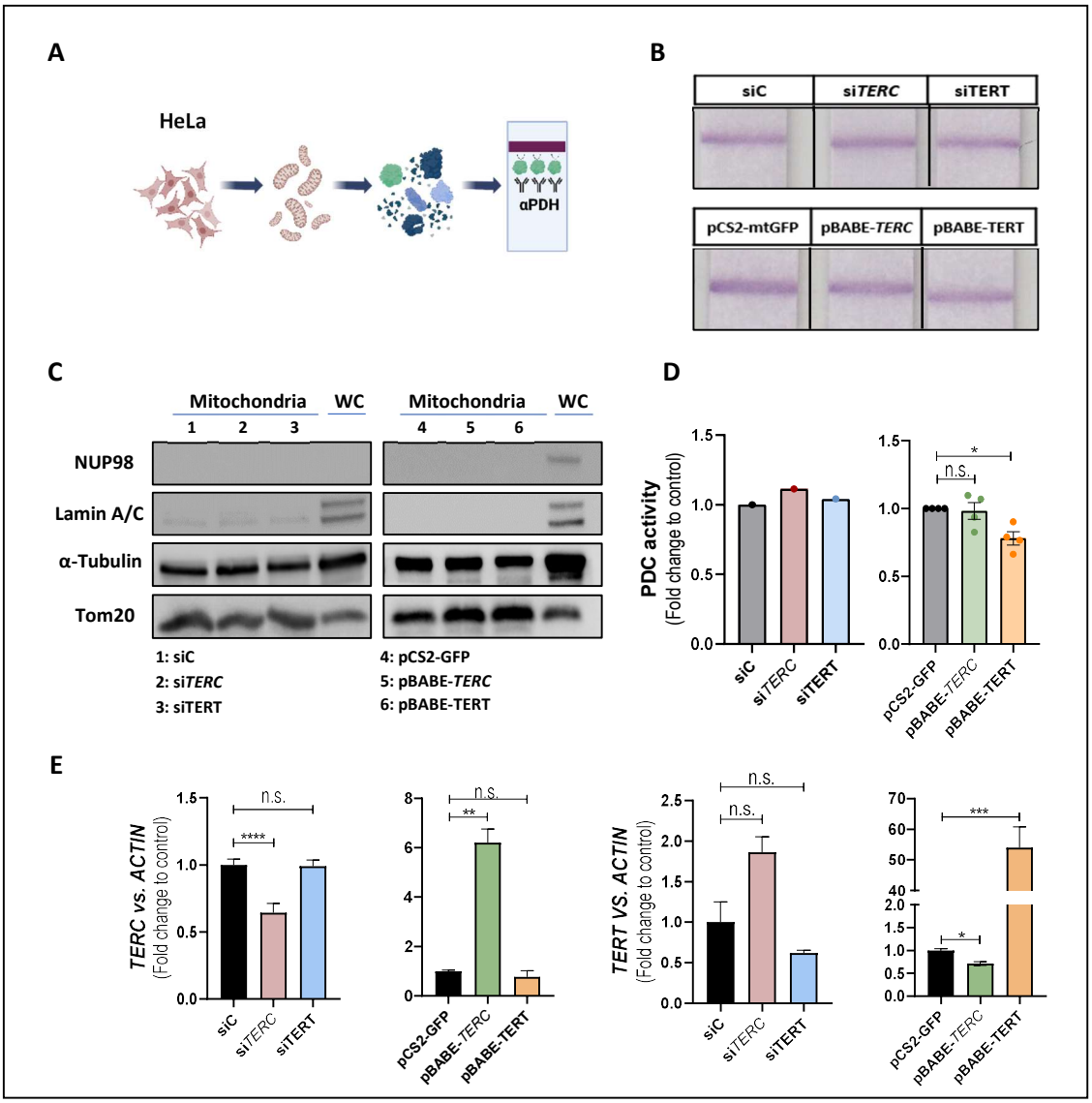

Figure 68. PDC activiy is reduced in mitochondria upon TERT overexpression. (A) Scheme of the followed protocol. After mitochondria isolation, the protein lysate was incubated with the comercial dipstick to retain the PDC in the nitrocelulose membrane. The intensity of the colored band correlates with the PDC activity. Created with BioRender.com. (B) Representative images of the band that apperared in the dipstick for the transfected HeLa cells. (C) Western blot membranes of isolated mitochondria and whole HeLa cells (WC) incubated with anti NUP98, Lamin A/C, α-Tubulin and Tom20. The absense of nuclear proteins (NUP98 and Lamin A/C) ensures that there was no nPDC in the samples. The enrichment in Tom20 shows the enrichment in mitochondria. (D) PDC activity quantification. The band intensity for each sample was measured in imageJ and normalized to control samples. The mean ± S.E.M for each group is shown. Each dot represents an experimental replicate. (E) RT-qPCR of transfected HeLa cells showing the *TERC* and *TERT* levels upon siRNA transfection (si*TERC*, siTERT) and the increase in expression with the plasmid transfection (pBABE-*TERC*/TERT). The mean ± S.E.M for each group is shown. (D and E) P value was calculated using Kruskal-Wallis and Dunn's multiple comparisons test, n.s.: not significant,*p≤0.05, **p≤0.01, ***p≤0.001.

Since the TERT-overexpressing cells showed a decrease in PDC activity, we wondered if there were changes in total levels of PDC-E1 or its phosphorylation status. The total levels of PDH (total E1) and serine 293 phosphorylated E1 (p-S293 E1) were determined by western blot in the isolated mitochondria (Fig. 69A). Neither *TERC* nor TERT overexpression changed total PDC-E1 levels (Fig. 69B). Interestingly, the levels of p-E1 showed an increase in *TERC*-overexpressing cells but in TERT-overexpressing cells weren't consistent with the previous results. (Fig. 69C).

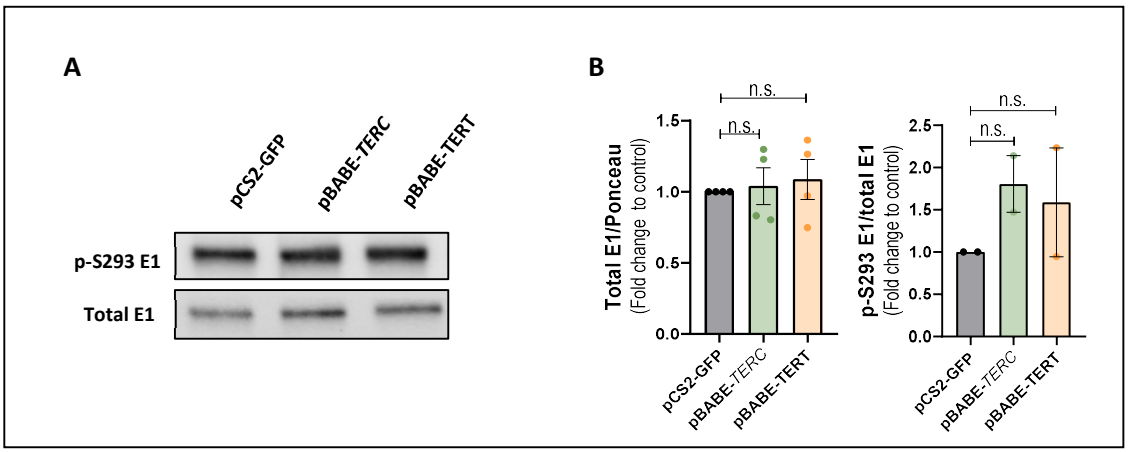

Figure 69. Total PDC-E1 and p-PDC-E1 protein levels do not change in the mitochondria of *TERC* and TERT-overexpressing HeLa cells. (A) Western blot membranes showing protein levels of PDC-E1 (total E1) and serine 293 phosphorylated E1 (p-S293 E1) in isolated mitochondria from transfected HeLa cells. (B) Quantification of the levels of total E1 in the samples. The levels of E1 were normalized to the Ponceau staning (total protein levels) and to control sample (pCS2-mtGFP). The levels of p-E1 were also normalized to total E1 levels. Each dot represents an experimental replicate. The mean ± S.E.M. for each group is shown. P value was calculated using Kruskal-Wallis and Dunn's multiple comparisons test, n.s.: not significant.

3.12. TERT and *TERC* weakly interact with PDC-E2

Finally, since the PDC complex is formed by the E1, E2 and E3 subunits, we wanted to know if *TERC* or TERT were also interacting with other subunits of PDC. Therefore, *TERC* and TERT interaction with the E2 component was investigated by PLA assays in HL60 and HeLa cells. The results showed that only a couple of cells were found to have a positive PLA signal in the case of TERC-PDC E2 interaction (Fig. 70D).

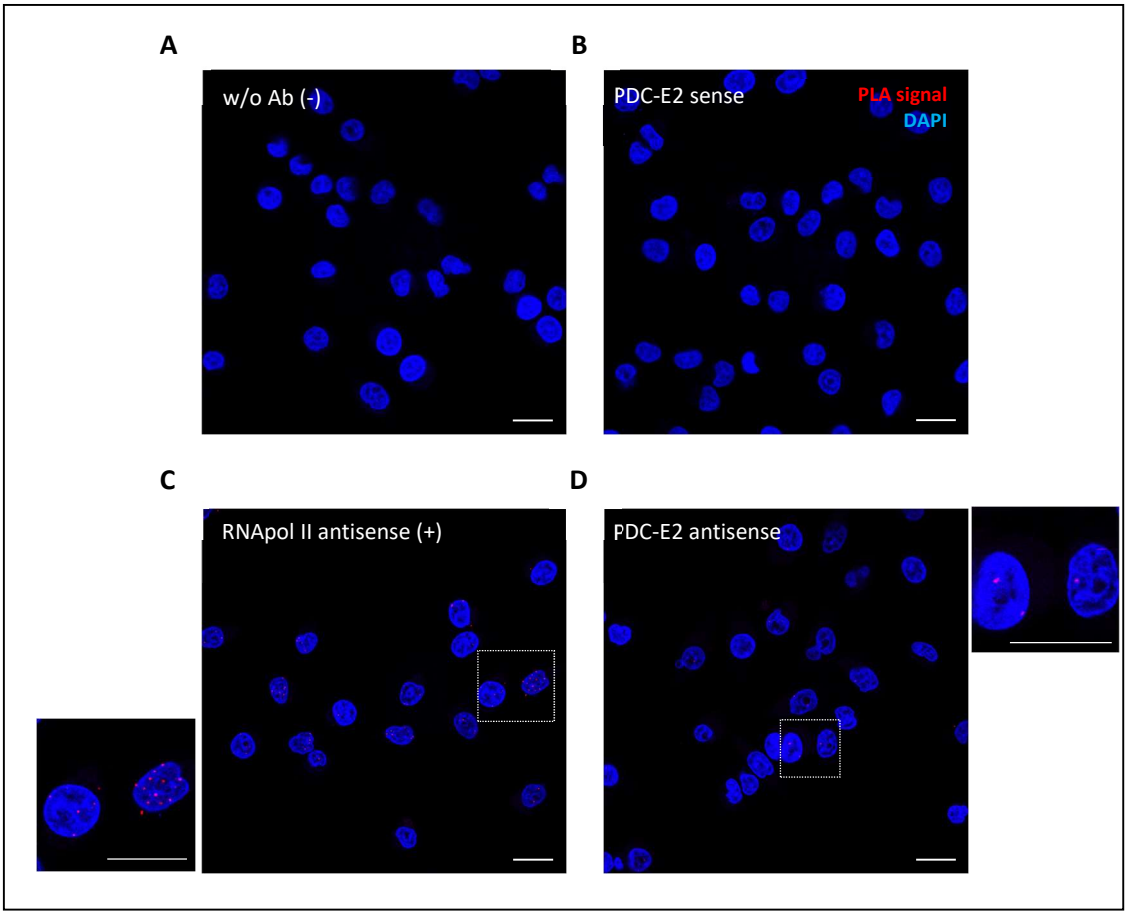

Figure 70. The telomerase RNA interacts with the PDC-E2 subunit. Representative images of the RNA-protein PLA experiment in HeLa cells. The foci of red fluorescence (PLA signal) indicate the places of interaction between *TERC* and the studied protein. The cell nucleus is stained with DAPI (blue). (A-B) Negative controls without the anti-PDC-E2 antibody or with the sense *TERC* probe. (C) Positive control with anti-RNA pol II and *TERC* antisense probe. (D) Interactions between *TERC* and PDC-E2 inside and outside the nucleus of the cells. Scale bar= 20 µm.

In the case of TERT-E2 interaction, the number of cells with a PLA signal and the number of signals in each cell was also lower than that observed in the TERT-E1 component interaction (Fig. 71C and 71F). HL60 cells presented a higher number of positive PLA signals than HeLa cells, in which again, the number of interactions increased upon transfection with the pBABE-TERT plasmid (Fig. 71C, 71F and 71H).

These results might suggest that the telomerase complex (or each component independently) interact with the whole PDC complex. Given that the PLA signal only appears if the interacting

molecules are closer than 40 nm, the lower number of PLA signals may be explained due to the fact that the PDC-E2 is found in the core of the complex, and the PDC-E1 protein is located in the periphery of the enzymatic complex.

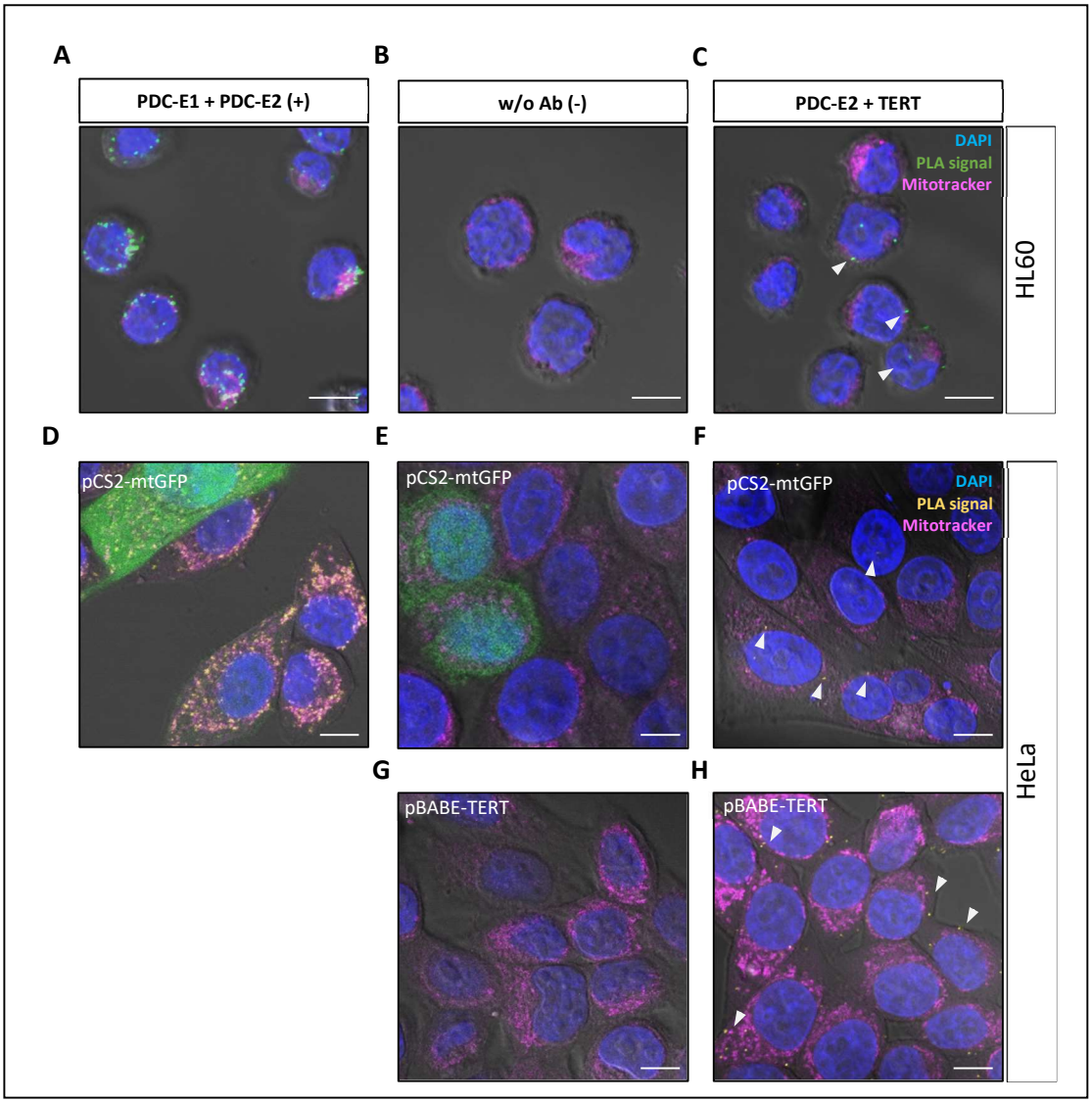

Figure 71. Telomerase (TERT) interacts with the PDC-E2 subunit. Representative confocal images of the TERT-PDC-E2 PLA in HL60 and HeLa cells. The PLA foci of interactinon can be observed in green in the upper panel (A-C) and in yellow in the other images (D-H). Mitochondria are stained with mitotracker (magenta) and the green cells correspond to HeLa cells transfected with the pCS2-mtGFP plasmid. (A and D) Positive control with anti-PDC-E1 and PDC-E2. (B, E and G) Negative controls without the primary antibodies. (C, F and H) Foci of interaction between TERT and PDC-E2 in the nucleus and cytoplasm of HL60 cells and HeLa cells (white arrowheads). The number of foci increases upon transfection with the pBABE-TERT plasmid.

4. Discussion

Long non-coding RNAs (lncRNAs) are known to have functions controlling gene expression by binding to specific motifs in the DNA[40] or by determining the localization of chromatin modificators or the transcription machinery[38]. The telomerase RNA (*TERC*) has been described to act as a lncRNA independently of telomerase performing those kinds of functions[45; 48]. In particular, our previous findings reveal the ability of *TERC* to interact with RNApol II to promote the transcription of myelopoietic genes[47]. However, although several loci containing the *TERC*-binding motif were found in the genome[37], the protein interactors of *TERC* haven't been described.

Considering all of the above, we decided to identify the protein interactome of *terc* to uncover additional non-canonical roles of the telomerase RNA using zebrafish as an *in vivo* model. Surprisingly, we found that most *terc*-interacting proteins were involved in carbon metabolism and oxidative phosphorylation pathways (Elena Martínez-Balsalobre PhD thesis, unpublished results).

In this work we demonstrated that the interaction found between *terc* and the E1 component of the pyruvate dehydrogenase complex (PDC-E1) in zebrafish was conserved in human cells. We validated the *TERC*-PDC-E1 interaction in two different human cell lines (HL60 and HeLa cells) by using RNA-pull down, RNA immunoprecipitation (RIP) and Proximity Ligation Assay (PLA) experiments. Additionally, by colocalization analysis of the PLA signal, we determined that this interaction was taking place inside the nucleus and in the cell cytosol and mitochondria. In the recent years, the number of reported glycolysis and TCA-related proteins interacting with RNAs has been widely increasing[286; 298]. Still, the pyruvate dehydrogenase has not been reported to be able to bind RNAs until now. Furthermore, this interaction also depicts another non-canonical role of *TERC*.

Since we found that *TERC*-PDC-E1 interaction was occurring in multiple cell sites, and it has been reported that *TERC* can be imported into the mitochondria[49] and PDC can translocate into the nucleus[105; 106], we wondered if *TERC* could be involved PDC-E1 localization. In fact, we found that a decrease in *TERC* expression led to an increase in nuclear levels of PDC-E1 and that *TERC* overexpression had the opposite effect. However, although we saw an increase in nuclear PDC levels when decreasing *TERC* expression, we did not see changes in global levels of acetylated histone 3 (H3) or histone 4 (H4). Besides, *TERC* expression did not affect PDC activity when measured in whole cells and mitochondria. Although global changes in PDC activity could not be appreciated, we wanted to address the question if, specifically, PDC activity could be changing in the nucleus when modifying *TERC* expression. Unfortunately, we couldn't isolate nuclei with enough purity to address this question. Furthermore, we cannot rule out that, despite the global acetylation status of histones is not altered, *TERC* might be recruiting PDC-E1 to specific loci to regulate histone acetylation. This would not be surprising considering the ability of *TERC* to bind to genomic DNA. Regarding this, it would be very interesting to assess PDC-E1 binding to genomic loci containing *TERC*-binding sites known to be bound by *TERC* and determine histone acetylation status in those loci.

It has been shown that *TERC*-TERT complexes regulate regeneration and tumorogenesis by binding to promoters of ribosomal DNA genes and stimulating its transcription by RNA polymerase I[299]. Furthermore, inhibition of both TERT and *TERC* impaired myelopoiesis in human iPS cells in a telomere length independent manner[46]. In addition, we have also shown that *terc* has a key role in the regulation of myelopoiesis in zebrafish and humans independently of TERT

and telomere length[21; 47]. Thus, we evaluated if PDC-E1-*TERC* interaction was *TERC*-exclusive, that is, a non-canonical role of telomerase RNA independent of TERT. We discovered that, in fact, TERT was also interacting with PDC-E1. Moreover, TERT overexpression reduced PDC activity in the mitochondria. In addition, we investigated if *TERC* and TERT were interacting with other proteins of the PDC. By using PLA, we detected some signals for both telomerase components interacting with PDC-E2, however, those were less intense and abundant than the ones obtained with PDC-E1. This may be due to the distribution of the PDC subunits in the complex, being the E1 in the periphery and E2 in the core. We need to further investigate if that interaction is performed by TERT and *TERC* separately or forming a complex, and in case of the latter, whether any of the components is dispensable for the interaction to happen.

Summarizing, in this work we show the interaction between both telomerase components with the E1 and E2 subunits of the PDC. We need to further investigate if that interaction is performed by TERT and *TERC* separately or altogether, and in case of the latter, if the presence of *TERC* or TERT is indispensable for the interaction to happen. Besides, all PDC components are known to perform independent functions in cytosol and nucleus of the cells. The PDC-E1α subunit has been reported to be in the cytosol, inhibiting the NFκB pathway by directly interacting with IKKβ and protein phosphatase 1B[300]. The E2 and E1 components have been shown to interact with the transcription factor STAT5, improving its function and upregulating the transcription of the genes under its control such as IL-3[301; 302]. Moreover, PDC-E2 has been described to form a complex with histone acetyltransferase p300 and pyruvate kinase (PKM2) to induce local production of acetyl-CoA in specific loci in the nucleus[303]. Lastly, the PDC-E3 protein has been shown to be able to bind TiO_2, and also to interact with doble strand DNA (dsDNA)[304].

Due to the numerous functions attributed to the E1, E2 and E3 components besides the production of acetyl-CoA when they're forming the PDC, and due to the several places of interaction found between PDC-E1 and E2 and the telomerase components, in order to stablish the biological role of this interaction, it would be useful to determine if the interactions found take place with the components separately of with the whole PDC (E1, E2 and E3 altogether). That is, if TERT and/or *TERC* are interacting with the PDC subunits separately, they may also be participating in their described non-canonical functions or being part of another non-canonical role of the PDC subunits not yet reported.

On the other hand, PDC has been recently described as a target to the aging process[305]. Not only PDC activity has been reported to be diminished in the muscle of aged mice[306] and in the brain of aged mice and Alzheimer's disease patients[307; 308], but also progeria patients, which have an accelerated aging process, have been described to have more nuclear PDC and decreased oxidative phosphorylation[106; 309; 310]. The telomerase complex is one of the key cellular mechanisms directly related to aging and immortalization[10; 218]. Several studies have already described the importance of the nucleus-to-mitochondria communication in cell function in general but also in the aging process[34; 104; 311]. Moreover, they point to histone modifications (specifically acetylation) as the main mechanism by which cell senescence and pluripotency are linked to cell metabolism[104; 312]. Due to the previous evidence linking the control of histone acetylation and aging, and due to the role of PDC in histone acetylation, we also have to consider that the interaction that we report in this work between the telomerase components and the subunits of PDC, may be indicating a new way in which aging and metabolism are connected.

Conclusions

The results obtained in this work led to the following conclusions:

1. *terc* levels affect the composition of the glycolytic and TCA cycle metabolites in zebrafish larvae. Moreover, *terc* functions as a lncRNA regulating the expression of *ldhbb* by binding to its promoter region in both larvae and adult hematopoietic tissue.

2. The pharmacological inhibition of lactate dehydrogenase (Ldh) with oxamate and exogenous lactate are able to alleviate skin inflammation in the *spint1a* mutant zebrafish by decreasing the NAD^+/NADH ratio. However, only the treatment with oxamate reduces the levels of DNA damage and oxidative stress (H_2O_2) in the skin of *spint1a* mutant larvae.

3. Manipulation of Ldh activity with oxamate and lactate alters gene expression profile of inflamed skin of *spint1a* mutant zebrafish larvae, including *rps6ka1*, *socs2* and *cxcl14*. However, genetic manipulation of selected differential expressed genes, such as *rps6ka1* and *socs2*, does not affect skin inflammation of *spint1a* mutant zebrafish larvae. In addition, *RPS6KA1* transcript levels increase in human skin psoriatic lesions and correlate with those of inflammation markers, whereas those of *SOCS2* are decreased.

4. *LDHA* transcript levels are higher in psoriatic lesions of human skin than in non-lesional and healthy skin, and positively correlate with those of inflammation markers. In addition, *CXCL14* mRNA levels are lower in human skin psoriatic lesions than in healthy skin and negatively correlate with those of *LDHA* and inflammation markers.

5. *terc* deficiency, but not Tert, alleviates skin inflammation of *spint1a* mutant larvae, assayed as the number of skin aggregates and neutrophil infiltration.

6. Overexpression of *terc* in hematopoietic cells restrains glioblastoma progression independently of Tert. This effect seems to be independent of the microglia, since its number and its polarization are both unaffected.

7. Both telomerase components (*TERC* and TERT) interact with the E1 and E2 subunits of the pyruvate dehydrogenase complex (PDC) in the nucleus, cytosol, and mitochondria of human cells.

8. Nuclear PDC correlates with *TERC* levels in human cells. Thus, increased *TERC* levels result in reduced nuclear PDC and, conversely, decreased *TERC* levels lead to increased nuclear PDC. These changes of PDC localization promoted by *TERC* affect neither global histone H3 and H4 acetylation nor PDC activity. However, TERT overexpression decreases PDC activity in the mitochondria.

References

1. Shay JW. 2018. Telomeres and aging. Curr Opin Cell Biol. 52:1-7.
2. Kim NW, Piatyszek MA, Prowse KR, Harley CB, West MD, Ho PL, Coviello GM, Wright WE, Weinrich SL, Shay JW. 1994. Specific association of human telomerase activity with immortal cells and cancer. Science. 266(5193):2011-2015.
3. Palm W, de Lange T. 2008. How shelterin protects mammalian telomeres. Annu Rev Genet. 42:301-334.
4. Teixeira MT, Gilson E. 2005. Telomere maintenance, function and evolution: The yeast paradigm. Chromosome Res. 13(5):535-548.
5. Blackburn EH. 2001. Switching and signaling at the telomere. Cell. 106(6):661-673.
6. de Lange T. 2005. Shelterin: The protein complex that shapes and safeguards human telomeres. Genes Dev. 19(18):2100-2110.
7. Low KC, Tergaonkar V. 2013. Telomerase: Central regulator of all of the hallmarks of cancer. Trends Biochem Sci. 38(9):426-434.
8. Lim CJ, Cech TR. 2021. Shaping human telomeres: From shelterin and cst complexes to telomeric chromatin organization. Nat Rev Mol Cell Biol. 22(4):283-298.
9. Wang Y, Feigon J. 2017. Structural biology of telomerase and its interaction at telomeres. Curr Opin Struct Biol. 47:77-87.
10. Aragona M, Maisano R, Panetta S, Giudice A, Morelli M, La Torre I, La Torre F. 2000. Telomere length maintenance in aging and carcinogenesis. Int J Oncol. 17(5):981-989.
11. Victorelli S, Passos JF. 2017. Telomeres and cell senescence - size matters not. EBioMedicine. 1(1):1-7.
12. Nandakumar J, Cech TR. 2013. Finding the end: Recruitment of telomerase to telomeres. Nat Rev Mol Cell Biol. 14(2):69-82.
13. Blackburn EH. 1990. Telomeres and their synthesis. Science. 249(4968):489-490.
14. Venteicher AS, Abreu EB, Meng Z, McCann KE, Terns RM, Veenstra TD, Terns MP, Artandi SE. 2009. A human telomerase holoenzyme protein required for cajal body localization and telomere synthesis. Science. 323(5914):644-648.
15. Garus A, Autexier C. 2021. Dyskerin: An essential pseudouridine synthase with multifaceted roles in ribosome biogenesis, splicing, and telomere maintenance. RNA. 27(12):1441-1458.
16. Tomlinson RL, Ziegler TD, Supakorndej T, Terns RM, Terns MP. 2006. Cell cycle-regulated trafficking of human telomerase to telomeres. Mol Biol Cell. 17(2):955-965.
17. Blackburn EH, Epel ES, Lin J. 2015. Human telomere biology: A contributory and interactive factor in aging, disease risks, and protection. Science. 350(6265):1193-1198.
18. Guterres AN, Villanueva J. 2020. Targeting telomerase for cancer therapy. Oncogene. 39(36):5811-5824.
19. Jaiswal RK, Kumar P, Yadava PK. 2013. Telomerase and its extracurricular activities. Cell Mol Biol Lett. 18(4):538-554.
20. Romaniuk A, Paszel-Jaworska A, Totoń E, Lisiak N, Hołysz H, Królak A, Grodecka-Gazdecka S, Rubiś B. 2019. The non-canonical functions of telomerase: To turn off or not to turn off. Mol Biol Rep. 46(1):1401-1411.
21. Alcaraz-Pérez F, García-Castillo J, García-Moreno D, López-Muñoz A, Anchelin M, Angosto D, Zon LI, Mulero V, Cayuela ML. 2014. A non-canonical function of telomerase rna in the regulation of developmental myelopoiesis in zebrafish. Nat Commun. 5:3228.
22. Choi J, Southworth LK, Sarin KY, Venteicher AS, Ma W, Chang W, Cheung P, Jun S, Artandi MK, Shah N et al. 2008. Tert promotes epithelial proliferation through transcriptional control of a myc- and wnt-related developmental program. PLoS Genet. 4(1):e10.
23. Liu H, Liu Q, Ge Y, Zhao Q, Zheng X, Zhao Y. 2016. Htert promotes cell adhesion and migration independent of telomerase activity. Sci Rep. 6:22886.
24. Mukherjee S, Firpo EJ, Wang Y, Roberts JM. 2011. Separation of telomerase functions by reverse genetics. Proc Natl Acad Sci U S A. 108(50):E1363-1371.

25. Bernabé-García M, Martínez-Balsalobre E, García-Moreno D, García-Castillo J, Revilla-Nuin B, Blanco-Alcaina E, Mulero V, Alcaraz-Pérez F, Cayuela ML. 2021. Telomerase reverse transcriptase activates transcription of mir500a to inhibit hedgehog signalling and promote cell invasiveness. Mol Oncol. 15(7):1818-1834.
26. Park JI, Venteicher AS, Hong JY, Choi J, Jun S, Shkreli M, Chang W, Meng Z, Cheung P, Ji H et al. 2009. Telomerase modulates wnt signalling by association with target gene chromatin. Nature. 460(7251):66-72.
27. Liu Z, Li Q, Li K, Chen L, Li W, Hou M, Liu T, Yang J, Lindvall C, Björkholm M et al. 2013. Telomerase reverse transcriptase promotes epithelial-mesenchymal transition and stem cell-like traits in cancer cells. Oncogene. 32(36):4203-4213.
28. Koh CM, Khattar E, Leow SC, Liu CY, Muller J, Ang WX, Li Y, Franzoso G, Li S, Guccione E et al. 2015. Telomerase regulates myc-driven oncogenesis independent of its reverse transcriptase activity. J Clin Invest. 125(5):2109-2122.
29. Liu T, Zhang L, Joo D, Sun SC. 2017. Nf-κb signaling in inflammation. Signal Transduct Target Ther. 2:17023-.
30. Yin L, Hubbard AK, Giardina C. 2000. Nf-kappa b regulates transcription of the mouse telomerase catalytic subunit. J Biol Chem. 275(47):36671-36675.
31. Wu Y, Bian C, Zhen C, Liu L, Lin Z, Nisar MF, Wang M, Bartsch JW, Huang E, Ji P et al. 2017. Telomerase reverse transcriptase mediates emt through nf-κb signaling in tongue squamous cell carcinoma. Oncotarget. 8(49):85492-85503.
32. Ghosh A, Saginc G, Leow SC, Khattar E, Shin EM, Yan TD, Wong M, Zhang Z, Li G, Sung WK et al. 2012. Telomerase directly regulates nf-κb-dependent transcription. Nat Cell Biol. 14(12):1270-1281.
33. Dolcet X, Llobet D, Pallares J, Matias-Guiu X. 2005. Nf-kb in development and progression of human cancer. Virchows Arch. 446(5):475-482.
34. Haendeler J, Dröse S, Büchner N, Jakob S, Altschmied J, Goy C, Spyridopoulos I, Zeiher AM, Brandt U, Dimmeler S. 2009. Mitochondrial telomerase reverse transcriptase binds to and protects mitochondrial dna and function from damage. Arterioscler Thromb Vasc Biol. 29(6):929-935.
35. Santos JH, Meyer JN, Skorvaga M, Annab LA, Van Houten B. 2004. Mitochondrial htert exacerbates free-radical-mediated mtdna damage. Aging Cell. 3(6):399-411.
36. Indran IR, Hande MP, Pervaiz S. 2011. Htert overexpression alleviates intracellular ros production, improves mitochondrial function, and inhibits ros-mediated apoptosis in cancer cells. Cancer Res. 71(1):266-276.
37. Chu C, Qu K, Zhong FL, Artandi SE, Chang HY. 2011. Genomic maps of long noncoding rna occupancy reveal principles of rna-chromatin interactions. Mol Cell. 44(4):667-678.
38. Yao RW, Wang Y, Chen LL. 2019. Cellular functions of long noncoding rnas. Nat Cell Biol. 21(5):542-551.
39. Sun M, Kraus WL. 2015. From discovery to function: The expanding roles of long noncoding rnas in physiology and disease. Endocr Rev. 36(1):25-64.
40. Kopp F, Mendell JT. 2018. Functional classification and experimental dissection of long noncoding rnas. Cell. 172(3):393-407.
41. Cayuela ML, Flores JM, Blasco MA. 2005. The telomerase rna component terc is required for the tumour-promoting effects of tert overexpression. EMBO Rep. 6(3):268-274.
42. Blasco MA, Rizen M, Greider CW, Hanahan D. 1996. Differential regulation of telomerase activity and telomerase rna during multi-stage tumorigenesis. Nat Genet. 12(2):200-204.
43. Wang J, Wu M, Chang L, Jin Z, Yang X, Li D, Qu J, Hou Q, Huang X, Xu C. 2022. The *lncrna terc* promotes gastric cancer cell proliferation, migration, and invasion by sponging *mir-423-5p* to regulate *sox12* expression. Ann Transl Med. 10(18):963.
44. Gazzaniga FS, Blackburn EH. 2014. An antiapoptotic role for telomerase rna in human immune cells independent of telomere integrity or telomerase enzymatic activity. Blood. 124(25):3675-3684.

45. Wu S, Ge Y, Lin K, Liu Q, Zhou H, Hu Q, Zhao Y, He W, Ju Z. 2022. Telomerase rna terc and the pi3k-akt pathway form a positive feedback loop to regulate cell proliferation independent of telomerase activity. Nucleic Acids Res. 50(7):3764-3776.
46. Jose SS, Tidu F, Burilova P, Kepak T, Bendickova K, Fric J. 2018. The telomerase complex directly controls hematopoietic stem cell differentiation and senescence in an induced pluripotent stem cell model of telomeropathy. Front Genet. 9:345.
47. García-Castillo J, Alcaraz-Pérez F, Martínez-Balsalobre E, García-Moreno D, Rossmann MP, Fernández-Lajarín M, Bernabé-García M, Pérez-Oliva AB, Rodríguez-Cortez VC, Bueno C et al. 2021. Telomerase rna recruits rna polymerase ii to target gene promoters to enhance myelopoiesis. Proc Natl Acad Sci U S A. 118(32).
48. Liu H, Yang Y, Ge Y, Liu J, Zhao Y. 2019. Terc promotes cellular inflammatory response independent of telomerase. Nucleic Acids Res. 47(15):8084-8095.
49. Cheng Y, Liu P, Zheng Q, Gao G, Yuan J, Wang P, Huang J, Xie L, Lu X, Tong T et al. 2018. Mitochondrial trafficking and processing of telomerase rna terc. Cell Rep. 24(10):2589-2595.
50. Zheng Q, Liu P, Gao G, Yuan J, Wang P, Huang J, Xie L, Lu X, Di F, Tong T et al. 2019. Mitochondrion-processed terc regulates senescence without affecting telomerase activities. Protein Cell. 10(9):631-648.
51. Nelson DL, Cox MM. 2008. Lehninger principles of biochemistry. AHR K, editor. SARA TENNEY.
52. Navale AM, Paranjape AN. 2016. Glucose transporters: Physiological and pathological roles. Biophys Rev. 8(1):5-9.
53. Kaneko JJ. 2008. Carbohydrate metabolism and its diseases. In: Kaneko JJ, Harvey JW, Bruss M, L., editors. Clinical biochemistry of domestic animals. Sixth Edition ed. Academic Press. p. 45-80.
54. Owen OE, Kalhan SC, Hanson RW. 2002. The key role of anaplerosis and cataplerosis for citric acid cycle function. J Biol Chem. 277(34):30409-30412.
55. Bradshaw PC. 2021. Acetyl-coa metabolism and histone acetylation in the regulation of aging and lifespan. Antioxidants (Basel). 10(4).
56. Kolliniati O, Ieronymaki E, Vergadi E, Tsatsanis C. 2022. Metabolic regulation of macrophage activation. J Innate Immun. 14(1):51-68.
57. Sun L, Suo C, Li ST, Zhang H, Gao P. 2018. Metabolic reprogramming for cancer cells and their microenvironment: Beyond the warburg effect. Biochim Biophys Acta.
58. Wang YH, Israelsen WJ, Lee D, Yu VWC, Jeanson NT, Clish CB, Cantley LC, Vander Heiden MG, Scadden DT. 2014. Cell-state-specific metabolic dependency in hematopoiesis and leukemogenesis. Cell. 158(6):1309-1323.
59. Eniafe J, Jiang S. 2021. The functional roles of tca cycle metabolites in cancer. Oncogene. 40(19):3351-3363.
60. Takeno T, Li SS. 1989. Structure of the human lactate dehydrogenase b gene. Biochem J. 257(3):921-924.
61. Krieg AF, Rosenblum LJ, Henry JB. 1967. Lactate dehydrogenase isoenzymes a comparison of pyruvate-to-lactate and lactate-to-pyruvate assays. Clin Chem. 13(3):196-203.
62. Lewis C, Schmitt M, Hershey FB. 1967. Heterogeneity of lactic dehydrogenase of human skin. J Invest Dermatol. 48(3):221-225.
63. Bauhammer I, Sacha M, Haltner E. 2019. Validation and stability analysis of a modified lactate dehydrogenase (ldh) test method to be employed for an. Heliyon. 5(5):e01618.
64. Goldberg E, Eddy EM, Duan C, Odet F. 2010. Ldhc: The ultimate testis-specific gene. J Androl. 31(1):86-94.
65. Monroe GR, van Eerde AM, Tessadori F, Duran KJ, Savelberg SMC, van Alfen JC, Terhal PA, van der Crabben SN, Lichtenbelt KD, Fuchs SA et al. 2019. Identification of human d lactate dehydrogenase deficiency. Nat Commun. 10(1):1477.

66. Quattro JM, Woods HA, Powers DA. 1993. Sequence analysis of teleost retina-specific lactate dehydrogenase c: Evolutionary implications for the vertebrate lactate dehydrogenase gene family. Proc Natl Acad Sci U S A. 90(1):242-246.
67. Taylor JS, Braasch I, Frickey T, Meyer A, Van de Peer Y. 2003. Genome duplication, a trait shared by 22000 species of ray-finned fish. Genome Res. 13(3):382-390.
68. Markert CL. 1984. Lactate dehydrogenase. Biochemistry and function of lactate dehydrogenase. Cell Biochem Funct. 2(3):131-134.
69. Read JA, Winter VJ, Eszes CM, Sessions RB, Brady RL. 2001. Structural basis for altered activity of m- and h-isozyme forms of human lactate dehydrogenase. Proteins. 43(2):175-185.
70. Farhana A, Lappin SL. 2022. Biochemistry, lactate dehydrogenase. In: LLC SP, editor. Biochemistry, lactate dehydrogenase.
71. Ždralević M, Brand A, Di Ianni L, Dettmer K, Reinders J, Singer K, Peter K, Schnell A, Bruss C, Decking SM et al. 2018. Double genetic disruption of lactate dehydrogenases a and b is required to ablate the "Warburg effect" Restricting tumor growth to oxidative metabolism. J Biol Chem. 293(41):15947-15961.
72. Feng Y, Xiong Y, Qiao T, Li X, Jia L, Han Y. 2018. Lactate dehydrogenase a: A key player in carcinogenesis and potential target in cancer therapy. Cancer Med. 7(12):6124-6136.
73. Claps G, Faouzi S, Quidville V, Chehade F, Shen S, Vagner S, Robert C. 2022. The multiple roles of ldh in cancer. Nat Rev Clin Oncol. 19(12):749-762.
74. Marín-Hernández A, Gallardo-Pérez JC, Ralph SJ, Rodríguez-Enríquez S, Moreno-Sánchez R. 2009. Hif-1alpha modulates energy metabolism in cancer cells by inducing over-expression of specific glycolytic isoforms. Mini Rev Med Chem. 9(9):1084-1101.
75. He TL, Zhang YJ, Jiang H, Li XH, Zhu H, Zheng KL. 2015. The c-myc-ldha axis positively regulates aerobic glycolysis and promotes tumor progression in pancreatic cancer. Med Oncol. 32(7):187.
76. Fu D, Li J, Wei J, Zhang Z, Luo Y, Tan H, Ren C. 2018. Hmgb2 is associated with malignancy and regulates warburg effect by targeting ldhb and fbp1 in breast cancer. Cell Commun Signal. 16(1):8.
77. Zha X, Wang F, Wang Y, He S, Jing Y, Wu X, Zhang H. 2011. Lactate dehydrogenase b is critical for hyperactive mtor-mediated tumorigenesis. Cancer Res. 71(1):13-18.
78. Maekawa M, Taniguchi T, Ishikawa J, Sugimura H, Sugano K, Kanno T. 2003. Promoter hypermethylation in cancer silences ldhb, eliminating lactate dehydrogenase isoenzymes 1-4. Clin Chem. 49(9):1518-1520.
79. Cui J, Quan M, Jiang W, Hu H, Jiao F, Li N, Jin Z, Wang L, Wang Y. 2015. Suppressed expression of ldhb promotes pancreatic cancer progression via inducing glycolytic phenotype. Med Oncol. 32(5):143.
80. Leiblich A, Cross SS, Catto JW, Phillips JT, Leung HY, Hamdy FC, Rehman I. 2006. Lactate dehydrogenase-b is silenced by promoter hypermethylation in human prostate cancer. Oncogene. 25(20):2953-2960.
81. Jin L, Chun J, Pan C, Alesi GN, Li D, Magliocca KR, Kang Y, Chen ZG, Shin DM, Khuri FR et al. 2017. Phosphorylation-mediated activation of ldha promotes cancer cell invasion and tumour metastasis. Oncogene. 36(27):3797-3806.
82. Zhao D, Zou SW, Liu Y, Zhou X, Mo Y, Wang P, Xu YH, Dong B, Xiong Y, Lei QY et al. 2013. Lysine-5 acetylation negatively regulates lactate dehydrogenase a and is decreased in pancreatic cancer. Cancer Cell. 23(4):464-476.
83. Cheng A, Zhang P, Wang B, Yang D, Duan X, Jiang Y, Xu T, Shi J, Ding C, Wu G et al. 2019. Aurora-a mediated phosphorylation of ldhb promotes glycolysis and tumor progression by relieving the substrate-inhibition effect. Nat Commun. 10(1):5566.
84. Shi L, Yan H, An S, Shen M, Jia W, Zhang R, Zhao L, Huang G, Liu J. 2019. Sirt5-mediated deacetylation of ldhb promotes autophagy and tumorigenesis in colorectal cancer. Mol Oncol. 13(2):358-375.

85. What is cancer? 2021. [accessed 2023 March, 23rd]. https://www.cancer.gov/about-cancer/understanding/what-is-cancer#definition.
86. Warburg OH. 1956. On the origin of cancer cells. Science. 123(3191):309-314.
87. Zhang W, Wang C, Hu X, Lian Y, Ding C, Ming L. 2022. Inhibition of ldha suppresses cell proliferation and increases mitochondrial apoptosis via the jnk signaling pathway in cervical cancer cells. Oncol Rep. 47(4).
88. Cattaneo A, Biocca S, Corvaja N, Calissano P. 1985. Nuclear localization of a lactic dehydrogenase with single-stranded dna-binding properties. Exp Cell Res. 161(1):130-140.
89. Castonguay Z, Auger C, Thomas SC, Chahma M, Appanna VD. 2014. Nuclear lactate dehydrogenase modulates histone modification in human hepatocytes. Biochem Biophys Res Commun. 454(1):172-177.
90. Latham T, Mackay L, Sproul D, Karim M, Culley J, Harrison DJ, Hayward L, Langridge-Smith P, Gilbert N, Ramsahoye BH. 2012. Lactate, a product of glycolytic metabolism, inhibits histone deacetylase activity and promotes changes in gene expression. Nucleic Acids Res. 40(11):4794-4803.
91. Hou X, Shi X, Zhang W, Li D, Hu L, Yang J, Zhao J, Wei S, Wei X, Ruan X et al. 2021. Ldha induces emt gene transcription and regulates autophagy to promote the metastasis and tumorigenesis of papillary thyroid carcinoma. Cell Death Dis. 12(4):347.
92. Li X, Yang Y, Zhang B, Lin X, Fu X, An Y, Zou Y, Wang JX, Wang Z, Yu T. 2022. Lactate metabolism in human health and disease. Signal Transduct Target Ther. 7(1):305.
93. Brooks GA. 2018. The science and translation of lactate shuttle theory. Cell Metab. 27(4):757-785.
94. Vander Heiden MG, Cantley LC, Thompson CB. 2009. Understanding the warburg effect: The metabolic requirements of cell proliferation. Science. 324(5930):1029-1033.
95. Mishra D, Banerjee D. 2019. Lactate dehydrogenases as metabolic links between tumor and stroma in the tumor microenvironment. Cancers (Basel). 11(6).
96. Patel BB, Ackerstaff E, Serganova IS, Kerrigan JE, Blasberg RG, Koutcher JA, Banerjee D. 2017. Tumor stroma interaction is mediated by monocarboxylate metabolism. Exp Cell Res. 352(1):20-33.
97. Škerlová J, Berndtsson J, Nolte H, Ott M, Stenmark P. 2021. Structure of the native pyruvate dehydrogenase complex reveals the mechanism of substrate insertion. Nat Commun. 12(1):5277.
98. Yu X, Hiromasa Y, Tsen H, Stoops JK, Roche TE, Zhou ZH. 2008. Structures of the human pyruvate dehydrogenase complex cores: A highly conserved catalytic center with flexible n-terminal domains. Structure. 16(1):104-114.
99. Wagenknecht T, Grassucci R, Radke GA, Roche TE. 1991. Cryoelectron microscopy of mammalian pyruvate dehydrogenase complex. J Biol Chem. 266(36):24650-24656.
100. Kolobova E, Tuganova A, Boulatnikov I, Popov KM. 2001. Regulation of pyruvate dehydrogenase activity through phosphorylation at multiple sites. Biochem J. 358(Pt 1):69-77.
101. Rardin MJ, Wiley SE, Naviaux RK, Murphy AN, Dixon JE. 2009. Monitoring phosphorylation of the pyruvate dehydrogenase complex. Anal Biochem. 389(2):157-164.
102. Patel MS, Nemeria NS, Furey W, Jordan F. 2014. The pyruvate dehydrogenase complexes: Structure-based function and regulation. J Biol Chem. 289(24):16615-16623.
103. Klyuyeva A, Tuganova A, Popov KM. 2008. Allosteric coupling in pyruvate dehydrogenase kinase 2. Biochemistry. 47(32):8358-8366.
104. Boukouris AE, Zervopoulos SD, Michelakis ED. 2016. Metabolic enzymes moonlighting in the nucleus: Metabolic regulation of gene transcription. Trends Biochem Sci. 41(8):712-730.

105. Sutendra G, Kinnaird A, Dromparis P, Paulin R, Stenson TH, Haromy A, Hashimoto K, Zhang N, Flaim E, Michelakis ED. 2014. A nuclear pyruvate dehydrogenase complex is important for the generation of acetyl-coa and histone acetylation. Cell. 158(1):84-97.
106. Zervopoulos SD, Boukouris AE, Saleme B, Haromy A, Tejay S, Sutendra G, Michelakis ED. 2022. Mfn2-driven mitochondria-to-nucleus tethering allows a non-canonical nuclear entry pathway of the mitochondrial pyruvate dehydrogenase complex. Mol Cell. 82(5):1066-1077.e1067.
107. Zhang L, Jiang X, Liu N, Li M, Kang J, Chen L, Tang J, Dong S, Lu F, Zhang W. 2021. Exogenous h2s prevents the nuclear translocation of pdc-e1 and inhibits vascular smooth muscle cell proliferation in the diabetic state. J Cell Mol Med. 25(17):8201-8214.
108. Pal S, Tyler JK. 2016. Epigenetics and aging. Sci Adv. 2(7):e1600584.
109. Zhou W, Niu YJ, Nie ZW, Kim JY, Xu YN, Yan CG, Cui XS. 2020. Nuclear accumulation of pyruvate dehydrogenase alpha 1 promotes histone acetylation and is essential for zygotic genome activation in porcine embryos. Biochim Biophys Acta Mol Cell Res. 1867(4):118648.
110. Li W, Long Q, Wu H, Zhou Y, Duan L, Yuan H, Ding Y, Huang Y, Wu Y, Huang J et al. 2022. Nuclear localization of mitochondrial tca cycle enzymes modulates pluripotency via histone acetylation. Nat Commun. 13(1):7414.
111. Sutendra G, Michelakis ED. 2013. Pyruvate dehydrogenase kinase as a novel therapeutic target in oncology. Front Oncol. 3:38.
112. Murphy K, Travers P, Walport M. 2008. Janeway's immunobiology.
113. de Szalay S, Wertz PW. 2023. Protective barriers provided by the epidermis. Int J Mol Sci. 24(4).
114. Coates M, Blanchard S, MacLeod AS. 2018. Innate antimicrobial immunity in the skin: A protective barrier against bacteria, viruses, and fungi. PLoS Pathog. 14(12):e1007353.
115. Trompette A, Ubags ND. 2023. Skin barrier immunology from early life to adulthood. Mucosal Immunol.
116. van de Vyver M. 2023. Immunology of chronic low-grade inflammation: Relationship with metabolic function. J Endocrinol. 257(1).
117. Lippolis JD. 2008. Immunological signaling networks: Integrating the body's immune response. J Anim Sci. 86(14 Suppl):E53-63.
118. Azuma M. 2006. Fundamental mechanisms of host immune responses to infection. J Periodontal Res. 41(5):361-373.
119. Kalia V, Sarkar S, Gourley TS, Rouse BT, Ahmed R. 2006. Differentiation of memory b and t cells. Curr Opin Immunol. 18(3):255-264.
120. O'Neill LA, Kishton RJ, Rathmell J. 2016. A guide to immunometabolism for immunologists. Nat Rev Immunol. 16(9):553-565.
121. Mockler MB, Conroy MJ, Lysaght J. 2014. Targeting t cell immunometabolism for cancer immunotherapy; understanding the impact of the tumor microenvironment. Front Oncol. 4:107.
122. Zhao H, Raines LN, Huang SC. 2020. Carbohydrate and amino acid metabolism as hallmarks for innate immune cell activation and function. Cells. 9(3).
123. Orliaguet L, Dalmas E, Drareni K, Venteclef N, Alzaid F. 2020. Mechanisms of macrophage polarization in insulin signaling and sensitivity. Front Endocrinol (Lausanne). 11:62.
124. Wang T, Liu G, Wang R. 2014. The intercellular metabolic interplay between tumor and immune cells. Front Immunol. 5:358.
125. Kornberg MD. 2020. The immunologic warburg effect: Evidence and therapeutic opportunities in autoimmunity. Wiley Interdiscip Rev Syst Biol Med.e1486.
126. Kumar S, Dikshit M. 2019. Metabolic insight of neutrophils in health and disease. Front Immunol. 10:2099.

127. Zhou W, Cao L, Jeffries J, Zhu X, Staiger CJ, Deng Q. 2018. Neutrophil-specific knockout demonstrates a role for mitochondria in regulating neutrophil motility in zebrafish. Dis Model Mech. 11(3).
128. Zhang D, Tang Z, Huang H, Zhou G, Cui C, Weng Y, Liu W, Kim S, Lee S, Perez-Neut M et al. 2019. Metabolic regulation of gene expression by histone lactylation. Nature. 574(7779):575-580.
129. Irizarry-Caro RA, McDaniel MM, Overcast GR, Jain VG, Troutman TD, Pasare C. 2020. Tlr signaling adapter bcap regulates inflammatory to reparatory macrophage transition by promoting histone lactylation. Proc Natl Acad Sci U S A. 117(48):30628-30638.
130. Ryan DG, O'Neill LAJ. 2020. Krebs cycle reborn in macrophage immunometabolism. Annu Rev Immunol.
131. Tannahill GM, Curtis AM, Adamik J, Palsson-McDermott EM, McGettrick AF, Goel G, Frezza C, Bernard NJ, Kelly B, Foley NH et al. 2013. Succinate is an inflammatory signal that induces il-1β through hif-1α. Nature. 496(7444):238-242.
132. Meiser J, Krämer L, Sapcariu SC, Battello N, Ghelfi J, D'Herouel AF, Skupin A, Hiller K. 2016. Pro-inflammatory macrophages sustain pyruvate oxidation through pyruvate dehydrogenase for the synthesis of itaconate and to enable cytokine expression. J Biol Chem. 291(8):3932-3946.
133. Martínez-Reyes I, Chandel NS. 2020. Mitochondrial tca cycle metabolites control physiology and disease. Nat Commun. 11(1):102.
134. Netea MG, Balkwill F, Chonchol M, Cominelli F, Donath MY, Giamarellos-Bourboulis EJ, Golenbock D, Gresnigt MS, Heneka MT, Hoffman HM et al. 2017. A guiding map for inflammation. Nat Immunol. 18(8):826-831.
135. Furman D, Campisi J, Verdin E, Carrera-Bastos P, Targ S, Franceschi C, Ferrucci L, Gilroy DW, Fasano A, Miller GW et al. 2019. Chronic inflammation in the etiology of disease across the life span. Nat Med. 25(12):1822-1832.
136. Kotas ME, Medzhitov R. 2015. Homeostasis, inflammation, and disease susceptibility. Cell. 160(5):816-827.
137. Yunna C, Mengru H, Lei W, Weidong C. 2020. Macrophage m1/m2 polarization. Eur J Pharmacol. 877:173090.
138. Biswas SK, Mantovani A. 2010. Macrophage plasticity and interaction with lymphocyte subsets: Cancer as a paradigm. Nat Immunol. 11(10):889-896.
139. Franceschi C, Garagnani P, Parini P, Giuliani C, Santoro A. 2018. Inflammaging: A new immune-metabolic viewpoint for age-related diseases. Nat Rev Endocrinol. 14(10):576-590.
140. Kim WB, Jerome D, Yeung J. 2017. Diagnosis and management of psoriasis. Can Fam Physician. 63(4):278-285.
141. Raharja A, Mahil SK, Barker JN. 2021. Psoriasis: A brief overview. Clin Med (Lond). 21(3):170-173.
142. Ni X, Lai Y. 2020. Keratinocyte: A trigger or an executor of psoriasis? J Leukoc Biol. 108(2):485-491.
143. Pasparakis M, Haase I, Nestle FO. 2014. Mechanisms regulating skin immunity and inflammation. Nat Rev Immunol. 14(5):289-301.
144. Albanesi C, Scarponi C, Giustizieri ML, Girolomoni G. 2005. Keratinocytes in inflammatory skin diseases. Curr Drug Targets Inflamm Allergy. 4(3):329-334.
145. Kim J, Krueger JG. 2015. The immunopathogenesis of psoriasis. Dermatol Clin. 33(1):13-23.
146. Chiang CC, Cheng WJ, Korinek M, Lin CY, Hwang TL. 2019. Neutrophils in psoriasis. Front Immunol. 10:2376.
147. Lowes MA, Suárez-Fariñas M, Krueger JG. 2014. Immunology of psoriasis. Annu Rev Immunol. 32:227-255.
148. Wang WM, Jin HZ. 2020. Role of neutrophils in psoriasis. J Immunol Res. 2020:3709749.

149. Weaver CT, Elson CO, Fouser LA, Kolls JK. 2013. The th17 pathway and inflammatory diseases of the intestines, lungs, and skin. Annu Rev Pathol. 8:477-512.
150. Albanesi C, Pastore S. 2010. Pathobiology of chronic inflammatory skin diseases: Interplay between keratinocytes and immune cells as a target for anti-inflammatory drugs. Curr Drug Metab. 11(3):210-227.
151. Toussirot E. 2012. The il23/th17 pathway as a therapeutic target in chronic inflammatory diseases. Inflamm Allergy Drug Targets. 11(2):159-168.
152. Cannavò SP, Riso G, Casciaro M, Di Salvo E, Gangemi S. 2019. Oxidative stress involvement in psoriasis: A systematic review. Free Radic Res. 53(8):829-840.
153. Kadam DP, Suryakar AN, Ankush RD, Kadam CY, Deshpande KH. 2010. Role of oxidative stress in various stages of psoriasis. Indian J Clin Biochem. 25(4):388-392.
154. Becatti M, Barygina V, Mannucci A, Emmi G, Prisco D, Lotti T, Fiorillo C, Taddei N. 2018. Sirt1 protects against oxidative stress-induced apoptosis in fibroblasts from psoriatic patients: A new insight into the pathogenetic mechanisms of psoriasis. Int J Mol Sci. 19(6).
155. Lin X, Huang T. 2016. Oxidative stress in psoriasis and potential therapeutic use of antioxidants. Free Radic Res. 50(6):585-595.
156. Niethammer P, Grabher C, Look AT, Mitchison TJ. 2009. A tissue-scale gradient of hydrogen peroxide mediates rapid wound detection in zebrafish. Nature. 459(7249):996-999.
157. Candel S, de Oliveira S, López-Muñoz A, García-Moreno D, Espín-Palazón R, Tyrkalska SD, Cayuela ML, Renshaw SA, Corbalán-Vélez R, Vidal-Abarca I et al. 2014. Tnfa signaling through tnfr2 protects skin against oxidative stress-induced inflammation. PLoS Biol. 12(5):e1001855.
158. Martínez-Morcillo FJ, Cantón-Sandoval J, Martínez-Navarro FJ, Cabas I, Martínez-Vicente I, Armistead J, Hatzold J, López-Muñoz A, Martínez-Menchón T, Corbalán-Vélez R et al. 2021. Nampt-derived nad+ fuels parp1 to promote skin inflammation through parthanatos cell death. PLoS Biol. 19(11):e3001455.
159. Mercurio L, Morelli M, Scarponi C, Scaglione GL, Pallotta S, Avitabile D, Albanesi C, Madonna S. 2021. Enhanced nampt-mediated nad salvage pathway contributes to psoriasis pathogenesis by amplifying epithelial auto-inflammatory circuits. Int J Mol Sci. 22(13).
160. Cibrian D, de la Fuente H, Sánchez-Madrid F. 2020. Metabolic pathways that control skin homeostasis and inflammation. Trends Mol Med. 26(11):975-986.
161. Chang SC, Yang WV. 2016. Hyperglycemia, tumorigenesis, and chronic inflammation. Crit Rev Oncol Hematol. 108:146-153.
162. Zezina E, Sercan-Alp O, Herrmann M, Biesemann N. 2020. Glucose transporter 1 in rheumatoid arthritis and autoimmunity. Wiley Interdiscip Rev Syst Biol Med. 12(4):e1483.
163. Cairns RA, Harris IS, Mak TW. 2011. Regulation of cancer cell metabolism. Nat Rev Cancer. 11(2):85-95.
164. Palmer CS, Ostrowski M, Balderson B, Christian N, Crowe SM. 2015. Glucose metabolism regulates t cell activation, differentiation, and functions. Front Immunol. 6:1.
165. Zhang Z, Zi Z, Lee EE, Zhao J, Contreras DC, South AP, Abel ED, Chong BF, Vandergriff T, Hosler GA et al. 2018. Differential glucose requirement in skin homeostasis and injury identifies a therapeutic target for psoriasis. Nat Med. 24(5):617-627.
166. Huang X, Chen J, Zeng W, Wu X, Chen M, Chen X. 2019. Membrane-enriched solute carrier family 2 member 1 (slc2a1/glut1) in psoriatic keratinocytes confers sensitivity to 2-deoxy-d-glucose (2-dg) treatment. Exp Dermatol. 28(2):198-201.
167. Fatás-Lalana B, Cantón-Sandoval J, Rodríguez-Ruiz L, Corbalán-Vélez R, Martínez-Menchón T, Pérez-Oliva AB, Mulero V. 2022. Impact of comorbidities of patients with psoriasis on phototherapy responses. Int J Mol Sci. 23(17).
168. Manosalva C, Quiroga J, Hidalgo AI, Alarcón P, Anseoleaga N, Hidalgo MA, Burgos RA. 2021. Role of lactate in inflammatory processes: Friend or foe. Front Immunol. 12:808799.

169. Certo M, Tsai CH, Pucino V, Ho PC, Mauro C. 2021. Lactate modulation of immune responses in inflammatory versus tumour microenvironments. Nat Rev Immunol. 21(3):151-161.
170. Pucino V, Certo M, Bulusu V, Cucchi D, Goldmann K, Pontarini E, Haas R, Smith J, Headland SE, Blighe K et al. 2019. Lactate buildup at the site of chronic inflammation promotes disease by inducing cd4+ t cell metabolic rewiring. Cell Metab. 30(6):1055-1074.e1058.
171. Haas R, Smith J, Rocher-Ros V, Nadkarni S, Montero-Melendez T, D'Acquisto F, Bland EJ, Bombardieri M, Pitzalis C, Perretti M et al. 2015. Lactate regulates metabolic and pro-inflammatory circuits in control of t cell migration and effector functions. PLoS Biol. 13(7):e1002202.
172. Arra M, Swarnkar G, Ke K, Otero JE, Ying J, Duan X, Maruyama T, Rai MF, O'Keefe RJ, Mbalaviele G et al. 2020. Ldha-mediated ros generation in chondrocytes is a potential therapeutic target for osteoarthritis. Nat Commun. 11(1):3427.
173. Hanahan D, Weinberg RA. 2011. Hallmarks of cancer: The next generation. Cell. 144(5):646-674.
174. Fouad YA, Aanei C. 2017. Revisiting the hallmarks of cancer. Am J Cancer Res. 7(5):1016-1036.
175. Ponomarev AV, Shubina IZ. 2019. Insights into mechanisms of tumor and immune system interaction: Association with wound healing. Front Oncol. 9:1115.
176. Upadhyay S, Sharma N, Gupta KB, Dhiman M. 2018. Role of immune system in tumor progression and carcinogenesis. J Cell Biochem. 119(7):5028-5042.
177. Beatty GL, Gladney WL. 2015. Immune escape mechanisms as a guide for cancer immunotherapy. Clin Cancer Res. 21(4):687-692.
178. Coulie PG, Van den Eynde BJ, van der Bruggen P, Boon T. 2014. Tumour antigens recognized by t lymphocytes: At the core of cancer immunotherapy. Nat Rev Cancer. 14(2):135-146.
179. Coussens LM, Werb Z. 2002. Inflammation and cancer. Nature. 420(6917):860-867.
180. Hiam-Galvez KJ, Allen BM, Spitzer MH. 2021. Systemic immunity in cancer. Nat Rev Cancer. 21(6):345-359.
181. Gao J, Liang Y, Wang L. 2022. Shaping polarization of tumor-associated macrophages in cancer immunotherapy. Front Immunol. 13:888713.
182. Whiteside TL. 2008. The tumor microenvironment and its role in promoting tumor growth. Oncogene. 27(45):5904-5912.
183. Briukhovetska D, Dörr J, Endres S, Libby P, Dinarello CA, Kobold S. 2021. Interleukins in cancer: From biology to therapy. Nat Rev Cancer. 21(8):481-499.
184. Biswas SK. 2015. Metabolic reprogramming of immune cells in cancer progression. Immunity. 43(3):435-449.
185. Comito G, Iscaro A, Bacci M, Morandi A, Ippolito L, Parri M, Montagnani I, Raspollini MR, Serni S, Simeoni L et al. 2019. Lactate modulates cd4 + t-cell polarization and induces an immunosuppressive environment, which sustains prostate carcinoma progression via tlr8/mir21 axis. Oncogene. 38(19):3681-3695.
186. Davis ME. 2016. Glioblastoma: Overview of disease and treatment. Clin J Oncol Nurs. 20(5 Suppl):S2-8.
187. Alifieris C, Trafalis DT. 2015. Glioblastoma multiforme: Pathogenesis and treatment. Pharmacol Ther. 152:63-82.
188. Lim M, Xia Y, Bettegowda C, Weller M. 2018. Current state of immunotherapy for glioblastoma. Nat Rev Clin Oncol. 15(7):422-442.
189. Medikonda R, Dunn G, Rahman M, Fecci P, Lim M. 2021. A review of glioblastoma immunotherapy. J Neurooncol. 151(1):41-53.
190. Janjua TI, Rewatkar P, Ahmed-Cox A, Saeed I, Mansfeld FM, Kulshreshtha R, Kumeria T, Ziegler DS, Kavallaris M, Mazzieri R et al. 2021. Frontiers in the treatment of glioblastoma: Past, present and emerging. Adv Drug Deliv Rev. 171:108-138.
191. Wang C, Thudium KB, Han M, Wang XT, Huang H, Feingersh D, Garcia C, Wu Y, Kuhne M, Srinivasan M et al. 2014. In vitro characterization of the anti-pd-1 antibody nivolumab,

bms-936558, and in vivo toxicology in non-human primates. Cancer Immunol Res. 2(9):846-856.
192. Gutic B, Bozanovic T, Mandic A, Dugalic S, Todorovic J, Stanisavljevic D, Dugalic MG, Sengul D, Detanac DA, Sengul I et al. 2023. Programmed cell death-1 and its ligands: Current knowledge and possibilities in immunotherapy. Clinics (Sao Paulo). 78:100177.
193. Tang Q, Zhao S, Zhou N, He J, Zu L, Liu T, Song Z, Chen J, Peng L, Xu S. 2023. Pd-1/pd-l1 immune checkpoint inhibitors in neoadjuvant therapy for solid tumors (review). Int J Oncol. 62(4).
194. Medikonda R, Pant A, Lim M. 2023. Immunotherapy as a new therapeutic approach for brain and spinal cord tumors. Adv Exp Med Biol. 1394:73-84.
195. Zhao L, Xu DG, Hu YH. 2023. The regulation of microglial cell polarization in the tumor microenvironment: A new potential strategy for auxiliary treatment of glioma-a review. Cell Mol Neurobiol. 43(1):193-204.
196. Friedmann-Morvinski D, Hambardzumyan D. 2023. Monocyte-neutrophil entanglement in glioblastoma. J Clin Invest. 133(1).
197. Kuntzel T, Bagnard D. 2022. Manipulating macrophage/microglia polarization to treat glioblastoma or multiple sclerosis. Pharmaceutics. 14(2).
198. Cartner S, Eisen JS, Farmer SF, Guillemin KJ, Kent ML, Sanders GE. 2019. The zebrafish in biomedical research: Biology, husbandry, diseases, and research applications. Academic Press.
199. Howe K, Clark MD, Torroja CF, Torrance J, Berthelot C, Muffato M, Collins JE, Humphray S, McLaren K, Matthews L et al. 2013. The zebrafish reference genome sequence and its relationship to the human genome. Nature. 496(7446):498-503.
200. Beddington RS, Smith JC. 1993. Control of vertebrate gastrulation: Inducing signals and responding genes. Curr Opin Genet Dev. 3(4):655-661.
201. Kimmel CB, Ballard WW, Kimmel SR, Ullmann B, Schilling TF. 1995. Stages of embryonic development of the zebrafish. Dev Dyn. 203(3):253-310.
202. Patton EE, Zon LI. 2001. The art and design of genetic screens: Zebrafish. Nat Rev Genet. 2(12):956-966.
203. Lantz-McPeak S, Guo X, Cuevas E, Dumas M, Newport GD, Ali SF, Paule MG, Kanungo J. 2015. Developmental toxicity assay using high content screening of zebrafish embryos. J Appl Toxicol. 35(3):261-272.
204. Patton EE, Zon LI, Langenau DM. 2021. Zebrafish disease models in drug discovery: From preclinical modelling to clinical trials. Nat Rev Drug Discov. 20(8):611-628.
205. Nasevicius A, Ekker SC. 2000. Effective targeted gene 'knockdown' in zebrafish. Nat Genet. 26(2):216-220.
206. Liu K, Petree C, Requena T, Varshney P, Varshney GK. 2019. Expanding the crispr toolbox in zebrafish for studying development and disease. Front Cell Dev Biol. 7:13.
207. Villefranc JA, Amigo J, Lawson ND. 2007. Gateway compatible vectors for analysis of gene function in the zebrafish. Dev Dyn. 236(11):3077-3087.
208. Scheer N, Campos-Ortega JA. 1999. Use of the gal4-uas technique for targeted gene expression in the zebrafish. Mech Dev. 80(2):153-158.
209. Asakawa K, Kawakami K. 2008. Targeted gene expression by the gal4-uas system in zebrafish. Dev Growth Differ. 50(6):391-399.
210. Ko SK, Chen X, Yoon J, Shin I. 2011. Zebrafish as a good vertebrate model for molecular imaging using fluorescent probes. Chem Soc Rev. 40(5):2120-2130.
211. Choi TY, Choi TI, Lee YR, Choe SK, Kim CH. 2021. Zebrafish as an animal model for biomedical research. Exp Mol Med. 53(3):310-317.
212. Lau BW, Wong AO, Tsao GS, So KF, Yip HK. 2008. Molecular cloning and characterization of the zebrafish (danio rerio) telomerase catalytic subunit (telomerase reverse transcriptase, tert). J Mol Neurosci. 34(1):63-75.

213. Xie M, Mosig A, Qi X, Li Y, Stadler PF, Chen JJ. 2008. Structure and function of the smallest vertebrate telomerase rna from teleost fish. J Biol Chem. 283(4):2049-2059.
214. Chen JL, Blasco MA, Greider CW. 2000. Secondary structure of vertebrate telomerase rna. Cell. 100(5):503-514.
215. McChesney PA, Elmore LW, Holt SE. 2005. Vertebrate marine species as model systems for studying telomeres and telomerase. Zebrafish. 1(4):349-355.
216. Anchelin M, Alcaraz-Pérez F, Martínez CM, Bernabé-García M, Mulero V, Cayuela ML. 2013. Premature aging in telomerase-deficient zebrafish. Dis Model Mech. 6(5):1101-1112.
217. Carneiro MC, de Castro IP, Ferreira MG. 2016. Telomeres in aging and disease: Lessons from zebrafish. Dis Model Mech. 9(7):737-748.
218. Anchelin M, Murcia L, Alcaraz-Pérez F, García-Navarro EM, Cayuela ML. 2011. Behaviour of telomere and telomerase during aging and regeneration in zebrafish. PLoS One. 6(2):e16955.
219. Henriques CM, Carneiro MC, Tenente IM, Jacinto A, Ferreira MG. 2013. Telomerase is required for zebrafish lifespan. PLoS Genet. 9(1):e1003214.
220. Imamura S, Uchiyama J, Koshimizu E, Hanai J, Raftopoulou C, Murphey RD, Bayliss PE, Imai Y, Burns CE, Masutomi K et al. 2008. A non-canonical function of zebrafish telomerase reverse transcriptase is required for developmental hematopoiesis. PLoS One. 3(10):e3364.
221. Martínez-Navarro FJ, Martínez-Menchón T, Mulero V, Galindo-Villegas J. 2019. Models of human psoriasis: Zebrafish the newly appointed player. Dev Comp Immunol. 97:76-87.
222. Galindo-Villegas J. 2016. Recent findings on vertebrate developmental immunity using the zebrafish model. Mol Immunol. 69:106-112.
223. Meeker ND, Trede NS. 2008. Immunology and zebrafish: Spawning new models of human disease. Dev Comp Immunol. 32(7):745-757.
224. Carney TJ, von der Hardt S, Sonntag C, Amsterdam A, Topczewski J, Hopkins N, Hammerschmidt M. 2007. Inactivation of serine protease matriptase1a by its inhibitor hai1 is required for epithelial integrity of the zebrafish epidermis. Development. 134(19):3461-3471.
225. Kirschner N, Poetzl C, von den Driesch P, Wladykowski E, Moll I, Behne MJ, Brandner JM. 2009. Alteration of tight junction proteins is an early event in psoriasis: Putative involvement of proinflammatory cytokines. Am J Pathol. 175(3):1095-1106.
226. Mathias JR, Dodd ME, Walters KB, Rhodes J, Kanki JP, Look AT, Huttenlocher A. 2007. Live imaging of chronic inflammation caused by mutation of zebrafish hai1. J Cell Sci. 120(Pt 19):3372-3383.
227. Amatruda JF, Shepard JL, Stern HM, Zon LI. 2002. Zebrafish as a cancer model system. Cancer Cell. 1(3):229-231.
228. White R, Rose K, Zon L. 2013. Zebrafish cancer: The state of the art and the path forward. Nat Rev Cancer. 13(9):624-636.
229. Stern HM, Zon LI. 2003. Cancer genetics and drug discovery in the zebrafish. Nat Rev Cancer. 3(7):533-539.
230. Liu S, Leach SD. 2011. Zebrafish models for cancer. Annu Rev Pathol. 6:71-93.
231. Ceol CJ, Houvras Y, Jane-Valbuena J, Bilodeau S, Orlando DA, Battisti V, Fritsch L, Lin WM, Hollmann TJ, Ferré F et al. 2011. The histone methyltransferase setdb1 is recurrently amplified in melanoma and accelerates its onset. Nature. 471(7339):513-517.
232. Teng Y, Xie X, Walker S, White DT, Mumm JS, Cowell JK. 2013. Evaluating human cancer cell metastasis in zebrafish. BMC Cancer. 13:453.
233. Astell KR, Sieger D. 2020. Zebrafish in vivo models of cancer and metastasis. Cold Spring Harb Perspect Med. 10(8).
234. Fazio M, Ablain J, Chuan Y, Langenau DM, Zon LI. 2020. Zebrafish patient avatars in cancer biology and precision cancer therapy. Nat Rev Cancer. 20(5):263-273.

235. Lawson ND, Weinstein BM. 2002. In vivo imaging of embryonic vascular development using transgenic zebrafish. Dev Biol. 248(2):307-318.
236. Ellett F, Pase L, Hayman JW, Andrianopoulos A, Lieschke GJ. 2011. Mpeg1 promoter transgenes direct macrophage-lineage expression in zebrafish. Blood. 117(4):e49-56.
237. Detrich HW. 2008. Fluorescent proteins in zebrafish cell and developmental biology. Methods Cell Biol. 85:219-241.
238. Santoriello C, Gennaro E, Anelli V, Distel M, Kelly A, Köster RW, Hurlstone A, Mione M. 2010. Kita driven expression of oncogenic hras leads to early onset and highly penetrant melanoma in zebrafish. PLoS One. 5(12):e15170.
239. Ignatius MS, Langenau DM. 2011. Fluorescent imaging of cancer in zebrafish. Methods Cell Biol. 105:437-459.
240. Mayrhofer M, Gourain V, Reischl M, Affaticati P, Jenett A, Joly JS, Benelli M, Demichelis F, Poliani PL, Sieger D et al. 2017. A novel brain tumour model in zebrafish reveals the role of yap activation in mapk- and pi3k-induced malignant growth. Dis Model Mech. 10(1):15-28.
241. Distel M, Wullimann MF, Köster RW. 2009. Optimized gal4 genetics for permanent gene expression mapping in zebrafish. Proc Natl Acad Sci U S A. 106(32):13365-13370.
242. Li Z, Li X, Wu S, Xue M, Chen W. 2014. Long non-coding rna uca1 promotes glycolysis by upregulating hexokinase 2 through the mtor-stat3/microrna143 pathway. Cancer Sci. 105(8):951-955.
243. Cui H, Banerjee S, Guo S, Xie N, Ge J, Jiang D, Zörnig M, Thannickal VJ, Liu G. 2019. Long noncoding rna malat1 regulates differential activation of macrophages and response to lung injury. JCI Insight. 4(4).
244. Westerfield M. 2000. The zebrafish book a guide for the laboratory use of zebrafish (danio rerio). Eugene: University of Oregon Press.
245. Westerfield M, Zon LI, Detrich III HW. 2009. Essential zebrafish methods: Cell and developmental biology. Elsevier.
246. Hall C, Flores MV, Storm T, Crosier K, Crosier P. 2007. The zebrafish lysozyme c promoter drives myeloid-specific expression in transgenic fish. BMC Dev Biol. 7:42.
247. Amsterdam A, Burgess S, Golling G, Chen W, Sun Z, Townsend K, Farrington S, Haldi M, Hopkins N. 1999. A large-scale insertional mutagenesis screen in zebrafish. Genes Dev. 13(20):2713-2724.
248. Renshaw SA, Loynes CA, Trushell DM, Elworthy S, Ingham PW, Whyte MK. 2006. A transgenic zebrafish model of neutrophilic inflammation. Blood. 108(13):3976-3978.
249. Mosimann C, Panáková D, Werdich AA, Musso G, Burger A, Lawson KL, Carr LA, Nevis KR, Sabeh MK, Zhou Y et al. 2015. Chamber identity programs drive early functional partitioning of the heart. Nat Commun. 6:8146.
250. Nguyen-Chi M, Laplace-Builhe B, Travnickova J, Luz-Crawford P, Tejedor G, Phan QT, Duroux-Richard I, Levraud JP, Kissa K, Lutfalla G et al. 2015. Identification of polarized macrophage subsets in zebrafish. Elife. 4:e07288.
251. Tan JL, Fogley RD, Flynn RA, Ablain J, Yang S, Saint-André V, Fan ZP, Do BT, Laga AC, Fujinaga K et al. 2016. Stress from nucleotide depletion activates the transcriptional regulator hexim1 to suppress melanoma. Mol Cell. 62(1):34-46.
252. Yuan M, Breitkopf SB, Yang X, Asara JM. 2012. A positive/negative ion-switching, targeted mass spectrometry-based metabolomics platform for bodily fluids, cells, and fresh and fixed tissue. Nat Protoc. 7(5):872-881.
253. Cortés MA. 2016. Función no canónica de la telomerasa en el modelo animal del pez cebra (trabajo fin de grado). Universidad de Murcia.
254. Farnsworth DR, Saunders LM, Miller AC. 2020. A single-cell transcriptome atlas for zebrafish development. Dev Biol. 459(2):100-108.

255. Fan L, Huang C, Li J, Gao T, Lin Z, Yao T. 2018. Long non-coding rna urothelial cancer associated 1 regulates radioresistance via the hexokinase 2/glycolytic pathway in cervical cancer. Int J Mol Med. 42(4):2247-2259.
256. Hua Q, Mi B, Xu F, Wen J, Zhao L, Liu J, Huang G. 2020. Hypoxia-induced lncrna-ac020978 promotes proliferation and glycolytic metabolism of non-small cell lung cancer by regulating pkm2/hif-1α axis. Theranostics. 10(11):4762-4778.
257. Sun L, Zhang H, Gao P. 2022. Metabolic reprogramming and epigenetic modifications on the path to cancer. Protein Cell. 13(12):877-919.
258. Go S, Kramer TT, Verhoeven AJ, Oude Elferink RPJ, Chang JC. 2021. The extracellular lactate-to-pyruvate ratio modulates the sensitivity to oxidative stress-induced apoptosis via the cytosolic nadh/nad. Apoptosis. 26(1-2):38-51.
259. Quinn WJ, Jiao J, TeSlaa T, Stadanlick J, Wang Z, Wang L, Akimova T, Angelin A, Schäfer PM, Cully MD et al. 2020. Lactate limits t cell proliferation via the nad(h) redox state. Cell Rep. 33(11):108500.
260. Lu J, Chatterjee M, Schmid H, Beck S, Gawaz M. 2016. Cxcl14 as an emerging immune and inflammatory modulator. J Inflamm (Lond). 13:1.
261. Maerki C, Meuter S, Liebi M, Mühlemann K, Frederick MJ, Yawalkar N, Moser B, Wolf M. 2009. Potent and broad-spectrum antimicrobial activity of cxcl14 suggests an immediate role in skin infections. J Immunol. 182(1):507-514.
262. Lv J, Wu ZL, Gan Z, Gui P, Yao SL. 2020. Cxcl14 overexpression attenuates sepsis-associated acute kidney injury by inhibiting proinflammatory cytokine production. Mediators Inflamm. 2020:2431705.
263. Kast RE, Hill QA, Wion D, Mellstedt H, Focosi D, Karpel-Massler G, Heiland T, Halatsch ME. 2017. Glioblastoma-synthesized g-csf and gm-csf contribute to growth and immunosuppression: Potential therapeutic benefit from dapsone, fenofibrate, and ribavirin. Tumour Biol. 39(5):1010428317699797.
264. Jamieson T, Clarke M, Steele CW, Samuel MS, Neumann J, Jung A, Huels D, Olson MF, Das S, Nibbs RJ et al. 2012. Inhibition of cxcr2 profoundly suppresses inflammation-driven and spontaneous tumorigenesis. J Clin Invest. 122(9):3127-3144.
265. Michael BD, Bricio-Moreno L, Sorensen EW, Miyabe Y, Lian J, Solomon T, Kurt-Jones EA, Luster AD. 2020. Astrocyte- and neuron-derived cxcl1 drives neutrophil transmigration and blood-brain barrier permeability in viral encephalitis. Cell Rep. 32(11):108150.
266. Yee PP, Wei Y, Kim SY, Lu T, Chih SY, Lawson C, Tang M, Liu Z, Anderson B, Thamburaj K et al. 2020. Neutrophil-induced ferroptosis promotes tumor necrosis in glioblastoma progression. Nat Commun. 11(1):5424.
267. Bambury RM, Teo MY, Power DG, Yusuf A, Murray S, Battley JE, Drake C, O'Dea P, Bermingham N, Keohane C et al. 2013. The association of pre-treatment neutrophil to lymphocyte ratio with overall survival in patients with glioblastoma multiforme. J Neurooncol. 114(1):149-154.
268. Ferrero G, Mahony CB, Dupuis E, Yvernogeau L, Di Ruggiero E, Miserocchi M, Caron M, Robin C, Traver D, Bertrand JY et al. 2018. Embryonic microglia derive from primitive macrophages and are replaced by cmyb-dependent definitive microglia in zebrafish. Cell Rep. 24(1):130-141.
269. Bohaud C, Cruz J, Terraza C, Barthelaix A, Laplace-Builhé B, Jorgensen C, Arribat Y, Djouad F. 2022. Lactate metabolism coordinates macrophage response and regeneration in zebrafish. Theranostics. 12(8):3995-4009.
270. Zhou HC, Xin-Yan Yan, Yu WW, Liang XQ, Du XY, Liu ZC, Long JP, Zhao GH, Liu HB. 2022. Lactic acid in macrophage polarization: The significant role in inflammation and cancer. Int Rev Immunol. 41(1):4-18.
271. Yu MY, Jia HJ, Zhang J, Ran GH, Liu Y, Yang XH. 2023. Exosomal mirnas-mediated macrophage polarization and its potential clinical application. Int Immunopharmacol. 117:109905.

272. Longhitano L, Vicario N, Forte S, Giallongo C, Broggi G, Caltabiano R, Barbagallo GMV, Altieri R, Raciti G, Di Rosa M et al. 2023. Lactate modulates microglia polarization via igfbp6 expression and remodels tumor microenvironment in glioblastoma. Cancer Immunol Immunother. 72(1):1-20.
273. Pimtong W, Datta M, Ulrich AM, Rhodes J. 2014. Drl.3 governs primitive hematopoiesis in zebrafish. Sci Rep. 4:5791.
274. Zhao S, Feng S, Tian Y, Wen Z. 2022. Hemogenic and aortic endothelium arise from a common hemogenic angioblast precursor and are specified by the etv2 dosage. Proc Natl Acad Sci U S A. 119(13):e2119051119.
275. Donaldson IJ, Chapman M, Kinston S, Landry JR, Knezevic K, Piltz S, Buckley N, Green AR, Göttgens B. 2005. Genome-wide identification of cis-regulatory sequences controlling blood and endothelial development. Hum Mol Genet. 14(5):595-601.
276. Landry JR, Kinston S, Knezevic K, Donaldson IJ, Green AR, Göttgens B. 2005. Fli1, elf1, and ets1 regulate the proximal promoter of the lmo2 gene in endothelial cells. Blood. 106(8):2680-2687.
277. Serina Secanechia YN, Bergiers I, Rogon M, Arnold C, Descostes N, Le S, López-Anguita N, Ganter K, Kapsali C, Bouilleau L et al. 2022. Identifying a novel role for the master regulator tal1 in the endothelial to hematopoietic transition. Sci Rep. 12(1):16974.
278. Ahir BK, Engelhard HH, Lakka SS. 2020. Tumor development and angiogenesis in adult brain tumor: Glioblastoma. Mol Neurobiol. 57(5):2461-2478.
279. Cai H, Liu X, Zheng J, Xue Y, Ma J, Li Z, Xi Z, Bao M, Liu Y. 2017. Long non-coding rna taurine upregulated 1 enhances tumor-induced angiogenesis through inhibiting microrna-299 in human glioblastoma. Oncogene. 36(3):318-331.
280. Blackburn EH, Collins K. 2011. Telomerase: An rnp enzyme synthesizes dna. Cold Spring Harb Perspect Biol. 3(5).
281. Huangyang P, Simon MC. 2018. Hidden features: Exploring the non-canonical functions of metabolic enzymes. Dis Model Mech. 11(8).
282. Snaebjornsson MT, Schulze A. 2018. Non-canonical functions of enzymes facilitate cross-talk between cell metabolic and regulatory pathways. Exp Mol Med. 50(4):1-16.
283. Gao X, Wang H, Yang JJ, Liu X, Liu ZR. 2012. Pyruvate kinase m2 regulates gene transcription by acting as a protein kinase. Mol Cell. 45(5):598-609.
284. McEwen BS, Allfrey VG, Mirsky AE. 1963. Studies on energy-yielding reactions in thymus nuclei : Ii. Pathways of aerobic carbohydrate catabolism. J Biol Chem. 238(7):2571-2578.
285. Castello A, Hentze MW, Preiss T. 2015. Metabolic enzymes enjoying new partnerships as rna-binding proteins. Trends Endocrinol Metab. 26(12):746-757.
286. Wegener M, Dietz KJ. 2022. The mutual interaction of glycolytic enzymes and rna in post-transcriptional regulation. RNA. 28(11):1446-1468.
287. Walden WE, Selezneva AI, Dupuy J, Volbeda A, Fontecilla-Camps JC, Theil EC, Volz K. 2006. Structure of dual function iron regulatory protein 1 complexed with ferritin ire-rna. Science. 314(5807):1903-1908.
288. White MR, Garcin ED. 2016. The sweet side of rna regulation: Glyceraldehyde-3-phosphate dehydrogenase as a noncanonical rna-binding protein. Wiley Interdiscip Rev RNA. 7(1):53-70.
289. Counter CM, Hahn WC, Wei W, Caddle SD, Beijersbergen RL, Lansdorp PM, Sedivy JM, Weinberg RA. 1998. Dissociation among in vitro telomerase activity, telomere maintenance, and cellular immortalization. Proc Natl Acad Sci U S A. 95(25):14723-14728.
290. Wong JM, Collins K. 2006. Telomerase rna level limits telomere maintenance in x-linked dyskeratosis congenita. Genes Dev. 20(20):2848-2858.
291. Pérez-Oliva AB, Olivares C, Jiménez-Cervantes C, García-Borrón JC. 2009. Mahogunin ring finger-1 (mgrn1) e3 ubiquitin ligase inhibits signaling from melanocortin receptor by competition with galphas. J Biol Chem. 284(46):31714-31725.

292. Tsai MC, Manor O, Wan Y, Mosammaparast N, Wang JK, Lan F, Shi Y, Segal E, Chang HY. 2010. Long noncoding rna as modular scaffold of histone modification complexes. Science. 329(5992):689-693.
293. Lorenzana-Carrillo MA, Gopal K, Byrne NJ, Tejay S, Saleme B, Das SK, Zhang Y, Haromy A, Eaton F, Mendiola Pla M et al. 2022. Trim35-mediated degradation of nuclear pkm2 destabilizes gata4/6 and induces p53 in cardiomyocytes to promote heart failure. Sci Transl Med. 14(669):eabm3565.
294. Zhang W, Xie M, Shu MD, Steitz JA, DiMaio D. 2016. A proximity-dependent assay for specific rna-protein interactions in intact cells. RNA. 22(11):1785-1792.
295. Alam MS. 2018. Proximity ligation assay (pla). Curr Protoc Immunol. 123(1):e58.
296. Manders EMM, Verbeek FJ, Aten JA. 1993. Measurement of co-localization of objects in dual-colour confocal images. J Microsc. 169(3):375-382.
297. Bolte S, Cordelières FP. 2006. A guided tour into subcellular colocalization analysis in light microscopy. J Microsc. 224(Pt 3):213-232.
298. Cieśla J. 2006. Metabolic enzymes that bind rna: Yet another level of cellular regulatory network? Acta Biochimica Polonica. 53.
299. Gonzalez OG, Assfalg R, Koch S, Schelling A, Meena JK, Kraus J, Lechel A, Katz SF, Benes V, Scharffetter-Kochanek K et al. 2014. Telomerase stimulates ribosomal dna transcription under hyperproliferative conditions. Nat Commun. 5:4599.
300. Zhang Y, Zhao M, Gao H, Yu G, Zhao Y, Yao F, Yang W. 2022. Mapk signalling-induced phosphorylation and subcellular translocation of pdhe1α promotes tumour immune evasion. Nat Metab. 4(3):374-388.
301. Chueh FY, Leong KF, Cronk RJ, Venkitachalam S, Pabich S, Yu CL. 2011. Nuclear localization of pyruvate dehydrogenase complex-e2 (pdc-e2), a mitochondrial enzyme, and its role in signal transducer and activator of transcription 5 (stat5)-dependent gene transcription. Cell Signal. 23(7):1170-1178.
302. Richard AJ, Hang H, Stephens JM. 2017. Pyruvate dehydrogenase complex (pdc) subunits moonlight as interaction partners of phosphorylated stat5 in adipocytes and adipose tissue. J Biol Chem. 292(48):19733-19742.
303. Matsuda S, Adachi J, Ihara M, Tanuma N, Shima H, Kakizuka A, Ikura M, Ikura T, Matsuda T. 2016. Nuclear pyruvate kinase m2 complex serves as a transcriptional coactivator of arylhydrocarbon receptor. Nucleic Acids Res. 44(2):636-647.
304. Fleminger G, Dayan A. 2021. The moonlighting activities of dihydrolipoamide dehydrogenase: Biotechnological and biomedical applications. J Mol Recognit. 34(11):e2924.
305. Stacpoole PW. 2012. The pyruvate dehydrogenase complex as a therapeutic target for age-related diseases. Aging Cell. 11(3):371-377.
306. Gurd BJ, Peters SJ, Heigenhauser GJ, LeBlanc PJ, Doherty TJ, Paterson DH, Kowalchuk JM. 2008. O2 uptake kinetics, pyruvate dehydrogenase activity, and muscle deoxygenation in young and older adults during the transition to moderate-intensity exercise. Am J Physiol Regul Integr Comp Physiol. 294(2):R577-584.
307. Blass JP, Sheu RK, Gibson GE. 2000. Inherent abnormalities in energy metabolism in alzheimer disease. Interaction with cerebrovascular compromise. Ann N Y Acad Sci. 903:204-221.
308. Yao J, Hamilton RT, Cadenas E, Brinton RD. 2010. Decline in mitochondrial bioenergetics and shift to ketogenic profile in brain during reproductive senescence. Biochim Biophys Acta. 1800(10):1121-1126.
309. Goldstein S, Ballantyne SR, Robson AL, Moerman EJ. 1982. Energy metabolism in cultured human fibroblasts during aging in vitro. J Cell Physiol. 112(3):419-424.
310. Rivera-Torres J, Acín-Perez R, Cabezas-Sánchez P, Osorio FG, Gonzalez-Gómez C, Megias D, Cámara C, López-Otín C, Enríquez JA, Luque-García JL et al. 2013. Identification of

mitochondrial dysfunction in hutchinson-gilford progeria syndrome through use of stable isotope labeling with amino acids in cell culture. J Proteomics. 91:466-477.
311. Zhu D, Li X, Tian Y. 2022. Mitochondrial-to-nuclear communication in aging: An epigenetic perspective. Trends Biochem Sci. 47(8):645-659.
312. Ren R, Ocampo A, Liu GH, Izpisua Belmonte JC. 2017. Regulation of stem cell aging by metabolism and epigenetics. Cell Metab. 26(3):460-474.

Resumen en castellano

1. Introducción

Los telómeros son estructuras conformadas por una secuencia de ADN repetida en tándem (TTAGGG) y un conjunto de proteínas accesorias, localizadas en los extremos de los cromosomas eucariotas[1; 2]. La secuencia telomérica no es una secuencia codificante, siendo la principal función de los telómeros la protección del ADN cromosómico[3]. El ADN telomérico sufre un pequeño acortamiento en cada división celular., y cuando se alcanza una longitud telomérica crítica, la célula entra en senescencia y es incapaz de seguir dividiéndose. Sin embargo, existen mecanismos en la célula para poder solventar este problema, como la telomerasa.

La telomerasa es un complejo ribonucleoproteico compuesto principalmente por dos componentes: una subunidad catalítica (TERT) y un componente de ARN (*TERC*). TERT es capaz de emplear a *TERC* como molde para completar la síntesis de los telómeros y mantener la longitud telomérica de las células[4; 5]. Dado que la telomerasa es capaz de mantener la longitud telomérica y, por ende, la capacidad de división de la célula, la telomerasa se ha relacionado directamente con los procesos de envejecimiento y cáncer[2; 6]. Sin embargo, en los últimos años se ha determinado que tanto TERT como *TERC* son capaces de realizar funciones extracurriculares o no canónicas, es decir, independientes del alargamiento telomérico[7-9].

La expresión de TERT se reactiva en el 90% de los tumores[2], y se ha demostrado que TERT es capaz de incentivar la progresión tumoral de forma independiente al alargamiento telomérico interviniendo en procesos como la transición epitelio-mesénquima[10; 11], y aumentando la señalización de factores de transcripción pro-tumorales como c-MYC[12]. Por otro lado, TERT ejerce otras funciones extracurriculares en la mitocondria, donde se ha determinado que es capaz de proteger el ADN mitocondrial del daño de la luz ultravioleta y además disminuye el estrés oxidativo inhibiendo la producción de especies reactivas de oxígeno (ROS)[13; 14].

En el caso de *TERC*, se conoce que es capaz de unirse a más de 2.000 loci en el genoma mediante una secuencia consenso (*TERC*-bs), y que es capaz de actuar como un ARN largo no-codificante (lnc-ARN) modificando la transcripción de genes, independientemente de TERT y de la actividad telomerasa[15]. Concretamente en nuestro laboratorio hemos determinado que su expresión es imprescindible para la correcta formación de la población mieloide (macrófagos y neutrófilos)[9]: *TERC* se une a los *TERC*-bs de las regiones promotoras de los genes que controlan la diferenciación mieloide (*CSF2*, *CSF3* y *SPI1*), reclutando a la ARN polimerasa II (ARN-pol II), y promoviendo la transcripción de esos genes y, por tanto, la mielopoyesis[16]. *TERC* también es importando a la mitocondria, donde es procesado, generándose una forma corta (*TERC*-53) relacionada con el control de la función mitocondrial y la senescencia celular[17; 18]. Además, tanto TERT como *TERC* poseen funciones extracurriculares regulado procesos de inflamación, regulando, entre otros, la señalización a través del factor nuclear-kappa B (NF-κB)[19-21].

La célula utiliza como principal fuente de energía las moléculas de glucosa, que se hidrolizan en un proceso en dos fases: la glucólisis y la fosforilación oxidativa[22]. La glucólisis se produce en el citosol y consiste en una oxidación parcial de la glucosa, dando lugar a dos moléculas de adenosina trifosfato (ATP) y dos moléculas de piruvato. El piruvato puede convertirse en lactato para recuperar el poder reductor perdido en la glucólisis, o puede convertirse en acetil-CoA en la mitocondria para entrar en el ciclo de ácidos tricarboxílicos (CAT) y así continuar con el proceso de fosforilación oxidativa (oxidación completa de la glucosa), que reporta más moléculas de energía (ATP)[22; 23].

La enzima encargada de la conversión del piruvato a lactato es la lactato deshidrogenasa (LDH)[22]. La reacción que cataliza es una reacción reversible y la regulación de su actividad viene dada tanto por su composición de subunidades (LDHA y LDHB) como por modificaciones transcripcionales y post-traduccionales, aunque en términos generales, una mayor composición de subunidades LDHA implica una mayor producción de lactato, y en el caso de LDHB, una mayor producción de piruvato[24]. El estudio de la LDH es de especial interés en las células tumorales debido a que es clave en la reprogramación metabólica que sufren para hacer frente a la demanda de producción de energía para su rápida proliferación (efecto Warburg)[25; 26]. Además, se ha establecido que el lactato ejerce un papel fundamental inmunomodulador en el microambiente tumoral[26; 27].

El piruvato puede también ser destinado a la generación de acetil-CoA por el complejo piruvato deshidrogenasa (PDC). Se trata de un complejo enzimático mitocondrial formado por tres subunidades[28]: E1 (piruvato deshidrogenasa), E2 (dihidrolipoil transacetilasa) y E3 (dihidrolipoil deshidrogenasa), donde el componente E1 está sujeto a una regulación mediante fosforilación que inactiva la actividad enzimática del complejo[29]. Aunque el PDC es mitocondrial, se ha demostrado que es capaz de translocarse al núcleo, donde controla la expresión de genes relacionados con el ciclo celular mediante la regulación de la acetilación de histonas[30]. Asimismo, su presencia en el núcleo se ha relacionado con los procesos de envejecimiento y desarrollo embrionario[31-33].

El sistema inmunitario está compuesto por barreras físicas y celulares y su principal función es la defensa del organismo frente a daño tisular y patógenos[34]. Se conoce que la regulación del metabolismo energético de las células inmunitarias es importante para el desarrollo de sus funciones, siendo el metabolismo de la glucosa uno de los más estudiados[35; 36]. Tanto la glucólisis como el CAT son fundamentales no solo para la proliferación de las células inmunitarias, sino que también los metabolitos generados poseen funciones de señalización importantes para el control de la expresión de genes y la generación de citoquinas[35; 37; 38].

Uno de los principales mecanismos de defensa del sistema inmunitario es la inflamación[39]. Este proceso se ha caracterizado clásicamente por el enrojecimiento, tumoración, dolor y calor[34; 39]. Cuando la inflamación se produce de forma controlada, se considera una inflamación aguda, donde hay una respuesta localizada en el espacio y el tiempo. Sin embargo, cuando los mecanismos de control de la inflamación se desajustan, se puede producir una inflamación crónica, donde la inflamación persiste en el tiempo, y puede producirse de forma sistémica[40; 41]. La inflamación crónica está presente en numerosas enfermedades, siendo una de ellas la psoriasis.

La psoriasis es una enfermedad multifactorial con un elevado componente genético que cursa con inflamación crónica en la piel, donde suelen aparecer lesiones en forma de placas enrojecidas con descamación[42; 43]. Molecularmente se caracteriza por una hiperproliferación de queratinocitos y la infiltración de células inmunitarias en la piel, donde se genera un bucle de alimentación positivo de moléculas pro-inflamatorias sintetizadas tanto por las células de la piel como por las del sistema inmunitario[44-47]. Además, se produce un incremento del estrés oxidativo en la piel que contribuye a la patogénesis de la enfermedad, y se ha determinado que moléculas como el NAD^+ son clave en la patología de la psoriasis ya que aumentan este estrés oxidativo[48]. Por otro lado, también se conoce que la regulación del metabolismo de la glucosa juega un papel fundamental ya que interviene en la proliferación de los queratinocitos[49; 50]. Además, el lactato producido por las células hiperproliferativas en condiciones de inflamación

crónica es capaz de retener a las células inmunitarias en el tejido, aumentando los niveles de inflamación en el mismo[51; 52].

Otro proceso patológico donde también la respuesta inflamatoria es clave es en el cáncer. Las células tumorales son capaces de evadir la respuesta inmunitaria anti-tumoral y crear un ambiente de citoquinas y moléculas de señalización para inducir una respuesta inmunitaria que favorezca el desarrollo del tumor[53-55].

El glioblastoma es el tumor cerebral más común y uno de los más agresivos, donde la supervivencia media de los pacientes es de aproximadamente 15 meses, a pesar de su tratamiento con terapias convencionales[56; 57]. Uno de los motivos por los que este tumor es tan agresivo es debido a su gran ambiente inmunosupresor[58]. Por ello, en la actualidad se considera que la inmunoterapia puede ser un tratamiento efectivo para los pacientes con glioblastoma[59].

El pez cebra (Danio rerio) es un pequeño pez tropical que pertenece a la familia Cyprinidae, orden de los Cypriniformes[60]. El uso de este pez como modelo animal en la investigación biomédica ha ido creciendo exponencialmente en los últimos años debido a sus numerosas ventajas frente a otros modelos vertebrados, como su elevada fecundidad y fertilización externa, la fácil manipulación genética de los embriones; su rápido desarrollo (organogénesis completa en 24 horas) y la transparencia de las larvas, que permite la visualización *in vivo* de células y moléculas mediante el uso de proteínas fluorescentes[61-63].

Se ha demostrado que el pez cebra es un gran modelo para el estudio de la biología de los telómeros ya que existe una gran similitud tanto estructural como funcional entre la telomerasa humana y la del pez cebra[64]. Además, el pez cebra posee una longitud telomérica similar a la del humano (5-15 kb)[65], y está relacionada con el envejecimiento del pez y su esperanza de vida[64-66]. Igualmente, el pez cebra se ha empleado como modelo para el descubrimiento de nuevas funciones extracurriculares tanto de Tert como de *terc*[9; 16; 67].

El pez cebra también es un gran modelo para el estudio del sistema inmunitario[68; 69] y la inflamación crónica[70]. Existen numerosos modelos de inflamación crónica en piel, como por ejemplo el mutante en el gen *spint1a* (*spint1a*$^{-/-}$), en el que el nivel de inflamación puede detectarse fácilmente debido a su fenotipo de agregados de queratinocitos y dispersión de neutrófilos fuera del tejido hematopoyético caudal[71].

Por otro lado, también se han establecido varios modelos de cáncer en el pez empleando el sistema de generación de transgénicos Gal4/UAS, por el que se puede inducir la expresión de un oncogén en un tejido específico[72]. Por ejemplo, uno de los modelos de glioblastoma más empleados se genera mediante la expresión del oncogén HRAS fusionado a la proteína fluorescente verde GFP (UAS:eGFP-*HRAS_V12*) en la línea transgénica *zic4:*GAL4, que expresa Gal4 específicamente en el tejido cerebral[73].

2. Objetivos

Los objetivos de este trabajo son los siguientes:

3. Estudiar la relación entre *terc* y la regulación del metabolismo de la glucosa en el contexto de inflamación crónica y en la respuesta inmunitaria antitumoral.

4. Validar y caracterizar la interacción entre el complejo piruvato deshidrogenasa y los componentes de la telomerasa *TERC* y TERT.

3. Resultados y discusión

3.1. Regulación del metabolismo de la glucosa por *terc*

En nuestro grupo de investigación hemos descrito que *TERC* posee una función extracurricular evolutivamente conservada regulado la generación de células de la estirpe mieloide. Concretamente, hemos demostrado que *TERC* es capaz de unirse su secuencia consenso específica (*TERC*-bs) en las regiones promotoras de los principales genes en control de la mielopoyesis, *SPI1* and *CSF3*, reclutando a la ARN pol II para iniciar su transcripción[9; 16].

Se conoce que los *TERC*-bs se encuentran en más de 2000 loci diferentes en todo el genoma humano, por lo que *TERC* puede estar regulando la transcripción de muchos más genes[15]. Por otro lado, ya hay descritos muchos lnc-ARNs que están involucrados en la regulación del metabolismo de la glucosa, como por ejemplo lncRNA-UCA1[88; 89], que aumenta la expresión de la hexoquinasa 2 (HK2) o el lncRNA-AC020978, que se expresa en condiciones de hipoxia, aumentando la transcripción de enzimas implicadas en la glucólisis[90].

Por ese motivo, decidimos evaluar si la expresión de *terc* podría estar afectando la composición de los metabolitos glucídicos, realizando un análisis metabolómico en larvas de pez cebra con una expresión de *terc* reducida o incrementada.

En este trabajo se presentan los primeros datos que apuntan a la existencia de una regulación del metabolismo de la glucosa por *terc*, ya que la concentración de varios metabolitos de la glucólisis y del ciclo de Krebs (CAT) se vio modificada atendiendo a la expresión de *terc*, especialmente, la concentración de lactato. Los niveles de lactato se vieron incrementados cuando se redujeron los niveles de *terc* y viceversa. Además, se encontró una *terc*-bs en el promotor del gen *ldhbb* y se comprobó que su expresión se reducía al disminuir los niveles de *terc*, y que la regulación se llevaba a cabo a través de su secuencia promotora. También pudimos establecer que esta regulación se producía no solo en larvas de pez cebra sino también en el tejido hematopoyético del pez adulto, siendo necesaria la caracterización de esta regulación mediante mutagénesis del *tercbs* en la región promotora del gen *ldhbb* y con un ensayo de aislamiento de cromatina mediante purificación de ARN (ChIRP) para detectar directamente la unión de *terc* a esta región promotora.

Una vez establecida esta regulación, se decidió estudiar el impacto de la expresión de *terc* en dos modelos de enfermedad en los que el lactato juega un papel importante en la modulación de la respuesta inmunitaria, comenzando por la inflamación crónica en piel.

En el contexto de inflamación crónica se ha descrito que el lactato es capaz de incrementar la respuesta inmunitaria, aumentando los niveles de inflamación[37; 51; 91]. Por ese motivo, comenzamos caracterizando el efecto de la regulación del lactato en un modelo de inflamación crónica en piel, como es el modelo de pez cebra mutante para *spint1a* (*spint1a*$^{-/-}$).

En primer lugar, encontramos que el tratamiento con un inhibidor de LDH (oxamato), redujo los niveles de inflamación en las larvas *spint1a*$^{-/-}$, aunque no se consiguió confirmar este resultado mediante la inhibición genética de los genes de *ldha* ni *ldhba*. Este resultado puede deberse a la presencia de otras isoformas de Ldh en la piel del pez cebra y a la dificultad para inhibir completamente la expresión de *ldha* y *ldhba* mediante la microinyección de las guías de CRISPR-Cas9, que generan una deleción en mosaico en la primera generación.

Por otro lado, el tratamiento con lactato también redujo los agregados y la dispersión en las larvas con inflamación crónica. Esto nos hizo plantearnos la hipótesis de que la reducción en la

inflamación se debiera no solo la producción de lactato, sino que la regulación de la actividad LDH mediante el oxamato o el lactato, estuviera afectando al balance NAD^+/NADH. Así, a través de ensayos de rescate mediante el tratamiento con NAD^+ y a través de la medición de NAD^+ y NADH mediante ensayos de luciferasa, comprobamos que tanto el tratamiento con oxamato como el lactato exógeno estaban reduciendo la ratio NAD^+/NADH. Existen evidencias previas de que la reducción en esta ratio mejora la inflamación en la piel[48], y nuestros resultados también confirman otros estudios de la literatura donde se establece que el lactato en exceso es capaz de producir cambios en los niveles de NAD^+/NADH[92; 93].

Asimismo, decidimos estudiar los cambios transcriptómicos que se estaban produciendo en la piel de las larvas tratadas con ambos tratamientos, y nos centramos en los genes comúnmente regulados por oxamato y lactato con el objetivo de encontrar genes candidatos a mediar esta mejora en la inflamación. Concretamente, establecimos que la mayoría de los genes identificados estaban implicados en rutas metabólicas, de señalización celular mediante citoquinas y en rutas de proliferación. Algunos de ellos (*rps6ka1*, *socs2*, *ctnnb1*, *pfas* or *cxcl14*) fueron seleccionados para realizar ensayos funcionales en las larvas *spint1a*$^{-/-}$, donde en el caso de *rps6ka1* y *socs2*, concluimos que ni su aumento ni su disminución era suficiente para causar cambios en el estado de inflamación de las larvas deficientes en *spint1a*.

Además, realizamos un análisis bioinformático empleando datos de transcriptómica de muestras de piel de pacientes de psoriasis, disponibles en la base de datos GEO (GDS4602). En este análisis comprobamos que la expresión de *LDHA* y *LDHB* estaba aumentada en las lesiones de piel de los pacientes de psoriasis y encontramos una correlación positiva entre la expresión de *LDHA* y el marcador de inflamación *IL-1B*. También evaluamos la expresión de los genes candidatos encontrados en el análisis de microarray realizado con las muestras de piel de pez cebra, encontrando varias diferencias en el patrón de expresión de los genes, como en el caso de *RPS6KA1* cuya expresión estaba aumentada en las muestras humanas y correlacionaba positivamente con la expresión de genes inflamatorios como *IL-1B* e *IL-17A*. Sin embargo, determinamos otros genes como *CXCL14*, cuya expresión estaba disminuida en la piel de las larvas *spint1a*$^{-/-}$ y también en las lesiones de piel de los pacientes de psoriasis, y aumentaba con los tratamientos de oxamato y lactato. Además, su expresión correlacionaba negativamente con la expresión de *LDHA* y los marcadores de inflamación estudiados, corroborando los resultados de otros estudios en la bibliografía, donde se ha descrito que sus niveles se encuentran reducidos en las lesiones de los pacientes de psoriasis, y que su falta aumenta la susceptibilidad de los pacientes a sufrir infecciones bacterianas[94].

Uno de los resultados más llamativos es la mejora de la inflamación en piel de las larvas deficientes en *terc*. Esto puede deberse a la reducción de la expresión de la *ldhbb* hepática, donde se acumularía el lactato. Este exceso de lactato en el hígado iría a la piel, donde la *ldhba* lo convertiría en piruvato, y generaría NADH, que restauraría el balance NAD^+/NADH.

Por otro lado, debido a la regulación de *ldhbb* por *terc* en las células hematopoyéticas, y a la implicación del metabolismo en la función del sistema inmunitario, estudiamos también el papel de *terc* en la respuesta inmunitaria antitumoral. Concretamente, encontramos que la sobreexpresión de terc en las células hematopoyéticas (peces *drl:terc*), resultó en una reducción del tamaño del tumor de glioblastoma, de forma independiente a la expresión de *tert*.

De esta forma, comenzamos a estudiar las posibles células inmunitarias involucradas en la reducción del tumor, comenzando por los neutrófilos debido al papel previamente descrito para terc regulando la mielopoyesis[16]. Mediante una tinción con negro Sudán, se vio que el número

de neutrófilos en la cabeza de las larvas *drl:terc* con tumor aumentaba de forma significativa, sin embargo, al estudiar la capacidad de migración de los neutrófilos en un ensayo de herida, no se encontraron diferencias con respecto a los neutrófilos sin sobreexpresión de *terc*. Ya que las citoquinas quimioatrayentes producidas por el tumor son diferentes a las producidas en una herida (G-CSF y GM-CSF en tumores[95], y gradientes de H_2O_2 como primera señal de reclutamiento en las heridas[98]), sería interesante estudiar las diferencias en la composición de citoquinas en ambos casos, e investigar si *terc* es capaz de inducir diferencias en la expresión de receptores de citoquinas, influyendo en el reclutamiento de los neutrófilos al tumor, pero sin tener efecto en el caso de las heridas.

Puesto que la mayor parte de las células que constituyen la respuesta inmunitaria frente al glioblastoma son las células de la microglía[101], decidimos estudiar si la sobreexpresión de *terc* era capaz de modificar su función antitumoral. Mediante inmunotinción de la microglía en larvas con y sin sobreexpresión de *terc*, comprobamos que el número de células de la microglía era similar en ambos casos, con independencia al desarrollo del glioblastoma. Asimismo, se comprobó si *terc* era capaz de inducir cambios en la polarización de los macrófagos (y, por ende, la microglía), realizando ensayos de infección en las larvas, previamente modificando los niveles de *terc*. Nuestros resultados indican que los cambios en la expresión en *terc* no son suficientes para producir cambios en el estado de polarización de los macrófagos, aunque sería necesario descartar al completo esta posibilidad estudiando marcadores de polarización directamente de la microglía que se localiza en el microambiente tumoral.

Finalmente, se decidió estudiar el interactoma de la proteína *Draculin* usando la base de datos STRING (https://string-db.org/) para establecer otras células que pudieran estar implicadas en la reducción del glioblastoma al aumentar la expresión de *terc*. En este estudio bioinformático se establecieron como posibles candidatas las células hemangiogénicas, que dan lugar tanto a las células hematopoyéticas como las células angiogénicas, es decir, las que dan lugar a los vasos sanguíneos. Los tumores sólidos como el glioblastoma inducen la formación de nuevos vasos sanguíneos para asegurar la llegada de nutrientes y oxígeno al tumor[115; 116], por lo que sería interesante indagar en la posibilidad de que *terc* esté involucrado en este proceso y que, por ello, los cambios en su expresión en estas células produzcan la reducción tumoral que hemos descrito.

3.2. Caracterización de la interacción entre piruvato deshidrogenasa y telomerasa

Se conoce que el ARN de la telomerasa (*TERC*) es capaz de funcionar como un lnc-ARN, uniéndose a una secuencia consenso específica en el genoma[15], y realizando funciones de forma independiente a TERT y al alargamiento telomérico[21; 74]. Concretamente, nuestro grupo de investigación ha demostrado que *TERC* es capaz de aumentar la transcripción de reguladores clave de la mielopoyesis, uniéndose en su región promotora y atrayendo y uniéndose a su vez a la ARN polimerasa II (ARN pol II)[16]. Sin embargo, aunque se conoce esta habilidad de *TERC* como regulador transcripcional, nunca se ha descrito si existen más proteínas que interaccionan con este ARN y que puedan dar más información sobre otras funciones extracurriculares que pueda estar llevando a cabo.

Teniendo esto en cuenta, decidimos identificar el interactoma proteico de *terc*, empleando al pez cebra como modelo *in vivo*. Una vez identificados los posibles interactores, descubrimos que la mayoría de ellos eran proteínas involucradas en el metabolismo de carbohidratos y la fosforilación oxidativa (tesis doctoral de Elena Martínez-Balsalobre, resultados no publicados).

En este trabajo hemos demostrado que la interacción identificada en el pez cebra entre *terc* y el componente E1 del complejo piruvato deshidrogenasa (PDC-E1), se encuentra conservada en el humano. Para ello, se han empleado dos líneas celulares diferentes y se han realizado ensayos de RNA-*pull down,* inmunoprecipitación de RNA (RIP) y ensayos de ligación por proximidad (PLA). Además, mediante ensayos de colocalización se ha determinado que esta interacción ocurre tanto en el núcleo como en el citosol y la mitocondria de la célula. En los últimos años, se ha incrementado considerablemente el número de enzimas glucolíticas y del CAT que tienen la capacidad de unir ARNs. Sin embargo, esta es la primera evidencia de la habilidad de la piruvato deshidrogenasa de unir ARN. Además, esta interacción evidencia un nuevo papel extracurricular de *TERC*.

Se determinó que los niveles de *TERC* son importantes para determinar la localización nuclear de la enzima, ya que una disminución de la expresión de *TERC* conllevaba un aumento de los niveles de PDC nuclear, y viceversa. Sin embargo, la expresión de *TERC* no indujo cambios en la actividad enzimática de PDC ni en los niveles globales de acetilación de las histonas H3 y H4. Sin embargo, ya que *TERC* es capaz de unirse a sitios específicos en el genoma a través de su secuencia consenso, no se puede descartar la posibilidad de que *TERC* pueda estar guiando al PDC para controlar la transcripción en sitios específicos del genoma.

También se evaluó si la interacción entre *TERC* y PDC era exclusiva del ARN de la telomerasa o si también estaba implicada la subunidad catalítica (TERT). Mediante la realización de PLA, concluimos que también TERT era capaz de interaccionar con la subunidad E1 del PDC. Además, comprobamos que la sobreexpresión de TERT era capaz de reducir la actividad PDC en la mitocondria. Asimismo, se estableció que ambos componentes de la telomerasa eran capaces de interaccionar con la subunidad E2 del PDC, aunque de forma más débil.

Es necesario conocer aún si esta novedosa interacción entre los componentes de la telomerasa y el PDC se produce por *TERC* y TERT por separado o formando un complejo, y, en ese caso, si alguno de los dos componentes es un factor limitante para la interacción. Además, se han descrito funciones independientes para las subunidades del PDC tanto en el núcleo como en el citosol. Por ejemplo, se ha determinado que la subunidad PDC-E1α se localiza también en el citosol y es capaz de inhibir la señalización del factor proinflamatorio NFκB, interaccionando con su inhibidor IKKβ[75]. También se ha descrito que tanto la subunidad E1 como la E2 son capaces

de interaccionar con el factor de transcripción STAT5, aumentando la transcripción de sus genes diana, como la interleucina 3 (IL-3)[76; 77]. Por tanto, para conocer la función biológica de esta interacción, es necesario dilucidar si la interacción con *TERC* y TERT se produce con las subunidades del PDC por separado, o con el complejo enzimático al completo.

Por otro lado, el PDC ha sido descrito recientemente como una proteína clave a estudiar en el proceso de envejecimiento[78], ya que se ha visto que su actividad se encuentra disminuida tanto en ratones envejecidos como en el cerebro de los pacientes con alzheimer[79-81]. Además, se ha determinado que las personas con progeria (síndrome que produce un envejecimiento acelerado), poseen una mayor cantidad de PDC nuclear y una disminución en su capacidad para realizar la fosforilación oxidativa[33; 82; 83].

El complejo de la telomerasa es uno de los mecanismos celulares directamente relacionados con los procesos de envejecimiento e inmortalidad[64; 84], y numerosos estudios han descrito la importancia de la comunicación núcleo-mitocondria tanto para la normal función celular como durante el envejecimiento[13; 85; 86]. Más aún, los estudios señalan que las modificaciones de histonas, y específicamente la acetilación, es el principal mecanismo por el que la senescencia y la pluripotencia celular se encuentra ligada al metabolismo[85; 87]. Debido a los estudios previos que relacionan el control de la acetilación de histonas con el envejecimiento, y debido al papel de PDC en la acetilación de histonas, también se debe considerar la posibilidad de que la interacción que reportamos en este trabajo entre los componentes de la telomerasa y las subunidades del PDC, pueda indicar una nueva forma por la que los procesos de envejecimiento y el metabolismo celular están conectados.

4. Conclusiones

Las conclusiones obtenidas a partir de los resultados de este trabajo son las siguientes:

1. Los cambios en la expresión de *terc* inducen modificaciones en la composición de los metabolitos de la glucólisis y el CAT en las larvas de pez cebra. Asimismo, *terc* funciona como un ARN largo no codificante regulando la expresión del gen *ldhbb* uniéndose a su región promotora tanto en larvas como en el tejido hematopoyético adulto.

2. La inhibición farmacológica de la lactato deshidrogenasa (Ldh) con oxamato y el tratamiento con lactato exógeno, mejoran la inflamación en piel en las larvas de pez cebra deficientes en *spint1a*, disminuyendo la ratio NAD^+/NADH. Sin embargo, solo el tratamiento con oxamato es capaz de reducir los niveles de daño en el ADN y de estrés oxidativo (H_2O_2) en la piel de las larvas deficientes en *spint1a*.

3. La manipulación de la actividad Ldh con oxamato y lactato altera el patrón de expresión génica de la piel inflamada de las larvas deficientes en *spint1a*, incluyendo *rps6ka1*, *socs2* y *cxcl14*. Sin embargo, la manipulación genética de los genes diferencialmente expresados seleccionados, como *rps6ka1* y *socs2*, no afecta a la inflamación crónica en piel de estas larvas. Además, los niveles de *RPS6KA1* están aumentados en las muestras de lesiones de pacientes psoriásicos y correlacionan con los niveles de marcadores de inflamación, mientras que los de *SOCS2* están disminuidos.

4. Los niveles de *LDHA* están aumentados en las lesiones de pacientes psoriásicos con respecto a la piel sin lesiones y aquella de pacientes sanos, y correlacionan positivamente con marcadores de inflamación. Además, los niveles de ARNm de *CXCL14* se encuentran disminuidos en las muestras de lesiones de pacientes psoriásicos con respecto a la piel sana, y correlacionan negativamente con los niveles de *LDHA* y los marcadores de inflamación.

5. Solo la deficiencia de *terc*, pero no la de Tert, es capaz de mejorar la inflamación crónica en piel de las larvas deficientes en *spint1a*, como muestra la disminución en la formación de agregados de queratinocitos y en la infiltración de neutrófilos en la piel.

6. La sobreexpresión de *terc* en células hematopoyéticas restringe el desarrollo tumoral del glioblastoma de forma independiente a Tert. Este efecto parece ser independiente de la microglía ya que tanto su número como su polarización permanecen inalterados.

7. Ambos componentes de la telomerasa (TERT y *TERC*) interaccionan con las subunidades E1 y E2 del complejo piruvato deshidrogenasa (PDC) en el núcleo, citosol y la mitocondria de células humanas.

8. La PDC nuclear correlaciona con los niveles de *TERC* en células humanas. Así, el incremento de *TERC* resulta en una disminución de PDC nuclear, mientras que una disminución de *TERC* produce un aumento en PDC nuclear. Los cambios de localización de PDC promovidos por *TERC* no afectan a los niveles generales de acetilación de histonas H3 y H4 ni a la actividad enzimática del PDC. Sin embargo, la sobreexpresión de TERT produce una disminución de la actividad PDC mitocondrial.